

University of Alberta

**Lung Injury and Repair:
Early Therapeutic Considerations**

by

Gloria Juliana Rey-Parra

A thesis submitted to the Faculty of Graduate Studies and Research in partial
fulfillment of the requirements for the degree of

Doctor of Philosophy

in

Medical Sciences-Pediatrics

Department of Pediatrics
©Gloria Juliana Rey-Parra
Spring 2012
Edmonton, Alberta

Permission is hereby granted to the University of Alberta Libraries to reproduce single copies of this thesis and to lend or sell such copies for private, scholarly or scientific research purposes only. Where the thesis is converted to, or otherwise made available in digital form, the University of Alberta will advise potential users of the thesis of these terms.

The author reserves all other publication and other rights in association with the copyright in the thesis and, except as herein before provided, neither the thesis nor any substantial portion thereof may be printed or otherwise reproduced in any material form whatsoever without the author's prior written permission.

Dedicated to my God,
beloved husband Hernando,
Little Princess Sylvia,
parents, sister and grandparents

ACKNOWLEDGEMENTS

I would like to express my deepest gratitude and admiration to my supervisor *Dr. Bernard Thébaud*, for giving me the opportunity to pursue a dream. Bernard became my mentor and a true model to follow. Despite his numerous commitments, he always kept the door open for an academic discussion, advice and guidance. I thank him for all the constructive criticism and encouraging words at the right time.

The work behind this thesis would not have been possible without the collaboration of my fellow graduate students, postdoctoral fellows and laboratory technicians. I am very grateful for all the shared knowledge, important discussions and long days of work. I would like to specially mention *Dr. Arul Vadivel*, *Ms. Farah Eaton*, *Ms. Beth Kirby* and *Mrs. Bev Morgan*, I will always remember your support, teachings and the good laughs we had together. I would also like to thank *Mrs. Bronwyn Appleyard* and *Mrs. Trish Kryzanowski* for all the administrative support.

I would like to thank *Dr. Stephen Archer*, *Dr. Richard Bland* and *Dr. Marleen Rabinovitch* for sharing their experience, teaching and support at different moments of my training.

I want to acknowledge the financial support from the Maternal Fetal – Newborn Health program-CIHR and Alberta Heritage Foundation for Medical Research.

I want to acknowledge the support from my family-in law during all this years. Specially *Daniel* and *Diana* for being there when I tried to balance all the aspects of my life. Special thanks to my friends for their encouraging words at all times. From all my good friends special thanks to *Margaret Lozano*, *Dr. Marcelo*

Marcet and *Candy Marcet* for all their help at different stages of the thesis writing process.

Finally, I want to thank from the bottom of my heart to my husband *Hernando* for being my continuous support, for walking with me during this crucial steps for all the love and laughter. To my daughter *Sylvia* for being my light and driving force beyond imagination. To my parents *Jorge* and *Gloria Isabel* for giving me all the possible love, great example of hard and honest work. For all their sacrifice and for encouraging me to become the best I could possibly be. To my beloved sister *Mona* for her support, trust and love during this years. To my grandparents *Jorge* and *Edelmira*, for all their care, example, values and understanding during this important part of my professional life.

ABSTRACT

Acute Lung Injury/Acute Respiratory Distress Syndrome (ALI/ARDS) remain a major health issue because of a high mortality and morbidity rate. Despite progress in understanding the pathogenesis of ALI, there is currently no drug-based therapy promoting lung repair. A predominant pathological finding in ALI is diffuse alveolar epithelial damage. Rapid recovery of the alveolar epithelium is crucial for lung repair and prevention of the development of lung fibrosis post-ALI/ARDS. In order to identify new therapeutic strategies aimed at improving epithelial function to accelerate repair and decrease the mortality/morbidity of patients with ARDS, we investigated two innovative concepts: (1) the lung healing capacity of the MRL (Murphy-Roth Large) mouse strain known for its unique capacity for both accelerated and regenerative wound healing, and (2) stem cell-based treatments. We used two well-established ALI/ARDS models: lipopolysaccharide, LPS-induced ALI/ARDS and bleomycin, BLM-induced ALI/ARDS complicated by fibrosis.

We found that MRL/MPJ mice have attenuated lung inflammation and injury in the LPS-induced model of ARDS compared to C57BL/6 control mice. The healing potential of MRL/MPJ mice is in part attributable to alveolar epithelial type 2 cells (AT2, putative distal lung progenitor cells) since they displayed an accelerated wound closure *in vitro* and their conditioned media attenuated LPS-induced ALI/ARDS in C57BL/6 mice. Conversely, in BLM-induced lung injury, MRL/MPJ healer mice showed no differences in their repair

capacity compared to C57BL6 controls. This could be attributable to the marked toxicity of BLM on AT2 cells.

We also tested the therapeutic potential of human umbilical cord blood cells (HUCBC) in BLM-induced lung injury. HUCB decreased collagen deposition, as well as improved lung function and exercise capacity. Moreover, HUCBC secreted relaxin and angiotensin converting enzyme 2 (ACE2), 2 molecules known for their antifibrotic effects. We further explored the antifibrotic effects of ACE2 by showing worsened lung fibrosis in ACE2 knock out, whereas exogenous administration of human recombinant ACE2 significantly attenuated fibrosis and improved lung function in BLM induced lung injury.

In summary, our studies provide new therapeutic options for lung repair after injury.

Table of Contents

CHAPTER 1

1. INTRODUCTION	1
1.1 Lung diseases: a major health care problem	1
1.2 Lung injury and resolution in ALI and IPF	1
1.2.1 Normal Lung repair after acute Injury	2
1.2.2 Injury resolution ALI/ARDS and IPF	2
1.3 Importance of Alveolar epithelial cells in lung repair	4
1.4 A mammal model of Scarless healing and its importance In lung repair	5
1.4.1 The regenerative capacity of the MRL mice	5
1.4.2 Increased healing in the MRL mice, an incidental finding	6
1.4.3 Early re-epithelization	6
1.4.4 Changes in the Extracellular Membrane	6
1.4.5 Gene mapping in the regenerating ear	7
1.4.6 Proteome of the regenerating wounds in MRL/MPJ	8
1.4.7 The scarless heart in MRL/MPJ mice	8
1.4.8 Other organs in the MRL/MPJ mice	10
1.5 Potential of Cell Therapy to Prevent/Repair the Damaged Lung	13
1.5.1 Stem Cells with reparative potential	11
<i>Mesenchymal Stem Cells</i>	11
<i>Embryonic Stem Cells</i>	12
<i>Induced Pluripotent Stem Cells</i>	13
<i>Endothelial progenitor cells</i>	13
1.5.2 Paracrine effect of Stem Cells	13
1.6 Overall hypothesis-objectives	15
1.7 References	16

CHAPTER 2

MRL/MPJ MICE ARE PROTECTED AGAINST LPS-INDUCED ACUTE RESPIRATORY DISTRESS	27
2.1 Introduction	28
2.2 Materials and Methods	28
2.2.1 Animals	28
2.2.2 Alveolar epithelial type 2 (AT2) Isolation and Primary Cell Culture	29
2.2.3 <i>In vitro</i> Scratch Assays	30
2.2.4 Analysis of AT2 cells secretome (Cdm) and Cytokine arrays	30
2.2.5 LPS Model	31
2.2.6 Histology and Lung Injury Score	31
2.2.7 Bronchoalveolar Lavage (BAL) protocol	32
2.2.8 Cytokine Quantification for BAL	32
2.2.9 Statistical Analysis	32
2.3 Results	32
2.3.1 MRL/MPJ LPS Challenged Mice Exhibit Improved Lung Architecture and decreased neutrophil cell count in BAL	32
2.3.2 Decreased Proinflammatory Cytokines in MRL/MPJ LPS Challenged Mice	33
2.3.3 MRL/MPJ Alveolar Type 2 (AT2) Cells Exhibit Accelerated Wound Healing Rate Compared to C57/BL6	33
2.3.4 MRL/MPJ AT2 Cdm Contains Soluble Factors That Accelerate Wound Healing Rate In C57/BL6 AT2 Cells	34
2.3.5 MRL/MPJ Cdm is Composed of Chemokines that Modulate Increased Wound Healing Rate	34
2.3.6 MRL/MPJ AT2 Cdm Attenuates Inflammation in C57/BL6 LPS Challenged Lungs <i>in vivo</i>	34
2.4 Discussion	35
2.4 References	37

CHAPTER 3

MRL/MPJ MICE ARE NOT PROTECTED AGAINST BLEOMYCIN-INDUCED PULMONARY FIBROSIS	48
3.1 Introduction	49
3.2 Materials and Methods	50
3.2.1 BLM Model	50
3.2.2 Hydroxyproline Assay	51
3.2.3 Measurement of Collagen Content in the lung	51
3.2.4 Histology	52
3.2.5 Lung Function testing	52
3.2.6 Exercise Capacity	53
3.2.7 Western Blot	53
3.2.8 Statistical Analysis	53
3.3 Results	54
3.3.1 Collagen Deposition in BLM induced Injury in MRL/MPJ and C57/BL6 mice	54
3.3.2 Lung Mechanics in BLM induced pulmonary fibrosis in MRL/MPJ and C57/BL6 mice	54
3.3.3 BLM induced pulmonary fibrosis decreases exercise capacity	54
3.3.4 Differences in TGF- β isoforms expression between BLM-exposed and saline treated mice	55
3.4 Discussion	55
3.5 References	58

CHAPTER 4	
THERAPEUTIC POTENTIAL OF HUMAN UMBILICAL CORD BLOOD DERIVED-CELLS IN FIBROTIC LUNG INJURY	68
4.1 Introduction	69
4.2 Materials and Methods	69
4.2.1 Characterization of human HUCBC	69
4.2.2 Experimental Design	69
4.2.3 Exercise Capacity	71
4.2.4 Lung Function testing	72
4.2.5 Lung Histology	73
4.2.6 Hydroxyproline Assay	73
4.2.7 Lung Collagen Content	74
4.2.8 Isolation and characterization of HUCBC	74
<i>Cell preparation</i>	74
<i>Evaluation of HUCBC proliferation</i>	74
<i>Angiogenesis assay</i>	75
<i>MSC differentiation assay</i>	75
4.2.9 Fluorescence-activated cell sorting of cell surface	75
4.2.10 Fibroblast Isolation	75
4.2.11 Cell engraftment	76.
4.2.12 Generation HUCBC Conditioned Media	76
4.2.13 ELISA to assess antifibrotic mediators in HUCBC Cdm	76
4.2.14 Statistical Analysis	77
4.3 Results	77
4.3.1 Characterization of HUCBC	77
4.3.2 HUCBC improve exercise capacity in BLM PF	77
4.3.3 HUCBC improve lung function in BLM PF	77
4.3.4 HUCBC ameliorate BLM PF	78
4.3.5 HUCBC engraftment	78
4.3.6 <i>In vitro</i> antifibrotic effects of HUCBC Cdm	78
4.4 Discussion	78
4.5 References	83

CHAPTER 5

ANGIOTENSIN CONVERTING ENZYME 2 ABROGATES 95

BLEOMYCIN-INDUCED LUNG INJURY: EFFECTS OF GENDER

5.1 Introduction	96
5.2 Materials and Methods	96
5.2.1 Experimental design	96
5.2.2 Recombinant human ACE2	97
5.2.3 TaqMan Real-Time Polymerase Chain Reaction	97
5.2.4 Exercise Capacity	98
5.2.5 Lung function testing	98
5.2.6 Lung histology	99
5.2.7 Hydroxyproline Assay	100
5.2.8 Lung Collagen Content	100
5.2.9 Statistical Analysis	100
5.2.10 Western Blot	101
5.2.11 Elisa	101
5.3 Results	101
5.3.1 Loss of ACE2 worsens lung fibrosis in BLM-induced lung injury	101
5.3.2 Loss of ACE2 worsens exercise capacity and lung function in BLM induced Lung injury	102
5.3.3 Male ACE2 ^{-y} display worse lung fibrosis than female ACE2 ^{-/-} in BLM-induced lung injury	102
5.3.4 rhACE2 improves lung architecture, function and attenuates lung collagen deposition in BLM treated mice	102
5.3.5 Effects of rhACE2 in male and female BLM-WT mice on lung architecture, function and lung collagen deposition WT treated mice	103
5.3.6 Angiotensin receptors in BLM induced Lung injury	103
5.4 Discussion	103
5.4.1 ACE2 in Lung injury and repair	104
5.4.2 Gender Differences in the susceptibility of ACE2 knockout mice to BLM induced lung injury	105
4.5 References	107

CHAPTER 6

CONCLUSIONS, LIMITATIONS AND FUTURE DIRECTIONS 123

6.1 Conclusions	124
6.2 Limitations	125
6.3 Future Directions	126
6.4 References	128

CHAPTER 7 APPENDIX 1

BLUNTED HYPOXIC PULMONARY VASOCONSTRICTION 131 IN EXPERIMENTAL NEONATAL CHRONIC LUNG DISEASE

7.1 Introduction 132

7.2 Materials and Methods 133

7.2.1 Chronic lung injury (CLI) in preterm lambs	133
7.2.2 CLI in newborn rats	133
7.2.3 Echo-Doppler in newborn rats	134
7.2.4 Organ bath studies of newborn rat PAs	134
7.2.5 Quantitative real-time polymerase chain reaction	134
7.2.6 Immunofluorescence	135
7.2.7 Adenovirus-mediated gene transfer	135
7.2.8 Electrophysiology	135
7.2.9 Statistical Analysis	135

7.3 Results 136

7.3.1 HPV is blunted in chronically ventilated newborn lambs	136
7.3.2 HPV is blunted in newborn rats with O ₂ -induced CLI <i>in vivo</i> and <i>ex vivo</i>	136
7.3.3 Vascular tone in rat distal PAs	136
7.3.4 Kv mRNA expression is decreased in dPAs from newborn rats with CLI	136
7.3.5 Intratracheal adenovirus-mediated Kv 1.5 gene transfer restores HPV in O ₂ -induced CLI in newborn rats	137
7.3.6 I _k is restored by Kv1.5 gene transfer	137

7.4 Discussion 138

7.5 Online Data Supplement 139

7.6 References 152

CHAPTER 8 APPENDIX 2

ANTENATAL SILDENAFIL TREATMENT	158
ATTENUATES PULMONARY HYPERTENSION IN	
EXPERIMENTAL CONGENITAL DIAPHRAGMATIC HERNIA	
8.1 Introduction	159
8.2 Materials and Methods	160
8.2.1 Animal Model	160
8.2.2 Plasma Sildenafil concentration	160
8.2.3 Lung cGMP levels	161
8.2.4 Lung morphology	161
8.2.5 Western blot analysis	161
8.2.6 Barium-gelatin arteriograms and arterial density counts	161
8.2.7 Medial wall thickness	163
8.2.8 Right ventricular hypertrophy	163
8.2.9 Organ bath studies of newborn rat PAs	163
8.2.10 Retina studies	163
8.2.11 Brain studies	164
8.2.12 Statistical analysis	165
8.3 Results	166
8.3.1 Maternal administered sildenafil crosses the placenta and inhibits PDE5 activity in fetal rat lungs	166
8.3.2 Effects of antenatal sildenafil on body weight, incidence of CDH, and lung hypoplasia	166
8.3.3 Antenatal sildenafil improves lung architecture in CDH rats	167
8.3.4 Antenatal sildenafil increases pulmonary vessel density in CDH	167
8.3.5 Antenatal sildenafil attenuates features of pulmonary hypertension in CDH	167
8.3.6 Antenatal sildenafil enhances PA responsiveness to the NO donor, DEANO	168
8.3.7 Retina studies	168
8.3.8 Sildenafil does not affect brain maturation	168
8.4 Discussion	169
7.6 References	182

List of Figures

Figure 2.1. Histological evaluation in LPS induced ALI	40
Figure 2.2 BAL Cell count in LPS induced ALI	41
Figure 2.3 Levels of Proinflammatory Cytokines in Lung homogenates	42
Figure 2.4 MRL/MPJ AT2 and C57/BL6 AT2 Cells Wound Healing Rate	43
Figure 2.5 MRL/MPJ AT2 and C57/BL6 AT2 Cdm Wound Healing Rate	44
Figure 2.6 Serum-free Cdm was analyzed using an antibody array	45
Figure 2.7 MRL/MPJ AT2 Cdm improves LPS induced lung injury in C57/BL6 mice	46
Figure 3.1 Collagen deposition in MRL/MPJ and C57/BL6 mice	63
Figure 3.2. Altered lung mechanics 21 days after BLM exposure	64
Figure 3.3 MRL/MPJ and C57/BL6 mice exhibit decreased exercise capacity during the fibrotic phase of BLM exposure	65
Figure 3.4 TGF- β isoform protein expression in MRL/MPJ and C57/BL6 after BLM or saline administration	66
Figure 4.1. HUCBC population contained monocytes, endothelial progenitor cells and MSCs	88
Figure 4.2. HUCBC improve exercise capacity in BLM challenged animals	89
Figure 4.3 HUCBC treated animals exhibit improved lung mechanics 21 days after BLM exposure	90
Figure 4.4 Collagen deposition is decreased in HUCBC treated animals	91

Figure 4.5 HUCBC enraftment in BLM+HUCBC treated mice	92
Figure 4.6 Antifibrotic effects of HUCBC Cdm	93
Figure 5.1 ACE2 deletion worsens lung fibrosis in BLM-induced lung injury	113
Figure 5.2 Exercise capacity in BLM induced lung injury in WT and ACE2 ^{-y}	114
Figure 5.3 Changes in lung mechanics at 21 days in BLM induced fibrosis in WT and ACE2 ^{-y}	115
Figure 5.4 Gender differences in response to BLM-induced lung injury	116
Figure 5.5 Lung function in ACE2 knockout mice	117
Figure 5.6 Survival, lung function and exercise capacity in BLM-WT mice and BLM WT+rhACE2 treated mice	118
Figure 5.7 Histology and collagen deposition in BLM-WT mice and BLM WT+rhACE2 treated mice	119
Figure 5.8 Histology, collagen deposition, exercise capacity and lung function testing in BLM-WT female mice and BLM-female WT+rhACE2 treated mice	120
Figure 5.9 Representative immunoblots for lung AT1R and Actin expression in WT mice	121
Figure 7.1 Pulmonary vascular response to hypoxia	141
Figure 7.2 Hypoxic Pulmonary Vasoconstriction	142
Figure 7.3 Contractile responses from distal pulmonary arteries of newborn rats	143
Figure 7.4 Voltage gated K channels mRNA expression in pulmonary arteries of newborn rats	144
Figure 7.5 <i>In vivo</i> Echo-Doppler	145

Figure 7.6 Effective $K_v1.5$ gene transfer in distal pulmonary arteries	147
Figure 7.7 Representative patch-clamp recording and mean current density–voltage plots	148
Figure 8.1 Sildenafil crosses the placenta and increases fetal lung cGMP and alters protein expression in fetal rat lung	174
Figure 8.2 Effect of antenatal sildenafil on body weight, incidence of CDH, and LW/BW ratio	175
Figure 8.3 Effect of antenatal sildenafil on lung morphometry	176
Figure 8.4 Antenatal sildenafil improves lung capillary density and lung expression of eNOS and VEGF	178
Figure 8.5 Antenatal sildenafil treatment attenuates features of pulmonary hypertension in the nitrofen-induced rat model of CDH	179
Figure 8.6 Sildenafil has no adverse effects on the Retina	180
Figure 8.7 Sildenafil has no adverse effects on the neonatal brain at postnatal day 30	181

Abbreviations

⁰C: degrees Celsius

<: less than

>: more than

=: equal

±: plus or minus

g: g force

µg: micrograms

mg: milligrams

ACE: Angiotensin converting enzyme

ACE2: Angiotensin converting enzyme 2

ALI: Acute lung injury

ANGII: Angiotensin II

ARDS: Acute respiratory distress syndrome

AT: Alveolar epithelial type cells

AT1: Alveolar epithelial cells type 1

AT2: Alveolar epithelial cells type 2

BAL: Bronchoalveolar lavage

BLM: Bleomycin

BrdU: Bromodeoxyuridine

Cdm: Conditioned media

DMEM: Dulbecco's modified Eagle's medium

eNOS: endothelial nitric oxide synthase

EPCs: Endothelial progenitor cells

ESCs: Embryonic stem cells

HEPES: 4-(2-hydroxyethyl)-1-piperazineethanesulfonic acid

HGF: Hepatocyte growth factor

HBSS: Hank's balanced salt solution

iPSCs: Induced pluripotent stem cells

IFN-gamma: Interferon gamma

KGF: Keratinocyte growth factor

LPS: Lipopolysaccharide

MALDI MS: Matrix-assisted laser desorption/ionization mass spectrometry

MRL: Murphy-Roth-Large

MRL/MPJ: Murphy-Roth-Large

MSCs: Mesenchymal stem cells

PF: pulmonary fibrosis

SDS-PAGE: Sodium dodecyl sulfate polyacrylamide gel electrophoresis

TGF- β : Transforming growth factor β

TGF- β $_{1}$: Transforming growth factor β $_{1}$

TGF- β $_{2}$: Transforming growth factor β $_{2}$

TGF- β $_{3}$: Transforming growth factor β $_{3}$

HUVEC: Human umbilical vein endothelial cells

VEGF: Vascular endothelial growth factor

1. Introduction

1.1 Lung diseases: a major health care problem

Respiratory diseases impose a significant economic impact on the Canadian health care system. Almost 6.5% of total health care costs are related to respiratory diseases¹. Acute and chronic lung diseases such as Acute Lung Injury (ALI) and its more severe form, Acute Respiratory Distress Syndrome (ARDS), can lead to chronic pulmonary fibrosis (PF), and represent a major health care challenge because of **lack of efficient therapies**. A **common denominator** of these diseases is the **absence of effective injury resolution leading to delayed/distorted tissue repair**. Despite improvements in supportive treatment – mainly mechanical ventilation and ultimately lung transplant for PF– no specific treatments exist for these diseases^{1 2, 3}. Therapies specifically targeting enhanced wound healing, inflammation resolution and scarless repair may lead to improved survival and decreased morbidity. Understanding/promoting efficient lung repair remains a sensible strategy for treating these lung diseases.

1.2 Lung injury and resolution in ALI and PF

The most distal portion of the lung, the alveoli, is composed of two distinct types of alveolar epithelial cells (AT): cuboidal AT2, responsible for surfactant production and presumed distal lung progenitor cells and flat AT1 cells, incapable of differentiating, but important for gas exchange in the alveolar-capillary membrane⁴.

1.2.1 Normal Lung repair after acute Injury

After injury to the alveolar-capillary membrane, hemorrhage and activation of the coagulation pathway occurs⁵. These mediators activate inflammatory cells, endothelial cells, fibroblast/myofibroblast and epithelial cells.

¹ http://www.phac-aspc.gc.ca/publicat/2007/lbrdc_vsmrc/pdf/PHAC-Respiratory-WEB-eng.pdf

Minutes following the injury, neutrophils migrate to the area, producing reactive oxygen species. A second cellular influx of mononuclear leukocytes releases cytokines and vasoactive mediators. Then, a matrix consisting of a mixture of connective tissue, leukocytes, myofibroblast and endothelial cells stimulate angiogenesis forming the base for re-epithelization/endothelization. The normal repair process is complete when the alveolar-capillary membrane has established its usual parenchymal cell distribution (i.e., alveolar epithelial cells). When the injury is acute and the stimulus is removed rapidly, the alveolar-capillary membrane will return to normal integrity ⁶. In ALI/ARDS and PF, there is an absence of effective injury resolution leading to abnormal repair ⁷. Characteristics similar to those seen in lungs of patients with ARDS have been modeled in mice exposed to bleomycin (BLM) induced lung injury complicated by fibrosis ⁸.

1.2.2 Injury resolution ALI/ARDS and PF

The pathologic features of ALI are edema, inflammation and damage of to the alveolar epithelium ⁷. The process is characterized by distinct phases that can be divided in to the following: an acute exudative phase, characterized by endothelial/epithelial injury leading to alveolar edema and an extended inflammatory and oxidative response. A proliferative phase, with gradual development of intra-alveolar and interstitial fibrosis, which leads to a chronic fibrotic phase with collagen deposition (scarring). The structure and function of the alveolar epithelium are important determinants of lung injury. ARDS survivors often exhibit decreased pulmonary function, impaired health-related quality of life and PF ⁹⁻¹¹.

In PF, sub epithelial fibrotic foci are the characteristic feature, believed to result form recurrent inflammatory insults and abnormal parenchymal- epithelial cell injury and fibroblast proliferation ^{12, 13}. There is an uncontrolled connective tissue remodeling characterized by accumulation of extracellular matrix with the consequent formation of a scar and destruction of organ architecture. In PF, aberrant alveolar epithelial cells synthesize factors that sustain the fibrotic

reaction by an inadequate “cross-talk” between parenchymal (epithelial) and mesenchymal (extracellular matrix, fibroblast) cells¹⁴⁻¹⁶.

Structural analysis from lung tissue of PF patients has uncovered AT1 destruction along with endothelial cell loss and disruption of the basement membrane^{6, 17}. The process is accompanied by intra-alveolar proliferation and migration of fibroblast and further differentiation into myofibroblasts.

Alveolar epithelial cell injury induces the proliferation of fibroblasts and their differentiation into myofibroblasts.

Myofibroblasts are, for the most part, considered to be responsible for the collagen production occurring in PF¹⁸. Moreover, myofibroblasts secrete a variety of cytokines, including the profibrotic transforming growth factor- β (TGF- β)¹⁸. In addition, these cells may induce alveolar epithelial cell death, perpetuating the damage of the alveolar epithelium and inhibiting appropriate and efficient re-epithelialization¹⁹.

1.3 Importance of Alveolar epithelial cells in lung repair

The critical importance of alveolar epithelial injury in the development of ALI/PF is now well established and it is clear that alveolar regeneration is crucial for injury resolution²⁰. One of the hallmarks of ALI/ARDS is diffuse alveolar damage, with occupation of the alveolar spaces with a proteinaceous liquid, inflammatory cells, fibrin and epithelial cell damage. These features are recapitulated in lipopolysaccharide (LPS, an endotoxin from Gram -negative bacteria)-induced ALI/ARDS in mice. As part of the repair process, AT2 proliferate and provide a provisional new epithelial barrier after the injury. The provision of a new epithelium is associated with a gradual regression of intra-alveolar granulation tissue¹².

The importance of epithelial cell injury, apoptosis and failed epithelial reconstitution is also important in the pathogenesis of PF. Epithelial cells in PF secrete different molecules such as growth factors and surfactant proteins that regulate the inflammatory and fibrotic response within the lung. AT2 cells are reparative and proliferate fast following injury²¹.

In fibrotic foci - the proposed areas of active scarring - prominent defects in the alveolar epithelium including hyperplasia and membrane denudation are evident in PF patients²² and rodents exposed to BLM²³⁻²⁶. BLM, a glycopeptide antibiotic produced by the bacterium *Streptomyces verticillus*, produces extensive damage to AT2²⁷. In fibrosis, AT2 fail to repair the damaged epithelium as a result of ineffective proliferation/differentiation leading to interstitial scarring¹⁵. The poor reconstitution of the epithelium is believed to drive fibrosis by inducing the proliferation of fibroblasts and the deposition of collagen. Studies on the repopulation of denuded tracheal explants show that these are rapidly repopulated by fibroblasts if insufficient epithelial cells are introduced to the lumen to control fibroblast proliferation²⁸. *In vitro* there is evidence to demonstrate that fibroblast differentiation and collagen production is enhanced in epithelial cell/fibroblast co-cultures by injury to the epithelial cell component²⁹.

The importance of the alveolar epithelium in the pathogenesis of PF and ARDS is further implied by the observation that epithelial cell growth factors - including keratinocyte growth factor (KGF) and hepatocyte growth factor (HGF) - enhance AT2 cell proliferation, migration and protect against scarring in various animal models (reviewed in³⁰). On the contrary, TGF- β a powerful profibrotic cytokine is an important regulator in pulmonary fibrosis that can induce apoptosis directly in various cell types²³. Different animal models over expressing TGF- β showed extensive progressive fibrosis but limited inflammation, indicating that TGF- β may play a predominant role in the progression of pulmonary fibrosis³¹. Inhibition of TGF- β activity by anti-TGF- β antibodies, or modulators of TGF- β such as pirfenidone which slows down the progression of PF³².

In summary, AT2 are an important site of initial injury¹² as well as a major determinant of repair³³. Harnessing the healing power of AT2 may lead to the identification of new treatment strategies specifically targeting lung injury prevention and/or repair.

Current management of lung diseases characterized by alveolar damage lacks drugs specifically targeting lung repair. In this thesis, we take advantage of 2 recent developments to discover new therapeutic options for lung diseases: 1) The

discovery of MRL mice (Murphy-Roth-Large), a particular strain of mice with enhanced tissue healing capacity and 2) novel insight into stem cell biology, as there is increasing evidence that stem cell-based strategies hold promise for the prevention of lung injury.

1.4 A mammal model of scarless healing and its importance in lung repair

1.4.1 Tissue regeneration in MRL mice

MRL mice possess an increased wound healing capacity. This characteristic is ideal for exploring new lung repair mechanisms in order to identify new therapeutic targets to *prevent* lung injury and/or to *promote* “scarless” lung repair. The MRL/MPJ (for Murphy, Roths and Large) mice was generated from a series of crosses of strains C57BL/6J (0.3%), C3H/HeDi (12.1%), AKR/J (12.6%) and LG/J (75%) and then followed by inbreeding³⁴. The MRL/MPJ mouse was developed for its large size as a control strain for the MRL *Ipr/Ipr*, which has been found to display a major defect in immune regulation leading to a generalized autoimmune arthritis like syndrome³⁵. On the contrary, MRL/MPJ mice do not develop autoimmune features until much later in life (around 6 months of age)³⁶.

Damaged tissues in these animals are quickly replaced with normal tissue architecture that retains its full functionality. This repair process is reminiscent of fetal healing³⁷ and amphibian regeneration, involving the absence of scarring and complete replacement of damaged organs^{13, 38}. In contrast, most other strains of mice demonstrate none or limited tissue regeneration and undergo extensive fibrosis that leads to scar formation³⁹.

Mice of the MRL/MPJ strain have a unique capacity for both accelerated and regenerative wound healing, as shown by the complete closure of ear hole punches, scarless heart regeneration following cryoinjury and complete healing of alkali burned corneas^{40,41}. Currently, the mechanisms of tissue regeneration in the MRL/MPJ remain unclear. Their regenerative capacity in the lung had never been explored.

1.4.2 Increased healing in the MRL mice, an incidental finding

While ear notching for identification of mice, Dr. Heber-Katz's group noticed that MRL/MPJ ear holes often closed completely in a short period of time⁴². They found that this recurrent event was actually a model of regeneration in mammals⁴⁰. The healing seen in these MRL/MPJ mice displays a normal macro and micro anatomic tissue architecture^{13,37}.

The holes made to MRL/MPJ mice ears were found to close and disappear after 30 days compared to the "non-healer" C57/BL6 mice³⁸. During these 30 days, at different time points, structural analyses, gene mapping and protein expression profiles were performed in attempt to understand the mechanisms behind the enhanced healing³⁹.

1.4.3 Early re-epithelization

During classical healing which involves scar formation, re-epithelization does not occur before 3-8 days after injury⁴³. As early as day 2 after the ear hole was inflicted, complete re-epithelization was observed in MRL/MPJ mice compared to C57/BL6 mice³⁹. In MRL/MPJ mice, non-injured epithelial cells appear to be in a "vigilant state," ready to migrate and proliferate when an injury occurs. This is supported by the fact that MRL/MPJ early ear-notched biopsies display almost intact epithelium in histological sections and messenger ribonucleic acid (mRNA) up regulation of keratins (necessary for epithelial growth)^{44, 45}. As well, there appears to be an increased BrdU incorporation in MRL/MPJ epithelial cells observed during week 1 and 2 after the ear hole punch⁴⁶, suggesting more a "active" epithelium compared to non-healing C57/BL6 mice.

1.4.4 Changes in the Extracellular Membrane

Besides the epithelial changes, the extracellular membrane exhibits different characteristics between healer (MRL/MPJ) and non-healer mice (C57/BL6). MRL/MPJ mice display a higher proliferation rate, increased angiogenic sprout and a thin extracellular membrane. Comparably, amphibians do

not, or posses a very thin extracellular membrane, so epithelial to mesenchymal transitions are more likely to occur^{47, 48}. As the extracellular membrane is responsible for initiating the changes required for repair and organization (collagen deposition, extracellular matrix growth, angiogenesis), the above mentioned structural changes suggest that the extracellular membrane composition may differ (functionally and chemically) between both strains of mice⁴². In fact, microarray analysis has shown that procollagen type I and III (increased in repair leading to scar formation) exhibit a 2.4 fold down regulation in MRL/MPJ mice when compared to C57/BL6 mice⁴⁵.

In the ear hole closure model, MRL/MPJ mice showed higher matrix metalloproteinases (MMP) 9 and 2 activity compared to C57/BL6⁴⁶. This traduces in an accelerated breakdown of the extracellular matrix- basement membrane, the hallmark of regeneration⁴⁶. To further confirm the role of MMPs in the healing process, a non-specific inhibitor, minocycline, administered to the animals blocked the ear hole closure in these mice^{46, 49}. Taken together, these data suggest that inflammation and MMPs facilitate the regenerative process.

1.4.5 Gene mapping in the regenerating ear

Because healer (MRL/MPJ) and non-healer (C57/BL6) mice are inbreed strains, quantitative gene mapping techniques (mapping of genes to specific locations on chromosomes) can be used to identify and trace genetic loci associated with regeneration^{40, 44, 50}. Using microsatellite mapping techniques, McBrearty et al⁵⁰ found five significant quantitative trait loci (QTL) on four different chromosomes: 7, 8, 12, 13 and 15^{42, 50}. Interestingly, chromosome 15 encodes for a variety of genes involved in limb regeneration, including members of the *hedgehog* family of signaling molecules, and genes of the *Hoxc* complex.^{51, 52} In studying ear-hole closure, Blankenhorn et al⁵¹, found that in both the MRL/MPJ and C57/BL6 strains, male and female mice healed ear holes differently, showing was sexually dimorphic healing response. In conclusion, the healer mouse offers some interesting insights into the mechanisms of regeneration and the lack of it in higher vertebrates.

1.4.6 Proteome of the regenerating wounds in MRL/MPJ

The existence of an ear model that shows remarkable regenerative properties provides an opportunity to characterize proteins that promote regeneration and restoration of tissue architecture. Using tissue profiling MALDI MS - a technique that permits the measurement of protein expression patterns from a variety of biological sources, including tissue sections - Caldwell et al⁵³ examined the wound healing phenomenon to detect candidate proteins that may promote tissue regeneration over fibrosis and scarring in the MRL/MPJ mouse. Protein expression at the sites of wound repair was profiled at 4 and 7 days post injury. The analysis revealed distinct differences in the magnitude, temporal sequence and composition of protein expression patterns between the regenerative (MRL/MPJ) and non-regenerative (C57/BL6) strains. Several dozen proteins were expressed differently between the two mouse strains. Some of the proteins that exhibited differences among strains: the calcium-binding proteins, calcyclin (S100A6), calgranulin A (S100A8/MRP8), calgranulin B (S100A9/MRP14), calgizzarin (S100A11), calvasculin (S100A4), and calmodulin. These molecules regulate a variety of cell functions, including chemotaxis, signal transduction, inflammation and cellular stress⁵³.

1.4.7 The scarless heart in MRL/MPJ mice

Besides cartilage regeneration, other organs have been explored in the MRL/MPJ mice. The heart is an organ considered not to regenerate in mammals. Heber-Katz et al⁵⁴ assessed the capability of MRL/MPJ mice to heal after a trans-diaphragmatic cryoinjury (inflicted with liquid nitrogen) to the right ventricle, compared to the non-healer C57/BL6. Their endpoints included tissue architecture assessed through trichrome Masson's staining (to visualize collagen), histological sections and echocardiography, among others. By day 5 in both strains of mice, the cryo-injured area was full of fibrotic cells, which had replaced the cardiomyocytes. By day 60, the MRL/MPJ mice showed normal myocardium and little or no scarring whereas the C57/BL6 mouse showed a non-cellular scar that

replaced the myocardium. Echocardiography was assessed several days after injury and then monthly. MRL/MPJ mice showed an enlarged right ventricle that returned to its normal size over a period of three months. Histological examination of the hearts after 1 year showed a normal MRL/MPJ heart compared with a non-healed and scarred C57/BL6 heart⁴¹. It is important to note that the echocardiographic data is only presented for the MRL/MPJ mice and there is no mention to the control non-healer C57/BL6⁵⁴.

To further explore which type of cell was responsible for the enhanced healing two possibilities were considered: the differentiated cardiomyocytes entered into the cell cycle and gave rise to new cells or stem cells were responsible for such replacement. To begin addressing the above issues, the authors examined a cell-cycle-associated molecule Ki-67. They found that early in the injury response, specifically between days 7 and 15 after injury, cardiomyocytes in the MRL/MPJ expressed Ki-67⁴¹. To determine the total number of cells that were dividing over the 60-day period, BrdU (a nucleic acid analogue) incorporation was determined.

At 60 days, the authors found that large numbers of cardiomyocytes were BrdU positive in MRL/MPJ compared to C57/BL6, suggesting myocardial regeneration in the adult heart. This is remarkable, taking into account that the adult heart is capable of limited regeneration. To address if the bone marrow was contributing with circulating stem cells to the enhanced healing, syngeneic chimeras were created by injecting male bone marrow cells from healer MRL/MPJ mice into lethally X-irradiated healer MRL/MPJ female mice and by injecting non-healer C57/BL6 male bone marrow into lethally X-irradiated non-healer C57/BL6 female mice. At the same time, BrdU was administered to the animals. Chimerism was shown to be positive in both the gut and spleen in these mice. The authors found that the number of BrdU-positive cardiomyocytes was far greater than chromosome Y-positive cardiomyocytes in all of the groups^{38, 41}. This indicates that the regenerating cells were mostly resident cardiac cells. These results are very interesting and reveal a mechanism of regeneration in a known non-regenerative organ such as the heart.

However, the literature on heart regeneration in MRL mice is not unanimous. Oh et al ⁵⁵ tested the healing capacity in MRL/MPJ mice using a model of myocardial infarction caused by coronary ligation. The presence of myocardial infarction was examined *in vivo* by repeated magnetic resonance imaging, which allows for serial imaging of the myocardial structure and function. The major finding of this study is that MRL/MPJ mice do not recover from ischemic myocardial infarction with scarless recovery. Rather, large myocardial scars persisted for at least 2 months following the creation of infarction in the majority of mice studied. These results could be explained by the different injury models, which could suggest that the enhanced healing in the MRL/MPJ mice is dependant on the type of injury inflicted.

1.4.8 Different organs in the MRL/MPJ mice

Other organs that have been investigated in MRL/MPJ mice are corneas and cortical stab wound in the brain. Ueno et al ⁵⁶, investigated the healing of alkali-burned corneas in MRL/MPJ mice, which showed accelerated corneal wound healing compared with C57/BL6 control animals. The rapid corneal wound healing in MRL/MPJ mice was accompanied by lowered inflammatory responses and highly activated re-epithelialization. MRL/MPJ mice showed accelerated rates of re-epithelialization, which were evident on days 3 through 7. There was massive infiltration of inflammatory cells in the corneal stroma and anterior chamber in C57/BL6 mice beginning on day 1. Inflammation was most severe on day 2 for the cornea and day 4 for the anterior chamber. In contrast to C57/BL6 mice, MRL/MPJ mice had minimal inflammation throughout the observation period (30 days). The neutrophil is the predominant cell type in the acute phase of inflammation followed by a wave of monocyte infiltration. One finding the authors report is the decreased neutrophil infiltration in MRL/MPJ mice and the improved healing in C57/BL6 mice when neutrophil depleted. However, the healing was still delayed compared to MRL/MPJ mice. These suggest that other mechanisms besides inflammation aid in the enhanced healing. As well, experiments performed using bone marrow chimeras show that rather than

hematopoietic cells being responsible for the enhanced healing, the local microenvironment (corneas) possess the factors necessary for wound healing³⁸.

Besides ear, heart and cornea, experiments employing a cortical stab wound showed some similarities in MRL/MPJ healing in the brain. It was found that MRL/MPJ mice suffered a more severe injury response than the control mice with more cell death but also with more BrdU-positive cells. There was also an enhanced inflammatory response and more widespread blood–brain-barrier leakage. By day 14, however, both the healer and the non-healer mice injuries looked the same⁵⁷. This suggests that the healing potential of the MRL/MPJ mice depends to a great extent in the tissue specific microenvironment.

A second major development in our understanding of how the body heals itself has come from new insights into stem cell biology. Stem cell based therapies hold promise for organ repair. Over the past ten years, evidence has accumulated suggesting that stem cells may be beneficial in the prevention of a variety of lung diseases⁵⁸⁻⁶⁴.

1.5 Potential of Cell Therapy to Prevent/Repair the Damaged Lung

Tissue resident cells are often incapable of self-renewal and regeneration in diseases such as ARDS and PF. However, exogenous administration of various reparative cells has been described in the literature.

1.5.1. Stem cells with reparative potential

Mesenchymal Stem Cells

Mesenchymal Stem Cells (MSCs) are multipotent cells that can differentiate into a variety of cell types, including: osteoblasts, chondrocytes and adipocytes. In terms of surface antigens, MSCs do not express CD34, CD45, CD117 (cKit), HLA class I, and HLA-DR antigens, whereas they are positive for CD13, CD29, CD44, CD73, CD90, CD105, and CD166⁶⁵. These cells can be obtained from bone marrow or from other sources such as umbilical cord blood⁶⁰. In rodent models of LPS induced ARDS and BLM induced PF, MSCs

administration improved survival and lung inflammation⁶⁰⁻⁶⁴.

Decreasing/modulating inflammation seems to be one of the mechanisms by which MSCs exert their beneficial effect. These include suppression of T cell and B cell proliferation, modulation of natural killers and monocytes⁶⁶⁻⁷¹.

MSCs inhibit the division of stimulated T cells by preventing their entry into the S phase of the cell cycle⁷². *In vitro*, they inhibit interferon- γ and tumor necrosis factor- α and increase IL-10, impeding T- cell expansion⁷³⁻⁷⁵. In addition, MSCs inhibit T cell activation through increased nitric oxide production⁷⁰. T cell inhibition does not appear to be antigen specific, working across human leukocyte antigen⁷⁶. Similar to T cell changes, MSCs inhibit B cell proliferation. They also reduce the expression of chemokine receptors and immunoglobulin production by stimulated B cells⁶⁹.

MSCs act upon specific cell types such as natural cell killers and monocytes inhibiting proliferation and cytotoxicity. They appear to affect the differentiation/blocking the cell cycle at the G0 phase and prevent the differentiation into dendritic cells^{77,78}. One of the mechanisms implicated is increased prostaglandin E2 and IL-10 production⁶⁷⁻⁷⁰.

Embryonic stem cells

Embryonic Stem Cells (ESC,) are pluripotent stem cells derived from the early blastocyst and capable of self-renewal. There is one study demonstrating attenuated fibrosis, improved lung function and survival following administration of ESC-derived AT2, in a model of bleomycin-induced acute lung injury. Targeted differentiation of ESC into alveolar epithelial cells, constitutes an exciting approach in cell therapy. However, ethical controversy, concerns regarding teratoma formation and immunoincompatibility hinder its clinical application^{79, 80}.

Induced pluripotent stem cells

Another potential approach in cell therapy is to administer functionally

mature cells generated by differentiation of ESCs. Recent engineering of somatic cells by expression of transcription factors linked to pluripotency, gave rise to induced pluripotent stem cells (iPSCs), which are functional equivalents of ESCs. It would be interesting to know how effective can they be in treating lung and other illness⁸¹.

Endothelial progenitor cells

Endothelial Progenitor Cells (EPCs) are a population of circulating and resident vascular precursor cells⁸². There is clinical evidence of reduced circulating EPCs in patients with obstructive/restrictive lung diseases⁸³. Moreover, increased circulating EPCs correlate with improved outcomes in lung injury^{84, 85}. Depletion of these cells may be involved in altered endothelial homeostasis of pulmonary circulation. Experimental lung vascular diseases such as monocrotaline induced pulmonary hypertension have shown structural and functional improvement with EPC administration⁸⁶, the mechanisms in these studies include e-NOS and VEGF induced vasodilatation. Together, these suggest that EPC supplementation may be a valid strategy to treat lung diseases^{58, 85}.

1.5.2 The paracrine effect of Stem cells.

Most of the beneficial effects seen with MSCs administration are believed to be due to a paracrine effect more than engraftment (not more than 5% in the majority of the studies)^{59, 87, 88}. MSCs dampen inflammation by secreting anti-inflammatory cytokines such as IL-10, KGF, TNF α n and more recently angiotensin converting enzyme 2 (ACE2, in human umbilical cord mesenchymal stem cells, unpublished data). Identification of paracrine factors may yield new efficacious molecules to promote lung repair.

Interestingly, ACE2 has recently been shown to play a role in the pathogenesis of ARDS and PF. The renin angiotensin system (RAS) is partially responsible for maintaining blood pressure homeostasis, salt and fluid balance. Angiotensin II (ANGII) causes vasoconstriction and cell proliferation which can

ultimately lead to pulmonary fibrosis and pulmonary hypertension⁸⁹. Angiotensin converting enzyme (ACE) generates ANGII from angiotensin I, being the capillary vessels in the lungs one of the major sites of ACE and ANG II production in the body. It has been elucidated that RAS is also critical in ALI/ARDS. ACE2 - a homologue of ACE - acts as a negative regulator of the RAS system, and there is evidence that supports its protective role in animal models of ARDS⁹⁰. ACE2 knockout mice display features seen in ARDS (increased vascular permeability) and worsened lung function⁹¹.

ACE levels in serum, bronchoalveolar lavage and lungs in PF are increased. Angiotensin and Angiotensinogen induce apoptosis of alveolar epithelial cells *in vitro*⁹². In an animal model of radiation-induced pulmonary fibrosis, concentrations of ACE and ANGII were increased in lung tissue homogenates and suggested that the process of pulmonary fibrosis was promoted by a local RAS in the lung⁹³. Moreover, ACE2 has been shown to be protective and down regulated in human and rodent models of PF⁸⁹. There is increasing evidence that ACE2 plays an important role in diverse lung pathologies and constitutes thoughtful approach for the treatment of progressive lung diseases^{91, 92}.

94-101

1.6 Overall hypothesis and objectives

The main objective of this thesis is to explore new lung repair mechanisms as means to identify innovative therapeutic targets to *prevent/repair* lung injury. In chapters 2 and 3, we investigated the lung healing potential of MRL/MPJ mice using an acute and chronic rodent model of lung injury (LPS induced ALI and BLM induced fibrosis, respectively). For chapter 4 we tested the therapeutic

potential of human umbilical cord blood cells in a BLM model of post ALI-PF and identified some of the paracrine factors. In chapter 5 we assessed the protective role of ACE2 in a rodent model of PF following ALI.

My overall hypothesis is that novel healing molecules derived from a mammal model of regeneration and from stem cells, cell can be used to treat ALI and to prevent the resulting lung fibrosis.

1.7 References

1. Chavasse R. The american thoracic society, toronto, may 2000. *Paediatr Respir Rev.* 2000;1:301-302
2. Wiedemann HP, Wheeler AP, Bernard GR, Thompson BT, Hayden D, deBoisblanc B, Connors AF, Jr., Hite RD, Harabin AL. Comparison of two fluid-management strategies in acute lung injury. *N Engl J Med.* 2006;354:2564-2575
3. Copland IB, Martinez F, Kavanagh BP, Engelberts D, McKerlie C, Belik J, Post M. High tidal volume ventilation causes different inflammatory responses in newborn versus adult lung. *Am J Respir Crit Care Med.* 2004;169:739-748
4. Thebaud B. Update in pediatric lung disease 2010. *Am J Respir Crit Care Med.* 2011;183:1477-1481
5. Clark RA. Basics of cutaneous wound repair. *J Dermatol Surg Oncol.* 1993;19:693-706
6. Wallace WA, Fitch PM, Simpson AJ, Howie SE. Inflammation-associated remodelling and fibrosis in the lung - a process and an end point. *Int J Exp Pathol.* 2007;88:103-110
7. Ware LB, Matthay MA. The acute respiratory distress syndrome. *N Engl J Med.* 2000;342:1334-1349
8. Wang D, Morales JE, Calame DG, Alcorn JL, Wetsel RA. Transplantation of human embryonic stem cell-derived alveolar epithelial type ii cells abrogates acute lung injury in mice. *Mol Ther.* 2010;18:625-634
9. Orme J, Jr., Romney JS, Hopkins RO, Pope D, Chan KJ, Thomsen G, Crapo RO, Weaver LK. Pulmonary function and health-related quality of life in survivors of acute respiratory distress syndrome. *Am J Respir Crit Care Med.* 2003;167:690-694
10. Miwa C, Koyama S, Watanabe Y, Tsubochi H, Endo S, Nokubi M, Kawabata Y. Pathological findings and pulmonary dysfunction after acute respiratory distress syndrome for 5 years. *Intern Med.* 2010;49:1599-1604

11. Davidson TA, Caldwell ES, Curtis JR, Hudson LD, Steinberg KP. Reduced quality of life in survivors of acute respiratory distress syndrome compared with critically ill control patients. *JAMA*. 1999;281:354-360
12. Snyder LS, Hertz MI, Peterson MS, Harmon KR, Marinelli WA, Henke CA, Greenheck JR, Chen B, Bitterman PB. Acute lung injury. Pathogenesis of intraalveolar fibrosis. *J Clin Invest*. 1991;88:663-673
13. Harty M, Neff AW, King MW, Mescher AL. Regeneration or scarring: An immunologic perspective. *Dev Dyn*. 2003;226:268-279
14. Ramos C, Montano M, Garcia-Alvarez J, Ruiz V, Uhal BD, Selman M, Pardo A. Fibroblasts from idiopathic pulmonary fibrosis and normal lungs differ in growth rate, apoptosis, and tissue inhibitor of metalloproteinases expression. *Am J Respir Cell Mol Biol*. 2001;24:591-598
15. Selman M, King TE, Pardo A. Idiopathic pulmonary fibrosis: Prevailing and evolving hypotheses about its pathogenesis and implications for therapy. *Ann Intern Med*. 2001;134:136-151
16. Selman M, Pardo A. Idiopathic pulmonary fibrosis: An epithelial/fibroblastic cross-talk disorder. *Respir Res*. 2002;3:3
17. Strieter RM, Gomperts BN, Keane MP. The role of cxc chemokines in pulmonary fibrosis. *J Clin Invest*. 2007;117:549-556
18. Gauldie J. Pro: Inflammatory mechanisms are a minor component of the pathogenesis of idiopathic pulmonary fibrosis. *Am J Respir Crit Care Med*. 2002;165:1205-1206
19. Wallach-Dayana SB, Golan-Gerstl R, Breuer R. Evasion of myofibroblasts from immune surveillance: A mechanism for tissue fibrosis. *Proc Natl Acad Sci U S A*. 2007;104:20460-20465
20. Crosby LM, Waters CM. Epithelial repair mechanisms in the lung. *Am J Physiol Lung Cell Mol Physiol*. 2010;298:L715-731
21. Coalson JJ. The ultrastructure of human fibrosing alveolitis. *Virchows Arch A Pathol Anat Histol*. 1982;395:181-199
22. Kasper M, Haroske G. Alterations in the alveolar epithelium after injury leading to pulmonary fibrosis. *Histol Histopathol*. 1996;11:463-483

23. Hagimoto N, Kuwano K, Inoshima I, Yoshimi M, Nakamura N, Fujita M, Maeyama T, Hara N. Tgf-beta 1 as an enhancer of fas-mediated apoptosis of lung epithelial cells. *J Immunol.* 2002;168:6470-6478
24. Vincent R, Bjarnason SG, Adamson IY, Hedgecock C, Kumarathasan P, Guenette J, Potvin M, Goegan P, Bouthillier L. Acute pulmonary toxicity of urban particulate matter and ozone. *Am J Pathol.* 1997;151:1563-1570
25. Ekimoto H, Takahashi K, Matsuda A, Umezawa H. [experimentally induced bleomycin pulmonary toxicity--comparison of the systemic (intraperitoneal) and local (intratracheal) administration]. *Gan To Kagaku Ryoho.* 1983;10:2550-2557
26. Pozzi E, Zanon P. On the pathogenesis of bleomycin lung toxicity. *Int J Clin Pharmacol Biopharm.* 1978;16:575-578
27. Harrison JH, Jr., Hoyt DG, Lazo JS. Acute pulmonary toxicity of bleomycin: DNA scission and matrix protein mrna levels in bleomycin-sensitive and -resistant strains of mice. *Mol Pharmacol.* 1989;36:231-238
28. Terzaghi M, Nettesheim P, Williams ML. Repopulation of denuded tracheal grafts with normal, preneoplastic, and neoplastic epithelial cell populations. *Cancer Res.* 1978;38:4546-4553
29. Morishima Y, Nomura A, Uchida Y, Noguchi Y, Sakamoto T, Ishii Y, Goto Y, Masuyama K, Zhang MJ, Hirano K, Mochizuki M, Ohtsuka M, Sekizawa K. Triggering the induction of myofibroblast and fibrogenesis by airway epithelial shedding. *Am J Respir Cell Mol Biol.* 2001;24:1-11
30. Berthiaume Y, Lesur O, Dagenais A. Treatment of adult respiratory distress syndrome: Plea for rescue therapy of the alveolar epithelium. *Thorax.* 1999;54:150-160
31. Sime PJ, Xing Z, Graham FL, Csaky KG, Gauldie J. Adenovector-mediated gene transfer of active transforming growth factor-beta1 induces prolonged severe fibrosis in rat lung. *J Clin Invest.* 1997;100:768-776
32. Raghu G, Johnson WC, Lockhart D, Mageto Y. Treatment of idiopathic pulmonary fibrosis with a new antifibrotic agent, pirfenidone: Results of a

- prospective, open-label phase ii study. *Am J Respir Crit Care Med.* 1999;159:1061-1069
33. dos Santos CC, Han B, Andrade CF, Bai X, Uhlig S, Hubmayr R, Tsang M, Lodyga M, Keshavjee S, Slutsky AS, Liu M. DNA microarray analysis of gene expression in alveolar epithelial cells in response to tnfa, lps, and cyclic stretch. *Physiol Genomics.* 2004;19:331-342
 34. Murphy ED, Roths JB. A y chromosome associated factor in strain bxsB producing accelerated autoimmunity and lymphoproliferation. *Arthritis Rheum.* 1979;22:1188-1194
 35. Watanabe-Fukunaga R, Brannan CI, Copeland NG, Jenkins NA, Nagata S. Lymphoproliferation disorder in mice explained by defects in fas antigen that mediates apoptosis. *Nature.* 1992;356:314-317
 36. Adachi M, Watanabe-Fukunaga R, Nagata S. Aberrant transcription caused by the insertion of an early transposable element in an intron of the fas antigen gene of lpr mice. *Proc Natl Acad Sci U S A.* 1993;90:1756-1760
 37. Dang C, Ting K, Soo C, Longaker MT, Lorenz HP. Fetal wound healing current perspectives. *Clin Plast Surg.* 2003;30:13-23
 38. Bedelbaeva K, Gourevitch D, Clark L, Chen P, Leferovich JM, Heber-Katz E. The mrl mouse heart healing response shows donor dominance in allogeneic fetal liver chimeric mice. *Cloning Stem Cells.* 2004;6:352-363
 39. Clark LD, Clark RK, Heber-Katz E. A new murine model for mammalian wound repair and regeneration. *Clin Immunol Immunopathol.* 1998;88:35-45
 40. Clark L, Otvos L, Jr., Stein PL, Zhang XM, Skorupa AF, Lesh GE, McMorris FA, Heber-Katz E. Golli-induced paralysis: A study in anergy and disease. *J Immunol.* 1999;162:4300-4310
 41. Leferovich JM, Bedelbaeva K, Samulewicz S, Zhang XM, Zwas D, Lankford EB, Heber-Katz E. Heart regeneration in adult mrl mice. *Proc Natl Acad Sci U S A.* 2001;98:9830-9835

42. Heber-Katz E. The regenerating mouse ear. *Semin Cell Dev Biol.* 1999;10:415-419
43. Clark RA, Tonnesen MG, Gailit J, Cheresch DA. Transient functional expression of alphavbeta 3 on vascular cells during wound repair. *Am J Pathol.* 1996;148:1407-1421
44. Beare AH, Metcalfe AD, Ferguson MW. Location of injury influences the mechanisms of both regeneration and repair within the mrl/mpj mouse. *J Anat.* 2006;209:547-559
45. American thoracic society/european respiratory society international multidisciplinary consensus classification of the idiopathic interstitial pneumonias. This joint statement of the american thoracic society (ats), and the european respiratory society (ers) was adopted by the ats board of directors, june 2001 and by the ers executive committee, june 2001. *Am J Respir Crit Care Med.* 2002;165:277-304
46. Gourevitch DL, Clark L, Bedelbaeva K, Leferovich J, Heber-Katz E. Dynamic changes after murine digit amputation: The mrl mouse digit shows waves of tissue remodeling, growth, and apoptosis. *Wound Repair Regen.* 2009;17:447-455
47. Stocum DL, Thoms SD. Retinoic-acid-induced pattern completion in regenerating double anterior limbs of urodeles. *J Exp Zool.* 1984;232:207-215
48. Stocum DL. The urodele limb regeneration blastema: A self-organizing system. I. Differentiation in vitro. *Dev Biol.* 1968;18:441-456
49. Kench JA, Russell DM, Fadok VA, Young SK, Worthen GS, Jones-Carson J, Henson JE, Henson PM, Nemazee D. Aberrant wound healing and tgf-beta production in the autoimmune-prone mrl/+ mouse. *Clin Immunol.* 1999;92:300-310
50. McBrearty BA, Clark LD, Zhang XM, Blankenhorn EP, Heber-Katz E. Genetic analysis of a mammalian wound-healing trait. *Proc Natl Acad Sci U S A.* 1998;95:11792-11797

51. Blankenhorn EP, Troutman S, Clark LD, Zhang XM, Chen P, Heber-Katz E. Sexually dimorphic genes regulate healing and regeneration in mrl mice. *Mamm Genome*. 2003;14:250-260
52. Masinde GL, Li X, Gu W, Davidson H, Mohan S, Baylink DJ. Identification of wound healing/regeneration quantitative trait loci (qtl) at multiple time points that explain seventy percent of variance in (mrl/mpj and sjl/j) mice f2 population. *Genome Res*. 2001;11:2027-2033
53. Caldwell RL, Opalenik SR, Davidson JM, Caprioli RM, Nanney LB. Tissue profiling maldi mass spectrometry reveals prominent calcium-binding proteins in the proteome of regenerative mrl mouse wounds. *Wound Repair Regen*. 2008;16:442-449
54. Heber-Katz E, Leferovich J, Bedelbaeva K, Gourevitch D, Clark L. The scarless heart and the mrl mouse. *Philos Trans R Soc Lond B Biol Sci*. 2004;359:785-793
55. Oh YS, Thomson LE, Fishbein MC, Berman DS, Sharifi B, Chen PS. Scar formation after ischemic myocardial injury in mrl mice. *Cardiovasc Pathol*. 2004;13:203-206
56. Ueno M, Lyons BL, Burzenski LM, Gott B, Shaffer DJ, Roopenian DC, Shultz LD. Accelerated wound healing of alkali-burned corneas in mrl mice is associated with a reduced inflammatory signature. *Invest Ophthalmol Vis Sci*. 2005;46:4097-4106
57. Hampton DW, Seitz A, Chen P, Heber-Katz E, Fawcett JW. Altered cns response to injury in the mrl/mpj mouse. *Neuroscience*. 2004;127:821-832
58. Alphonse RS, Thebaud B. Growth factors, stem cells and bronchopulmonary dysplasia. *Neonatology*. 2011;99:326-337
59. Matthay MA, Thompson BT, Read EJ, McKenna DH, Jr., Liu KD, Calfee CS, Lee JW. Therapeutic potential of mesenchymal stem cells for severe acute lung injury. *Chest*. 2010;138:965-972
60. Lee JW, Gupta N, Serikov V, Matthay MA. Potential application of mesenchymal stem cells in acute lung injury. *Expert Opin Biol Ther*. 2009;9:1259-1270

61. Gupta N, Su X, Popov B, Lee JW, Serikov V, Matthay MA. Intrapulmonary delivery of bone marrow-derived mesenchymal stem cells improves survival and attenuates endotoxin-induced acute lung injury in mice. *J Immunol.* 2007;179:1855-1863
62. Mei SH, McCarter SD, Deng Y, Parker CH, Liles WC, Stewart DJ. Prevention of lps-induced acute lung injury in mice by mesenchymal stem cells overexpressing angiopoietin 1. *PLoS Med.* 2007;4:e269
63. Ortiz LA, Dutreil M, Fattman C, Pandey AC, Torres G, Go K, Phinney DG. Interleukin 1 receptor antagonist mediates the antiinflammatory and antifibrotic effect of mesenchymal stem cells during lung injury. *Proc Natl Acad Sci U S A.* 2007;104:11002-11007
64. Xu J, Woods CR, Mora AL, Joodi R, Brigham KL, Iyer S, Rojas M. Prevention of endotoxin-induced systemic response by bone marrow-derived mesenchymal stem cells in mice. *Am J Physiol Lung Cell Mol Physiol.* 2007;293:L131-141
65. Park HW, Shin JS, Kim CW. Proteome of mesenchymal stem cells. *Proteomics.* 2007;7:2881-2894
66. Yamada A, Hatano K, Koyama T, Matsuoka K, Esumi Y, Terunuma D. Syntheses of a series of lacto-n-neotetraose clusters using a carbosilane dendrimer scaffold. *Carbohydr Res.* 2006;341:467-473
67. Uccelli A, Moretta L, Pistoia V. Mesenchymal stem cells in health and disease. *Nat Rev Immunol.* 2008;8:726-736
68. Tolar J, Le Blanc K, Keating A, Blazar BR. Concise review: Hitting the right spot with mesenchymal stromal cells. *Stem Cells.* 2010;28:1446-1455
69. Corcione A, Benvenuto F, Ferretti E, Giunti D, Cappiello V, Cazzanti F, Risso M, Gualandi F, Mancardi GL, Pistoia V, Uccelli A. Human mesenchymal stem cells modulate b-cell functions. *Blood.* 2006;107:367-372
70. Ren G, Zhang L, Zhao X, Xu G, Zhang Y, Roberts AI, Zhao RC, Shi Y. Mesenchymal stem cell-mediated immunosuppression occurs via

- concerted action of chemokines and nitric oxide. *Cell Stem Cell*. 2008;2:141-150
71. English K, French A, Wood KJ. Mesenchymal stromal cells: Facilitators of successful transplantation? *Cell Stem Cell*. 2010;7:431-442
 72. Glennie S, Soeiro I, Dyson PJ, Lam EW, Dazzi F. Bone marrow mesenchymal stem cells induce division arrest anergy of activated t cells. *Blood*. 2005;105:2821-2827
 73. Bartholomew A, Sturgeon C, Siatskas M, Ferrer K, McIntosh K, Patil S, Hardy W, Devine S, Ucker D, Deans R, Moseley A, Hoffman R. Mesenchymal stem cells suppress lymphocyte proliferation in vitro and prolong skin graft survival in vivo. *Exp Hematol*. 2002;30:42-48
 74. Maitra B, Szekely E, Gjini K, Laughlin MJ, Dennis J, Haynesworth SE, Koc ON. Human mesenchymal stem cells support unrelated donor hematopoietic stem cells and suppress t-cell activation. *Bone Marrow Transplant*. 2004;33:597-604
 75. Maccario R, Podesta M, Moretta A, Cometa A, Comoli P, Montagna D, Daudt L, Ibatici A, Piaggio G, Pozzi S, Frassoni F, Locatelli F. Interaction of human mesenchymal stem cells with cells involved in alloantigen-specific immune response favors the differentiation of cd4+ t-cell subsets expressing a regulatory/suppressive phenotype. *Haematologica*. 2005;90:516-525
 76. Krampera M, Cosmi L, Angeli R, Pasini A, Liotta F, Andreini A, Santarlasci V, Mazzinghi B, Pizzolo G, Vinante F, Romagnani P, Maggi E, Romagnani S, Annunziato F. Role for interferon-gamma in the immunomodulatory activity of human bone marrow mesenchymal stem cells. *Stem Cells*. 2006;24:386-398
 77. Nauta AJ, Kruisselbrink AB, Lurvink E, Willemze R, Fibbe WE. Mesenchymal stem cells inhibit generation and function of both cd34+-derived and monocyte-derived dendritic cells. *J Immunol*. 2006;177:2080-2087

78. Ramasamy R, Lam EW, Soeiro I, Tisato V, Bonnet D, Dazzi F. Mesenchymal stem cells inhibit proliferation and apoptosis of tumor cells: Impact on in vivo tumor growth. *Leukemia*. 2007;21:304-310
79. Agostini C. Stem cell therapy for chronic lung diseases: Hope and reality. *Respir Med*. 2010;104 Suppl 1:S86-91
80. Daley GQ. Stem cells: Roadmap to the clinic. *J Clin Invest*. 2010;120:8-10
81. Li M, Chen M, Han W, Fu X. How far are induced pluripotent stem cells from the clinic? *Ageing Res Rev*. 2010;9:257-264
82. Borghesi A, Garofoli F, Cabano R, Tzialla C, Bollani L, Stronati M. Circulating endothelial progenitor cells and diseases of the preterm infant. *Minerva Pediatr*. 2010;62:21-23
83. Fadini GP, Schiavon M, Cantini M, Baesso I, Facco M, Miorin M, Tassinato M, de Kreutzenberg SV, Avogaro A, Agostini C. Circulating progenitor cells are reduced in patients with severe lung disease. *Stem Cells*. 2006;24:1806-1813
84. Burnham EL, Taylor WR, Quyyumi AA, Rojas M, Brigham KL, Moss M. Increased circulating endothelial progenitor cells are associated with survival in acute lung injury. *Am J Respir Crit Care Med*. 2005;172:854-860
85. Yamada M, Kubo H, Ishizawa K, Kobayashi S, Shinkawa M, Sasaki H. Increased circulating endothelial progenitor cells in patients with bacterial pneumonia: Evidence that bone marrow derived cells contribute to lung repair. *Thorax*. 2005;60:410-413
86. Zhao YD, Courtman DW, Deng Y, Kugathasan L, Zhang Q, Stewart DJ. Rescue of monocrotaline-induced pulmonary arterial hypertension using bone marrow-derived endothelial-like progenitor cells: Efficacy of combined cell and enos gene therapy in established disease. *Circ Res*. 2005;96:442-450
87. Ionescu LI, Alphonse RS, Arizmendi N, Morgan B, Abel M, Eaton F, Duszyk M, Vliagoftis H, Aprahamian TR, Walsh K, Thebaud B. Airway

- delivery of soluble factors from plastic-adherent bone marrow cells prevents murine asthma. *Am J Respir Cell Mol Biol.* 2011
88. Danchuk S, Ylostalo JH, Hossain F, Sorge R, Ramsey A, Bonvillain RW, Lasky JA, Bunnell BA, Welsh DA, Prockop DJ, Sullivan DE. Human multipotent stromal cells attenuate lipopolysaccharide-induced acute lung injury in mice via secretion of tumor necrosis factor- α -induced protein 6. *Stem Cell Res Ther.* 2011;2:27
89. Li X, Molina-Molina M, Abdul-Hafez A, Uhal V, Xaubet A, Uhal BD. Angiotensin converting enzyme-2 is protective but downregulated in human and experimental lung fibrosis. *Am J Physiol Lung Cell Mol Physiol.* 2008;295:L178-185
90. Kuba K, Imai Y, Rao S, Gao H, Guo F, Guan B, Huan Y, Yang P, Zhang Y, Deng W, Bao L, Zhang B, Liu G, Wang Z, Chappell M, Liu Y, Zheng D, Leibbrandt A, Wada T, Slutsky AS, Liu D, Qin C, Jiang C, Penninger JM. A crucial role of angiotensin converting enzyme 2 (ace2) in sars coronavirus-induced lung injury. *Nat Med.* 2005;11:875-879
91. Imai Y, Kuba K, Rao S, Huan Y, Guo F, Guan B, Yang P, Sarao R, Wada T, Leong-Poi H, Crackower MA, Fukamizu A, Hui CC, Hein L, Uhlig S, Slutsky AS, Jiang C, Penninger JM. Angiotensin-converting enzyme 2 protects from severe acute lung failure. *Nature.* 2005;436:112-116
92. Wang R, Zagariya A, Ibarra-Sunga O, Gidea C, Ang E, Deshmukh S, Chaudhary G, Baraboutis J, Filippatos G, Uhal BD. Angiotensin ii induces apoptosis in human and rat alveolar epithelial cells. *Am J Physiol.* 1999;276:L885-889
93. Song L, Wang D, Cui X, Shi Z, Yang H. Kinetic alterations of angiotensin-ii and nitric oxide in radiation pulmonary fibrosis. *J Environ Pathol Toxicol Oncol.* 1998;17:141-150
94. Marshall RP, Gohlke P, Chambers RC, Howell DC, Bottoms SE, Unger T, McAnulty RJ, Laurent GJ. Angiotensin ii and the fibroproliferative response to acute lung injury. *Am J Physiol Lung Cell Mol Physiol.* 2004;286:L156-164

95. Marshall RP, McAnulty RJ, Laurent GJ. Angiotensin ii is mitogenic for human lung fibroblasts via activation of the type 1 receptor. *Am J Respir Crit Care Med.* 2000;161:1999-2004
96. Reis FM, Bouissou DR, Pereira VM, Camargos AF, dos Reis AM, Santos RA. Angiotensin-(1-7), its receptor mas, and the angiotensin-converting enzyme type 2 are expressed in the human ovary. *Fertil Steril.* 2011;95:176-181
97. Ferreira AJ, Shenoy V, Qi Y, Fraga-Silva RA, Santos RA, Katovich MJ, Raizada MK. Angiotensin-converting enzyme 2 activation protects against hypertension-induced cardiac fibrosis involving extracellular signal-regulated kinases. *Exp Physiol.* 2010
98. Li W, Moore MJ, Vasilieva N, Sui J, Wong SK, Berne MA, Somasundaran M, Sullivan JL, Luzuriaga K, Greenough TC, Choe H, Farzan M. Angiotensin-converting enzyme 2 is a functional receptor for the sars coronavirus. *Nature.* 2003;426:450-454
99. Zhong J, Basu R, Guo D, Chow FL, Byrns S, Schuster M, Loibner H, Wang XH, Penninger JM, Kassiri Z, Oudit GY. Angiotensin-converting enzyme 2 suppresses pathological hypertrophy, myocardial fibrosis, and cardiac dysfunction. *Circulation.* 2010;122:717-728, 718 p following 728
100. Shenoy V, Ferreira AJ, Qi Y, Fraga-Silva RA, Diez-Freire C, Dooies A, Jun JY, Sriramula S, Mariappan N, Pourang D, Venugopal CS, Francis J, Reudelhuber T, Santos RA, Patel JM, Raizada MK, Katovich MJ. The angiotensin-converting enzyme 2/angiogenesis-(1-7)/mas axis confers cardiopulmonary protection against lung fibrosis and pulmonary hypertension. *Am J Respir Crit Care Med.* 2010;182:1065-1072
101. Wysocki J, Ye M, Rodriguez E, Gonzalez-Pacheco FR, Barrios C, Evora K, Schuster M, Loibner H, Brosnihan KB, Ferrario CM, Penninger JM, Battle D. Targeting the degradation of angiotensin ii with recombinant angiotensin-converting enzyme 2: Prevention of angiotensin ii-dependent hypertension. *Hypertension.* 2010;55:90-98

CHAPTER 2

MRL/MPJ MICE ARE PROTECTED AGAINST LPS-INDUCED ACUTE RESPIRATORY DISTRESS

2.1 Introduction

Acute Respiratory Distress Syndrome (ARDS) is a severe subtype of Acute Lung Injury (ALI), characterized by hypoxemia, acute inflammatory response and neutrophilic alveolitis, with an annual mortality rate of 30 to 50%^{1,2}. Sepsis and pneumonia are leading causes of ARDS¹. The lung epithelium plays a central role in the pathogenesis and resolution of ARDS regulating fluid balance at the air-liquid interface and constituting a line of defense against infection³. Exposed to the external environment, it is a target for injury and infection. In mice, intratracheal lipopolysaccharide (LPS) instillation activates alveolar macrophages and neutrophils, causing diffuse alveolar damage that resembles ARDS in humans^{4,5}. Despite advances in patient care ARDS remains an important contributor to prolonged mechanical ventilation in intensive care units¹.

Mice of the MRL/MPJ strain have a unique capacity for both accelerated and regenerative wound healing, as suggested by the complete closure of ear hole punches, scarless heart regeneration following cryoinjury and complete healing of alkali burned corneas⁶⁻⁸. Damaged tissues in these animals are quickly replaced with normal tissue architecture that retains its full functionality. This repair process is reminiscent of fetal healing^{9, 10} and amphibian regeneration involving the formation of scarless healing and complete replacement of damaged organs as opposed to scarring^{11, 12-16}. In contrast, most other strains of mice demonstrate none or limited tissue regeneration¹⁷. The healing potential in the lung of the strain of MRL/MPJ mice remains unknown. This led us to hypothesize that MRL/MPJ mice are protected against LPS-induced ALI.

2.2 Materials and Methods

2.2.1 Animals

All procedures involving animals were approved by the Animal Welfare Committee of the University of Alberta. Eight to 12 week old MRL/MPJ and

C57/BL6 mice were obtained from Jackson (Bar Harbor, ME) and used in all the experiments described ahead.

2.2.2 Alveolar epithelial type 2 cells (AT2) Isolation and Primary Cell Culture

Primary AT2 cells were prepared using a modified protocol from a previously published method¹⁸. MRL/MPJ and C57BL6 mice were euthanized with an overdose of Sodium Pentobarbital (65mg/kg). The trachea was exposed and cannulated and lungs were perfused with 10 ml of heparinized sterile Phosphate Buffered Saline (PBS) through the pulmonary artery. 2 ml dispase (BD Biosciences, USA) was instilled into the lungs, followed by instillation of 500 μ l 1% low-melt agarose. Instilled lungs were immediately covered with ice and incubated for 2 min to gel the agarose. Lungs were removed, placed in a culture vessel containing an additional 1 ml of dispase and incubated for 45 min at room temperature. The lungs were then transferred to a culture dish and 7 ml serum free DMEM + 25 mM HEPES (GIBCO, USA) containing 100U/ml DNase I (Sigma Aldrich, St Louis, MO, USA) was added. The tissue was separated from the airways and lungs carefully dissociated. Cell suspensions were sequentially filtered through nylon gauze (100 μ m, 45 μ m, 30 μ m) followed by centrifugation (12 min, 130 \times g) to pellet the cells. To further purify AT2 cells, the cells were incubated with biotinylated anti-CD-32 (0.65 μ g/million cells) and biotinylated anti-CD-45 (1.5 μ g/million cells) for 30 min at 37°C (Pharmigen, San Diego, CA, USA). Meanwhile, streptavidin-coated magnetic particles were washed in PBS (Sigma-Aldrich, St. Louis, MO, USA). After incubation, the cells were centrifuged (130 \times g for 8 min at 4°C), resuspended in 7 ml DMEM, added to the magnetic particles and incubated with gentle rocking for 30 min at room temperature. At the end of the incubation, the tube was attached to the magnetic tube separator. The cells suspension was centrifuged and resuspended in culture media¹⁸. Isolated cells were plated at a known density and cultured for 48 h in 12 well culture plates until confluence was reached. AT2 cells were then used for *in vitro* scratch assays to assess wound healing potential or to collect serum free

conditioned media. Cells were cultured in Dulbecco modified Eagle medium (DMEM, Sigma-Aldrich, St. Louis, MO, USA) with 4.5 g/L glucose, with 10% fetal bovine serum (Sigma-Aldrich, St. Louis, MO, USA), 100 U/ml penicillin, 100 µg/ml streptomycin, and 250 ng/ml amphotericin B (antibiotic antimycotic solution, Sigma-Aldrich, St. Louis, MO, USA), at 37°C, 95% humidity and 5% CO₂.

2.2.3 *In vitro* Scratch Assays

Scratch assays to assess wound closure were performed as previously described^{19,20}. AT2 cells from both strains of mice were grown in 12-well plates until confluence, and serum deprived for 24 h in DMEM. In each well, a scratch was made using a sterile tip, and cellular debris was removed by washing with DMEM. The width of the scratch was determined microscopically immediately after creation and 2, 6, 12 and 24 h later. In the first set of experiments, serum starved AT2 cells from MRL/MPJ and C57/BL6 were compared. In the second set of experiments, the effects of the following conditions on wound closure were analyzed: MRL/MPJ AT2 cells/ MRL/MPJ Conditioned Media (Cdm); MRL/MPJ AT2 cells/ C57/BL6 Cdm; C57/BL6 AT2 cells/ C57/BL6 Cdm. All the comparisons were performed at 2, 6, 12 and 24 h. All images were acquired using an inverted light microscope (Leica Microsystems, Canada). Relative closure was calculated as $(X_0 - X_{yh})$, where X_0 = width of the scratch at time 0, X_{yh} = width of the scratch after 2, 6, and 12 h at baseline or after exposure to Cdm. Percentage closure was calculated as follows: $[(X_0 - X_{yh}) / X_0] 100$.

2.2.4 Analysis of AT2 cells secretome (Cdm) and Cytokine arrays

We analyzed Cdm from both: MRL/MPJ AT2 cells and C57/BL6 using The RayBio® Mouse Cytokine Antibody Array G series 1000 (protein array system), which detects 96 mouse cytokines using microspheres labeled with fluorophoresin.

Lungs were minced, and lysed with RIPA buffer (1x PBS, 1% Nonidet P-40, 0.5% sodium deoxyolate, 0.1% SDS, and protease inhibitor) for cell and tissue lysis, and protein was quantified by Bradford method. The cytokine arrays were performed by Ray Biotech according to their protocols for the RayBio Quantibody Mouse Inflammation Array 1 (RayBiotech, Norcross, GA). Relative intensities of obtained spots were measured by densitometry and corrected by background subtraction. Results of duplicate readings were averaged.

2.2.5 LPS Model

Eight to 12 week old MRL/MPJ and C57/BL6 mice were obtained from Jackson (Bar Harbor, ME) and randomized into 4 groups: (1) C57BL6 control group (saline), (2) MRL/MPJ control group (saline), (3) C57/BL6 LPS, (4) MRL/MPJ LPS, the animals were anesthetized using a mixture of oxygen and Isoflurane® 2.5%. Then, mice were weighted and LPS (Sigma Aldrich, St. Louis, MO) administered intratracheally at a dose of 4 mg/Kg in 50 μ l²¹. Control animals were injected intratracheally with 50 μ l of sterile saline 0.9%. Mice were monitored every day and harvested after 72 h. The lungs were either inflated and fixed in 10% Formaldehyde, snap frozen in liquid nitrogen (cytokine measurements) or used for BAL.

2.2.6 Histology and Lung Injury Score

Lungs were inflation fixed, embedded in paraffin, sectioned and stained with hematoxilin & eosin as described²². For histological evaluation of the lungs, 4 midlung sections per lung were examined, using a lung injury score, previously described²³. Each slide was evaluated by two separate investigators (GJRP and CL; GJRP and AV) in a blinded manner. A total of 10 sections/ lung counted on each slide at 400x magnification. Within each field, points were assigned according to predetermined criteria. All of the points for each category were added and weighted according to their relative importance. The injury score was calculated according to the following formula: injury score = [(alveolar hemorrhage points/no. of fields) + 2 x (alveolar infiltrate points/no. of fields) + 3 x

(fibrin points/no. of fields) + (alveolar septal congestion/no. of fields)]/total number of alveoli counted²³.

2.2.7 Bronchoalveolar lavage (BAL) Protocol

BAL was performed by instilling intratracheally 0.9% NaCl (1 ml). The fluid was recovered by gentle suction and placed on ice for immediate processing. An aliquot of the BAL fluid was processed immediately for cytokine quantification, total and differential cell counts. Total cell counts were performed with a hemocytometer, whereas differential cell counts were performed on cytospin preparations stained with modified Wright-Giemsa stain (Diff-Quik; American Scientific Products, McGaw Park, IL)²³.

2.2.8 Cytokine Quantification for BAL

Cytokine concentrations in BAL from LPS challenged C57/BL6 + CdM and LPS C57/BL6 +DMEM were determined using commercially available ELISA kits for detection of IL1 β , KC and RANTES (eBioscience, San Diego, CA) and APN (Millipore).

2.2.9 Statistical Analysis

Data are expressed as means \pm Standard Error Mean (SEM). Statistical analysis was performed using ANOVA and post hoc tests (Least Significant Difference), as appropriate. Values were considered significant with $P < 0.05$.

2.3 Results

2.3.1 MRL/MPJ LPS Challenged Mice Exhibit Improved Lung Architecture and decreased neutrophil cell count in BAL

To further assess the healing capacity and immunomodulatory activity in MRL/MPJ mice lungs, we administered LPS or saline intratracheally to adult MRL/MPJ and C57/BL6 mice and compared their lung architecture using a

quantitative lung injury score (assessed by two independent observers) on hematoxylin & eosin stained lung sections²³. MRL/MPJ LPS challenged lungs show decreased severity of lung injury compared to C57/BL6 mice (1.788 ± 0.206 vs. 2.642 ± 0.107 , $p < 0.05$). Figure 2.1 A-B.

LPS administration significantly increased total and neutrophil cell count assessed through BAL (Figure 2.2 A-B). However, MRL/MPJ LPS challenged lungs exhibit significantly decreased total ($3.3 \times 10^5 \pm 1.38 \times 10^5$ vs. $47.7 \times 10^5 \pm 23.0 \times 10^5$ cells, $p < 0.05$) neutrophil cell count in BAL compared to C57/BL6 lungs ($36.9 \times 10^5 \pm 16.8 \times 10^5$ vs. $1.3 \times 10^5 \pm 0.89 \times 10^5$ cells, $p < 0.05$).

2.3.2 Decreased Proinflammatory Cytokines in MRL/MPJ LPS Challenged Mice

To further evaluate the inflammatory response in MRL/MPJ LPS challenged mice, levels of proinflammatory cytokines and chemokines were measured in lung homogenates from control and LPS challenged lungs in both strains of mice. Proinflammatory cytokines (KC, RANTES, Fas-L and IL1 β) were significantly increased in C57/BL6 LPS challenged lungs as compared to C57/BL6 controls and MRL/MPJ controls. Conversely, the pro-inflammatory cytokine levels were decreased in MRL/MPJ LPS lungs compared to C57/BL6 LPS mice (Figure 2.3).

2.3.3 MRL/MPJ Alveolar Type 2 (AT2) Cells Exhibit Accelerated Wound Healing Rate Compared to C57/BL6

AT2 cells were isolated from both MRL/MPJ and C57/BL6 mice ($n=3$ animals, respectively). AT2 cells ($n=5$ wells) were grown for 48 h until confluent and the rate of wound closure, at different time points (2, 6, and 12 h), measured after a scratch was made. MRL/MPJ AT2 cells healed significantly faster at 6 h (62.5 ± 7.9 vs. 31.0 ± 3.7 percentage closure, $p < 0.05$) 12 h (92.5 ± 2.0 vs. 65.0 ± 1.7 percentage closure, $p < 0.05$) compared to C57/BL6 (Figure 2.4 A-B).

2.3.4 MRL/MPJ AT2 Cdm Contains Soluble Factors That Accelerate Wound Healing Rate In C57/BL6 AT2 Cells

To address if MRL/MPJ AT2 cells secreted soluble factors that contributed to their enhanced healing ability, Cdm was obtained from both MRL/MPJ and C57/BL6 AT2 cells and the wound closure rate after a scratch compared as follows (Figure 2.5): MRL/MPJ AT2 cells/ MRL/MPJ Cdm; MRL/MPJ AT2 cells/ C57/BL6 Cdm; C57/BL6 AT2 cells/ C57/BL6 Cdm. All the comparisons were performed at 12h. MRL/MPJ AT2 cells retained their increased healing ability regardless of the Cdm used (Figure 2.5). MRL/MPJ Cdm accelerated the healing potential of C57/BL6 AT2 cells compared to C57/BL6 Cdm (86.6 ± 7.3 vs. 43.8 ± 8.5 , $p<0.05$).

2.3.5 MRL/MPJ Cdm is Composed of Chemokines that Modulate Increased Wound Healing Rate

To understand the molecular mediators of the observed effects of MRL/MPJ Cdm, we examined Cdm from both MRL/MPJ and C57/BL6 AT2 cells using a Multiplex antibody array (Figure 2.6 A), which included a broad spectrum of molecules analyzed (Figure 2.6B). Cluster analysis revealed Cdm composition, 31% chemokines, 27% binding proteins, 21% cytokines, 14% growth factors, 4% cytokine antagonists, 3% extracellular matrix proteins. Among all the factors analyzed in AT2 Cdm, MRL/MPJ exhibit decreased levels of proinflammatory cytokines (Fas-L, IL-1 β , M-CSF, MCP-5, RANTES, TNF α , INF-gamma, GM-CSF and G-CSF).

2.3.6 MRL/MPJ AT2 Cdm Attenuates Inflammation in C57/BL6 LPS Challenged Lungs *in vivo*

MRL/MPJ AT2 Cdm was administered daily, intranasally to LPS challenged C57/BL6 mice in order to assess the *in vivo* anti-inflammatory effect of MRL/MPJ AT2 Cdm. H&E lung sections exhibit decreased cellularity in MRL/MPJ AT2 Cdm treated mice compared to DMEM treated mice and improved lung injury score (1.965 ± 0.509 vs. 2.84 ± 0.685 , $p<0.05$, Figure 2.7A-B).

BAL cytokine quantification revealed significantly decreased pro-inflammatory IL1 β and KC levels in MRL/MPJ AT2 Cdm treated mice compared to DMEM treated mice, RANTES levels exhibited no differences between groups (Figure 2.7 C).

2.4. Discussion

The MRL/MPJ mice constitute a very interesting inbred strain that possesses enhanced healing properties, reminiscent of fetal healing and amphibian regeneration^{6-8, 13-16}. We used the well-characterized model of LPS-induced ALI to evaluate the lung healing capacity in MRL/MPJ compared to C57/BL6 mice²¹. *In vivo*, MRL/MPJ LPS challenged mice exhibit attenuated lung injury with decreased BAL inflammatory influx and pro-inflammatory cytokines as compared to C57/BL6 LPS mice. This enhanced healing capacity is due, at least in part, to an accelerated wound healing rate in AT2 cells MRL/MPJ mice. Moreover, MRL/MPJ AT2 cells secrete soluble factors that enhance wound closure in C57/BL6 AT2 Cells.

To the best of our knowledge, this is the first time that MRL/MPJ mice enhanced healing capacity in an acute model of lung injury is assessed from a lung perspective in the AT2 cells. During the early phase of ARDS, the lung is the site of an intense inflammatory process with sequential activation of cytokines, chemokines, and secretion of proteases²⁴. The inflammation is mostly limited to the lung, with low levels of inflammatory mediators in the systemic circulation²⁴²⁵. LPS induced ALI alters AT2 surfactant secretion and stimulates inflammatory cells (i.e alveolar macrophages and neutrophils) which as well suppress surfactant by AT2 cells²⁶.

The neutrophil is the predominant cell type in the acute phase of inflammation (including LPS induced ALI) followed by a wave of monocyte infiltration. One interesting finding by Ueno et al²⁷, is decreased neutrophil infiltration in MRL/MPJ mice and improved healing in C57/BL6 mice when neutrophil depleted. This is consistent with our *in vivo* results, where decreased

lung cellularity and pro-inflammatory cytokines are evident in wild type LPS challenged mice treated with MRL/MPJ AT2 Cdm (Figure 2.7). However, despite the neutrophil depletion in C57/BL6 mice ²⁷, the healing was still delayed compared to MRL/MPJ mice. These suggest that other mechanisms besides inflammation contribute to enhanced healing. Recently, mesenchymal stem cells isolated from MRL/MPJ mice demonstrated enhanced regenerative capacity compared to those from C57/BL6 mice, through a Wnt modulator sFRP2 pathway ²⁸. More interestingly, experiments performed using bone marrow chimeras show that rather than hematopoietic cells being responsible for the enhanced healing, MRL/MPJ mice have accelerated corneal wound healing compared with C57/BL6 control animals ²⁷ and the local microenvironment (corneas) possess the factors necessary for wound healing. The rapid corneal wound healing in MRL mice was accompanied by lowered inflammatory responses and highly activated reepithelialization. MRL/MPJ mice showed accelerated rates of reepithelialization had minimal inflammation throughout the observation period (30 days). This is consistent with our findings in the lung suggesting that a highly specialized lung cell, AT2, possess an increased wound healing rate in MRL/MPJ compared to non healer mice AT2 cells. Moreover, administration of AT2 Cdm from MRL mice was able to attenuate lung inflammation in LPS-induced ALI in C57/BL6 mice.

Among all the factors analyzed in AT2 Cdm, MRL/MPJ exhibit decreased levels of proinflammatory cytokines (Fas-L, IL-1 β , M-CSF, MCP-5, RANTES, TNF α , INF-gamma, GM-CSF and G-CSF), which have been found to be increased in murine models of LPS-induced ALI ⁵. Further identification of AT2 Cdm may yield new therapeutic targets for ALI/ARDS.

In conclusion, the MRL/MPJ mice constitute an interesting inbred strain that possesses enhanced healing properties, reminiscent of fetal healing and amphibian regeneration. Understanding the mechanisms by which MRL/MPJ mice exert improved healing, may lead to the identification of new therapeutic targets promoting scarless healing.

2.5 References

1. Ware LB, Matthay MA. The acute respiratory distress syndrome. *N Engl J Med.* 2000;342:1334-1349
2. Mendez JL, Hubmayr RD. New insights into the pathology of acute respiratory failure. *Curr Opin Crit Care.* 2005;11:29-36
3. Gropper MA, Wiener-Kronish J. The epithelium in acute lung injury/acute respiratory distress syndrome. *Curr Opin Crit Care.* 2008;14:11-15
4. Mei SH, McCarter SD, Deng Y, Parker CH, Liles WC, Stewart DJ. Prevention of lps-induced acute lung injury in mice by mesenchymal stem cells overexpressing angiopoietin 1. *PLoS Med.* 2007;4:e269
5. Rojas M, Woods CR, Mora AL, Xu J, Brigham KL. Endotoxin-induced lung injury in mice: Structural, functional, and biochemical responses. *Am J Physiol Lung Cell Mol Physiol.* 2005;288:L333-341
6. Heber-Katz E, Leferovich J, Bedelbaeva K, Gourevitch D, Clark L. The scarless heart and the mrl mouse. *Philos Trans R Soc Lond B Biol Sci.* 2004;359:785-793
7. Heber-Katz E. The regenerating mouse ear. *Semin Cell Dev Biol.* 1999;10:415-419
8. Leferovich JM, Bedelbaeva K, Samulewicz S, Zhang XM, Zwas D, Lankford EB, Heber-Katz E. Heart regeneration in adult mrl mice. *Proc Natl Acad Sci U S A.* 2001;98:9830-9835
9. Dang CM, Beanes SR, Lee H, Zhang X, Soo C, Ting K. Scarless fetal wounds are associated with an increased matrix metalloproteinase-to-tissue-derived inhibitor of metalloproteinase ratio. *Plast Reconstr Surg.* 2003;111:2273-2285
10. Dang C, Ting K, Soo C, Longaker MT, Lorenz HP. Fetal wound healing current perspectives. *Clin Plast Surg.* 2003;30:13-23
11. Bedelbaeva K, Gourevitch D, Clark L, Chen P, Leferovich JM, Heber-Katz E. The mrl mouse heart healing response shows donor dominance in allogeneic fetal liver chimeric mice. *Cloning Stem Cells.* 2004;6:352-363

12. Harty M, Neff AW, King MW, Mescher AL. Regeneration or scarring: An immunologic perspective. *Dev Dyn.* 2003;226:268-279
13. Brockes JP, Kumar A. Plasticity and reprogramming of differentiated cells in amphibian regeneration. *Nat Rev Mol Cell Biol.* 2002;3:566-574
14. Brockes JP, Kumar A, Velloso CP. Regeneration as an evolutionary variable. *J Anat.* 2001;199:3-11
15. Stocum DL. The urodele limb regeneration blastema: A self-organizing system. I. Differentiation in vitro. *Dev Biol.* 1968;18:441-456
16. Stocum DL, Thoms SD. Retinoic-acid-induced pattern completion in regenerating double anterior limbs of urodeles. *J Exp Zool.* 1984;232:207-215
17. Clark LD, Clark RK, Heber-Katz E. A new murine model for mammalian wound repair and regeneration. *Clin Immunol Immunopathol.* 1998;88:35-45
18. Corti M, Brody AR, Harrison JH. Isolation and primary culture of murine alveolar type ii cells. *Am J Respir Cell Mol Biol.* 1996;14:309-315
19. Matthay MA, Thompson BT, Read EJ, McKenna DH, Jr., Liu KD, Calfee CS, Lee JW. Therapeutic potential of mesenchymal stem cells for severe acute lung injury. *Chest.* 2010;138:965-972
20. Oudhoff MJ, Bolscher JG, Nazmi K, Kalay H, van 't Hof W, Amerongen AV, Veerman EC. Histatins are the major wound-closure stimulating factors in human saliva as identified in a cell culture assay. *FASEB J.* 2008;22:3805-3812
21. LoCicero J, 3rd, Xu X, Zhang L. Heat shock protein suppresses the senescent lung cytokine response to acute endotoxemia. *Ann Thorac Surg.* 1999;68:1150-1153
22. van Haften T, Byrne R, Bonnet S, Rochefort GY, Akabutu J, Bouchentouf M, Rey-Parra GJ, Galipeau J, Haromy A, Eaton F, Chen M, Hashimoto K, Abley D, Korbitt G, Archer SL, Thebaud B. Airway delivery of mesenchymal stem cells prevents arrested alveolar growth in

- neonatal lung injury in rats. *Am J Respir Crit Care Med.* 2009;180:1131-1142
23. Matute-Bello G, Winn RK, Jonas M, Chi EY, Martin TR, Liles WC. Fas (cd95) induces alveolar epithelial cell apoptosis in vivo: Implications for acute pulmonary inflammation. *Am J Pathol.* 2001;158:153-161
 24. Pugin J, Verghese G, Widmer MC, Matthay MA. The alveolar space is the site of intense inflammatory and profibrotic reactions in the early phase of acute respiratory distress syndrome. *Crit Care Med.* 1999;27:304-312
 25. Liu L, Li TP. Ultrastructure of type ii alveolar epithelial cells in rats with acute respiratory distress syndrome. *Di Yi Jun Yi Da Xue Xue Bao.* 2003;23:690-691, 695
 26. Touqui L, Arbibe L. A role for phospholipase a2 in ards pathogenesis. *Mol Med Today.* 1999;5:244-249
 27. Ueno M, Lyons BL, Burzenski LM, Gott B, Shaffer DJ, Roopenian DC, Shultz LD. Accelerated wound healing of alkali-burned corneas in mrl mice is associated with a reduced inflammatory signature. *Invest Ophthalmol Vis Sci.* 2005;46:4097-4106
 28. Alfaro MP, Pagni M, Vincent A, Atkinson J, Hill MF, Cates J, Davidson JM, Rottman J, Lee E, Young PP. The wnt modulator sfrp2 enhances mesenchymal stem cell engraftment, granulation tissue formation and myocardial repair. *Proc Natl Acad Sci U S A.* 2008;105:18366-18371

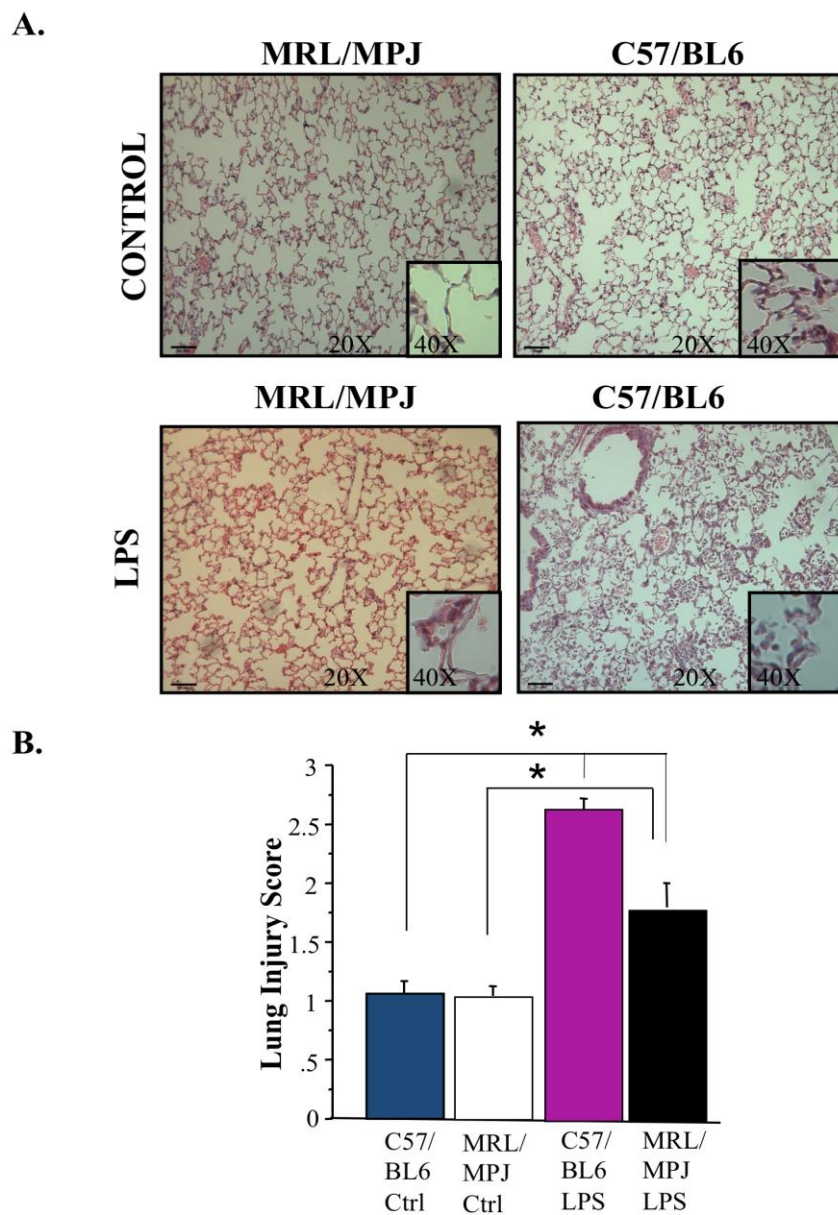


Figure 2.1. Histological evaluation in LPS induced ALI. **A.** Representative H&E stained lung sections from 4 experimental groups **B.** Lung Injury Score, mean data \pm SEM, (n=5/group, *p<0.05).

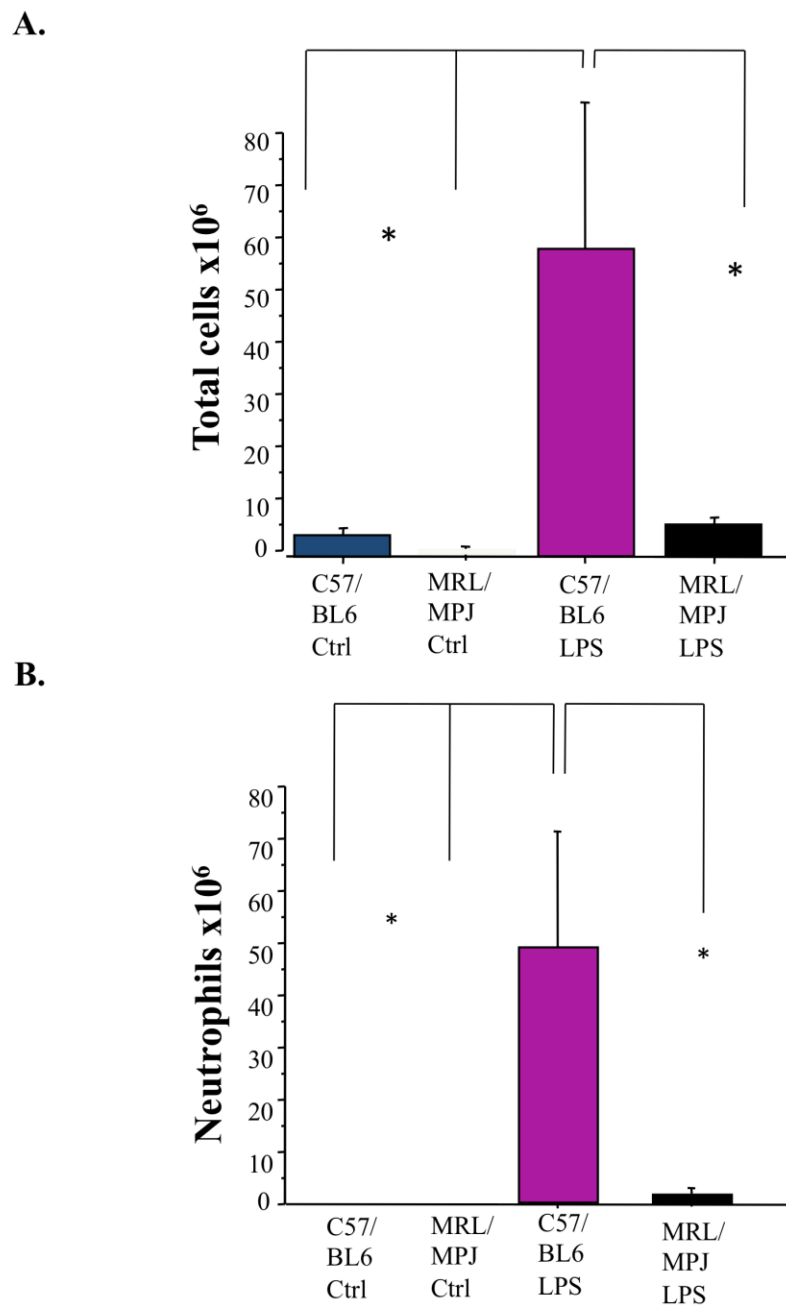


Figure 2.2 BAL Cell count in LPS induced ALI. **A** and **B** Total and neutrophil cell counts performed in BAL fluid 72 h after injury. (n=7/group, p<0.05).

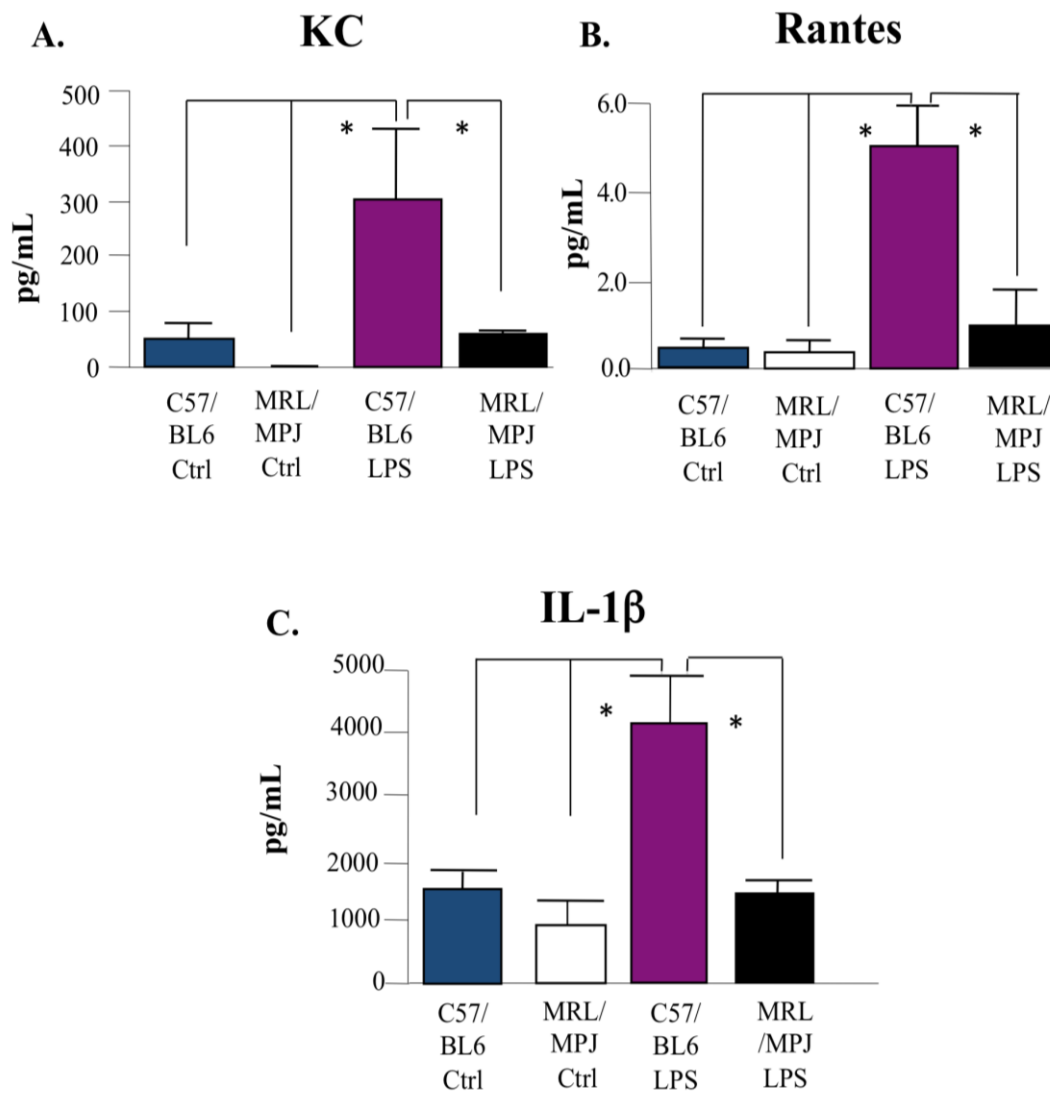


Figure 2.3 Levels of Proinflammatory Cytokines in Lung homogenates. A. KC (murine IL8 homolog), **B. RANTES**, and **C. IL-1 β** measured by multiplex immunoassay (n=7/group, *p<0.05).

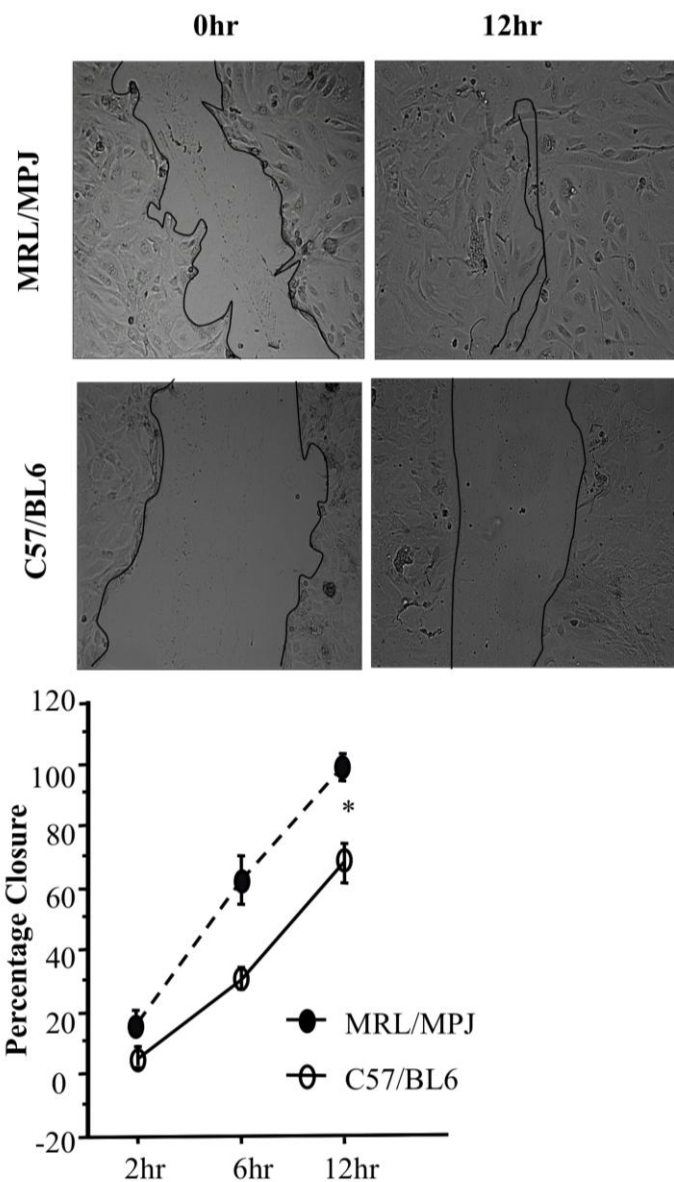


Figure 2.4 MRL/MPJ AT2 and C57/BL6 AT2 Cells Wound Healing Rate. A. Representative micrograph of a confluent monolayer of AT2 cells at time 0 and 12 h. **B.** Mean data \pm SEM, percentage wound closure after 2, 6, and 12 h of scratch assay. (n=5/group, *p<0.05).

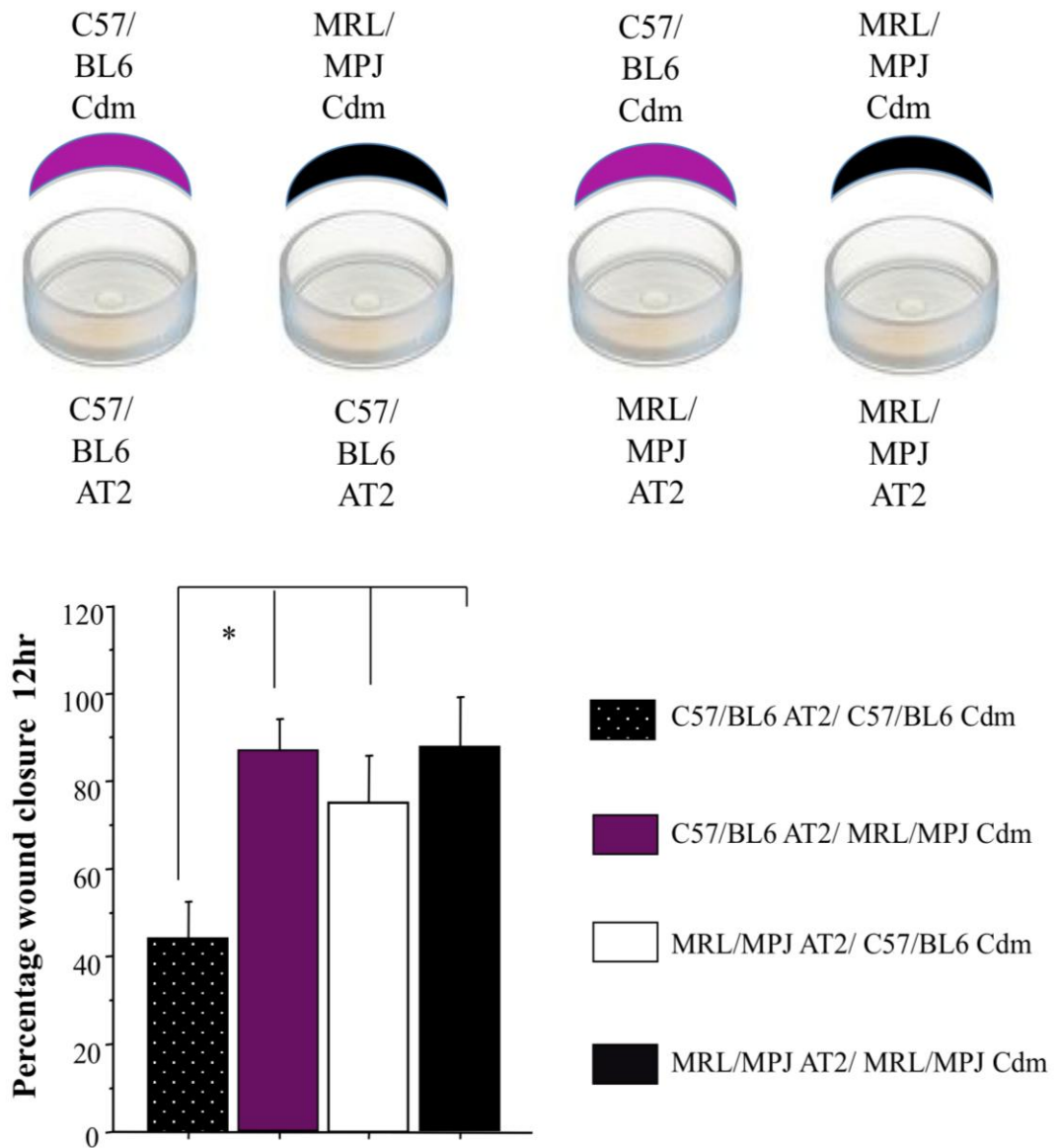


Figure 2.5 MRL/MPJ AT2 and C57/BL6 AT2 Cdm Wound Healing Rate.

Mean data \pm SEM, percentage wound closure after 12h of scratch assay

(n=5/group, p<0.05).

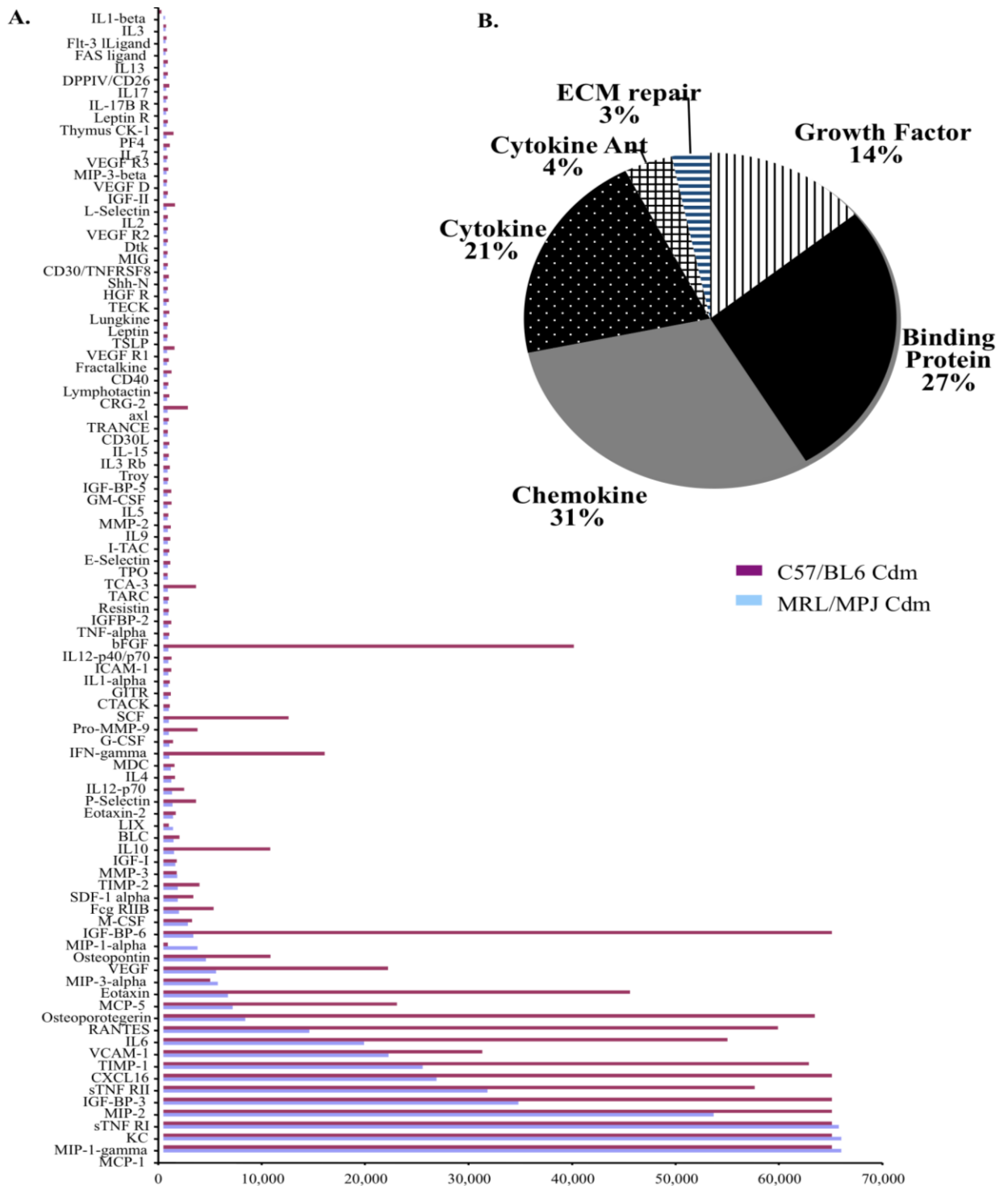


Figure 2.6 Serum-free Cdm was analyzed using an antibody array .A. Antibody array results. Data are presented as spot intensity relative to the negative control and normalized to positive control. **B.** Pie chart showing cluster analysis of Cdm secreted proteins based on reported function. (n=1/group)

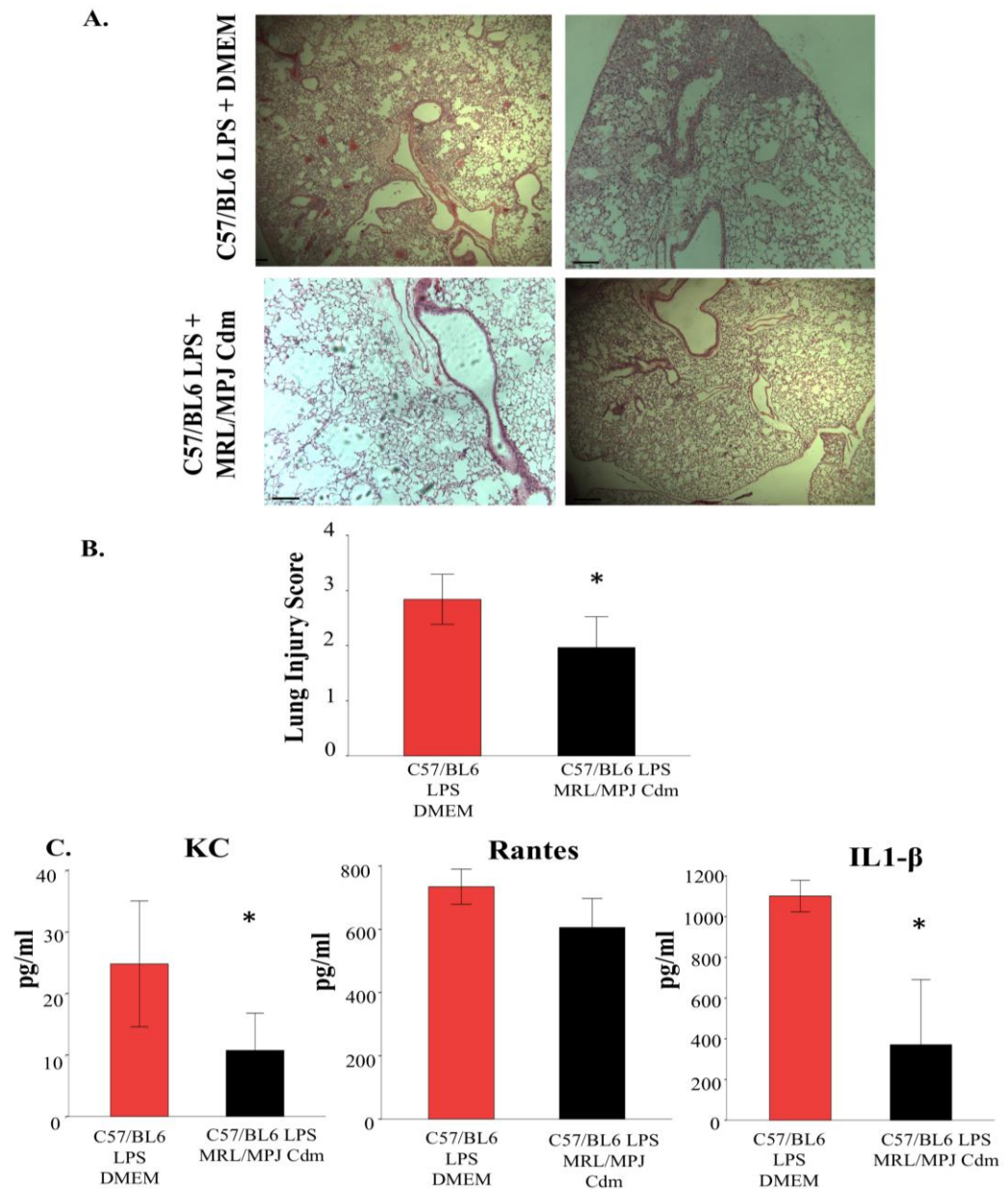


Figure 2.7 MRL/MPJ AT2 Cdm improves LPS induced lung injury in C57/BL6 mice. **A.** Representative H&E lung sections from C57/BL6 LPS challenged mice treated with MRL/MPJ Cdm or DMEM. **B.** Lung Injury Score. Levels of Proinflammatory Cytokines in Bronchoalveolar Lavage. KC (murine IL8 homolog), RANTES, and IL-1 β measured by ELISA. Mean data \pm SEM, (n=5-7/group, p<0.05).

CHAPTER 3

MRL/MPJ MICE ARE NOT PROTECTED AGAINST BLEOMYCIN-INDUCED PULMONARY FIBROSIS

Rey-Parra GJ, Vadivel A, Archer SL, Eaton F, Korbitt G, Thebaud B.

3.1 Introduction

Pulmonary fibrosis (PF) is a disease characterized by progressive dyspnea and pulmonary function abnormalities (i.e. reduced lung volumes, impaired gas exchange). Once diagnosed, it confers a poor prognosis. From the time of initial clinical evaluation, the disease follows an inexorable course that evolves to hypoxic respiratory failure, with a median survival of 2-3 years¹. Sub epithelial fibroblast foci are the characteristic feature of PF, believed to result from recurrent inflammatory insults and abnormal parenchymal repair. Acute lung injury (ALI) and acute respiratory distress syndrome (ARDS) are known severe inflammatory lung diseases, often complicated by the development of PF. ARDS patients often experience changes in pulmonary function, compatible with PF^{2, 34}. Similar features to those seen in PF in humans have been demonstrated in mice exposed to bleomycin (BLM)^{5, 6}.

Wound healing is an essential process in the maintenance of body integrity. The wound repair response initiates complex processes with the purpose of restoring architecture and function of the tissue^{7, 8}. In adult mammals, the mechanism of healing is repair which results in a scar formation. In contrast, scarless regeneration is seen in more primitive vertebrates and fetal wounds^{9, 10}. The inhibition of certain pro-inflammatory cytokines (TGF- β) and the activation/response of certain inflammatory cells (i.e fibroblast) may play a role in determining the nature of tissue repair^{11, 12}. TGF- β 1 and TGF- β 2, are profibrotic growth factors which induce myofibroblast differentiation, increasing collagen synthesis and reducing collagenases activity¹³. Other isoform of TGF- β , TGF- β 3 exhibits a protective effect in scarring.¹⁴

Mice of the MRL/MPJ strain have a unique capacity for both accelerated and regenerative wound healing, as shown by the complete closure of earhole punches with rapid peripheral nerve re-growth^{15, 16}, scarless heart regeneration following cryoinjury¹⁷, accelerated healing in alkali burn corneas¹⁸ and decreased uterine scarring after cesarean section¹⁹. Damaged tissues in these animals are quickly replaced with normal tissue architecture that retains its full functionality. This repair process is reminiscent of fetal healing²⁰ and amphibian

regeneration involving the formation of scarless healing and complete replacement of damaged organs as opposed to scarring^{21, 22}. In contrast, most other strains of mice demonstrate no or limited tissue regeneration and undergo extensive fibrosis that leads to scar formation^{7, 8, 12, 15, 19, 23, 24}. Currently, the mechanism of tissue regeneration in the MRL/MPJ is unclear. We have previously shown that MRL mice have attenuated inflammatory lung injury in a model of LPS-induced ARDS. Consequently, we hypothesized that MRL/MPJ mice will exhibit increased repair/healing capacity after BLM-induced lung fibrosis.

3.2 Materials and Methods

3.2.1 BLM Model

All procedures involving animals were approved by the Animal Welfare Committee of the University of Alberta. Eight-week old MRL/MPJ/MPJ and C57/BL6 mice were obtained from Jackson (Bar Harbor, ME) and randomized into 4 groups: (1) C57/BL6 control group (saline), (2) MRL/MPJ control group (saline), (3) C57/BL6 BLM (BLM-fibrosis model), (4) MRL/MPJ BLM. Before intratracheal administration of BLM or saline, all MRL/MPJ and C57/BL6 mice underwent an exercise test capacity. After, the animals were anesthetized using a mixture of oxygen and Isoflurane® 2.5%. Then, mice were weighted and BLM (Sigma Aldrich, St. Louis, MO) administered intratracheally at a dose of 1.5 U/Kg in 50 µl (~0.04 U/mice)²⁵. Control animals were injected intratracheally with 50 µl of sterile saline 0.9%. Buprenorphine was administered subcutaneously for pain relief (0.05-0.1 mg/kg) after the procedure and repeated every 12 hours for the first 48 hours. Mice were monitored every day. A new exercise test was performed 14 and 21 days after BLM or saline injection. Twenty-one days after intratracheal injection lungs were harvested for hydroxyproline and collagen assays and histology, after assessing lung mechanics with Flexivent (Scireq, Montreal).

3.2.2 Hydroxyproline Assay

Lungs from MRL/MPJ and C57/BL6 mice were harvested 21 days after BLM/saline administration and perfused with heparinized saline, to remove blood. The right bronchus was ligated and the left lung inflated with formaldehyde 10% at a pressure of 20 cm H₂O, for histology. Each of the right lung lobes were weighted, snap frozen in liquid nitrogen and stored at -80 °C for Hydroxyproline and total collagen content assays. Briefly, lungs were homogenized, incubated in 50% trichloroacetic acid (Sigma Aldrich, St Louis, MO) and hydrolyzed with 12N HCL. Samples were then baked at 110°C for 12 hours. Hydroxyproline is oxidized using chloramine T (Sigma Aldrich, St Louis, MO) and pink colored with Ehrlich's solution (Sigma, St Louis, MO). The concentration of hydroxyproline is calculated against a hydroxyproline standard curve and the values of the samples are normalized to dry tissue weight, expressed as µg/mg.^{26, 27}.

3.2.3 Measurement of Collagen Content in the Lung

Collagen content of the lung was determined by assaying soluble collagen using the Sircol Collagen Assay kit, a modification of the sirius red method (Biocolor, Belfast, Northern Ireland), according to the manufacturer's instructions. Briefly, frozen samples were thawed incubated at 4°C overnight in lysis buffer according to tissue weight (0.5 M acetic acid and protein inhibitor cocktail, Sigma Aldrich, St Louis MO). Supernatants (50 µl) were added to 1 mL of Sircol Dye Reagent and then mixed for 30 minutes at room temperature in a mechanical shaker. The collagen-dye complex was precipitated by centrifugation at 10000 × g for 10 min. The unbound dye solution was carefully removed. The precipitated complex was resuspended in 1 mL of alkali reagent. The obtained solution was placed in a 96 wells plate and evaluated in a plate reader (absorbance = 540 nm). Obtained values were then compared to the standard curve as recommended to obtain absolute collagen content. Shown data represent the mean collagen content, expressed as µg/mg of right lobes.

3.2.4 Histology

Lungs were inflation fixed, embedded in paraffin, sectioned and stained with Masson's trichrome; muscles and cells are stained red, nuclei black and collagen blue. For histologic evaluation of the lungs, four mid-lung random sections per lung were examined.

3.2.5 Lung Function Testing

Mice were anesthetized 21 days after bleomycin administration with 70–90 mg/kg pentobarbital sodium, tracheotomized, and mechanically ventilated at a rate of 350 breaths/min, tidal volume of 6 ml/kg, and positive end-expiratory pressure of 3–4 cmH₂O with a computer-controlled small-animal ventilator (Scireq, Montreal, QC, Canada). Once ventilated, mice were paralyzed with 1 mg/kg pancuronium bromide i.p (Sigma Aldrich, St Louis, MO). Airway pressure, volume, and airflow were recorded using a controlled piston to evaluate lung mechanics.

Pressure-volume curves were generated by a sequential and increasing delivery of air into the lungs from resting pressure (zero volume) to total lung capacity followed by sequential expiratory steps during which air was incrementally released. The plateau pressure was recorded when airflow returned to zero at each step. To determine static compliance (C_{st}) of the lung, the Salazar-Knowles equation was applied to the pressure measurements obtained between total lung capacity (TLC) and functional residual capacity (FRC) during the expiratory phase of the pressure-volume loop²⁸. C_{st} was determined from the analysis of pressure-volume curves.

Forced oscillation technique measures the impedance (alveolar pressure to central airflow ratios) of the lung to an oscillatory flow wave controlled by the computer piston. These impedance values are applied to a mathematical model of the lung, the constant phase model²⁹.

The computer-controlled piston applies a 1.25 to 8-s perturbation to the lungs consisting priming frequencies from 1 to 20.5 Hz. Multiple linear regression is used to fit impedance spectra derived from measured pressure and volume changes to the constant phase model of the lung.

To ensure proper recruitment of all alveolar spaces, three pressure-volume curves were generated for each animal. After this maneuver, a 3-s prime wave was performed followed by a second pressure-volume curve to obtain reported values. Each perturbation was followed by 10 s of ventilation before the next measurement was taken^{28, 29}.

3.2.6 Exercise capacity

C57/BL6 and MRL/MPJ mice were run on a treadmill with an inclination of 5° at different speeds/time as follows: 1 min at 3m/min, 4m/min, 5m/min respectively and 3 min at 6 m/min, as a warm up. This followed by 24 min at 8m/min, 7 min at 10 m/min and 8 min at 12m/min. Mice were run until they could not maintain sufficient speed to remain off the shock grid.

3.2.7 Western Blot

Right lungs were flash-frozen in liquid nitrogen and homogenized in buffer containing an antiprotease cocktail before electrophoresis on 7.5% or 10% SDS-PAGE gels using Bradford method. Lung expression of TGF- β 1, TGF- β 2, TGF- β 3 isoforms were quantified by densitometry, relative to a reporter (actin, 43 KDa). TGF- β 1, TGF- β 2 primary antibodies were purchased from Santa Cruz (location), TGF- β 3 from Abcam, (location).

3.2.8 Statistical Analysis

Data are expressed as means \pm Standard Error. Statistical analysis was performed using ANOVA and post hoc tests (Least Significant Difference), as appropriate. Values were considered significant with $P < 0.05$.

3.3 Results

3.3.1 Collagen Deposition in BLM induced Injury in MRL/MPJ and C57/BL6 mice

We used the well characterized model of BLM pulmonary fibrosis to evaluate the healing process between “healer” (MRL/MPJ) and “non-healer” mice (C57/BL6). The degree of fibrosis between both strains of mice was compared in lung sections stained with trichrome masson’s and quantitatively by hydroxyproline and total collagen content (Figure 3.1 A-C respectively). Representative H&E stained lung sections of BLM exposed animals show marked fibrosis with complete loss of lung architecture and increased collagen deposition in the parenchyma (blue) in both mice strains (Figure 3.1A).

The hydroxyproline and total collagen concentration was significantly increased in both BLM-treated groups compared to controls (Figure 3.1 B-C). No statistically significant differences were observed between BLM-exposed C57/BL6 and MRL/MPJ mice. Among controls the collagen deposition was comparable between strains.

3.3.2 Lung Mechanics in BLM- induced pulmonary fibrosis in MRL/MPJ and C57/BL6 mice

In addition to using traditional methods such as histology and biochemical assays to assess the disease progression in the BLM challenged mice compared to controls, we evaluated changes in lung mechanics at 21 days. Interstitial lung fibrosis was associated with decreased compliance and increased elastance in both BLM treated groups as compared to controls (Figure 3.2 A-B respectively). No differences between MRL/MPJ and C57/BL6 were observed.

3.3.3 BLM-Induced Pulmonary Fibrosis Decreases Exercise Capacity

Mice underwent 3 exercise tests before, 14 and 21 days after BLM or saline administration (Figure 3.3 A-B). At 14 and 21 days after BLM administration,

exercise capacity was markedly decreased in both BLM groups compared to controls. There were no differences between C57/BL6 and MRL/MPJ mice.

3.3.4 Differences in TGF- β isoforms expression between BLM-exposed and saline-treated mice

TGF- β isoforms protein expression was assessed in lungs from both MRL/MPJ and C57/BL6 mice, 21 days after BLM or saline administration (Figure 3.4). TGF- β 1 expression was significantly increased in BLM-exposed lungs compared to controls (Figure 3.4 A). No significant differences were observed in TGF- β 2 expression among groups, (Figure 3.4 B). Finally, TGF- β 3 was increased in BLM exposed mice compared to saline control groups and no differences between mice strains were observed (Figure 3.4 C).

3.4 Discussion

MRL/MPJ ability to heal without a scar has been previously shown in cartilage, heart (following cryoinjury), alkali-burned corneas and decreased uterine scarring after cesarean section^{19, 8, 16-18}. In contrast, MRL/MPJ mice have shown to repair tissue leading to scar formation after myocardial ischemic injury and dorsal skin wounds^{30, 31}. In this study we assessed the potential of MRL/MPJ mice to repair/heal after BLM-induced pulmonary fibrosis. We show that MRL/MPJ mice develop a similar degree of pulmonary fibrosis, both structurally and functionally, as wild type mice when exposed to BLM. This suggests that the mechanisms governing wound healing in these mice are dependent of the anatomical site of injury, type/severity, and possibly, activity of pro-inflammatory and pro-fibrotic cytokines. The lung's end respiratory unit, the alveoli (composed of AT2, alveolar type 2 cells-AT1, alveolar type 1 cells and endothelial cells) possess a delicate balance both structurally and functionally that allows for appropriate gas exchange. In PF recreated by BLM administration, alveolar cells, particularly AT2 undergo severe damage³²⁻³⁵.

In PF, AT2 are believed to fail to repair the damaged epithelium as a result of ineffective proliferation/differentiation leading to interstitial scarring³⁶. Persistent denudation of the epithelium in fibrotic lesions suggests that the remaining cells are unsuccessful/overwhelmed in their reparative efforts, allowing for abnormal collagen deposition³⁷. Although many studies have suggested a link between an injury to AT2 and the development of pulmonary fibrosis³²⁻³⁵, there is no data that had directly tested whether they are mechanistically related. MRL/MPJ mice may have enhanced lung healing capacities as suggested by our previous findings in the acute LPS-induced lung injury model. MRL AT2 seem to promote the repair capabilities in the injured MRL lung. However, in BLM induced PF the lung repairing mechanisms, specifically AT2 cells may be overwhelmed failing to repair effectively. In pulmonary fibrosis, the healing potential of the lungs in MRL/MPJ mice has never been examined. Other studies, where different lung fibrosis models are used (i.e TGF- β 1, radiation induced PF³⁸⁻⁴¹), where alveolar cell injury is not as prominent, may hold the key to decreased fibrosis.

BLM induced PF is characterized by a bi-phasic response. The initial phase is characterized by an inflammatory response followed by a fibrotic phase: dividing the BLM model into two phases, allows to discriminate between an inflammatory and fibrotic process⁴². In the present study, we were interested in the fibrotic phase and the ability of the MRL/MPJ to overcome this injury. This resembles more closely the clinical setting where patients with PF often seek medical attention in the fibrotic phase when the symptoms appear, presumably after the inflammatory phase. We did not study the inflammatory phase of the model, where differences between MRL/MPJ and non-healer mice may have emerged. It is known that minimal inflammation is associated with regenerative capacity as shown in amphibians and fetal wounds^{16, 43}. Microarray analysis in MRL/MPJ mice ears have shown that the majority of genes differentially upregulated in MRL/MPJ tissue are involved in tissue repair, while those upregulated in C57/BL6 involve inflammation⁴⁴. This suggest that there must be

other mechanisms involved that lead to the fibrotic phase seen in BLM induced injury besides the inflammatory response.

Different cytokines have been involved in the pathogenesis of lung fibrosis¹³. TGF- β 1 is a profibrotic cytokine that induces differentiation of fibroblast into myofibroblast, increases collagen synthesis and reduces collagenases activity¹³. Other isoforms of TGF- β , TGF- β 2 and β 3 have been implicated in scarring. Most studies performed in skin, show a similar pro-fibrotic effect of TGF- β 2 but a protective effect of TGF- β 3¹⁴. We had hypothesized that TGF- β 3 (protective) was increased, while TGF- β 1 and TGF- β 2 decreased in BLM exposed MRL/MPJ compared to BLM non-healer mice. Although it has been reported that MRL/MPJ mice display increased production of this cytokine, here, TGF- β 1 protein expression did not differ between mice strains but was increased in BLM treated mice¹¹. We did not find differences in TGF- β 2 expression among groups or strains. However, TGF- β 3 appeared significantly increased in BLM treated mice as compared to controls. TGF- β 3 as a protective mechanism could be overwhelmed by the injury and incapable of protecting the already challenged lung.

The discovery of the MRL/MPJ increased wound healing has motivated further studies to characterize this process³⁰. In this study, using a model of pulmonary fibrosis we show using histological, biochemical and lung mechanics examination, that MRL/MPJ mice do not regenerate or show decreased pulmonary fibrosis. We conclude that the mechanisms involved in wound healing in MRL/MPJ depend on the organ and severity of the injury. It remains important to test the regenerative potential of MRL/MPJ in other lung injury models and in other organs in order to gain new insight into successful, scarless healing and identification new therapeutic targets.

3.5 References

1. Demedts M, Costabel U. Ats/ers international multidisciplinary consensus classification of the idiopathic interstitial pneumonias. *Eur Respir J*. 2002;19:794-796
2. Orme J, Jr., Romney JS, Hopkins RO, Pope D, Chan KJ, Thomsen G, Crapo RO, Weaver LK. Pulmonary function and health-related quality of life in survivors of acute respiratory distress syndrome. *Am J Respir Crit Care Med*. 2003;167:690-694
3. Miwa C, Koyama S, Watanabe Y, Tsubochi H, Endo S, Nokubi M, Kawabata Y. Pathological findings and pulmonary dysfunction after acute respiratory distress syndrome for 5 years. *Intern Med*. 2010;49:1599-1604
4. Davidson TA, Caldwell ES, Curtis JR, Hudson LD, Steinberg KP. Reduced quality of life in survivors of acute respiratory distress syndrome compared with critically ill control patients. *JAMA*. 1999;281:354-360
5. Orr FW, Adamson IY, Young L. Promotion of pulmonary metastasis in mice by bleomycin-induced endothelial injury. *Cancer Res*. 1986;46:891-897
6. Ortiz LA, Gambelli F, McBride C, Gaupp D, Baddoo M, Kaminski N, Phinney DG. Mesenchymal stem cell engraftment in lung is enhanced in response to bleomycin exposure and ameliorates its fibrotic effects. *Proc Natl Acad Sci U S A*. 2003;100:8407-8411
7. Bedelbaeva K, Gourevitch D, Clark L, Chen P, Leferovich JM, Heber-Katz E. The mrl mouse heart healing response shows donor dominance in allogeneic fetal liver chimeric mice. *Cloning Stem Cells*. 2004;6:352-363
8. Heber-Katz E, Leferovich J, Bedelbaeva K, Gourevitch D, Clark L. The scarless heart and the mrl mouse. *Philos Trans R Soc Lond B Biol Sci*. 2004;359:785-793
9. Fini ME. Keratocyte and fibroblast phenotypes in the repairing cornea. *Prog Retin Eye Res*. 1999;18:529-551

10. Garg HG, Thompson BT, Hales CA. Structural determinants of antiproliferative activity of heparin on pulmonary artery smooth muscle cells. *Am J Physiol Lung Cell Mol Physiol*. 2000;279:L779-789
11. Kench JA, Russell DM, Fadok VA, Young SK, Worthen GS, Jones-Carson J, Henson JE, Henson PM, Nemazee D. Aberrant wound healing and tgf-beta production in the autoimmune-prone mrl/+ mouse. *Clin Immunol*. 1999;92:300-310
12. Davis TA, Longcor JD, Hicok KC, Lennon GG. Prior injury accelerates subsequent wound closure in a mouse model of regeneration. *Cell Tissue Res*. 2005;320:417-426
13. Kolb M, Bonniaud P, Galt T, Sime PJ, Kelly MM, Margetts PJ, Gauldie J. Differences in the fibrogenic response after transfer of active transforming growth factor-beta1 gene to lungs of "Fibrosis-prone" And "Fibrosis-resistant" Mouse strains. *Am J Respir Cell Mol Biol*. 2002;27:141-150
14. Metcalfe AD, Ferguson MW. Tissue engineering of replacement skin: The crossroads of biomaterials, wound healing, embryonic development, stem cells and regeneration. *J R Soc Interface*. 2007;4:413-437
15. Buckley G, Metcalfe AD, Ferguson MW. Peripheral nerve regeneration in the mrl/mpj ear wound model. *J Anat*. 2011;218:163-172
16. Heber-Katz E. The regenerating mouse ear. *Semin Cell Dev Biol*. 1999;10:415-419
17. Leferovich JM, Bedelbaeva K, Samulewicz S, Zhang XM, Zwas D, Lankford EB, Heber-Katz E. Heart regeneration in adult mrl mice. *Proc Natl Acad Sci U S A*. 2001;98:9830-9835
18. Ueno M, Lyons BL, Burzenski LM, Gott B, Shaffer DJ, Roopenian DC, Shultz LD. Accelerated wound healing of alkali-burned corneas in mrl mice is associated with a reduced inflammatory signature. *Invest Ophthalmol Vis Sci*. 2005;46:4097-4106
19. Buhimschi CS, Zhao G, Sora N, Madri JA, Buhimschi IA. Myometrial wound healing post-cesarean delivery in the mrl/mpj mouse model of uterine scarring. *Am J Pathol*. 2010;177:197-207

20. Dang C, Ting K, Soo C, Longaker MT, Lorenz HP. Fetal wound healing current perspectives. *Clin Plast Surg*. 2003;30:13-23
21. Clark LD, Clark RK, Heber-Katz E. A new murine model for mammalian wound repair and regeneration. *Clin Immunol Immunopathol*. 1998;88:35-45
22. Harty M, Neff AW, King MW, Mescher AL. Regeneration or scarring: An immunologic perspective. *Dev Dyn*. 2003;226:268-279
23. Vorotnikova E, McIntosh D, Dewilde A, Zhang J, Reing JE, Zhang L, Cordero K, Bedelbaeva K, Gourevitch D, Heber-Katz E, Badylak SF, Braunhut SJ. Extracellular matrix-derived products modulate endothelial and progenitor cell migration and proliferation in vitro and stimulate regenerative healing in vivo. *Matrix Biol*. 2010;29:690-700
24. Hampton DW, Seitz A, Chen P, Heber-Katz E, Fawcett JW. Altered cns response to injury in the mrl/mpj mouse. *Neuroscience*. 2004;127:821-832
25. Casey J, Kaplan J, Atochina-Vasserman EN, Gow AJ, Kadire H, Tomer Y, Fisher JH, Hawgood S, Savani RC, Beers MF. Alveolar surfactant protein d content modulates bleomycin-induced lung injury. *Am J Respir Crit Care Med*. 2005;172:869-877
26. Reddy GK, Enwemeka CS. A simplified method for the analysis of hydroxyproline in biological tissues. *Clin Biochem*. 1996;29:225-229
27. Woessner JF, Jr. The determination of hydroxyproline in tissue and protein samples containing small proportions of this imino acid. *Arch Biochem Biophys*. 1961;93:440-447
28. Lovgren AK, Jania LA, Hartney JM, Parsons KK, Audoly LP, Fitzgerald GA, Tilley SL, Koller BH. Cox-2-derived prostacyclin protects against bleomycin-induced pulmonary fibrosis. *Am J Physiol Lung Cell Mol Physiol*. 2006;291:L144-156
29. Hantos Z, Daroczy B, Suki B, Nagy S, Fredberg JJ. Input impedance and peripheral inhomogeneity of dog lungs. *J Appl Physiol*. 1992;72:168-178

30. Beare AH, Metcalfe AD, Ferguson MW. Location of injury influences the mechanisms of both regeneration and repair within the mrl/mpj mouse. *J Anat.* 2006;209:547-559
31. Oh YS, Thomson LE, Fishbein MC, Berman DS, Sharifi B, Chen PS. Scar formation after ischemic myocardial injury in mrl mice. *Cardiovasc Pathol.* 2004;13:203-206
32. Lee VY, Schroedl C, Brunelle JK, Buccellato LJ, Akinci OI, Kaneto H, Snyder C, Eisenbart J, Budinger GR, Chandel NS. Bleomycin induces alveolar epithelial cell death through jnk-dependent activation of the mitochondrial death pathway. *Am J Physiol Lung Cell Mol Physiol.* 2005;289:L521-528
33. Moore BB, Hogaboam CM. Murine models of pulmonary fibrosis. *Am J Physiol Lung Cell Mol Physiol.* 2008;294:L152-160
34. Serrano-Mollar A, Nacher M, Gay-Jordi G, Closa D, Xaubet A, Bulbena O. Intratracheal transplantation of alveolar type ii cells reverses bleomycin-induced lung fibrosis. *Am J Respir Crit Care Med.* 2007;176:1261-1268
35. Adamson IY, Bakowska J. Relationship of keratinocyte growth factor and hepatocyte growth factor levels in rat lung lavage fluid to epithelial cell regeneration after bleomycin. *Am J Pathol.* 1999;155:949-954
36. Selman M, King TE, Pardo A. Idiopathic pulmonary fibrosis: Prevailing and evolving hypotheses about its pathogenesis and implications for therapy. *Ann Intern Med.* 2001;134:136-151
37. Morishima Y, Nomura A, Uchida Y, Noguchi Y, Sakamoto T, Ishii Y, Goto Y, Masuyama K, Zhang MJ, Hirano K, Mochizuki M, Ohtsuka M, Sekizawa K. Triggering the induction of myofibroblast and fibrogenesis by airway epithelial shedding. *Am J Respir Cell Mol Biol.* 2001;24:1-11
38. Mi S, Li Z, Yang HZ, Liu H, Wang JP, Ma YG, Wang XX, Liu HZ, Sun W, Hu ZW. Blocking il-17a promotes the resolution of pulmonary inflammation and fibrosis via tgf- β 1-dependent and -independent mechanisms. *J Immunol.* 2011

39. Luckhardt TR, Coomes SM, Trujillo G, Stoolman JS, Vannella KM, Bhan U, Wilke CA, Moore TA, Toews GB, Hogaboam CM, Moore BB. Tlr9-induced interferon beta is associated with protection from gammaherpesvirus-induced exacerbation of lung fibrosis. *Fibrogenesis Tissue Repair*. 2011;4:18
40. Katre A, Ballinger C, Akhter H, Fanucchi M, Kim DK, Postlethwait E, Liu RM. Increased transforming growth factor beta 1 expression mediates ozone-induced airway fibrosis in mice. *Inhal Toxicol*. 2011;23:486-494
41. Degryse AL, Lawson WE. Progress toward improving animal models for idiopathic pulmonary fibrosis. *Am J Med Sci*. 2011;341:444-449
42. Chaudhary NI, Schnapp A, Park JE. Pharmacologic differentiation of inflammation and fibrosis in the rat bleomycin model. *Am J Respir Crit Care Med*. 2006;173:769-776
43. Grose R, Martin P. Parallels between wound repair and morphogenesis in the embryo. *Semin Cell Dev Biol*. 1999;10:395-404
44. Colwell AS, Krummel TM, Kong W, Longaker MT, Lorenz HP. Skin wounds in the mrl/mpj mouse heal with scar. *Wound Repair Regen*. 2006;14:81-90

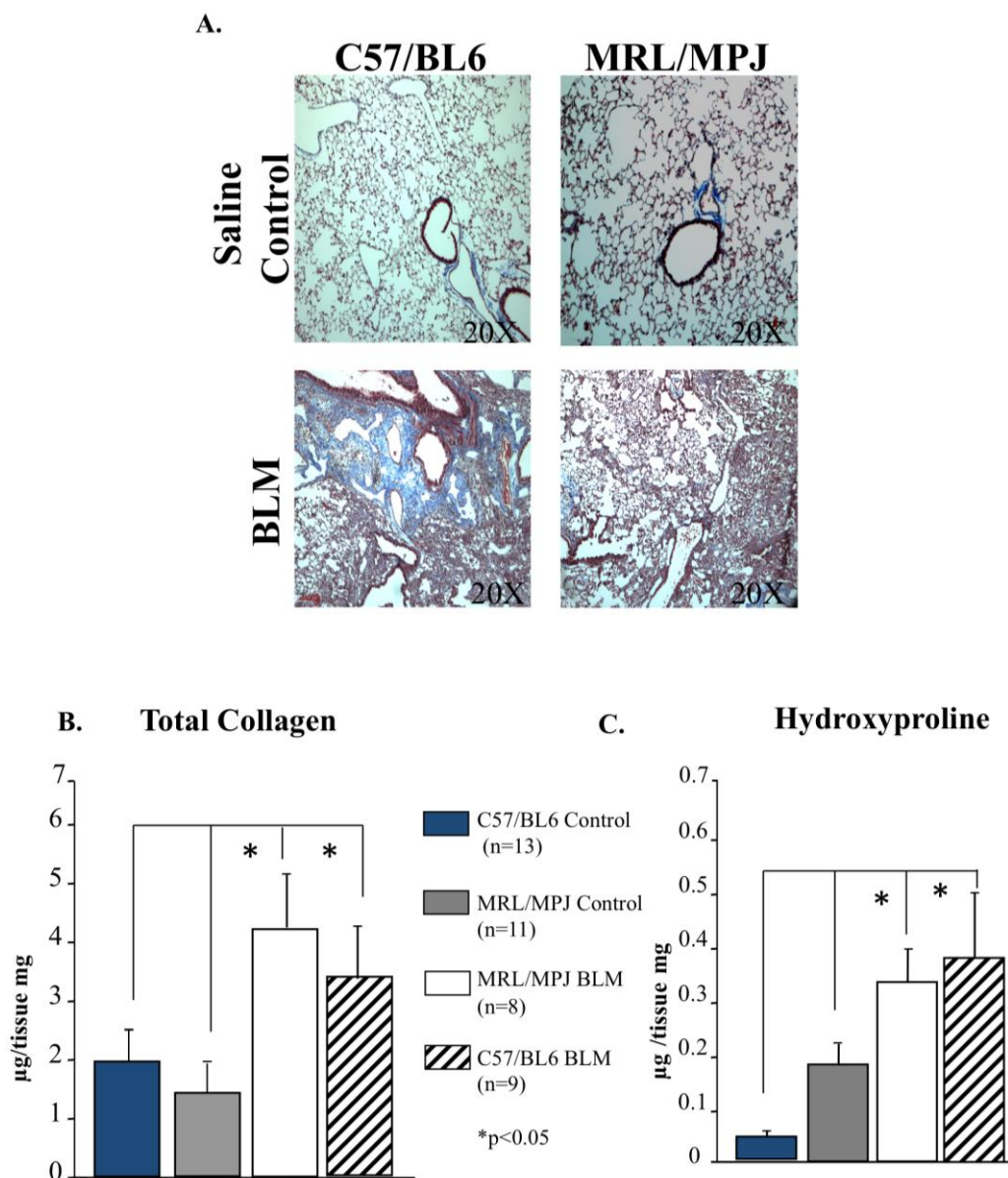


Figure 3.1. Collagen deposition in MRL/MPJ and C57/BL6 mice. A. Representative lung sections stained with Masson's trichrome, from BLM treated animals and saline controls (21 days after BLM or saline administration). Total collagen **B.** and hydroxyproline **C.** content in lungs from all experimental groups, significantly increased in BLM exposed animals compared to controls; no differences between strains were detected. *P<0.05 mean data expressed as \pm SEM.

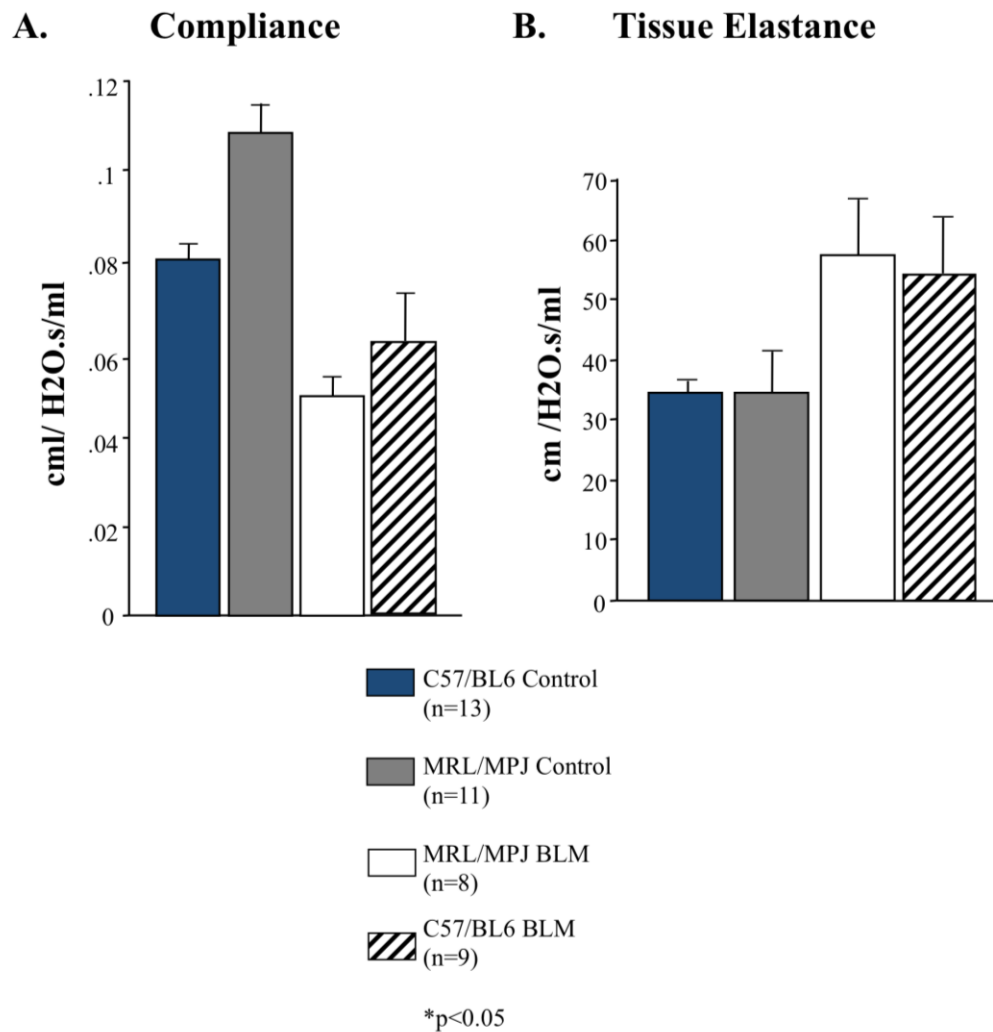


Figure 3.2. Altered lung mechanics 21 days after BLM exposure. Lung mechanics were measured in anesthetized, paralyzed and mechanically ventilated mice after BLM or saline instillation. **A.** Lung compliance is significantly decreased in both strains of mice after BLM exposure. **B.** Tissue elastance (rigidity) is significantly increased in MRL/MPJ and C57/BL6 after BLM administration. *P<0.05 mean data expressed as \pm SEM.

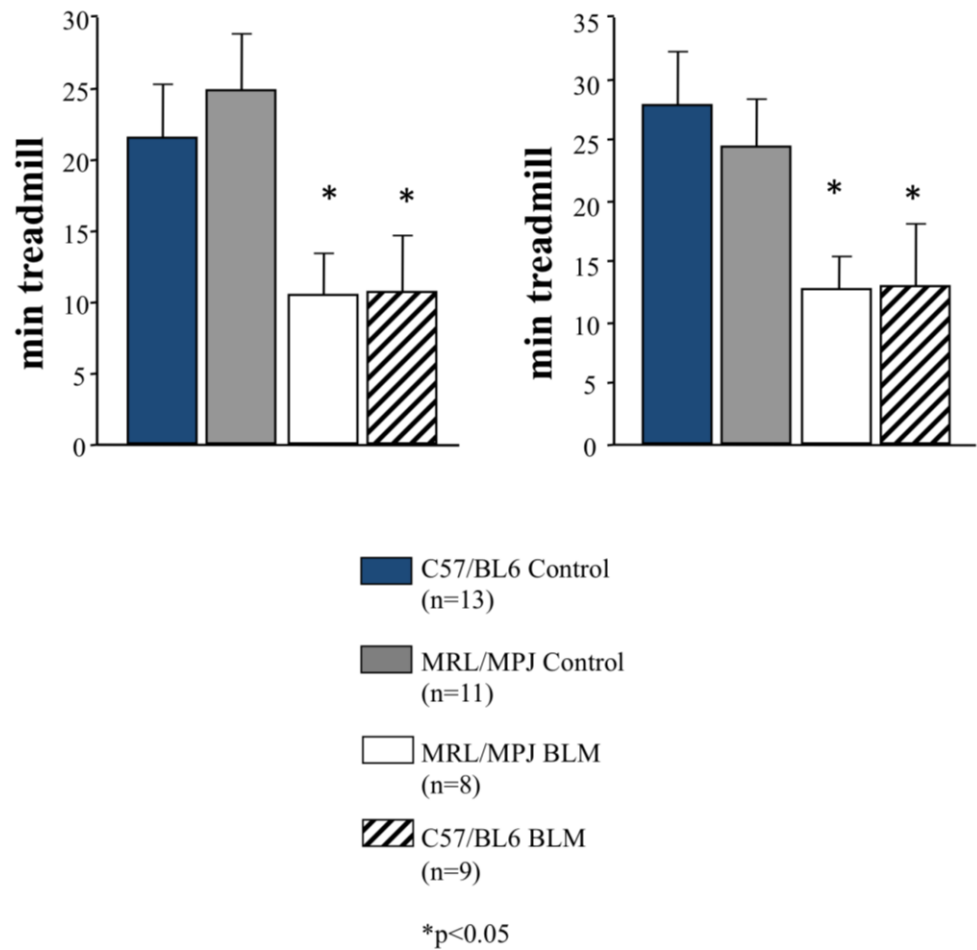
A. 14 days after Saline or bleomycin**B. 21 days after Saline or bleomycin**

Figure 3.3 MRL/MPJ and C57/BL6 mice exhibit decreased exercise capacity during the fibrotic phase of BLM exposure. A. and B. exercise capacity is significantly decreased 14 and 21 days after BLM in both MRL/MPJ and C57/BL6 mice. *P<0.05 mean data expressed as \pm SEM.

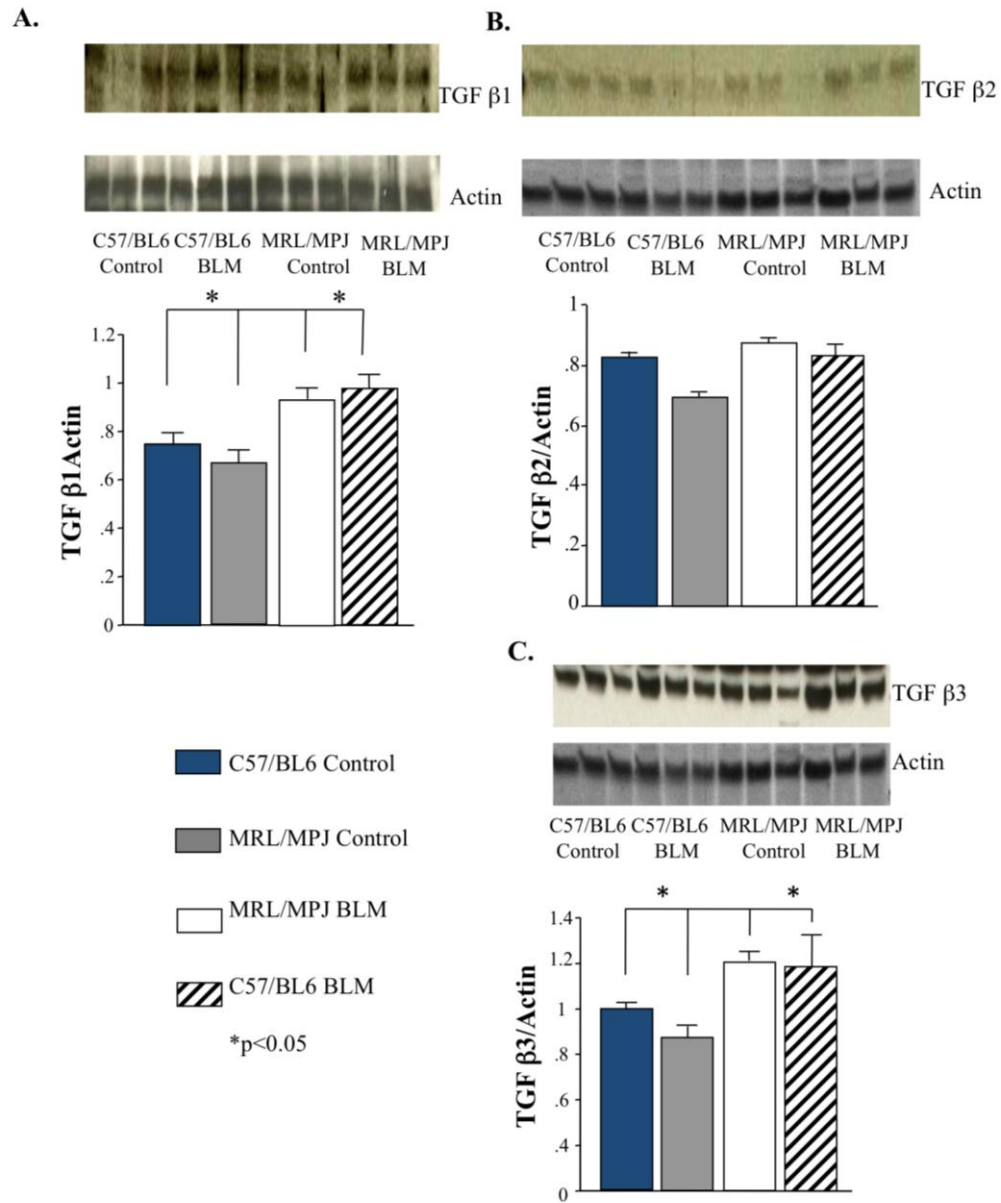


Figure 3.4. TGF- β isoform protein expression in MRL/MPJ and C57/BL6 after BLM or saline administration. A. TGF- β 1 and TGF- β 3 C. are significantly increased in BLM exposed mice compared to saline controls. B. No difference in TGF- β 2 protein expression is seen among groups. N=3/group. P<0.05 mean data expressed as \pm SEM.

CHAPTER 4

THERAPEUTIC POTENTIAL OF HUMAN UMBILICAL CORD BLOOD DERIVED- CELLS IN FIBROTIC LUNG INJURY

Rey-Parra GJ, Vadivel A, Byrne R, Akabutu J, Bouchentouf M, Galipeau J, Haromy A, Eaton F, Abley D, Thébaud B.

4.1 Introduction

Acute lung injury (ALI) and its more severe form acute respiratory distress syndrome (ARDS), are characterized by diffuse lung damage, pulmonary edema¹ and can be complicated by pulmonary fibrosis (PF)²⁻⁴. Currently, there is no effective pharmacological therapy to attenuate ALI/ARDS and prevent subsequent PF⁵. At present, treatment for ALI/ARDS includes prolonged mechanical ventilation which can contribute to ARDS related PF⁶. Once PF is diagnosed, it confers a poor prognosis, leading to impaired pulmonary function and decreased health-related quality of life^{3,4,7}. Similar features to those seen in ARDS with fibrotic lung injury are recapitulated in mice exposed to bleomycin (BLM)^{8,9}.

Cell-based strategies hold tremendous promise for preventing organ injury in general and lung damage in particular⁷. The therapeutic potential of bone marrow-derived cells has been demonstrated in numerous animal models of lung diseases⁷, including BLM-induced pulmonary fibrosis⁸⁻¹⁰. Besides the bone marrow, human umbilical cord blood (HUCB) represents a rich source of stem/progenitor cells^{11,12}. HUCB remains in the cord and placenta following birth and is routinely discarded. As a potential source of therapeutic cells, HUCBC offer few ethical concerns and are easy to obtain without jeopardizing the newborn or mother's health. HUCBC injected into experimental models of spinal cord injury or ischemic brain injury have shown migration, repair or alleviation of motor behavior deficits in the central nervous system suggesting a potential for HUCBC to prevent organ damage¹³. The therapeutic potential of HUCBC for the prevention of fibrosis post ALI/ARDS is not well explored. We hypothesized that HUCBC would preserve lung structure and function in BLM induced lung injury in mice.

4.2 Materials and Methods

4.2.1 Characterization of human HUCBC.

HUCBC were extracted from frozen cord blood collected from healthy term deliveries at the University of Alberta Cord Blood Bank.

Cell preparation: Frozen UCB units were thawed at 37°C and HUCBC were transferred to 50 ml tubes and washed 5 to 6 times with HBSS. Tubes were then centrifuged at 1200 RPM for 20 min at 4°C. CB cells were cultured in DMEM-HG (10% FBS) and incubated in humidified atmosphere at 37°C and 5% CO₂. Medium was changed twice a week and adherent cells were harvested for characterization after one week of culture.

Cell labeling for FACS analysis: Cells were resuspended in PBS containing 1% FBS buffer and incubated with either a unique antibody conjugated to APC (CD14, CD31, VEGFR1, VEGFR2, CD44 and CD45) or a PE conjugated antibody (CD34, CD90, CD105 and CD73) for 2 hours at 4°C. Direct fluorescent staining was used to detect dual binding of FITC-labeled Ulex europeus agglutinin (UEA)-1 (Sigma, Deisenhofen, Germany) and 1,1-dioctadecyl-3,3,3,3-tetramethylindocarbocyanine (DiI)-labeled acetylated low density lipoproteins (acLDL, Cedarlane, MA, USA). AcLDL staining was performed by incubating some adherent CB cells with 10 µg/ml DiIacLDL in complete growth medium for 4 hours at 37°C. Lectin labeling was induced by incubating cells with 10 µg/ml of (UEA)-1 for 2 hours at room temperature. FACS was performed using a FACScalibur analyzer (BD Bioscience).

Evaluation of HUCBC proliferation: Cells were seeded in 6 well plates in complete culture medium composed of EBM-2 supplemented with 1% FBS, 1% Pen/Strep, IGF-1, EGF, FGF, VEGF, ascorbic acid. Cells were harvested at the beginning of the experiments (T₀) and 2 and 5 days later. 100 µl of cell suspension was diluted in 10 ml of shed fluid and counted using Z2 Beckman Coulter particle counter and size analyzer (Miami, Florida, USA) at the indicated time points.

Angiogenesis assay: This test was performed in order to evaluate the ability of HUCBC to form vessel *in vitro* when cultured on wells coated with a matrix made of laminin, collagen type IV, heparin sulfate proteoglycans, entactin and nidogen (Chemicon, Montreal, Canada). 96 well plates were first coated at 37°C for 2

hours with the matrix and 1×10^4 cells were seeded then in each well onto the surface of the polymerized matrix. Cells were incubated in complete medium at 37°C for 16 hours in a tissue culture incubator (37°C , 5% CO_2). Visual patterns were defined on photos of five random view-fields per well and a semi-quantitative analysis was performed for each condition according to the degree of angiogenesis progression as previously described ¹⁴. The pattern association criterion was defined by the number and size of polygons formed, capillary thickness, and cell alignment and fusion. Monocytes were used as negative control for the test. Monocytes were cultured in RPMI-based medium supplemented with 10% FBS, 1% HEPES, 1% sodium pyruvate, and 1% Pen/Strep.

Mesenchymal Stem Cell (MSC) differentiation assay: Osteogenic and adipogenic induction was performed on HUCBC population as previously described ¹⁵.

4.2.2 Experimental Design

Ten to 12 week old male C57BL6 were allocated to the following groups: (1) control group (saline), (2) BLM + DMEM, (3) BLM + HUCBC. The mice were anesthetized using a mixture of oxygen and Isoflurane® 2.5%, weighed and BLM (Sigma Aldrich, St. Louis, MO) administered intratracheally (i.t) at a dose of 1.5 U/Kg in 50 μl (~ 0.04 U/mice) ¹⁶. Control animals were injected i.t with 50 μl of sterile saline 0.9%, HUCBC cells 500.000 cells/animal, or DMEM. Mice were monitored every day. An exercise test was performed before, 7, 14 and 21 days after BLM, BLM+cells and saline injection. Twenty-one days after i.t injection lungs were harvested for hydroxyproline and collagen assays and histology, after assessing lung mechanics.

4.2.3 Exercise capacity

The animals run on a treadmill with an inclination of 5° at different speeds/time as follows: 1 min at 3m/min, 4m/min, 5m/min respectively and 3 min

at 6 m/min, as a warm up. This followed by 24 min at 8m/min, 7 min at 10 m/min and 8 min at 12m/min. Mice were run until they could not maintain sufficient speed to remain off the shock grid.

4.2.4 Lung Function Testing

Mice were anesthetized 21 days after BLM administration with 70–90 mg/kg pentobarbital sodium, tracheotomized, and mechanically ventilated at a rate of 350 breaths/min, tidal volume of 6 ml/kg, and positive end-expiratory pressure of 3–4 cmH₂O with a computer-controlled small-animal ventilator (Scireq, Montreal, Canada). Once ventilated, mice were paralyzed with 1 mg/kg pancuronium bromide given intraperitoneally (Sigma Aldrich, St Louis, MO). Flexivent, Scireq, we recorded airway pressure, volume, and airflow using a controlled piston to evaluate lung mechanics.

Pressure-volume curves were generated by a sequential and increasing delivery of air into the lungs from resting pressure (zero volume) to total lung capacity followed by sequential expiratory steps during which air was incrementally released. The plateau pressure was recorded when airflow returned to zero at each step. To determine compliance of the lung, the Salazar-Knowles equation was applied to the pressure measurements obtained between total lung capacity (TLC) and functional residual capacity (FRC) during the expiratory phase of the pressure-volume loop¹⁷. Compliance was determined from the analysis of pressure-volume curves.

Forced oscillation technique measures the impedance (alveolar pressure to central airflow ratios) of the lung to an oscillatory flow wave controlled by the computer piston. These impedance values are applied to a mathematical model of the lung, the constant phase model¹⁸. This model provides a clear distinction between central and peripheral airways and lung parenchyma.

The computer-controlled piston applies a 1.25 to 8-s perturbation to the lungs consisting priming frequencies from 1 to 20.5 Hz. Multiple linear regression is

used to fit impedance spectra derived from measured pressure and volume changes to the constant phase model of the lung.

To ensure proper recruitment of all alveolar spaces, three pressure-volume curves were generated for each animal. After this maneuver, a 3-s prime wave was performed followed by a second pressure-volume curve to obtain reported values. Each perturbation was followed by 10 s of ventilation before the next measurement was taken^{17, 18}.

4.2.5 Lung Histology

The right bronchus was ligated and the left lung inflated with formaldehyde 10% at a pressure of 20 cm H₂O, for histology. Lungs were inflation fixed, embedded in paraffin, sectioned as described and stained with Masson's trichrome; muscles and cells are stained red, nuclei black and collagen blue. For histologic evaluation of the lungs, four midlung sections per lung were examined.

4.2.6 Hydroxyproline Assay

Mice lungs were harvested 21 days after BLM/saline administration and perfused with heparinized saline, to remove blood. The right bronchi was ligated and the left lung inflated with formaldehyde 10% at a pressure of 20 cm H₂O, for histology. Each right lobe (4 total) was weighted, snap frozen in liquid nitrogen and stored at -80 °C, for Hydroxyproline and total collagen content assays. Briefly, lungs were homogenized, incubated in 50% trichloroacetic acid (Sigma Aldrich, St Louis, MO) and hydrolyzed with 12N HCL. Samples were then baked at 110°C for 12 hours. Hydroxyproline is oxidized using chloramine T (Fluka) and pink colored with Ehrlich's solution (Sigma, St Louis, MO). The concentration of hydroxyproline is calculated against a hydroxyproline standard curve and the values of the samples are normalized to dry tissue weight, expressed as µg/mg.^{19,}

4.2.7 Lung Collagen Content

Collagen content of the lung was determined by assaying soluble collagen using the Sircol Collagen Assay kit, a modification of the sirius red method (Biocolor, Belfast, Northern Ireland), according to the manufacturer's instructions. Briefly, frozen samples were thawed incubated at 4°C overnight in lysis buffer according to tissue weight (0.5 M acetic acid and protein inhibitor cocktail, Sigma Aldrich, St Louis MO). Supernatants (50 µl) were added to 1 mL of Sircol Dye Reagent and then mixed for 30 minutes at room temperature in a mechanical shaker. The collagen-dye complex was precipitated by centrifugation at 10000 × g for 10 min. The unbound dye solution was carefully removed. The precipitated complex was resuspended in 1 mL of alkali reagent. The obtained solution was placed in a 96 wells plate and evaluated in a plate reader (absorbance = 540 nm). Obtained values were then compared to the standard curve as recommended to obtain absolute collagen content. Shown data represent the mean collagen content, expressed as µg/µg of right lobes.

4.2.8 Isolation and characterization of HUCBC

Cell preparation: Frozen HUCBC units were thawed at 37°C and HUCBC cells were transferred to 50 ml tubes and washed 5 to 6 times with HBSS. Tubes were then centrifuged at 1200 RPM for 20 min at 4°C. HUCBC were cultured in DMEM-HG (10% FBS) and incubated in humidified atmosphere at 37°C and 5% CO₂. Medium was changed twice a week and adherent cells were harvested for characterization after one week of culture.

Evaluation of HUCBC proliferation: Cells were seeded in 6 well plates in complete culture medium. Cells were harvested at the beginning of the experiments (T0) and 2 and 5 days later. 100 µl of cell suspension was diluted in 10 ml of shed fluid and counted using Z2 Beckman Coulter particle counter and size analyzer (Miami, Florida, USA) at the indicated time points.

Angiogenesis assay: This test was performed in order to evaluate the ability of HUCBC to form vessel *in vitro* when cultured on wells coated with a matrix made of laminin, collagen type IV, heparin sulfate proteoglycans, entactin and nidogen (Chemicon, Montreal, Canada). 96 well plates were first coated at 37°C for 2 hours with the matrix and 1×10^4 cells were seeded then in each well onto the surface of the polymerized matrix. Cells were incubated in complete medium at 37°C for 16 hours in a tissue culture incubator (37°C, 5% CO₂).

MSC differentiation assay: Osteogenic and adipogenic induction was performed on HUCBC population as previously described²¹.

HUCBC were extracted from frozen cord blood collected from healthy term deliveries, kindly provided by Dr. Akabutu, University of Alberta. Plastic adherent-mononuclear cells were cultured (DMEM-10%FBS-1%PSF) for two weeks and characterized using FACS analysis.

4.2.9 Fluorescence-activated Cell Sorting of Cell Surface

Cell labeling for FACS analysis: Cells were resuspended in PBS containing 1% FBS buffer and incubated with either a unique antibody conjugated to APC (CD14, CD31, VEGFR1, VEGFR2, CD44 and CD45) or a conjugated antibody (CD34, CD90, CD105 and CD73) for 2 hours at 4°C. Direct fluorescent staining was used to detect dual binding of FITC-labeled Ulex europeus agglutinin (UEA)-1 (Sigma, Deisenhofen, Germany) and 1,1-dioctadecyl-3,3,3,3-tetramethylindocarbocyanine (DiI)-labeled acetylated low density lipoproteins (acLDL, Cedarlane, MA, USA). AcLDL staining was performed by incubating some adherent CB cells with 10 µg/ml DiIacLDL in complete growth medium for 4 hours at 37°C. Lectin labeling was induced by incubating cells with 10 µg/ml of (UEA)-1 for 2 hours at room temperature. FACS was performed using a FACScalibur analyzer (BDbioscience).

4.2.10 Fibroblast isolation

Mouse lungs were dissected and rinsed in sterile PBS following removal

of tracheas and extrapulmonary airways and were finely minced with sterile scissors and incubated in 1 mg/mL Collagenase Type I (Sigma Adrich, St Louis, Missouri) in PBS in a volume of 2 mL per lung for 60 min at 37°C in a shaking incubator. The resulting cell suspension was further disaggregated by trituration through an 18- gauge needle, diluted in PBS, filtered through a 40- μ m nylon cell strainer (Falcon; Becton Dickinson) and washed twice in PBS. After centrifugation of 1500 rpm for 5 min, 3 times, the resulting cells were plated in DMEM 10% FBS 1% PSF²². Fibroblast were isolated from saline control animals and BLM exposed mice 7 days following intratracheal injection.

4.2.11 Cell engraftment

Mouse lungs (n=3 per/group) were inflated with Tissue-Tek optimal cutting temperature (O.C.T.) medium (Ted Pella, Inc., Redding, CA) and subsequently frozen in a block of O.C.T. medium. Lungs were stained for the type 2 alveolar epithelial cell (AT2)–specific marker SP-C, pro-SP-C, and cellular nuclei (4',6-diamidino-2-phenylindole, DAPI) and imaged with a confocal microscope. HUCBC labeled with the Human Nuclear Antigen (HNA, chemicon)²² were manually counted in 25 random fields throughout the lung for a total cell count of 8,224 cells day 4 post-injury.

4.2.12 Generation of HUCBC Conditioned Medium

Passage 2 HUCBC were grown to about 80% confluency. Medium was aspirated and cells were rinsed three times with phosphate-buffered saline. Cells were cultured in serum-free medium for 12 hours. Conditioned medium (Cdm) was removed and filtered through a 50- μ m mesh to remove cellular debris, as previously described¹¹.

4.2.13 ELISA to assess antifibrotic mediators in HUCBC Cdm

Cdm and fibroblast supernatant were snap frozen in liquid nitrogen and stored at -80°C. Transforming growth factor β 1, (TGF β 1), human Relaxin and

human Angiotensin converting enzyme 2 (ACE2) were measured using ELISA kits (R&D Systems and Enzo life Sciences).

4.2.14 Statistical Analysis

Data are expressed as mean \pm SE, except where stated otherwise. Statistical analysis was performed using ANOVA, *post hoc* test (least significant difference). Values were considered significant with $P < 0.05$.

4.3 Results

4.3.1 Characterization of HUCBC

HUCBC from healthy term newborns formed a heterogeneous cell population (Figure 4.1 A). Accordingly, FACS analysis revealed that HUCBC expressed cell surface markers (Figure 4.1B-C) compatible with monocytes, and proliferating, putative endothelial progenitor cells (EPCs) and MSCs (Figure 4.1D). MSC differentiation assays showed few proliferating cell clusters but no adipocyte or osteocyte positive staining (not shown). In an *in vitro* angiogenic assay, HUCBC formed some vascular networks with a low cell density while other HUCBCs (putative monocytes) were unable to form vascular networks (Figure 4.1E) as compared to HUVEC (Figure 4.1F). Monocytes used as negative controls, were unable to form vascular networks (Figure 4.1G).

4.3.2 HUCBC improve exercise capacity in BLM PF

Exercise capacity was significantly decreased in BLM challenged mice compared to controls and BLM+HUCBC treated animals, at 7, 14 and 21 days. BLM+HUCBC treated animals, at 14 and 21 days had significantly improved exercise capacity as compared to BLM group (Figure 4.2).

4.3.3 HUCBC improve lung function in BLM PF

BLM significantly decreased lung compliance by 32%(Figure 4.3 A) and increased lung elastance by 37%(Figure 4.3 B) 21 days after BLM injury

compared to controls. HUCBC administration significantly improved compliance (Figure 4.3 A) and elastance (Figure 4.3 B) compared to BLM treated group.

4.3.4 HUCBC ameliorate BLM PF

BLM induced marked fibrosis and distorted lung architecture compared to controls as shown on lung sections stained with Trichrome Masson's (Figure 4.4A). HUCBC significantly attenuated BLM-induced fibrosis (Figure 4.4B-C). Hydroxyproline (Figure 4.4B) and sircol collagen (Figure 4.4 C) assays confirmed quantitatively the decrease in lung collagen content with HUCB treatment.

4.3.5 HUCBC engraftment

HNA labeled cells accounted for 0.2% of cells counted in UCBC treated animals (Figure 4.5A).

4.3.6 *In vitro* antifibrotic effects of HUCBC Cdm

In vitro, exposure of lung fibroblasts to BLM significantly increased the levels of the potent pro-fibrotic molecule TGF β 1 (Figure 4.6A). Cell free Cdm derived from HUCBC significantly decreased TGF β 1 levels in BLM treated fibroblast. Conversely, Cdm derived from Human Dermal Fibroblast (HDF) had no effect (Figure 4.6 A). The antifibrotic mediators, Human relaxin and ACE2, were detected exclusively in HUCBC Cdm samples but not in HDF Cdm (Figure 4.6 B-C respectively).

4.4 Discussion

In this study we provide proof of principle that HUCBC exert a therapeutic benefit even after 10 years of cryopreservation. *In vivo* HUCBC administered concomitantly with BLM improved exercise capacity, lung compliance, and attenuated lung fibrosis. The therapeutic benefit is likely mediated via a paracrine mechanism because lung engraftment was low and *in vitro* findings revealed

decreased BLM-induced production of TGF- β 1 by fibroblasts with cell free HUCBC-derived CdM, which contained ACE2 and relaxin, known antifibrotic compounds.

Numerous studies have demonstrated the therapeutic potential of bone marrow-derived cells to prevent lung damage in various experimental models of lung disease ⁷. Ortiz and Rojas et al showed that myelosuppression increased the susceptibility to BLM-induced lung injury and that bone marrow-derived MSCs were protective against lung fibrosis in this model ⁸⁻¹⁰. Increasingly, UCB is being recognized as a valuable source of stem cells for regenerative purposes. The annual global 100 million human birth rate places UCB as the largest untouched stem cell source, with advantages of naive immune status ^{11, 12}. UCB is a currently discarded, yet easily accessible, ethically appropriate, clinically relevant source of potent stem cells. Studies suggest that UCB yields higher numbers of stem and progenitor cells with a higher proliferation rate and expansion potential than those of adult BM ¹¹. Recent findings suggest an age-related decline in progenitor cells and a higher regenerative potential of “young” vs. “old” stem cells ¹⁸. Finally, UCB transplantation is already successfully used clinically for a variety of nonmalignant and malignant hematopoietic as well as metabolic diseases in children and adults ¹⁹ and is feasible despite HLA incompatibility of 1-3 antigens, thus offering new possibilities in allogenic regenerative medicine.

There is only one study exploring the role of cord blood-derived cells in lung fibrosis. Moodley showed that systemically administered human Wharton Jelly-derived MSCs reduced inflammation, TGF- β 1 expression and lung collagen concentration in BLM-induced lung injury ²⁰. In our study, we administered intratracheally human UCB-derived cells that were stored for over ten years. HUCBC consisted of a heterogeneous cell population as assessed by morphological and immunological analyses. Differentiation and angiogenesis assays suggest that at the time of injection (1 week culture), the HUCBC population was composed mainly of monocytes and EPCs while no MSC subpopulation could be detected. It is well established that UCB MSCs take a

long time (30 to 60 days) to start proliferating *in vitro*, suggesting that during the time lapse of cell preparation and injection, these cells were still very rare and may not account for the beneficial effect of HUCBC. More recently, it has been shown that HUCBC from term newborn yield predominantly endothelial colony forming cells, while UCB from preterm babies yielded predominantly MSC colonies ²¹. All together, this suggests that the beneficial effect may be explained by the presence of UCB-derived EPCs and monocytes.

EPCs serve as reparative cells and promote vessel formation ²². Recent evidence suggest a role for EPCs in lung repair ²³. Specifically, circulating EPCs are decreased in patients with pulmonary fibrosis complicated by pulmonary arterial hypertension ²⁴. Little is known about the role of angiogenesis in the occurrence of pulmonary fibrosis. In BLM-induced lung injury, the normal lung architecture is replaced by a mix of collagen and myofibroblasts with few blood vessels. Angiogenic factors such as vascular endothelial growth factor (VEGF), may aid in allowing adequate blood supply to the fibrotic area thereby decreasing the extent of fibrotic damage. This is supported by the fact that loss of myeloid cell-derived VEGF worsens lung fibrosis and significantly reduces the formation of blood vessels ²⁵. This suggests that the process of angiogenesis, driven by myeloid cell-derived VEGF, is essential for the prevention of fibrosis. Indeed, EPCs participate in tissue regeneration by promoting endothelial cell proliferation via paracrine secretion of angiogenic factors ²⁶. This is consistent with the role of angiogenesis in promoting alveolar development and the protective effect of angiogenic growth factors in a model of O₂-induced arrested alveolar growth ²⁷. Monocytes, the other cell type present in our heterogeneous HUCBC, may also be beneficial for angiogenesis via MCP-1 that promotes endothelial progenitor cell proliferation and migration ²⁸. Cell-to-cell interaction between monocytes and vascular smooth muscle cells induce VEGF synthesis in both types of cell and IL-6 is partially involved in VEGF production ²⁹.

However, the benefit of pro-angiogenic therapies in preventing pulmonary fibrosis is controversial. Farkas et al found that VEGF worsened lung fibrosis in a rat model of idiopathic pulmonary fibrosis induced by adenoviral delivery of

TGF- β 1³⁰. These data showed that experimental pulmonary fibrosis lead to loss of the microvasculature through increased endothelial apoptosis and to remodeling of the pulmonary arteries, resulting in pulmonary hypertension. While adenoviral mediated overexpression of VEGF resulted in reduced endothelial apoptosis, increased vascularization, and attenuated pulmonary hypertension, pulmonary fibrosis worsened. The reason for the apparent discrepancy between studies is unclear.

Consistent with various cell therapy studies in various models of lung injury⁷, we found low engraftment of cells in our treated group. These findings suggest that beyond cell replacement, cells may be releasing factors *in situ* responsible for the beneficial effects observed. Increasing evidence suggest that the therapeutic benefit of stem cells is mediated via a paracrine effect, opening new avenues for the use of cell-based approaches to treating lung injury³¹. Accordingly, we found that cell free Cdm derived from HUCBC, but not from HDF, attenuated the release of the pro-fibrotic molecule TGF- β 1 from BLM-stimulated lung fibroblasts. HUCBC-derived Cdm, but not HDF Cdm, contained molecules that exert anti-fibrotic effects including relaxin and ACE2.

Relaxin is a hormone released primarily during pregnancy by the teca cells³². Its main role is extracellular matrix remodeling to facilitate the ligament laxity needed during pregnancy and delivery. More recently, relaxin was shown to exert antifibrotic and anti-inflammatory properties³². Relaxin acts at multiple levels to inhibit fibrogenesis, including attenuating TGF- β 1-induced differentiation/growth of myofibroblasts and collagen deposition³³. Relaxin also acts directly on profibrotic factors, primarily TGF- β 1 to inhibit their ability to accelerate myofibroblast accumulation and collagen production, the net effect being a relaxin-induced reduction of fibrosis. The effects of long-term relaxin deficiency on ageing Rln1^{-/-} mice have demonstrated an age related progression of interstitial fibrosis various organs including the lung³⁴ leading to organ damage and dysfunction. Likewise, mice deficient in the relaxin family peptides receptor 1 (Rxfp1) also experience lung fibrosis³². Conversely, treatment of male Rln1^{-/-} mice with exogenous human relaxin consistently led to the reversal of collagen

accumulation (fibrosis) in the various organs studied ³⁴. In BLM-induced pulmonary fibrosis in mice, the administration of recombinant human relaxin over a 2-week treatment period prevented collagen accumulation and restored lung function ³⁵. More recently, a novel peptide that targets the relaxin Rxfp1/LGR7 receptor was found to inhibit TGF- β 1-induced collagen deposition in human dermal fibroblasts and to attenuate BLM-induced pulmonary fibrosis in mice ³⁶.

ACE2, a homologue to Angiotensin Converting Enzyme (ACE), exhibits cardiopulmonary antifibrotic effects and is primarily found in endothelial cells ³⁷. In various ALI/ARDS models, ACE2 deletion worsened lung injury promoting enhanced vascular permeability/edema, inflammation and worsened lung function ³⁸. Importantly, in BLM-induced lung injury, ACE2 appears to prevent alveolar epithelial cell apoptosis balancing ANGII (proapoptotic) and its antiapoptotic degradation product ANG1-7 ³⁹.

Overall, our study provides proof concept that HUCBC is an ethically acceptable source of cell-based therapy for ALI/ARDS with anti-fibrotic properties. In addition, our data suggest that similar to MSC and vascular progenitor cells, HUCBC exert their effects via a paracrine activity, opening novel avenues for identifying pharmacological therapies for lung repair.

4.5 References

1. Ware LB, Matthay MA. The acute respiratory distress syndrome. *N Engl J Med*. 2000;342:1334-1349
2. Cepkova M, Matthay MA. Pharmacotherapy of acute lung injury and the acute respiratory distress syndrome. *J Intensive Care Med*. 2006;21:119-143
3. Davidson TA, Caldwell ES, Curtis JR, Hudson LD, Steinberg KP. Reduced quality of life in survivors of acute respiratory distress syndrome compared with critically ill control patients. *JAMA*. 1999;281:354-360
4. Miwa C, Koyama S, Watanabe Y, Tsubochi H, Endo S, Nokubi M, Kawabata Y. Pathological findings and pulmonary dysfunction after acute respiratory distress syndrome for 5 years. *Intern Med*. 2010;49:1599-1604
5. Orme J, Jr., Romney JS, Hopkins RO, Pope D, Chan KJ, Thomsen G, Crapo RO, Weaver LK. Pulmonary function and health-related quality of life in survivors of acute respiratory distress syndrome. *Am J Respir Crit Care Med*. 2003;167:690-694
6. Moore BB, Hogaboam CM. Murine models of pulmonary fibrosis. *Am J Physiol Lung Cell Mol Physiol*. 2008;294:L152-160
7. Weiss DJ, Bertoncello I, Borok Z, Kim C, Panoskaltsis-Mortari A, Reynolds S, Rojas M, Stripp B, Warburton D, Prockop DJ. Stem cells and cell therapies in lung biology and lung diseases. *Proc Am Thorac Soc*. 2011;8:223-272
8. Ortiz LA, Dutreil M, Fattman C, Pandey AC, Torres G, Go K, Phinney DG. Interleukin 1 receptor antagonist mediates the antiinflammatory and antifibrotic effect of mesenchymal stem cells during lung injury. *Proc Natl Acad Sci U S A*. 2007;104:11002-11007
9. Ortiz LA, Gambelli F, McBride C, Gaupp D, Baddoo M, Kaminski N, Phinney DG. Mesenchymal stem cell engraftment in lung is enhanced in response to bleomycin exposure and ameliorates its fibrotic effects. *Proc Natl Acad Sci U S A*. 2003;100:8407-8411

10. Rojas M, Xu J, Woods CR, Mora AL, Spears W, Roman J, Brigham KL. Bone marrow-derived mesenchymal stem cells in repair of the injured lung. *Am J Respir Cell Mol Biol*. 2005;33:145-152
11. Broxmeyer HE. Biology of cord blood cells and future prospects for enhanced clinical benefit. *Cytotherapy*. 2005;7:209-218
12. Sullivan MJ. Banking on cord blood stem cells. *Nat Rev Cancer*. 2008;8:555-563
13. Newman MB, Davis CD, Borlongan CV, Emerich D, Sanberg PR. Transplantation of human umbilical cord blood cells in the repair of CNS diseases. *Expert Opin Biol Ther*. 2004;4:121-130
14. Bouchentouf M, Forner KA, Cuerquis J, Michaud V, Zheng J, Paradis P, Schifffrin EL, Galipeau J. Induction of cardiac angiogenesis requires killer cell lectin-like receptor 1 and alpha4beta7 integrin expression by NK cells. *J Immunol*. 2010;185:7014-7025
15. van Haaften T, Byrne R, Bonnet S, Rochefort GY, Akabutu J, Bouchentouf M, Rey-Parra GJ, Galipeau J, Haromy A, Eaton F, Chen M, Hashimoto K, Abley D, Korbitt G, Archer SL, Thebaud B. Airway delivery of mesenchymal stem cells prevents arrested alveolar growth in neonatal lung injury in rats. *Am J Respir Crit Care Med*. 2009;180:1131-1142
16. Reddy GK, Enwemeka CS. A simplified method for the analysis of hydroxyproline in biological tissues. *Clin Biochem*. 1996;29:225-229
17. Woessner JF, Jr. The determination of hydroxyproline in tissue and protein samples containing small proportions of this imino acid. *Arch Biochem Biophys*. 1961;93:440-447
18. Conboy IM, Conboy MJ, Wagers AJ, Girma ER, Weissman IL, Rando TA. Rejuvenation of aged progenitor cells by exposure to a young systemic environment. *Nature*. 2005;433:760-764
19. Broxmeyer HE, Douglas GW, Hangoc G, Cooper S, Bard J, English D, Arny M, Thomas L, Boyse EA. Human umbilical cord blood as a potential

- source of transplantable hematopoietic stem/progenitor cells. *Proc Natl Acad Sci U S A*. 1989;86:3828-3832
20. Moodley Y, Atienza D, Manuelpillai U, Samuel CS, Tchongue J, Ilancheran S, Boyd R, Trounson A. Human umbilical cord mesenchymal stem cells reduce fibrosis of bleomycin-induced lung injury. *Am J Pathol*. 2009;175:303-313
 21. Javed MJ, Mead LE, Prater D, Bessler WK, Foster D, Case J, Goebel WS, Yoder MC, Haneline LS, Ingram DA. Endothelial colony forming cells and mesenchymal stem cells are enriched at different gestational ages in human umbilical cord blood. *Pediatr Res*. 2008;64:68-73
 22. Schmidt-Lucke C, Rossig L, Fichtlscherer S, Vasa M, Britten M, Kamper U, Dimmeler S, Zeiher AM. Reduced number of circulating endothelial progenitor cells predicts future cardiovascular events: Proof of concept for the clinical importance of endogenous vascular repair. *Circulation*. 2005;111:2981-2987
 23. Thebaud B, Tibboel D. Pulmonary hypertension associated with congenital diaphragmatic hernia. *Cardiol Young*. 2009;19 Suppl 1:49-53
 24. Fadini GP, Schiavon M, Rea F, Avogaro A, Agostini C. Depletion of endothelial progenitor cells may link pulmonary fibrosis and pulmonary hypertension. *Am J Respir Crit Care Med*. 2007;176:724-725; author reply 725
 25. Stockmann C, Kerdiles Y, Nomaksteinsky M, Weidemann A, Takeda N, Doedens A, Torres-Collado AX, Iruela-Arispe L, Nizet V, Johnson RS. Loss of myeloid cell-derived vascular endothelial growth factor accelerates fibrosis. *Proc Natl Acad Sci U S A*. 2010;107:4329-4334
 26. Rehman J, Li J, Orschell CM, March KL. Peripheral blood "Endothelial progenitor cells" Are derived from monocyte/macrophages and secrete angiogenic growth factors. *Circulation*. 2003;107:1164-1169
 27. Thebaud B, Ladha F, Michelakis ED, Sawicka M, Thurston G, Eaton F, Hashimoto K, Harry G, Haromy A, Korbitt G, Archer SL. Vascular endothelial growth factor gene therapy increases survival, promotes lung

- angiogenesis, and prevents alveolar damage in hyperoxia-induced lung injury: Evidence that angiogenesis participates in alveolarization. *Circulation*. 2005;112:2477-2486
28. Ma J, Wang Q, Fei T, Han JD, Chen YG. Mcp-1 mediates tgf-beta-induced angiogenesis by stimulating vascular smooth muscle cell migration. *Blood*. 2007;109:987-994
 29. Hojo Y, Ikeda U, Maeda Y, Takahashi M, Takizawa T, Okada M, Funayama H, Shimada K. Interaction between human monocytes and vascular smooth muscle cells induces vascular endothelial growth factor expression. *Atherosclerosis*. 2000;150:63-70
 30. Farkas L, Farkas D, Ask K, Moller A, Gauldie J, Margetts P, Inman M, Kolb M. Vegf ameliorates pulmonary hypertension through inhibition of endothelial apoptosis in experimental lung fibrosis in rats. *J Clin Invest*. 2009;119:1298-1311
 31. Lee JW, Fang X, Krasnodembskaya A, Howard JP, Matthay MA. Concise review: Mesenchymal stem cells for acute lung injury: Role of paracrine soluble factors. *Stem Cells*. 2011;29:913-919
 32. Samuel CS, Hewitson TD, Unemori EN, Tang ML. Drugs of the future: The hormone relaxin. *Cell Mol Life Sci*. 2007;64:1539-1557
 33. Formigli L, Perna AM, Meacci E, Cinci L, Margheri M, Nistri S, Tani A, Silvertown J, Orlandini G, Porciani C, Zecchi-Orlandini S, Medin J, Bani D. Paracrine effects of transplanted myoblasts and relaxin on post-infarction heart remodelling. *J Cell Mol Med*. 2007;11:1087-1100
 34. Samuel CS, Zhao C, Bathgate RA, Bond CP, Burton MD, Parry LJ, Summers RJ, Tang ML, Amento EP, Tregear GW. Relaxin deficiency in mice is associated with an age-related progression of pulmonary fibrosis. *FASEB J*. 2003;17:121-123
 35. Unemori EN, Pickford LB, Salles AL, Piercy CE, Grove BH, Erikson ME, Amento EP. Relaxin induces an extracellular matrix-degrading phenotype in human lung fibroblasts in vitro and inhibits lung fibrosis in a murine model in vivo. *J Clin Invest*. 1996;98:2739-2745

36. Pini A, Shemesh R, Samuel CS, Bathgate RA, Zauberman A, Hermesh C, Wool A, Bani D, Rotman G. Prevention of bleomycin-induced pulmonary fibrosis by a novel antifibrotic peptide with relaxin-like activity. *J Pharmacol Exp Ther.* 2010;335:589-599
37. Kuba K, Imai Y, Penninger JM. Angiotensin-converting enzyme 2 in lung diseases. *Curr Opin Pharmacol.* 2006;6:271-276
38. Imai Y, Kuba K, Rao S, Huan Y, Guo F, Guan B, Yang P, Sarao R, Wada T, Leong-Poi H, Crackower MA, Fukamizu A, Hui CC, Hein L, Uhlig S, Slutsky AS, Jiang C, Penninger JM. Angiotensin-converting enzyme 2 protects from severe acute lung failure. *Nature.* 2005;436:112-116
39. Uhal BD, Li X, Xue A, Gao X, Abdul-Hafez A. Regulation of alveolar epithelial cell survival by the ace-2/angiotensin 1-7/mas axis. *Am J Physiol Lung Cell Mol Physiol.* 2011;301:L269-274

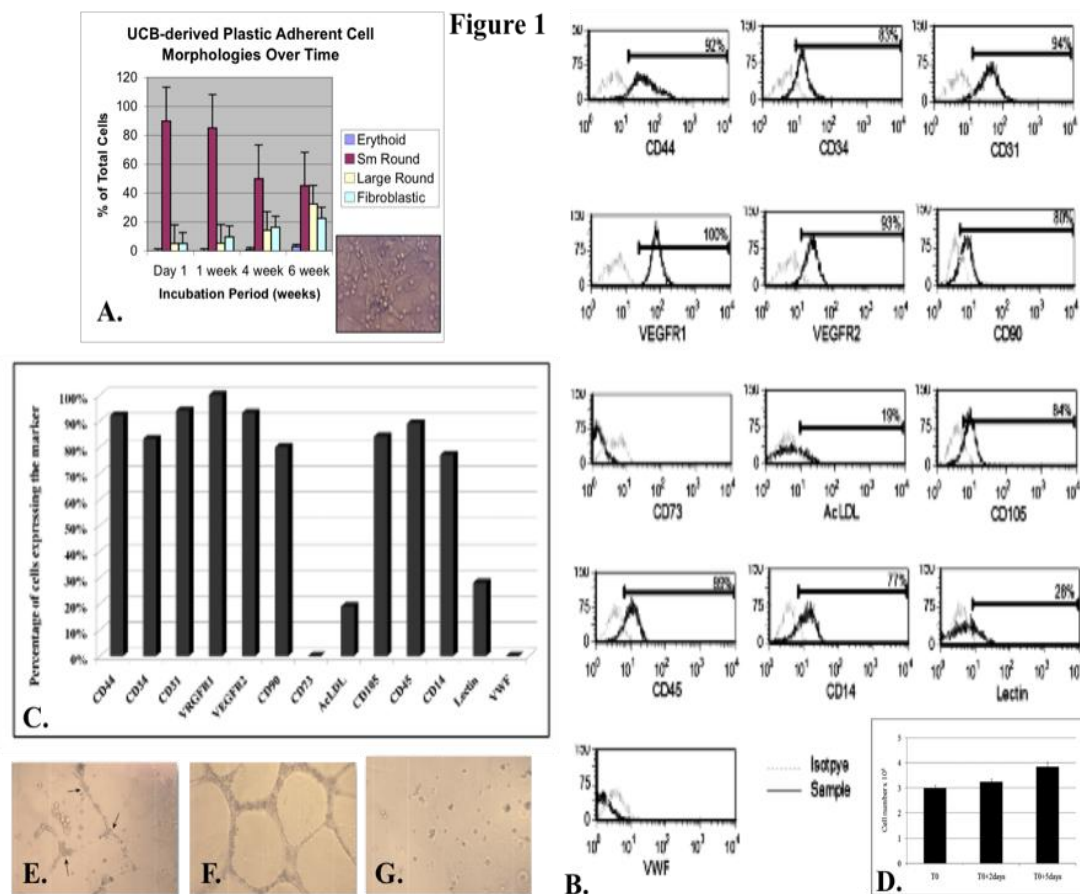


Figure 4.1. Characterization of HUCBC. **A.** Graphical representation of the percentage of UCBC showing various morphologies after 1 day of culture and 1, 4 and 6 weeks later. **B, C.** HUCBC molecular phenotype was performed after 1 week of culture in complete culture medium. UCBC were composed of various cells expressing cell surface markers compatible with monocytes (CD14+, VEGFR2+, VEGFR1+, CD31+, DiAcLDL+, Lectin +, CD105 and CD45+), EPCs (CD34+, VEGFR2+, DiAcLDL+, Lectin +) and MSCs (CD90+, CD44+). **D.** The proliferation assay showed that there were some cells with proliferative capacities. Since monocytes do not proliferate, this result confirms the presence of a subpopulation of proliferating cells (EPCs or MSCs). **E.** UCBC cultured on matrix coated flasks were able to form some networks still very sparse and with a low cell density. Arrows indicate cells aligning and fusing to form vascular structures. Some cells were unable to form vascular network and they were presumably monocytes. **F.** Human monocytes, used as negative control, formed no vascular networks. **G.** Conversely, HUVEC cells were used as positive control for the assay. All HUVEC fused to form vascular network.

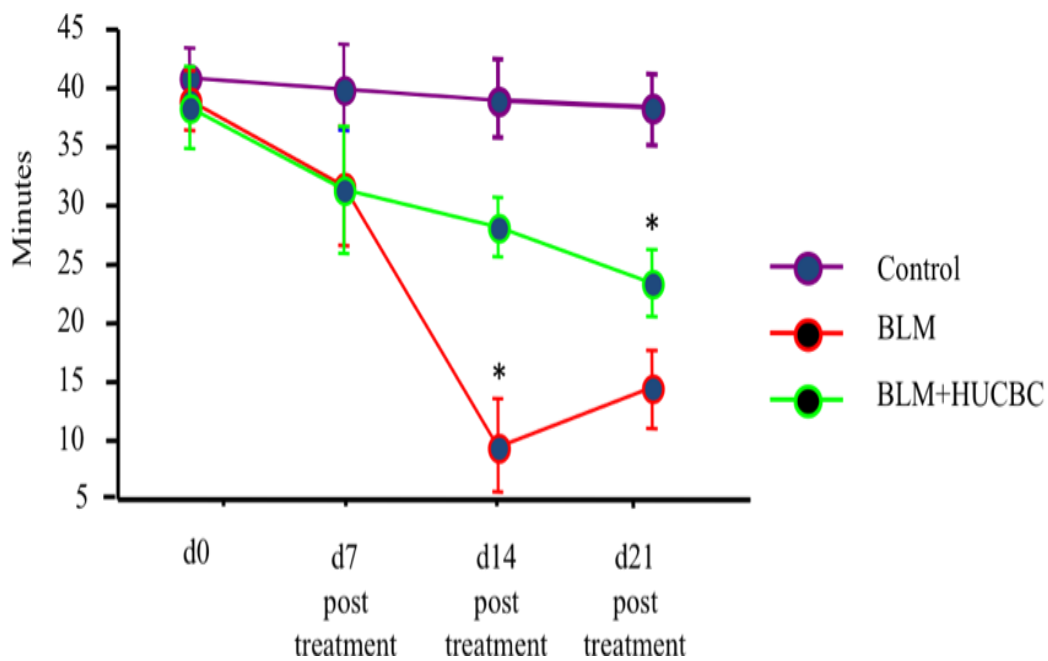


Figure 4.2. HUCBC improve exercise capacity in BLM challenged animals. C57BL/6 mice were run on a predetermined protocol on an animal treadmill to assess exercise capacity. Bleo-exposed mice had significant worsening of their exercise capacity over time. UCBC treatment attenuated the decline in exercise capacity (n= 6-7 mice/group, *P<0.05, mean data expressed as \pm SEM).

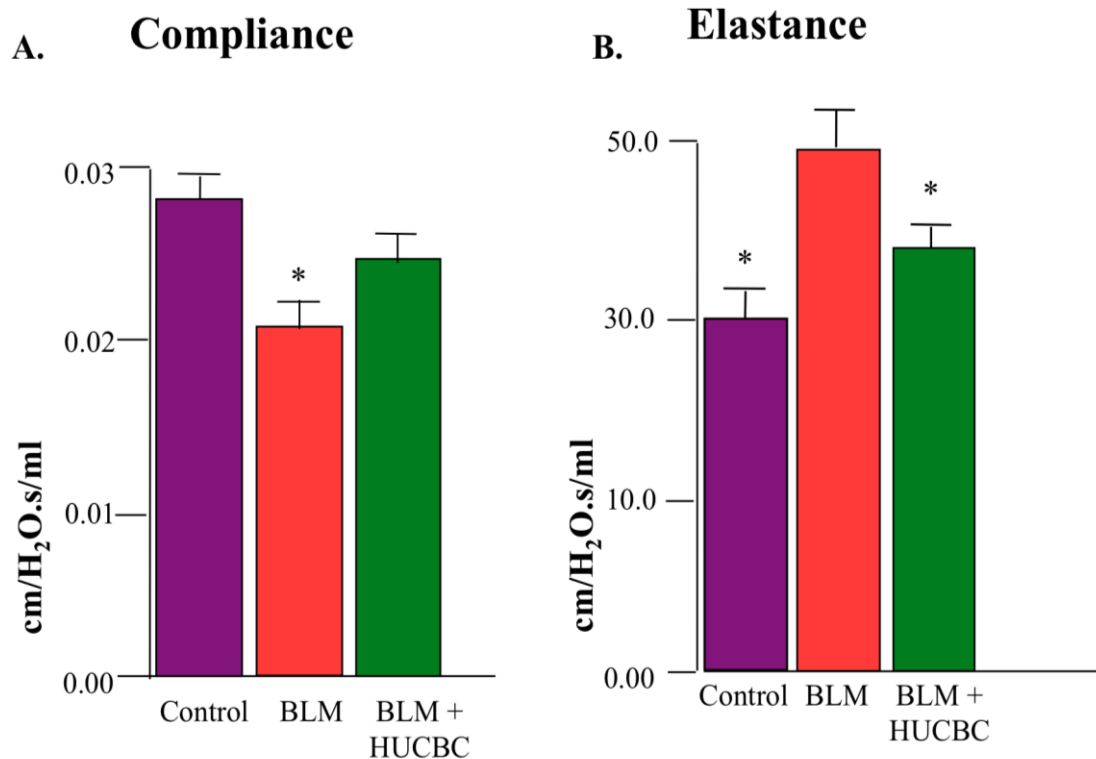


Figure 4.3 HUCBC treated animals exhibit improved lung mechanics 21 days after BLM exposure. **A.** Lung compliance was significantly decreased in BLM-induced lung injury. HUCBC treatment improved lung compliance in BLM-exposed mice. **B.** Tissue elastance (rigidity) was significantly increased in BLM-induced lung injury. UCBC treatment improved lung resistance in BLM-exposed mice (n=6-7 mice/group, *P<0.05, mean data expressed as \pm SEM).

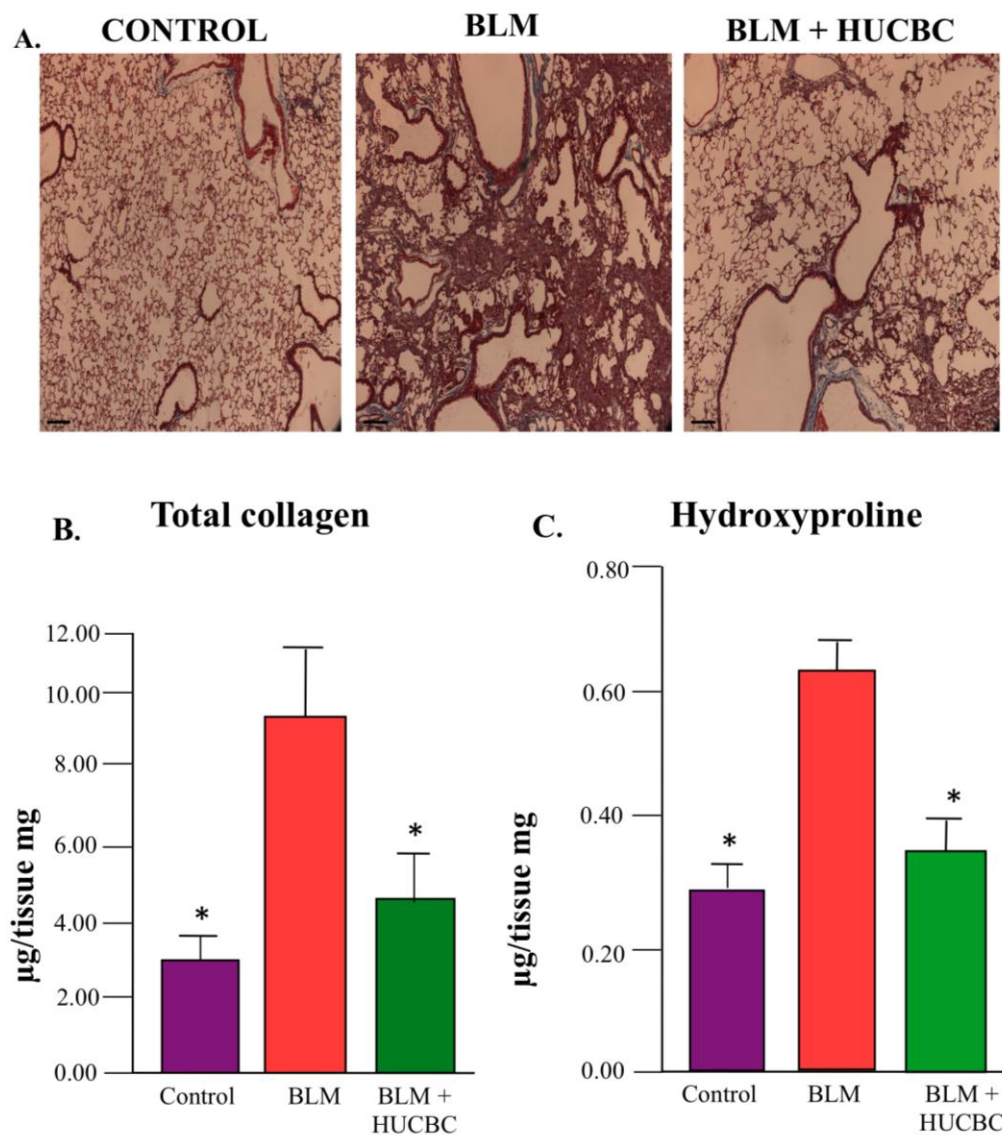


Figure 4.4. Collagen deposition is decreased in HUCBC treated animals. A. Representative lung sections stained with Masson's trichrome from control (saline treated mice), BLM and BLM+HUCBC treated mice at 21 days of the experimental protocol showing altered lung architecture and massive lung fibrosis in BLM treated mice. HUCBC treated mice show less distorted lung architecture and less lung fibrosis. **B. C.** Total collagen and Hydroxyproline content in lungs from all experimental groups provide quantitative assessment for excess collagen deposition in BLM-induced lung injury at 21 days. HUCBC treatment significantly attenuated lung collagen deposition in BLM exposed mice (n=6-7/group, *P<0.05, mean data expressed as \pm SEM).

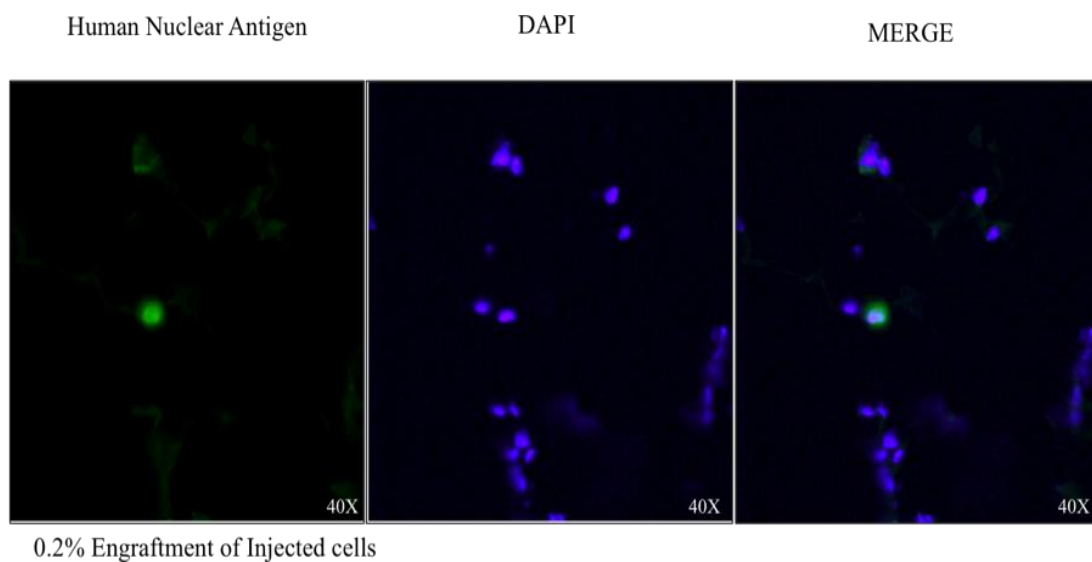


Figure 4.5. Intratracheal injection of HUCBC results in low lung engraftment. A. Immunofluorescence on frozen lung sections of HUCBC treated BLM-exposed mice examined under confocal microscopy reveals Human Nuclear Antigen (HNA) stain to detect HUCBC and DAPI staining to mark cell nuclei. HNA staining, after manually counting 25 random fields throughout the lung for a total cell count of 8,224 cells, revealed 0.2% cell engraftment.

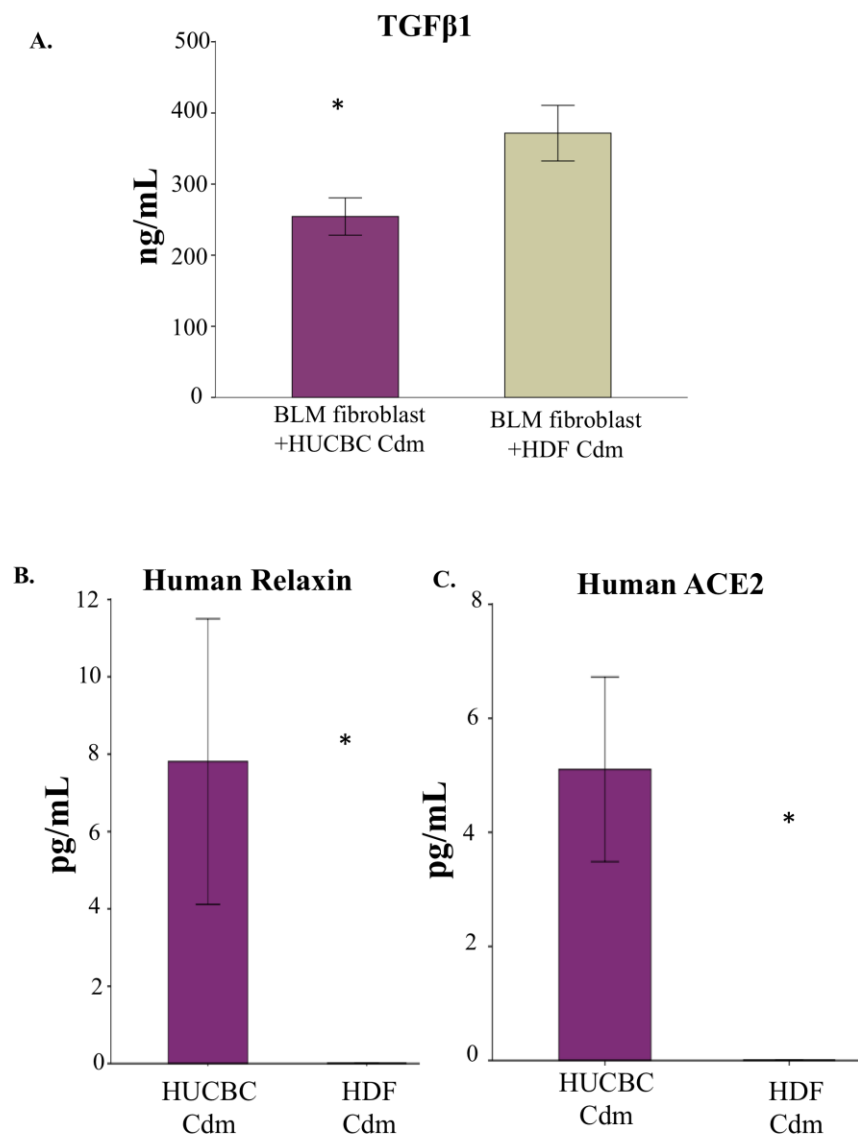


Figure 4.6. Antifibrotic effects of HUCBC Cdm. **A.** TGF- β 1 release from BLM-exposed lung fibroblasts treated with UCBC Cdm or Human Dermal Fibroblast (HDF) Cdm. **B. C.** Human relaxin and ACE2 were present in HUCBC Cdm, but undetectable in HDF Cdm (n=6/group, *P<0.05).

CHAPTER 5

ANGIOTENSIN CONVERTING ENZYME 2 ABROGATES BLEOMYCIN-INDUCED LUNG INJURY: EFFECTS OF GENDER

Rey-Parra GJ, Vadivel A, Coltan L, Hall A, Eaton F, Schuster M, Loibner H, Penninger JM, Kassiri Z, Oudit GY, Thébaud B. Angiotensin converting enzyme 2 abrogates bleomycin-induced lung injury. *J Mol Med (Berl)*. 2012 Jan 14. [Epub ahead of print] PubMed PMID: 22246130.

5.1 Introduction

Acute respiratory distress syndrome (ARDS), a severe form of acute lung injury (ALI), is characterized by diffuse lung damage, arterial hypoxaemia and decreased compliance¹. Despite advances in patient care, ALI/ARDS remains an important cause of death and morbidity in intensive care units². ARDS survivors often have impaired pulmonary function, decreased health-related quality of life and chronic pulmonary fibrosis³⁻⁵. At present, treatment is supportive and includes prolonged mechanical ventilation, which can further contribute to ARDS-related morbidity⁶. Currently, there is no effective pharmacological therapy to attenuate lung injury and promote lung repair in ALI/ARDS⁶⁻¹⁰.

Experimental and clinical evidence indicate that the renin angiotensin system (RAS) contributes to lung injury¹¹⁻¹⁴. ACE cleaves angiotensin (ANG) I to generate ANGII. Proliferative and fibrotic properties have been attributed to the ACE-ANGII-AT1 receptor axis^{15, 16}. ACE2, a homologue to ACE, degrades ANGII to ANG 1-7 peptides, limiting ANGII accumulation^{14, 17}. Thus, ACE2 counterbalances the deleterious effects of ACE and prevents lung injury. Angiotensin converting enzyme-2 (ACE2) knockout mice have enhanced vascular permeability, increased lung edema, neutrophil accumulation, and worsened lung function¹⁷. Characteristics similar to those seen in lungs of patients with ARDS have been modeled in mice exposed to bleomycin (BLM) induced lung injury complicated by fibrosis¹⁸. We hypothesized that ACE2 gene deletion would worsen BLM-induced lung injury and its resultant fibrosis; conversely, recombinant human (rh) ACE2 would attenuate BLM-induced lung injury. Furthermore, since lungs of female rats exhibit higher lung expression of ACE2 than male rats¹⁹, we assessed gender differences in ACE2 knockout mice in BLM-induced lung injury.

5.2 Materials and Methods

5.2.1 Experimental design

All procedures involving animals were approved by the Animal Welfare Committee of the University of Alberta. Fourteen to 16 week old male C57BL6 (wild type, WT, controls) mice and ACE2 knockouts - males (ACE2^{-y}) and females (ACE2^{-f})

- were allocated to the following groups: (1) WT control group (saline), (2) ACE2^{-y} control group (saline), (3) WT BLM (ALI/ARDS model), and (4) ACE2^{-y} BLM. The mice were anesthetized using a mixture of oxygen and Isoflurane® 2.5%, weighed and BLM (Sigma Aldrich, St. Louis, MO) administered intratracheally at a dose of 1.5 U/Kg in 50 µl (~0.04 U/mice)²⁰. Control animals were injected intratracheally with 50 µl of sterile saline 0.9%.

In a separate set of experiments, we compared gender differences in the following groups: (1) ACE2^{-y} controls (saline), (2) ACE2^{-/-} controls, (3) ACE2^{-y} BLM, and (4) ACE2^{-/-} BLM.

Finally, to explore the therapeutic potential of rhACE2, we performed a third set of experiments including (1) WT control group (saline), (2) WT BLM (ALI/ARDS model), and (3) WT BLM+rhACE2. rhACE2 was given intraperitoneally for 21 days at a dose of 2mg/kg.

Mice were monitored every day. An exercise test was performed 21 days after BLM or saline injection. Three weeks after BLM, lungs were harvested for hydroxyproline and collagen assays, profibrotic gene expression and histology, after assessing lung mechanics.

5.2.2 Recombinant human ACE2

The extracellular domain of rhACE2 (amino acid residues 1–740, MW = 101 kDa) was expressed recombinantly in Chinese hamster ovary cells under serum free conditions in a chemically defined medium as previously described¹⁶⁻¹⁹. The enzymatic turnover of rhACE2 with Ang II substrate was 5.2±0.1 µmol.mg⁻¹.min⁻¹ and the elimination half-life of rhACE2 was 10.4 hrs in Rhesus monkeys. The purity of the expression product was 99.99% as measured by HPLC^{17, 18}.

5.2.3 TaqMan Real-Time Polymerase Chain Reaction

mRNA expression levels of smooth muscle actin and transforming growth factor-β were determined by TaqMan (Applied Systems Inc, Streetsville, Ontario, Canada) real-time polymerase chain reaction as described previously^{21, 25-27}. Expression analysis of the reported genes was performed by TaqMan reverse-transcription polymerase chain

reaction using ABI 7900 sequence detection system; 18S rRNA was used as an endogenous control. The primer/probe for mRNA expression analysis by Taqman real-time polymerase chain reaction were purchased from Applied Biosystems for α -smooth muscle actin (α -SMA) (product #: Mm00725412_S1) and as follows for (Transforming Growth Factor β 1) TGF β 1 Forward Primer 5'-CCTGCAAGACCATCGACATG-3'; Reverse Primer 5'-ACAGGATCTGGCCACGGAT-3' and Probe 5'-FAMCTGGTGAAACGGAAGCGCATCGAA-TAMRA -3'. Results are presented as relative expression (R.E) to 18S.

5.2.4 Exercise capacity

The animals run on a treadmill with an inclination of 5° at different speeds/time as follows: 1 min at 3m/min, 4m/min, 5m/min respectively and 3 min at 6 m/min, as a warm up. This followed by 24 min at 8m/min, 7 min at 10 m/min and 8 min at 12m/min. Mice were run until they could not maintain sufficient speed to remain off the shock grid²⁸.

5.2.5 Lung Function Testing

Mice were anesthetized 21 days after BLM administration with 70–90 mg/kg pentobarbital sodium, tracheotomized, and mechanically ventilated at a rate of 350 breaths/min, tidal volume of 6 ml/kg, and positive end-expiratory pressure of 3–4 cmH₂O with a computer-controlled small-animal ventilator (Scireq, Montreal, Canada). Once ventilated, mice were paralyzed with 1 mg/kg pancuronium bromide i.p (Sigma Aldrich, St Louis, MO) to evaluate lung mechanics and record airway pressure, volume, and airflow using a controlled piston.

Pressure-volume curves were generated by a sequential and increasing delivery of air into the lungs from resting pressure (zero volume) to total lung capacity followed by sequential expiratory steps during which air was incrementally released. The plateau pressure was recorded when airflow returned to zero at each step. To determine compliance of the lung, the Salazar-Knowles equation was applied to the pressure measurements obtained between total lung capacity (TLC) and functional residual

capacity (FRC) during the expiratory phase of the pressure-volume loop²⁹. Compliance was determined from the analysis of pressure-volume curves.

Forced oscillation technique measures the impedance (alveolar pressure to central airflow ratios) of the lung to an oscillatory flow wave controlled by the computer piston. These impedance values are applied to a mathematical model of the lung, the constant phase model³⁰. This model provides a clear distinction between central and peripheral airways and lung parenchyma. The equation of the constant phase model is

$$Z(f) = R_{aw} + i2\pi f I_{aw} + \frac{G_{ti} - iH_{ti}}{(2\pi f)^\alpha}$$

where R_{aw} = a measure of central airways resistance, I_{aw} = inertance of the gas in the airways, G_{ti} = tissue resistance, H_{ti} = tissue elasticity and $i = \sqrt{-1}$. The computer-controlled piston applies a 1.25 to 8-s perturbation to the lungs consisting of priming frequencies from 1 to 20.5 Hz. Multiple linear regression is used to fit impedance spectra derived from measured pressure and volume changes to the constant phase model of the lung.

To ensure proper recruitment of all alveolar spaces, three pressure-volume curves were generated for each animal. After this maneuver, a 3-s prime wave was performed followed by a second pressure-volume curve to obtain reported values. Each perturbation was followed by 10s of ventilation before the next measurement was taken^{29, 30}.

5.2.6 Lung Histology

The right bronchus was ligated and the left lung inflated with 10% formaldehyde at a pressure of 20 cm H₂O for histology. Inflation fixed lungs were then embedded in paraffin, sectioned as described²⁸ and stained with trichrome Masson's; muscles and cells are stained red, nuclei black and collagen blue. For histologic evaluation of the lungs, four midlung sections per lung were examined.

5.2.7 Hydroxyproline Assay

Mice lungs were harvested 21 days after BLM/saline administration and perfused with heparinized saline to remove blood. The right bronchus was ligated and each of the 4 right lobes was weighted, snap frozen in liquid nitrogen and stored at -80°C , for hydroxyproline and total collagen content assays. Briefly, lungs were homogenized, incubated in 50% trichloroacetic acid (Sigma Aldrich, St Louis, MO) and hydrolyzed with 12N HCl. Samples were then baked at 110°C for 12 hours. Hydroxyproline is oxidized using chloramine T (Fluka,) and pink colored with Ehrlich's solution (Sigma, St Louis, MO). The concentration of hydroxyproline is calculated against a hydroxyproline standard curve and the values of the samples are normalized to dry tissue weight, expressed as $\mu\text{g}/\text{mg}$ ^{31,32}.

5.2.8 Lung Collagen Content

Collagen content of the lung was determined by assaying soluble collagen using the Sircol Collagen Assay kit, a modification of the sirius red method (Biocolor, Belfast, Northern Ireland), according to the manufacturer's instructions. Briefly, frozen samples were thawed, incubated at 4°C overnight in lysis buffer according to tissue weight (0.5 M acetic acid and protein inhibitor cocktail, Sigma Aldrich, St Louis MO). Supernatants (50 μl) were added to 1 mL of Sircol Dye Reagent and then mixed for 30 minutes at room temperature in a mechanical shaker. The collagen-dye complex was precipitated by centrifugation at $10000 \times g$ for 10 min. The unbound dye solution was carefully removed. The precipitated complex was resuspended in 1 mL of alkali reagent. The obtained solution was placed in a 96 wells plate and evaluated in a plate reader (absorbance =540 nm). Obtained values were then compared to the standard curve as recommended to obtain absolute collagen content. Shown data represent the mean collagen content expressed as $\mu\text{g}/\text{mg}$.

5.2.9 Statistical Analysis

Data are expressed as mean \pm SE, except where stated otherwise. Statistical analysis was performed using unpaired Student's *t* test or ANOVA, *post hoc* test (least significant

difference) and Mann-Whitney as appropriate. Values were considered significant with $p < 0.05$.

5.2.10. Western Blot

Right lungs were flash-frozen in liquid nitrogen and homogenized in buffer containing an antiprotease cocktail before electrophoresis on 7.5% or 10% SDS-PAGE gels. Protein was quantified using the Bradford method. Lung expression of AT1 and AT2 receptors were quantified by densitometry, relative to a reporter (actin, 43 KDa). AT1 and AT2 primary antibodies were purchased from Santa Cruz.

5.2.11. ELISA

Right lungs were flash-frozen in liquid nitrogen and homogenized in buffer containing an antiprotease cocktail before quantitative assessment of proinflammatory cytokines keratinocyte chemoattractant (KC), tumor necrosis factor alpha (TNF α), interleukin 1 β (IL1 β), TGF β were performed using ELISA kits (R&D Systems).

5.3 Results

5.3.1 Loss of ACE2 worsens lung fibrosis in BLM-induced lung injury

The severity of lung fibrosis between groups was assessed qualitatively on trichrome Masson's stained lung sections (Figure 1A) and quantitatively by measuring mRNA levels of profibrotic genes α -SMA (Figure 1B) and TGF β 1 (Figure 1C) as well as total lung collagen/hydroxyproline content (Fig. 1 D-E). As expected, no histological changes were observed in the lungs from saline (controls) treated WT and ACE2^{-/-} animals (Figure 1A). BLM-induced loss of lung architecture and fibrosis in the parenchyma (Figure 1A) were more evident in ACE2^{-/-}-BLM compared to controls and BLM-WT mice. These changes were associated with increased expression of the fibrosis-associated genes α -SMA and TGF β 1 (Figure 1B-C) in both BLM treated groups. Collagen and hydroxyproline levels were significantly higher in ACE2^{-/-} BLM compared to controls and BLM-WT (Figure 1D, E).

5.3.2 Loss of ACE 2 worsens exercise capacity and lung function in BLM-induced lung injury

After 21 days of BLM injection, all BLM exposed animals ($ACE2^{-/y}$ and WT) exhibited a significant decrease in exercise capacity compared with saline treated control mice (Figure 2). Exercise capacity was significantly worse in BLM- $ACE2^{-/y}$ compared to BLM-WT. Likewise, BLM- $ACE2^{-/y}$ mice exhibited decreased dynamic lung compliance (Figure 3A) and increased lung elastance (Figure 3B) compared to BLM-WT.

5.3.3 Male $ACE2^{-/y}$ display worse lung fibrosis than female $ACE2^{-/-}$ in BLM-induced lung injury

Trichrome Masson's stained lung sections showed loss of lung architecture and increased fibrosis in BLM- $ACE2^{-/y}$ as compared to saline controls and BLM- $ACE2^{-/-}$ (Figure 4A). Lung fibrosis appeared significantly milder in BLM- $ACE2^{-/-}$ females. BLM- $ACE2^{-/y}$ had significantly higher levels of α -SMA (Figure 4B) and TGF β 1 (Figure 4C) mRNA and collagen deposition compared to $ACE2^{-/-}$ BLM (Figure 4D-E). Likewise, these results were associated with decreased compliance and increased elastance in BLM- $ACE2^{-/y}$ compared to female BLM- $ACE2^{-/-}$ mice (Figure 5A-B).

5.3.4 Treatment with rhACE2 improves lung architecture and function and attenuates lung collagen deposition in BLM-induced lung injury in WT mice

We examined the protective effect of rhACE2 to prevent fibrosis in BLM-induced lung injury. Treatment with rhACE2 improved survival (Figure 6A), exercise capacity (Figure 6B) and lung function (dynamic compliance and elastance, Figure 6C-D) as compared to untreated BLM-WT mice. Treatment with rhACE2 also improved lung architecture in Trichrome Masson's stained lung sections (Figure 7A). rhACE2 significantly decreased lung collagen deposition in BLM-WT+rhACE2 compared to BLM-WT (Figure 7B), as well as levels of α -SMA (Figure 7C) and TGF β 1 mRNA (Figure 7D) and protein (Figure 7E) and lung TNF α protein expression (Figure 7F) as

compared to untreated BLM-WT mice.

5.3.5 Effects of rhACE2 in male and female BLM-WT mice on lung architecture, function and lung collagen deposition WT treated mice

Finally, we examined the protective effect of rhACE2 to prevent fibrosis in female BLM-induced lung injury (Figure 8). Surprisingly, BLM challenged WT females did not exhibit fibrotic changes. Trichrome Masson's stained lung sections revealed mild lung architecture distortion in BLM WT females compared to males (Figure 8A). WT females exposed to BLM had only mild increase in lung collagen (Figure 8B) and lung hydroxyproline (Figure 8C) compared to males. Likewise, WT females had unchanged lung function (Figure 8D-E) and exercise capacity (Figure 8F) compared to BLM WT males. rhACE2 significantly attenuated lung fibrosis (Figure 8A-C) and improved lung function (Figure 8D-E) and exercise capacity (Figure 8F) in BLM WT males.

5.3.6 Angiotensin receptors in BLM induced Lung injury

In order to explain the apparent protection of female WT mice from fibrosis, we explored other component of the RAS. Lung AT1R expression was unchanged between Control and BLM exposed WT female and WT male (Figure 9A). Conversely, lung AT2R expression was significantly increased in BLM female WT as compared with control female WT and BLM male WT (Figure 9B). The AT2/AT1 receptor ratio was significantly increased in BLM WT female (Figure 9C) compared to all other groups.

5.4 Discussion

We observed that ACE2 gene deletion aggravates BLM-induced lung injury. Conversely, rhACE2 treatment improves lung function and exercise capacity and attenuates lung fibrosis in BLM-induced lung injury. In addition, we found that BLM-induced lung injury was worse in ACE2 deficient male than female mice. Overall, our data suggest a protective role for rhACE2 in experimental ALI/ARDS.

5.4.1 ACE2 in lung injury and repair

Recent evidence suggests that the RAS has important functions outside the cardiovascular system. Latest since ACE2 was identified as a key receptor for coronavirus infections responsible for the severe acute respiratory syndrome (SARS)¹⁴ major attention has been drawn to the potential protective role of ACE2 in lung diseases. In three different ALI/ARDS models (acid-aspiration-induced ARDS, endotoxin-induced ARDS, and peritoneal sepsis-induced), ACE2 knockout mice exhibit exacerbated lung injury compared with WT mice¹²: loss of ACE2 caused enhanced vascular permeability, increased lung edema, neutrophil accumulation, and worsened lung function. Importantly, treatment with catalytically active recombinant ACE2 protein improved the symptoms of ALI in WT mice, as well as in ACE2 knockout mice¹². Furthermore, lung injury in experimental ARDS in mice can be attenuated by blocking the RAS¹². One complication of ARDS is lung fibrosis. Li et al³³ have demonstrated that ACE2 mRNA and activity are downregulated in human and experimental lung fibrosis and suggest that ACE2 limits the local accumulation of ANG II. Previous studies have not assessed the effect of ACE2 deletion on long-term complications of ALI/ARDS such as lung fibrosis. Our data demonstrates that loss of ACE2 aggravates exercise capacity, lung function and worsens subsequent lung fibrosis in BLM-induced experimental lung injury.

Currently, there is no efficacious pharmacological therapy to prevent the onset of pulmonary fibrosis post ALI/ARDS⁷. Consequently, we explored the therapeutic potential of rhACE2 to attenuate BLM-induced lung injury. rhACE2 improved survival, exercise capacity and lung function and abrogated lung fibrosis in this model. Our data are in accordance with recent findings showing that lentiviral packaged ANG-(1-7) fusion gene or ACE2 cDNA prevents BLM-induced lung fibrosis in male Sprague Dawley rats³⁴. This is also consistent with recent reports showing a protective effect of ACE2 in preventing fibrosis in other organs such as ANGII-induced cardiac hypertrophy and in diabetic nephropathy^{22, 24}. Our data provide additional proof of principle for the therapeutic benefit of ACE2 in improving lung function and structure post-ALI/ARDS. The therapeutic implications of these findings could potentially translate into decreased morbidity and mortality in ALI/ARDS patients.

6.2 Gender differences in the susceptibility of ACE2 knockout mice to BLM induced lung injury

In this study, we found gender differences in ACE2^{-/-} mice in BLM-induced lung injury. Men with idiopathic pulmonary fibrosis have decreased quality of life compared to women³⁵. In rodents, castrated male mice exhibited a female-like response to BLM while female mice given exogenous androgen exhibited a male-like response, suggesting a detrimental role of androgens in pulmonary function in fibrosis³⁶. Interestingly, in BLM-induced fibrosis in rats, female hormones appeared to have a detrimental role in BLM-exposed female compared to males³⁷. In our study, the effects of BLM in female ACE2^{-/-} mice were not only milder compared to male knock-out mice, but also milder compared to male Wt mice. These contradictory results, could potentially be explained by differences in species³⁸ and BLM doses. In our study, we selected a low to middle BLM dose in which a balance between survival and fibrotic response (functional and histological) was achieved. It is recognized that lung function correlates more directly with poor prognosis than fibrotic end-points³⁹. In our study, male mice exhibited a significant decline in compliance compared to females. Our data shows significantly worse lung function and higher lung collagen deposition in male ACE2 knockouts compared to females. This gender-based difference could suggest a hormonal involvement in the pathophysiology of BLM-induced lung injury. Indeed, 17 β -estradiol-mediated upregulation of ACE2 protects the kidney from the progression of hypertensive renal disease and female ACE2 knockout mice showed minimal age-related renal injury^{40, 41}. Likewise, other anti-fibrotic agents (i.e relaxin, an insulin-like hormone secreted during pregnancy with a demonstrated antifibrotic effect in experimentally induced pulmonary fibrosis) may play a role in the decreased collagen deposition seen in females⁴². Recently, Reis et al. reported that ANG-(1-7), its receptor Mas, and ACE2 are expressed in the human ovary⁴³. This could imply a constant endogenous source of ACE2 that would confer further cardiovascular protection. Besides estrogens, this could provide another explanation for cardiopulmonary protection in females.

Under no disease process, there is evidence that 17β -estradiol exerts differential regulation on components of the RAS, modifying both mostly AT1 receptor genes. In the lung 17β -estradiol administration downregulated AT1 receptor expression. However, no significant interaction in the regulation of AT2 receptor mRNA was evident⁴⁴. Waseda et al⁴⁵ demonstrated that both AT1 and AT2 aid in the pro-fibrotic effect of BLM in the lungs. In our study, lung AT1R expression was unchanged between control and BLM exposed WT female and WT male (Figure 9A). Conversely, lung AT2R expression was significantly increased in BLM female WT as compared with control female WT and BLM male WT (Figure 9B). The AT2/AT1 receptor ratio was significantly increased in BLM WT female (Figure 9C) compared to all other groups. This suggests that a compensatory increase in AT2 could be in part responsible for the decreased fibrosis seen in BLM WT females.

In conclusion, ACE2 exerts a protective effect in BLM-induced lung injury. Human recombinant ACE2 may have therapeutic potential to prevent lung fibrosis after ALI/ARDS. Attenuated fibrosis in BLM exposed ACE2^{-/-} mice compared with ACE2^{-y} suggest a hormonal involvement in lung fibrosis post ALI/ARDS.

5.5 References

1. Ashbaugh DG, Bigelow DB, Petty TL, Levine BE. Acute respiratory distress in adults. *Lancet*. 1967;2:319-323
2. Ware LB, Matthay MA. The acute respiratory distress syndrome. *N Engl J Med*. 2000;342:1334-1349
3. Orme J, Jr., Romney JS, Hopkins RO, Pope D, Chan KJ, Thomsen G, Crapo RO, Weaver LK. Pulmonary function and health-related quality of life in survivors of acute respiratory distress syndrome. *Am J Respir Crit Care Med*. 2003;167:690-694
4. Miwa C, Koyama S, Watanabe Y, Tsubochi H, Endo S, Nokubi M, Kawabata Y. Pathological findings and pulmonary dysfunction after acute respiratory distress syndrome for 5 years. *Intern Med*. 2010;49:1599-1604
5. Davidson TA, Caldwell ES, Curtis JR, Hudson LD, Steinberg KP. Reduced quality of life in survivors of acute respiratory distress syndrome compared with critically ill control patients. *JAMA*. 1999;281:354-360
6. Briel M, Meade M, Mercat A, Brower RG, Talmor D, Walter SD, Slutsky AS, Pullenayegum E, Zhou Q, Cook D, Brochard L, Richard JC, Lamontagne F, Bhatnagar N, Stewart TE, Guyatt G. Higher vs lower positive end-expiratory pressure in patients with acute lung injury and acute respiratory distress syndrome: Systematic review and meta-analysis. *JAMA*. 2010;303:865-873
7. Cepkova M, Matthay MA. Pharmacotherapy of acute lung injury and the acute respiratory distress syndrome. *J Intensive Care Med*. 2006;21:119-143
8. Peter JV, John P, Graham PL, Moran JL, George IA, Bersten A. Corticosteroids in the prevention and treatment of acute respiratory distress syndrome (ARDS) in adults: Meta-analysis. *BMJ*. 2008;336:1006-1009

9. Afshari A, Brok J, Moller AM, Wetterslev J. Aerosolized prostacyclin for acute lung injury (ali) and acute respiratory distress syndrome (ards). *Cochrane Database Syst Rev.* 2010:CD007733
10. Putensen C, Theuerkauf N, Zinserling J, Wrigge H, Pelosi P. Meta-analysis: Ventilation strategies and outcomes of the acute respiratory distress syndrome and acute lung injury. *Ann Intern Med.* 2009;151:566-576
11. Rockx B, Baas T, Zornetzer GA, Haagmans B, Sheahan T, Frieman M, Dyer MD, Teal TH, Proll S, van den Brand J, Baric R, Katze MG. Early upregulation of acute respiratory distress syndrome-associated cytokines promotes lethal disease in an aged-mouse model of severe acute respiratory syndrome coronavirus infection. *J Virol.* 2009;83:7062-7074
12. Imai Y, Kuba K, Rao S, Huan Y, Guo F, Guan B, Yang P, Sarao R, Wada T, Leong-Poi H, Crackower MA, Fukamizu A, Hui CC, Hein L, Uhlig S, Slutsky AS, Jiang C, Penninger JM. Angiotensin-converting enzyme 2 protects from severe acute lung failure. *Nature.* 2005;436:112-116
13. Kuba K, Imai Y, Rao S, Gao H, Guo F, Guan B, Huan Y, Yang P, Zhang Y, Deng W, Bao L, Zhang B, Liu G, Wang Z, Chappell M, Liu Y, Zheng D, Leibbrandt A, Wada T, Slutsky AS, Liu D, Qin C, Jiang C, Penninger JM. A crucial role of angiotensin converting enzyme 2 (ace2) in sars coronavirus-induced lung injury. *Nat Med.* 2005;11:875-879
14. Li W, Moore MJ, Vasilieva N, Sui J, Wong SK, Berne MA, Somasundaran M, Sullivan JL, Luzuriaga K, Greenough TC, Choe H, Farzan M. Angiotensin-converting enzyme 2 is a functional receptor for the sars coronavirus. *Nature.* 2003;426:450-454
15. Marshall RP, McAnulty RJ, Laurent GJ. Angiotensin ii is mitogenic for human lung fibroblasts via activation of the type 1 receptor. *Am J Respir Crit Care Med.* 2000;161:1999-2004
16. Marshall RP, Gohlke P, Chambers RC, Howell DC, Bottoms SE, Unger T, McAnulty RJ, Laurent GJ. Angiotensin ii and the fibroproliferative

- response to acute lung injury. *Am J Physiol Lung Cell Mol Physiol*. 2004;286:L156-164
17. Imai Y, Slutsky AS. High-frequency oscillatory ventilation and ventilator-induced lung injury. *Crit Care Med*. 2005;33:S129-134
 18. Wang D, Morales JE, Calame DG, Alcorn JL, Wetsel RA. Transplantation of human embryonic stem cell-derived alveolar epithelial type ii cells abrogates acute lung injury in mice. *Mol Ther*. 2010;18:625-634
 19. Xie X, Chen J, Wang X, Zhang F, Liu Y. Age- and gender-related difference of ace2 expression in rat lung. *Life Sci*. 2006;78:2166-2171
 20. Casey J, Kaplan J, Atochina-Vasserman EN, Gow AJ, Kadire H, Tomer Y, Fisher JH, Hawgood S, Savani RC, Beers MF. Alveolar surfactant protein d content modulates bleomycin-induced lung injury. *Am J Respir Crit Care Med*. 2005;172:869-877
 21. Zhong J, Guo D, Chen CB, Wang W, Schuster M, Loibner H, Penninger JM, Scholey JW, Kassiri Z, Oudit GY. Prevention of angiotensin ii-mediated renal oxidative stress, inflammation, and fibrosis by angiotensin-converting enzyme 2. *Hypertension*. 2011;57:314-322
 22. Oudit GY, Liu GC, Zhong J, Basu R, Chow FL, Zhou J, Loibner H, Janzek E, Schuster M, Penninger JM, Herzenberg AM, Kassiri Z, Scholey JW. Human recombinant ace2 reduces the progression of diabetic nephropathy. *Diabetes*. 2010;59:529-538
 23. Wysocki J, Ye M, Rodriguez E, Gonzalez-Pacheco FR, Barrios C, Evora K, Schuster M, Loibner H, Brosnihan KB, Ferrario CM, Penninger JM, Battle D. Targeting the degradation of angiotensin ii with recombinant angiotensin-converting enzyme 2: Prevention of angiotensin ii-dependent hypertension. *Hypertension*. 2010;55:90-98
 24. Zhong J, Basu R, Guo D, Chow FL, Byrns S, Schuster M, Loibner H, Wang XH, Penninger JM, Kassiri Z, Oudit GY. Angiotensin-converting enzyme 2 suppresses pathological hypertrophy, myocardial fibrosis, and cardiac dysfunction. *Circulation*. 2010;122:717-728, 718 p following 728

25. Wong DW, Oudit GY, Reich H, Kassiri Z, Zhou J, Liu QC, Backx PH, Penninger JM, Herzenberg AM, Scholey JW. Loss of angiotensin-converting enzyme-2 (ace2) accelerates diabetic kidney injury. *Am J Pathol.* 2007;171:438-451
26. Kassiri Z, Oudit GY, Sanchez O, Dawood F, Mohammed FF, Nuttall RK, Edwards DR, Liu PP, Backx PH, Khokha R. Combination of tumor necrosis factor-alpha ablation and matrix metalloproteinase inhibition prevents heart failure after pressure overload in tissue inhibitor of metalloproteinase-3 knock-out mice. *Circ Res.* 2005;97:380-390
27. Zhong JC, Ye JY, Jin HY, Yu X, Yu HM, Zhu DL, Gao PJ, Huang DY, Shuster M, Loibner H, Guo JM, Yu XY, Xiao BX, Gong ZH, Penninger JM, Oudit GY. Telmisartan attenuates aortic hypertrophy in hypertensive rats by the modulation of ace2 and profilin-1 expression. *Regul Pept.* 2011;166:90-97
28. van Haaften T, Byrne R, Bonnet S, Rochefort GY, Akabutu J, Bouchentouf M, Rey-Parra GJ, Galipeau J, Haromy A, Eaton F, Chen M, Hashimoto K, Abley D, Korbitt G, Archer SL, Thebaud B. Airway delivery of mesenchymal stem cells prevents arrested alveolar growth in neonatal lung injury in rats. *Am J Respir Crit Care Med.* 2009;180:1131-1142
29. Lovgren AK, Jania LA, Hartney JM, Parsons KK, Audoly LP, Fitzgerald GA, Tilley SL, Koller BH. Cox-2-derived prostacyclin protects against bleomycin-induced pulmonary fibrosis. *Am J Physiol Lung Cell Mol Physiol.* 2006;291:L144-156
30. Hantos Z, Daroczy B, Suki B, Nagy S, Fredberg JJ. Input impedance and peripheral inhomogeneity of dog lungs. *J Appl Physiol.* 1992;72:168-178
31. Reddy GK, Enwemeka CS. A simplified method for the analysis of hydroxyproline in biological tissues. *Clin Biochem.* 1996;29:225-229
32. Woessner JF, Jr. The determination of hydroxyproline in tissue and protein samples containing small proportions of this imino acid. *Arch Biochem Biophys.* 1961;93:440-447

33. Li X, Molina-Molina M, Abdul-Hafez A, Uhal V, Xaubet A, Uhal BD. Angiotensin converting enzyme-2 is protective but downregulated in human and experimental lung fibrosis. *Am J Physiol Lung Cell Mol Physiol.* 2008;295:L178-185
34. Shenoy V, Ferreira AJ, Qi Y, Fraga-Silva RA, Diez-Freire C, Dooies A, Jun JY, Sriramula S, Mariappan N, Pourang D, Venugopal CS, Francis J, Reudelhuber T, Santos RA, Patel JM, Raizada MK, Katovich MJ. The angiotensin-converting enzyme 2/angiogenesis-(1-7)/mas axis confers cardiopulmonary protection against lung fibrosis and pulmonary hypertension. *Am J Respir Crit Care Med.* 2010;182:1065-1072
35. Han MK, Swigris J, Liu L, Bartholmai B, Murray S, Giardino N, Thompson B, Frederick M, Li D, Schwarz M, Limper A, Flaherty K, Martinez FJ. Gender influences health-related quality of life in ipf. *Respir Med.* 2010;104:724-730
36. Voltz JW, Card JW, Carey MA, Degraff LM, Ferguson CD, Flake GP, Bonner JC, Korach KS, Zeldin DC. Male sex hormones exacerbate lung function impairment after bleomycin-induced pulmonary fibrosis. *Am J Respir Cell Mol Biol.* 2008;39:45-52
37. Gharaee-Kermani M, Hatano K, Nozaki Y, Phan SH. Gender-based differences in bleomycin-induced pulmonary fibrosis. *Am J Pathol.* 2005;166:1593-1606
38. Kolb M, Bonniaud P, Galt T, Sime PJ, Kelly MM, Margetts PJ, Gauldie J. Differences in the fibrogenic response after transfer of active transforming growth factor-beta1 gene to lungs of "Fibrosis-prone" And "Fibrosis-resistant" Mouse strains. *Am J Respir Cell Mol Biol.* 2002;27:141-150
39. Jegal Y, Kim DS, Shim TS, Lim CM, Do Lee S, Koh Y, Kim WS, Kim WD, Lee JS, Travis WD, Kitaichi M, Colby TV. Physiology is a stronger predictor of survival than pathology in fibrotic interstitial pneumonia. *Am J Respir Crit Care Med.* 2005;171:639-644
40. Ji H, Menini S, Zheng W, Pesce C, Wu X, Sandberg K. Role of angiotensin-converting enzyme 2 and angiotensin(1-7) in 17beta-

- oestradiol regulation of renal pathology in renal wrap hypertension in rats. *Exp Physiol.* 2008;93:648-657
41. Oudit GY, Herzenberg AM, Kassiri Z, Wong D, Reich H, Khokha R, Crackower MA, Backx PH, Penninger JM, Scholey JW. Loss of angiotensin-converting enzyme-2 leads to the late development of angiotensin ii-dependent glomerulosclerosis. *Am J Pathol.* 2006;168:1808-1820
 42. Tang ML, Samuel CS, Royce SG. Role of relaxin in regulation of fibrosis in the lung. *Ann N Y Acad Sci.* 2009;1160:342-347
 43. Reis FM, Bouissou DR, Pereira VM, Camargos AF, dos Reis AM, Santos RA. Angiotensin-(1-7), its receptor mas, and the angiotensin-converting enzyme type 2 are expressed in the human ovary. *Fertil Steril.* 2011;95:176-181
 44. Brosnihan KB, Hodgins JB, Smithies O, Maeda N, Gallagher P. Tissue-specific regulation of ace/ace2 and at1/at2 receptor gene expression by oestrogen in apolipoprotein e/oestrogen receptor-alpha knock-out mice. *Exp Physiol.* 2008;93:658-664
 45. Waseda Y, Yasui M, Nishizawa Y, Inuzuka K, Takato H, Ichikawa Y, Tagami A, Fujimura M, Nakao S. Angiotensin ii type 2 receptor antagonist reduces bleomycin-induced pulmonary fibrosis in mice. *Respir Res.* 2008;9:43

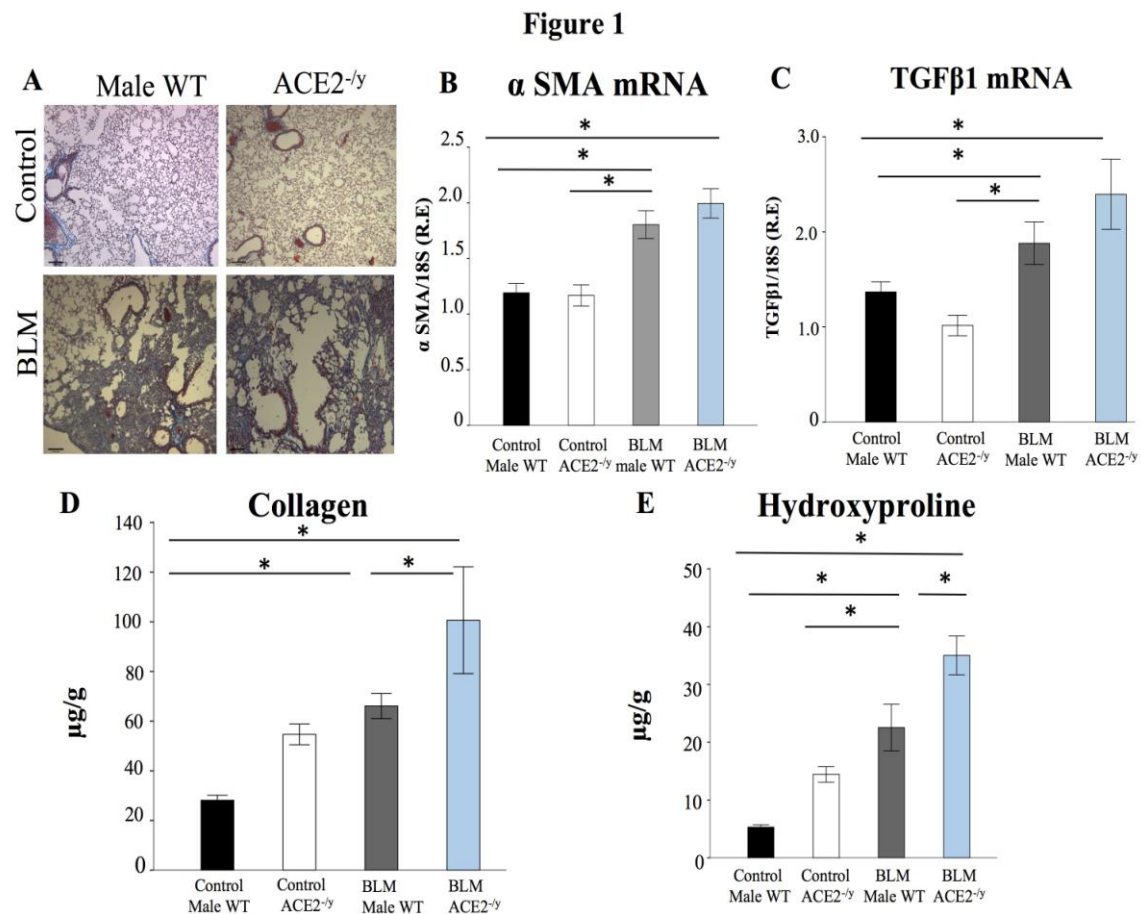


Figure 5.1. ACE2 deletion worsens lung fibrosis in BLM-induced lung injury. **A)** Representative Trichrome Masson's histological sections. BLM-induced lung injury, evidenced by loss of lung architecture and collagen deposition (blue), is more evident in BLM-ACE2^{-/-} compared to BLM-WT mice. **B, C)** Lung α SMA and TGF β 1 mRNA are significantly increased in BLM ACE2^{-/-} and WT BLM compared to WT and ACE2^{-/-} controls. R.E (relative exposure to 18S). **D, E)** Lung collagen and hydroxyproline content were significantly increased in BLM ACE2^{-/-} compared to WT and controls. Mean data \pm SEM. N=4-7/group, *p<0.05.

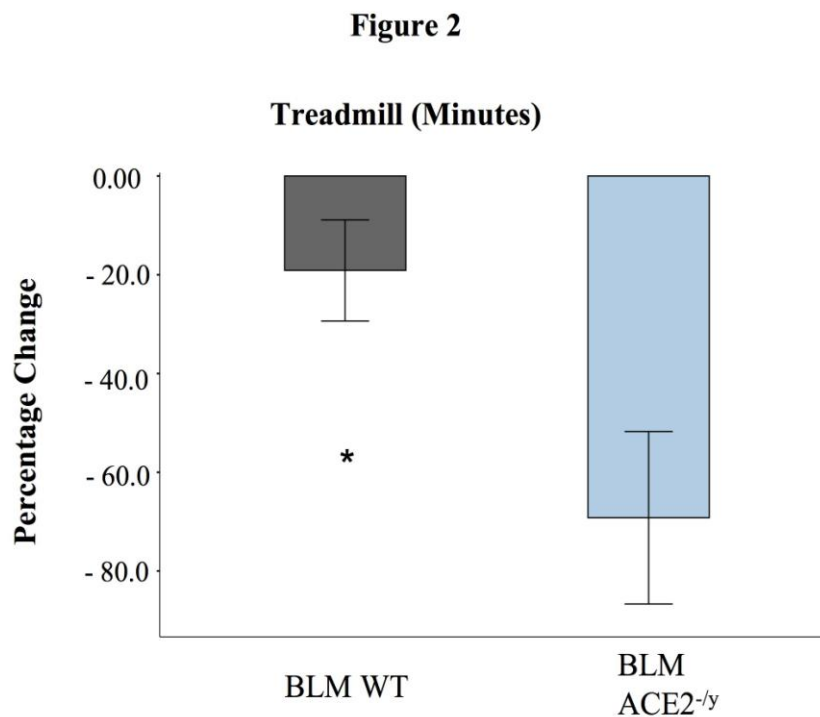


Figure 5.2. Exercise capacity in BLM induced lung injury in WT and ACE2^{-/-}. ACE2 deletion worsens exercise capacity 21 days after BLM exposure. Percentage change respective to controls (male WT and ACE2^{-/-} unexposed to BLM) \pm SEM. N=5-7/group, * p <0.05.

Figure 3

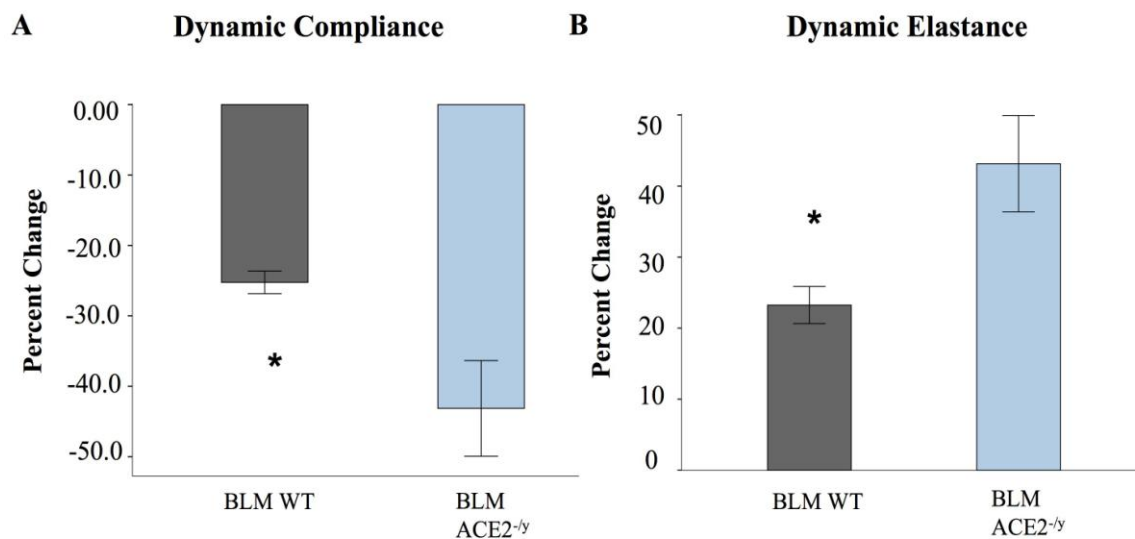


Figure 5.3. Changes in lung mechanics at 21 days in BLM induced fibrosis in WT and ACE2^{-/-}. **A)** Dynamic compliance is decreased in BLM challenged ACE2^{-/-} mice compared to BLM-WT. Data are expressed as percentage change respective to controls (male WT and ACE2^{-/-} unexposed to BLM) \pm SEM. **B)** Dynamic Elastance is increased in ACE2^{-/-} mice compared to BLM-WT, data expressed as percentage change respective to controls \pm SEM. N=4-7/group, * p<0.05.

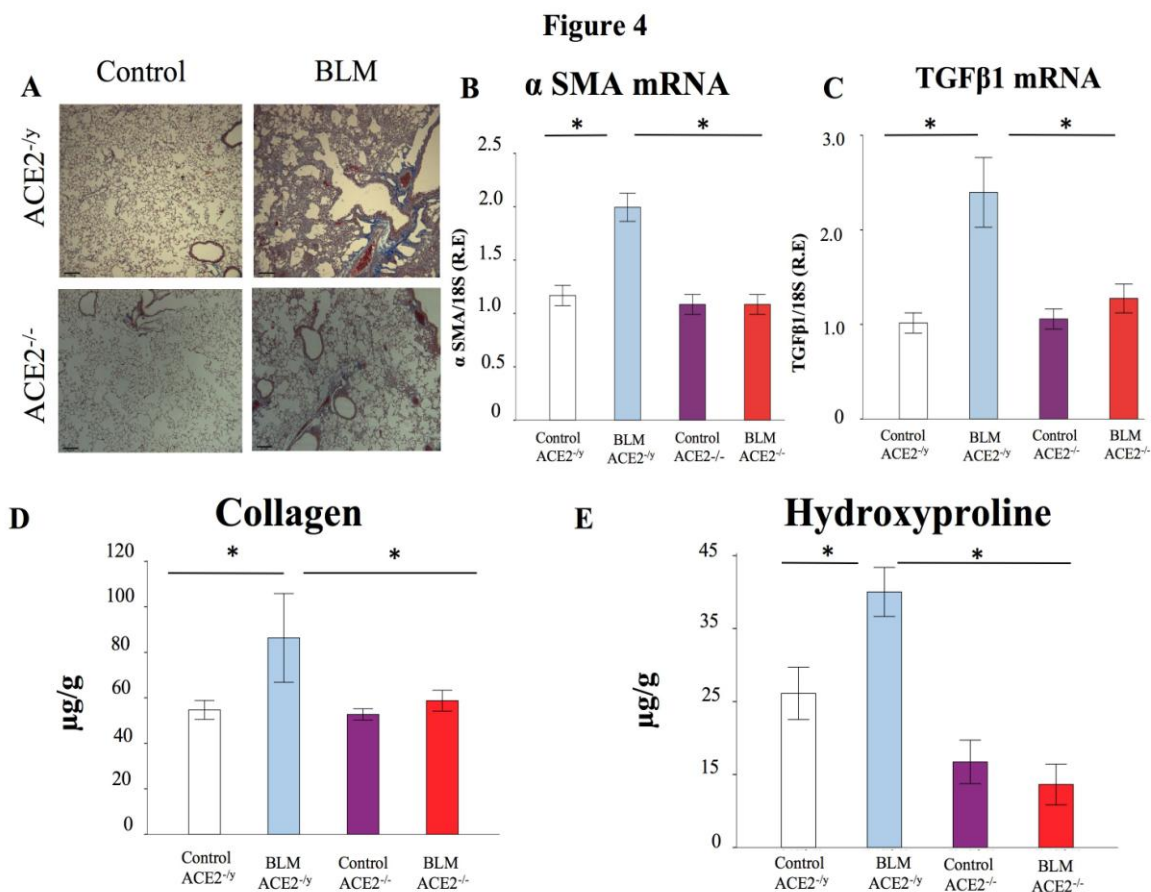


Figure 5.4. Gender differences in response to BLM-induced lung injury. **A)** Representative Trichrome Masson's histological sections. BLM ACE2^{-/-} shows milder disruption of lung architecture as compared to BLM ACE2^{-y} group. **B, C)** Lung α SMA and TGF β 1 mRNA are significantly decreased in BLM ACE2^{-/-} compared to BLM ACE2^{-y}. Mean data \pm SEM. R.E (relative exposure to 18S). **D, E)** Lung total collagen and hydroxyproline content are increased in BLM ACE2^{-y} compared to BLM ACE2^{-/-}. Mean data \pm SEM. N=4-7/group, * p<0.05.

Figure 5

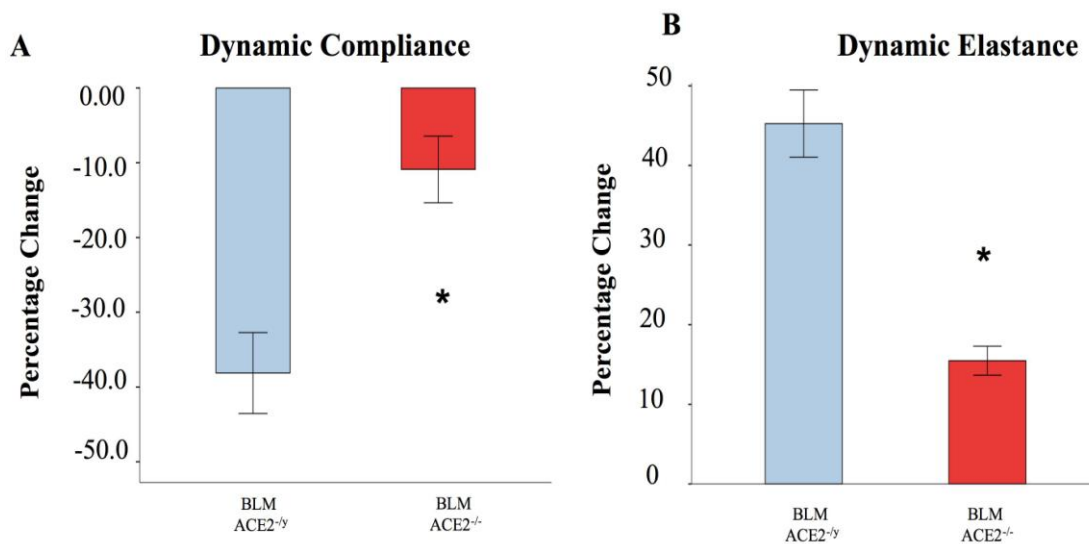


Figure 5.5. Lung function in ACE2 knockout mice. **A)** Dynamic Compliance is significantly decreased in BLM ACE2^{-/-} compared to ACE2^{-/-}. **B)** Dynamic Elastance is increased in ACE2^{-/-} BLM compared to BLM ACE2^{-/-}. Data expressed as percentage change respective to controls (ACE2^{-/-} and ACE2^{-/-} unexposed to BLM) \pm SEM. N=5-7/group, *p<0.05.

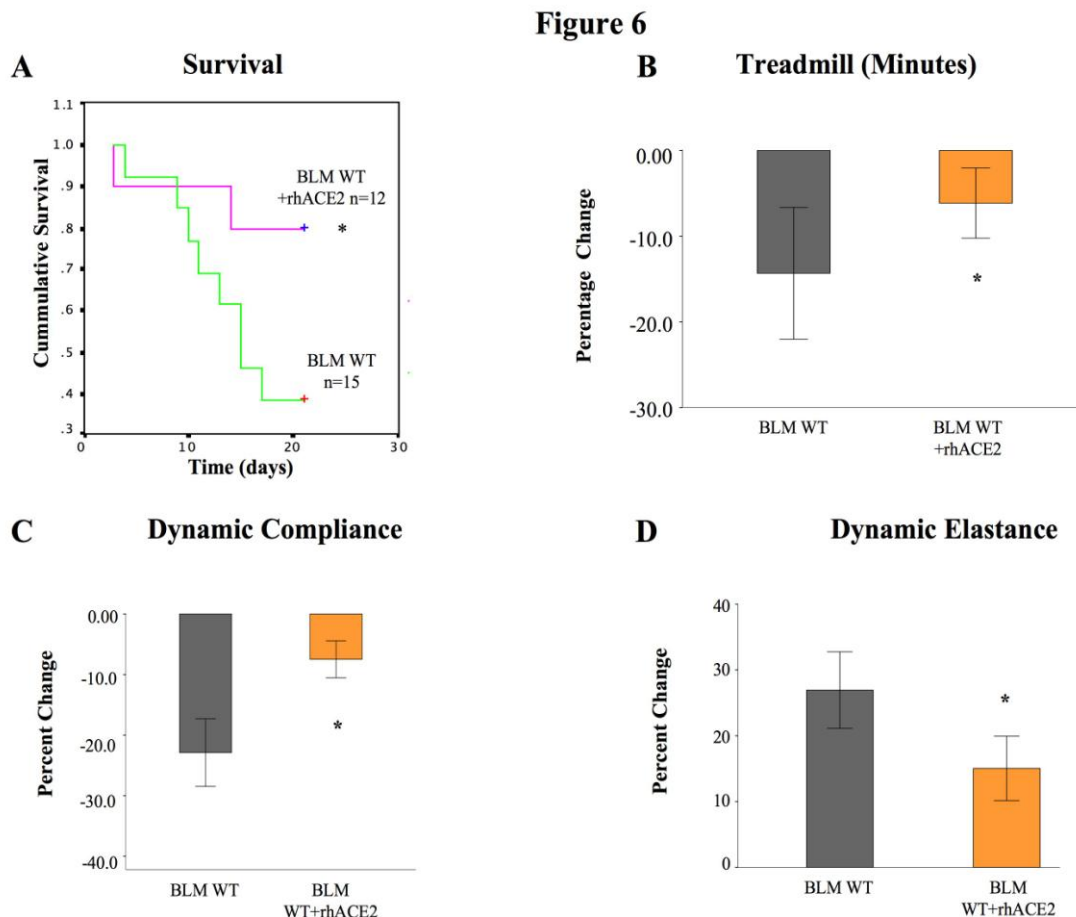


Figure 5.6. Survival, lung function and exercise capacity in BLM-WT mice and BLM WT+rhACE2 treated mice. **A)** Cumulative survival of BLM-WT mice and BLM WT+rhACE2 treated mice. rhACE2 treatment significantly improved survival compared to untreated BLM-WT mice. N=12-15/group, * $p < 0.05$. **B)** rhACE2 treatment improves exercise capacity compared to untreated WT BLM mice. **C-D)** rhACE2 treatment improves lung function: dynamic compliance is significantly increased in BLM-WT+rhACE2 compared to BLM-WT; Dynamic Elastance is significantly decreased in BLM-WT+rhACE2. Data expressed as percentage change respective to controls (male WT unexposed to BLM) \pm SEM. N=4-7/group, * $p < 0.05$.

Figure 7

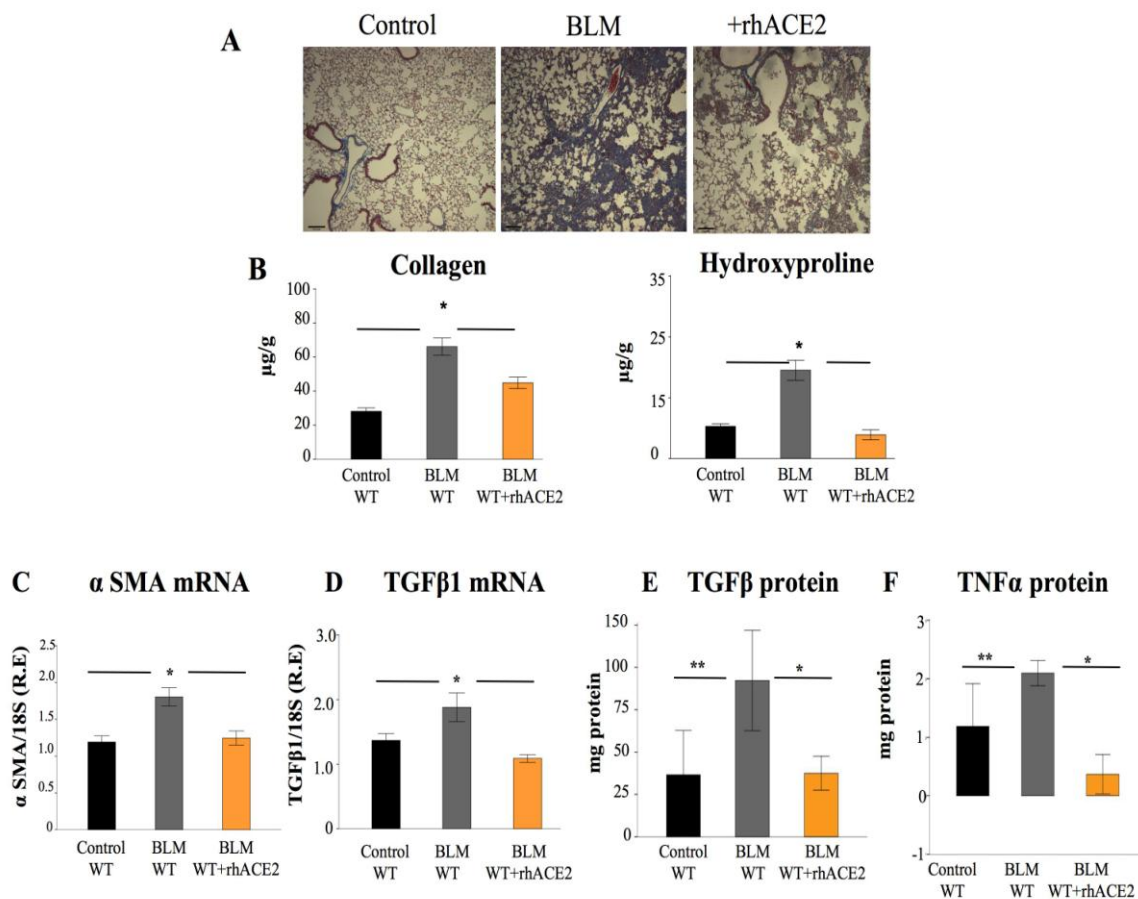


Figure 5.7. Histology and collagen deposition in BLM-WT mice and BLM WT+rhACE2 treated mice. **A)** Representative Trichrome Masson's histological sections. BLM-WT+rhACE2 showed improved lung architecture as compared to BLM-WT mice. **B)** Lung total collagen content and hydroxyproline are decreased in BLM-WT+rhACE2 compared to untreated BLM-WT mice. Mean data \pm SEM. **C-F)** Lung α SMA and TGF β 1 mRNA and protein as well as TNF α are significantly decreased in BLM-WT+rhACE2 compared to WT BLM mice. Mean data \pm SEM. R.E (relative exposure to 18S).

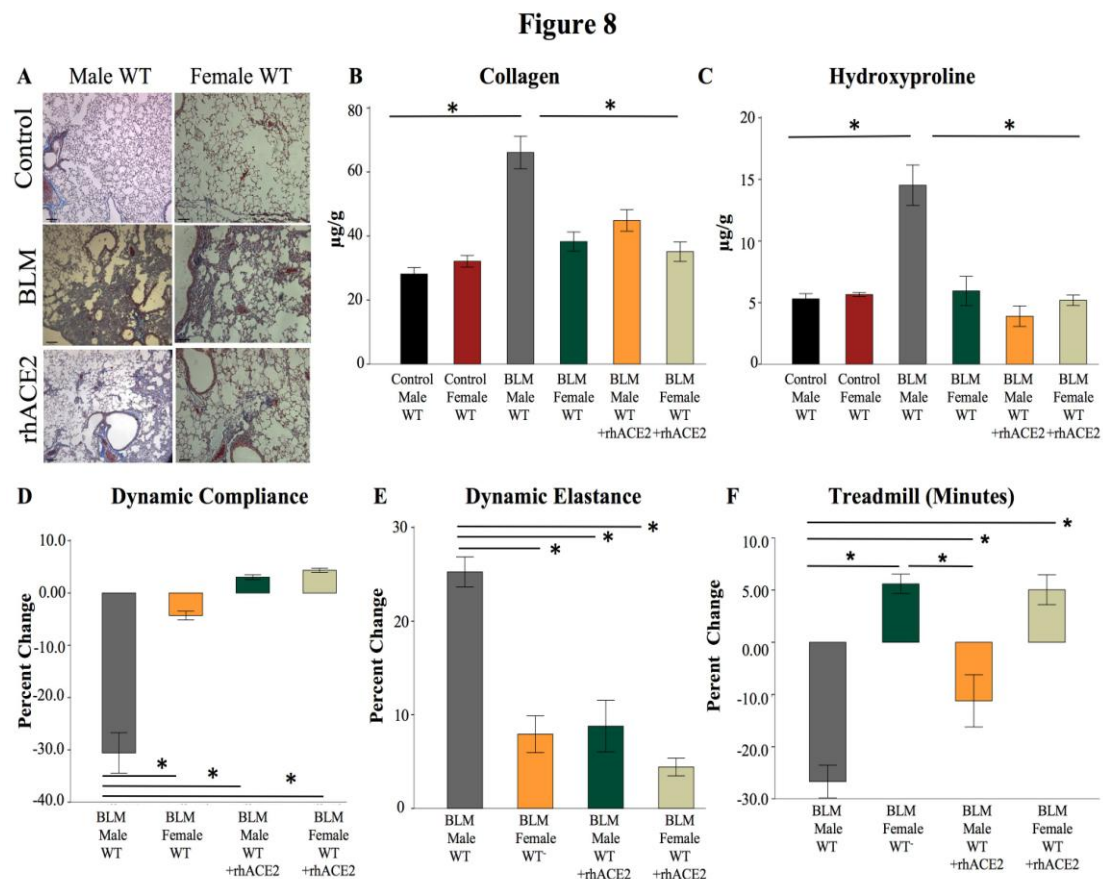


Figure 5.8. Histology, collagen deposition, exercise capacity and lung function testing in BLM-WT female mice and BLM-female WT+rhACE2 treated mice. **A)** Representative Trichrome Masson's histological sections. BLM-female WT showed decreased lung architecture distortion as compared to BLM-male WT mice. Moreover, rhACE2 further improved lung architecture in BLM-female WT. **B-C)** Lung total collagen content and hydroxyproline are decreased in BLM-female WT, BLM-female WT+rhACE2 and BLM-male WT+rhACE2, compared to untreated BLM-male WT mice. Mean data \pm SEM. **D-E)** BLM-female WT exhibit similar lung function to untreated controls and BLM-male WT+rhACE2: dynamic compliance is significantly increased in BLM-female WT and BLM-female WT+rhACE2 compared to BLM-male WT; Dynamic Elastance is significantly decreased in BLM-female WT and BLM-female WT+rhACE2 compared to BLM-male WT. **F)** Exercise capacity was unchanged in female treated and untreated groups compared to BLM-male WT. Data expressed as percentage change respective to controls (male and female WT unexposed to BLM) \pm SEM. N=4-7/group, * p <0.05.

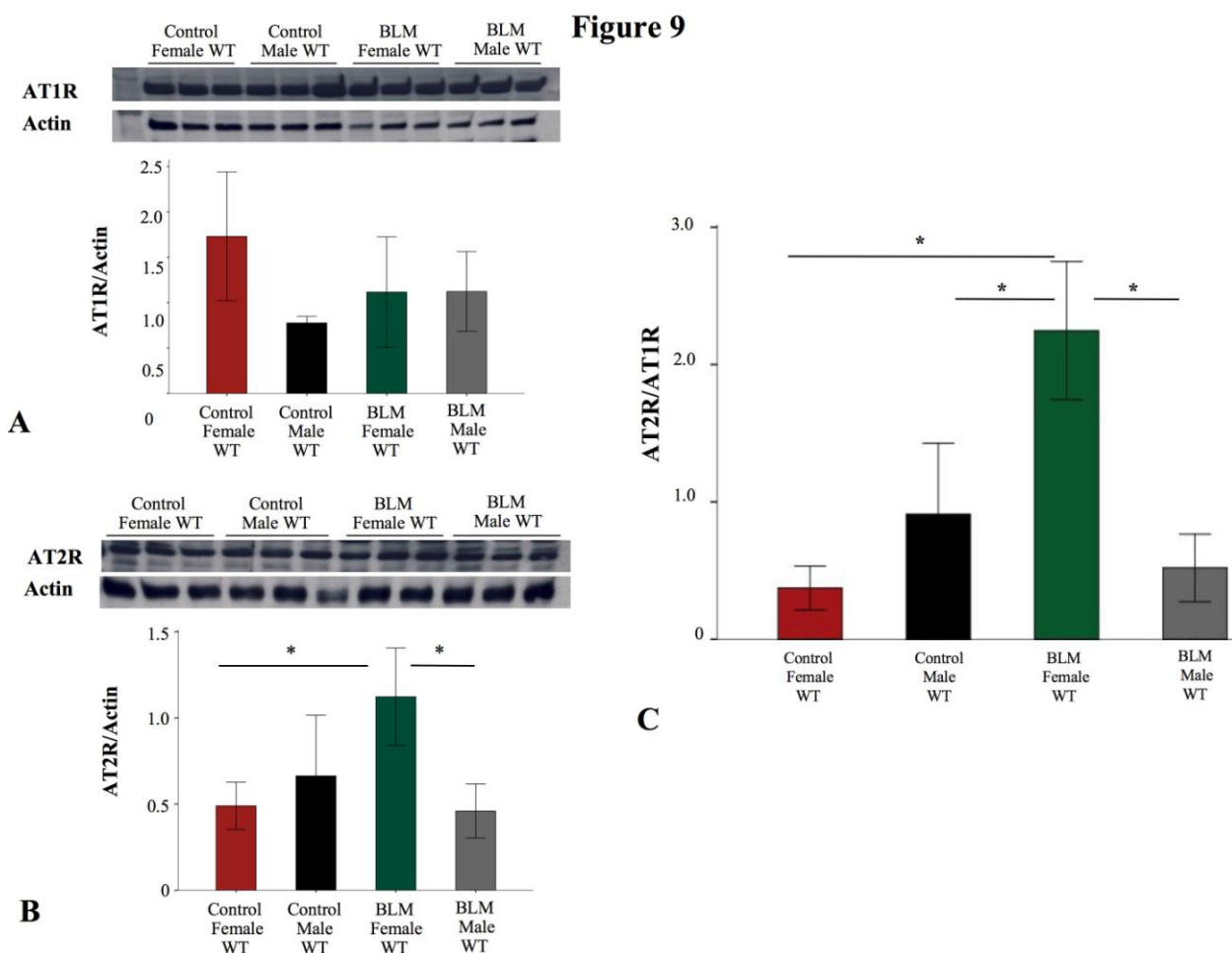


Figure 5.9. Representative immunoblots for lung AT1R and Actin expression in WT mice. A. Representative immunoblots for lung AT1R and Actin (control) expression in lung homogenates from WT control males/females and BLM WT challenged male and female mice and mean densitometry for lung AT1R expression. B. Representative immunoblots for lung AT2R and Actin (control) expression in lung homogenates from WT control males/females and BLM WT challenged male and female mice and mean densitometry for lung AT2R expression. C. AT2/AT1 receptor ratio is significantly increased in WT BLM challenged females. \pm SEM. N=3/group, * p <0.05.

CHAPTER 6

CONCLUSIONS, LIMITATIONS AND FUTURE DIRECTIONS

6.1 Conclusions

In our quest to discover new treatment options for incurable lung diseases, we explored the healing capacity after acute and chronic lung injury in a mammal model of regeneration. In addition, we tested the therapeutic potential of HUCBC and a putative lung protective factor derived from HUCB (ACE2) in a rodent model of ARDS complicated by lung fibrosis.

In Chapter 2, we reported the novel observation that the healer strain of MRL/MPJ mice are protected against LPS-induced ALI/ARDS, partially through an attenuated inflammatory response. We also identified an accelerated healing potential of their AT2 cells. In chapter 3, we showed in another model of lung injury - BLM induced fibrosis no differences between the non-healer control mice and MRL/MPJ.

In chapter 4, we provided proof of concept that HUCBC (after 10 years of cryopreservation) decreased collagen deposition and improved functional parameters in BLM induced fibrosis. We also found that HUCB had a low engraftment rate, in concordance with findings by other authors^{1-2, 3}, suggesting that other mechanisms may account for the therapeutic benefit of cell therapy. Thus we found that (a) *in vitro*, BLM exposed fibroblast treated with HUCBC Cdm exhibit decreased levels of the profibrotic growth factor TGF- β 1 and that (b) HUCBC secrete known antifibrotic mediators such as relaxin and ACE2⁴⁻⁸. These may be responsible for the beneficial paracrine effects seen with HUCBC administration.

In Chapter 5, we used ACE2 knockout mice to further explore the role of ACE2 in BLM induced lung injury. We observed that ACE2 gene deletion aggravates BLM-induced lung injury while conversely rhACE2 treatment improves lung function and structure in BLM challenged wild type mice. Interestingly, we found that BLM-induced lung injury was accentuated in ACE2 deficient male compared to female mice.

Overall, our studies provide new evidence regarding the healing properties of MRL mice in the so far unexplored lung and offer new therapeutic options for

cord blood derived cell therapies to prevent pulmonary fibrosis.

6.2 Limitations

There are several limitations that should be acknowledged and considered for future studies in this important area of lung research.

In chapter 2, we observed increased healing in an LPS induced ARDS model in MRL/MPJ. However, we did not explore the anti-inflammatory response in these mice. Instead, we tested the *in vivo* anti-inflammatory effects of AT2 secretome. No experiments to show attenuated inflammation by AT2 cells *in vitro*.

We used the scratch assay technique to test our hypothesis that AT2 cells in MRL mice had higher healing capacity. It is not *per se* a model of inflammation as LPS induced ARDS is. However, due to the sensitivity and rapid differentiation of AT2 *in vitro*, we chose this model of healing to initially assess the main differences between healer and non-healer mice.

One of the main animal models used in the process of generating this thesis, was BLM induced fibrosis for studies 3, 4 and 5. Although it is a well accepted and widely used model that mimics the heterogeneous distribution of fibrosis, there are certain disadvantages to its use. There is a wide range of doses reported as well as several routes for administration⁹⁻¹³. The BLM dose used in our study (previously reported by others) constitutes an intermediate dose that leads to increased collagen deposition and impaired lung function^{3, 14-16}. The intratracheal route was selected because of the isolated damage to the organ of interest and consistency in lesions observed, when compared to other routes (intravenously, intraperitoneal). In our pilot studies, using higher doses of BLM hindered survival in our animals and lower doses did not produce a strong fibrotic response to be detected by our biochemical assays.

In chapter 3 we did not observe differences in response to BLM injury in MRL/MPJ mice compared to non-healer mice. One explanation may rely on the toxic nature of BLM: this substance induces a particular destruction of AT2. These cells may hold the key for adequate balance in injury/repair. Interestingly,

MRL/MPJ mice appear to be protected in a model of TGF β 1 induced lung fibrosis (very preliminary data from our lab). This model is known to cause decreased injury to AT2 cells¹⁷⁻¹⁹.

In chapter 4, we found that HUCBC constituted a mixture of cells (MSCs, EPCs, other mononuclear cells). Even though, we find a therapeutic effect in BLM induced IPF, we are unable to determine which type of cells is exerting the beneficial effect. We think that the effect is given by the mixture of cells and its paracrine effect, rather than their engraftment.

In chapters 4 and 5 where therapeutic options for pulmonary fibrosis we explored, we found protective effects when therapies were administered immediately after the injury. This suggests prevention rather than regeneration/adequate repair after the injury was established. The prophylactic approach is clinically relevant to attenuated the complications post ALI/ARDS. However, the BLM model is also used to mimic IPF. IPF patients present after symptoms have started, usually in more advanced stages of the fibrotic process^{20, 21}. We were not able to demonstrate so far reversal of established lung fibrosis. Therefore, additional therapies that can overcome the fibrotic process need to be developed for these patients.

6.3 Future directions

This thesis presents exciting results that open an avenue for future studies regarding new therapeutic options for lung repair after injury. The finding that MRL/MPJ mice are protected against ALI model and their AT2 cells possess enhanced healing abilities, lead us to consider future studies to harness the mechanism behind the regenerative mechanism and identify putative healing factors that can be used clinically.

In BLM challenged MRL/MPJ lungs we could not find differences compared to wild type mice. Future studies using other models of lung fibrosis, where the damage to AT2 cells is less prominent may elicit different results. For instance, TGF β -1 induced lung fibrosis has been described to induce less toxicity to AT2 cells compared to BLM²². If AT2 cells are indeed responsible for

repairing the alveoli, I would expect less damage/improved healing to the lung architecture compared to BLM induced fibrosis. In MRL/MPJ mice different types of injury, even in the same organ, seem to elicit various responses (i.e the heart, where ischemic and cryoinjury exhibit almost an opposite effect on healing). This is the case of both of our models, LPS induced ALI/ARDS and BLM induced fibrosis. Both toxins act differently; BLM produces free radicals that can cleave DNA while LPS induces cytokine production from both local inflammatory cells and AT2 cells. The later, does not have a direct toxicity for alveolar epithelial cells²³. *In vitro* comparison of AT2 cells reaction to both toxins between wild type and MRL/MPJ may help determine how resistant MRL/MPJ AT2 cells are in different challenging environments.

In this thesis we describe for the first time gender differences in BLM IPF challenged ACE2 knockout mice. Further studies are needed to assess the mechanisms governing lung fibrosis as well as to explore the interactions of sex hormones and other molecular markers in the development of lung disease.

Finally, the results of this thesis could be applied in different areas including the design and application of current novel experimental approaches such as metabolomics. The development of this area can lead to have more reliable and simpler ways to analyze full spectrum of the metabolome in health and disease as well as in the application of this approach in clinical studies. Moreover, the results of this thesis could be the platform for designing clinical studies that may use recombinant therapies such as rh-ACE2 or other molecules to treat lung disease.

Likewise, current studies in our lab are aimed at the identification of other compounds responsible for the therapeutic effect seen with HUCBC. This research will enhance our knowledge on the therapeutic potential of HUCBC to prevent/treat debilitating and life-threatening lung injury and could improve the outcome of patients affected with these diseases.

6.4 References

1. van Haaften T, Byrne R, Bonnet S, Rochefort GY, Akabutu J, Bouchentouf M, Rey-Parra GJ, Galipeau J, Haromy A, Eaton F, Chen M, Hashimoto K, Abley D, Korbitt G, Archer SL, Thebaud B. Airway delivery of mesenchymal stem cells prevents arrested alveolar growth in neonatal lung injury in rats. *Am J Respir Crit Care Med.* 2009;180:1131-1142
2. Ortiz LA, Dutreil M, Fattman C, Pandey AC, Torres G, Go K, Phinney DG. Interleukin 1 receptor antagonist mediates the antiinflammatory and antifibrotic effect of mesenchymal stem cells during lung injury. *Proc Natl Acad Sci U S A.* 2007;104:11002-11007
3. Ortiz LA, Gambelli F, McBride C, Gaupp D, Baddoo M, Kaminski N, Phinney DG. Mesenchymal stem cell engraftment in lung is enhanced in response to bleomycin exposure and ameliorates its fibrotic effects. *Proc Natl Acad Sci U S A.* 2003;100:8407-8411
4. Bennett RG. Relaxin and its role in the development and treatment of fibrosis. *Transl Res.* 2009;154:1-6
5. Tang ML, Samuel CS, Royce SG. Role of relaxin in regulation of fibrosis in the lung. *Ann N Y Acad Sci.* 2009;1160:342-347
6. Royce SG, Miao YR, Lee M, Samuel CS, Tregear GW, Tang ML. Relaxin reverses airway remodeling and airway dysfunction in allergic airways disease. *Endocrinology.* 2009;150:2692-2699
7. Bathgate RA, Lekgabe ED, McGuane JT, Su Y, Pham T, Ferraro T, Layfield S, Hannan RD, Thomas WG, Samuel CS, Du XJ. Adenovirus-mediated delivery of relaxin reverses cardiac fibrosis. *Mol Cell Endocrinol.* 2008;280:30-38
8. Zhong J, Guo D, Chen CB, Wang W, Schuster M, Loibner H, Penninger JM, Scholey JW, Kassiri Z, Oudit GY. Prevention of angiotensin ii-mediated renal oxidative stress, inflammation, and fibrosis by angiotensin-converting enzyme 2. *Hypertension.* 2011;57:314-322

9. Lown JW, Sim SK. The mechanism of the bleomycin-induced cleavage of DNA. *Biochem Biophys Res Commun.* 1977;77:1150-1157
10. Ichikawa T, Matsuda A, Miyamoto K, Tsubosaki M, Umezawa H. Biological studies on bleomycin a. *J Antibiot (Tokyo).* 1967;20:149-155
11. Umezawa H, Ishizuka M, Maeda K, Takeuchi T. Studies on bleomycin. *Cancer.* 1967;20:891-895
12. Yagoda A, Mukherji B, Young C, Etcubanas E, Lamonte C, Smith JR, Tan CT, Krakoff IH. Bleomycin, an antitumor antibiotic. Clinical experience in 274 patients. *Ann Intern Med.* 1972;77:861-870
13. Adamson IY, Bowden DH. The pathogenesis of bleomycin-induced pulmonary fibrosis in mice. *Am J Pathol.* 1974;77:185-197
14. Yang Y, Zhe X, Phan SH, Ullenbruch M, Schuger L. Involvement of serum response factor isoforms in myofibroblast differentiation during bleomycin-induced lung injury. *Am J Respir Cell Mol Biol.* 2003;29:583-590
15. Murakami S, Nagaya N, Itoh T, Fujii T, Iwase T, Hamada K, Kimura H, Kangawa K. C-type natriuretic peptide attenuates bleomycin-induced pulmonary fibrosis in mice. *Am J Physiol Lung Cell Mol Physiol.* 2004;287:L1172-1177
16. Addis-Lieser E, Kohl J, Chiamonte MG. Opposing regulatory roles of complement factor 5 in the development of bleomycin-induced pulmonary fibrosis. *J Immunol.* 2005;175:1894-1902
17. Sime PJ, Xing Z, Graham FL, Csaky KG, Gauldie J. Adenovector-mediated gene transfer of active transforming growth factor-beta1 induces prolonged severe fibrosis in rat lung. *J Clin Invest.* 1997;100:768-776
18. Warshamana GS, Pociask DA, Sime P, Schwartz DA, Brody AR. Susceptibility to asbestos-induced and transforming growth factor-beta1-induced fibroproliferative lung disease in two strains of mice. *Am J Respir Cell Mol Biol.* 2002;27:705-713

19. Kenyon NJ, Ward RW, McGrew G, Last JA. Tgf-beta1 causes airway fibrosis and increased collagen i and iii mrna in mice. *Thorax*. 2003;58:772-777
20. Coalson JJ. The ultrastructure of human fibrosing alveolitis. *Virchows Arch A Pathol Anat Histol*. 1982;395:181-199
21. American thoracic society/european respiratory society international multidisciplinary consensus classification of the idiopathic interstitial pneumonias. This joint statement of the american thoracic society (ats), and the european respiratory society (ers) was adopted by the ats board of directors, june 2001 and by the ers executive committee, june 2001. *Am J Respir Crit Care Med*. 2002;165:277-304
22. Kolb M, Bonniaud P, Galt T, Sime PJ, Kelly MM, Margetts PJ, Gauldie J. Differences in the fibrogenic response after transfer of active transforming growth factor-beta1 gene to lungs of "Fibrosis-prone" And "Fibrosis-resistant" Mouse strains. *Am J Respir Cell Mol Biol*. 2002;27:141-150
23. Yang HZ, Wang JP, Mi S, Liu HZ, Cui B, Yan HM, Yan J, Li Z, Liu H, Hua F, Lu W, Hu ZW. Tlr4 activity is required in the resolution of pulmonary inflammation and fibrosis after acute and chronic lung injury. *Am J Pathol*. 2012;180:275-292

CHAPTER 7
APPENDIX 1

**BLUNTED HYPOXIC PULMONARY
VASOCONSTRICTION IN
EXPERIMENTAL NEONATAL CHRONIC
LUNG DISEASE**

Rey-Parra GJ, Archer SL, Bland RD, Albertine KH, Carlton DP, Cho S, Kirby B, Haromy A, Eaton F, Wu X, Thébaud B. Blunted hypoxic pulmonary vasoconstriction in experimental neonatal chronic lung disease. *Am J Respir Crit Care Med.* 2008 Aug 15;178(4):399-406

7.1 Introduction

Premature infants account for more than 12% of all US births (National Institute of Medicine report, July 13, 2006, <http://www.iom.edu/CMS/3740/25471/35813.aspx>). Recent advances in obstetrical management and neonatal intensive care have increased survival of extremely premature infants (<1000g). These infants are prone to respiratory failure, for which they receive mechanical ventilation (MV) with O₂-rich gas. Prolonged exposure to cyclic stretch and high concentrations of inspired O₂ often leads to a chronic form of lung disease (CLD) that remains the leading cause of long-term hospitalization and recurrent respiratory illness in infants born at <28 weeks of gestation¹.

Prominent histological features of CLD include arrested alveolar growth and decreased capillary density²⁻⁴. Extremely premature infants with CLD frequently experience severe episodes of hypoxemia. The mechanism accounting for these hypoxemic events in neonates is poorly understood, but more likely related to either acute changes in airway resistance^{5, 6} or increased pulmonary vasoconstriction. It is unknown whether impaired ventilation in CLD may lead to mismatching of ventilation and perfusion, which could contribute to episodic hypoxemia and cyanosis.

Hypoxic pulmonary vasoconstriction (HPV) is a unique and important physiological response that facilitates matching of ventilation and perfusion in the lung. In segmental hypoxia, as occurs in CLD, constriction of distal pulmonary arteries (PAs), which regulate vascular resistance, diverts blood from poorly ventilated areas to well ventilated areas of the lung, thereby optimizing oxygenation, usually without increasing pulmonary vascular resistance (PVR)⁷.

Although the mechanisms that control HPV have not been completely elucidated⁸⁻¹⁰, it appears that hypoxia initiates HPV through a redox mechanism^{11, 12} that inhibits K⁺ channels in pulmonary artery smooth muscle cells (PASMC)¹³. O₂-sensitive voltage gated K⁺ channels (K_v) play an important role in

regulating HPV through modulation of cell membrane potential (E_M)¹⁴. During HPV, hypoxia closes Kv channels. This leads to membrane depolarization, opening of voltage-gated L-type calcium (Ca^{++}) channels, and increased influx of extracellular Ca^{++} , thereby causing pulmonary vasoconstriction. Inhibition of O_2 -sensitive Kv channels Kv1.5 and Kv2.1 contribute to initiation of HPV^{15,16}.

Thus, we hypothesize that HPV is impaired in neonatal CLD and that the basis for impaired HPV is reduced expression and function of O_2 -sensitive Kv channels.

Some of the results of these studies have been previously reported in the form of an abstract¹⁷.

7.2 Materials and Methods

Detailed Methods are provided in the online supplement

All procedures were approved by the Institutional Animal Care and Use Committee at the University of Utah in Salt Lake City (preterm lambs) and the University of Alberta (newborn rats).

7.2.1 Chronic lung injury (CLI) in preterm lambs

Preterm lambs were mechanically ventilated for 3 weeks and chronically catheterized as previously described¹⁸⁻²¹. PVR was measured during a 2-h steady-state baseline period, followed by a 2-h steady-state period of hypoxemia, induced by lowering the FiO_2 so that PaO_2 decreased to <40 mmHg.

7.2.2 CLI in newborn rats

Sprague-Dawley rat pups were exposed to normoxia (21% O_2 , control group) or hyperoxia (95% O_2 , O_2 -CLI group) from birth to P14 in sealed Plexiglas chambers with continuous O_2 monitoring²²⁻²⁵. After P14, pups were euthanized and lungs processed for various analyses.

Exposure of newborn rats to hyperoxia from birth to P14 during the critical period of alveolar development impairs alveolar growth (larger but fewer alveoli)

and is associated with right ventricular hypertrophy, an indirect marker of pulmonary hypertension. These results have been previously reported ²⁶.

7.2.3 Echo-Doppler in newborn rats

PA acceleration time (PAAT) (Vevo 770B Visual Sonics, Inc. ON, Canada) was measured from the onset of the pulmonary flow to its peak as previously described ²⁶. For the HPV challenge, animals were briefly (~30 sec) exposed to hypoxia (2.5% O₂) until a saturation of ~60% (Mouse Ox, Starr Life Sciences Corp) was obtained.

7.2.4 Organ bath studies of newborn rat PAs

Third generation pulmonary arteries (diameter <100µm, length = 2 mm, here referred to as dPAs) were mounted in a wire myograph (Myodaq; Danish Myo Technology) and bathed in Krebs-Henseleit buffer bubbled with 21% O₂-5% CO₂-balance N₂ (normoxia, pO₂ ~120 mmHg) or 5% O₂-5% CO₂-balance N₂ (hypoxia, pO₂ ~50 mmHg) maintained at 37°C, pH 7.35-7.45 ^{27, 28}. Isometric changes in response to phenylephrine (10⁻⁵ mol/L), HPV, the non-specific Kv channel inhibitor 4-aminopyridine (10 mM), a specific Kv 1.x channel inhibitor Correolide (100µM, gift from John Obenchain, Merck & Co, Inc, Rahway, NJ), the calcium-sensitive K channel (BK_{Ca}) inhibitor Iberitoxin (10⁻⁷ M), and the ATP-dependent K channel (K_{ATP}) inhibitor Glyburide (5 x 10⁻⁶ M) and to 80 mmol/L KCl were compared between control and O₂-induced CLI PAs.

7.2.5 Quantitative real-time polymerase chain reaction

Quantitative real-time polymerase chain reaction (qRT-PCR) was performed on isolated dPAs from newborn rats as previously described ^{29, 30} using purchased primers for human Kv 1.5, rat Kv 1.5 and Kv 2.1, BK_{Ca} (Applied biosystems). Levels of mRNA were normalized to a stable control gene (β2MG, β2 Microglobulin) and expressed as 2^{-ΔΔCt} (cycle time) ^{29, 30}.

7.2.6 Immunofluorescence

Immunofluorescence for anti-Kv1.5 antibody (Sigma-Aldrich P9357) was performed on whole rat lung tissue as described^{29,30}.

7.2.7 Adenovirus-mediated gene transfer

A 2.1-kb cDNA fragment of Kv1.5 was obtained by reverse transcription of mRNA derived from the proximal PA of a cardiac transplant donor²⁹. The virus was given intratracheally to CLI rats at P10 (26).

7.2.8 Electrophysiology

PASMC were freshly isolated from dPAs of control, O₂-induced CLI, Ad5-Kv1.5 treated and Ad5-GFP treated rats. Their response to hypoxia was studied using a whole cell patch clamping technique. PASMCs were voltage-clamped at -70 mV, and currents were evoked from -70 to +50 mV by steps of 200ms, as previously described²⁹.

7.2.9 Statistical Analysis

Data are expressed as mean \pm standard error (SE), except where stated otherwise. Statistical analysis was performed using unpaired Student's t-test or ANOVA, post hoc test (least significant difference) and Mann-Whitney as appropriate. Values were considered significant with $P < 0.05$.

7.3 Results

7.3.1 HPV is blunted in chronically ventilated newborn lambs

Chronically mechanically ventilated preterm lambs had persistent baseline elevation of PVR for the entire 3 weeks. PVR increased significantly during hypoxia at the end of week 1, but HPV was blunted during weeks 2 and 3 (Figure 1).

7.3.2 HPV is blunted in newborn rats with O₂-induced CLI *in vivo* and *ex vivo*

In vivo echo-Doppler studies showed that PAAT was significantly decreased in newborn rats with O₂-induced CLI as compared with normoxic controls (Figure 2A). During the hypoxic challenge, PAAT decreased in control pups, but not in pups with O₂-induced CLI (Figure 2A).

In vitro, dPAs constricted in response to hypoxia while dPAs from newborn rats with O₂-induced CLI failed to constrict in response to hypoxia (Figure 2B).

7.3.3 Vascular tone in rat distal PAs

The contractile response to the α -agonist Phenylephrine (10 mmol/L) was decreased significantly in O₂-induced CLI as compared to controls (Figure 3A). KCl constriction (Figure 3B) and the response to the BK_{Ca} and K_{ATP} channel blockers Iberiotoxin and Glyburide were similar between groups (Figure 3C). There was no difference in constriction in response to the Kv channel inhibitor 4-AP (10 mmol/L) (Figure 3D). In contrast, the vascular reactivity in O₂-induced CLI arteries to the specific Kv 1.x inhibitor correolide was significantly decreased as compared to normoxic control arteries (figure 3E).

7.3.4 Kv mRNA expression is decreased in dPAs from newborn rats with CLI

Blunted HPV in newborn rats exposed to O₂ was associated with a decrease in mRNA expression of Kv1.5 and Kv2.1 in dPAs as compared with controls

(Figure 4A). There was no difference in BK_{Ca} mRNA expression between groups (Figure 4B).

7.3.5 Intratracheal adenovirus-mediated Kv 1.5 gene transfer restores HPV in O₂-induced CLI in newborn rats

In vivo, echo-doppler showed that PAAT was significantly decreased in newborn rats with O₂-induced CLI, Adv-Kv O₂-induced CLI and Adv-GFP O₂-induced CLI as compared with normoxic controls (Figure 5). During the hypoxic challenge, PAAT decreased only in Adv-Kv O₂-induced CLI and control pups, but not in pups with O₂-induced CLI or Adv-GFP O₂-induced CLI (Figure 5).

Intratracheal administration of Ad5-Kv1.5 increased Kv1.5 expression in PAs of O₂-induced CLI as shown by immunofluorescence imaging (Figure 6 A) and qRT-PCR. qRT-PCR analysis using species-specific Kv primer revealed that human Kv1.5 was only expressed in Ad5-Kv1.5 transfected PAs (Figure 6 B). In dPAs rings, Ad5-Kv1.5 gene transfer restored HPV as compared to Ad5-GFP dPAs and non-transfected O₂-induced CLI dPAs (Figure 6 C).

7.3.6 I_K is restored by Kv1.5 gene transfer

Consistent with our *in vivo* and *in vitro* studies, I_K was significantly decreased in PSMCs from experimental O₂-induced CLI compared to controls (Figure 7A and B). There was a loss of the outward rectifying portion of the whole cell K⁺ current (evident in a comparison of panels A vs D as less total current and less upward deflection from the linear, ohmic current between voltage steps +10-+70mV). In control PSMCs, I_K was inhibited by hypoxia (Figure 7A), whereas I_K in O₂-induced CLI remained unaffected (Figure 7B). CLI Kv1.5 gene therapy restored not only the net current, but specifically the outward rectifying portion of the current, so that panels A and C look similar. This (together with the qRT data in Figure 4) indicates the loss of K⁺ current with CLI is largely due to loss of Kv current. Conversely, I_K was low in PSMCs from Ad5-GFP transfected animals (Figure 7D).

7.4 Discussion

Many studies of CLI have focused on changes in lung mechanics and airway function³¹⁻³⁵ to explain hypoxic episodes in premature infants. However, little attention has been paid to the possible mismatch of ventilation and perfusion that may develop in CLD. In this study, we show for the first time *in vivo* and *in vitro* evidence that HPV is impaired in two experimental models, created in different species and by different approaches, that mimic human CLD. In addition, impaired HPV in newborn rats was associated with decreased expression of the O₂-sensitive Kv1.5 channel. And finally, HPV was restored after adenovirus-associated gene transfer of Kv1.5. These findings support the notion that blunted HPV may contribute to the impaired gas exchange seen in CLD, and that therapeutic targeting of O₂-sensitive Kv channels in the pulmonary circulation might restore HPV and thereby improve arterial oxygenation in lung vascular diseases associated with impaired O₂ responsiveness.

HPV is a unique and important physiological response that facilitates matching of ventilation and perfusion in the lung. In segmental hypoxia the blood is diverted from poorly ventilated areas to well ventilated segments of the lung, optimizing PO₂ without increasing systemic vascular resistance¹⁴. Hypoxia depolarizes the PASMC membrane and causes an increase in intracellular Ca⁺⁺. This is related to inhibition of O₂-sensitive Kv channels, particularly Kv1.5^{15, 16}. Decreased HPV in chronic hypoxia results from loss of Kv1.5 and 2.1^{29, 36}, and enhanced expression of Kv1.5 by adenovirus-mediated gene transfer restores HPV²⁹. Patients with pulmonary hypertension have decreased mRNA levels of the O₂ sensitive Kv 1.5 channel³⁷ suggesting an etiological role for O₂ sensitive Kv channels in the development of this disease.

During development, maturational changes in K⁺ channel expression account for differences in O₂ constriction. In the fetus, the resting membrane potential in PASMC is controlled by large-conductance Ca⁺⁺-sensitive K channels (BK_{Ca}), the predominant O₂ sensitive channel³⁸. After birth, there is a shift to O₂ sensitive Kv channels presumably enhancing the capacity for HPV, without increasing pulmonary vascular resistance³⁸. Whether there is a delay in the maturational

shift from BK_{Ca} to O_2 sensitive Kv channels in experimentally induced BPD is unknown. O_2 toxicity and/or chronic ventilation, the two main causes contributing to lung injury in premature infants, may impede Kv channel expression/function in the pulmonary vasculature. More recently, the deleterious effect of even brief (30 min) hyperoxia (decreased vasodilation to nitric oxide and acetylcholine) on the pulmonary circulation was reported^{39, 40}. Interestingly, the authors also show that lambs previously exposed for a brief period (30 min) to 100% O_2 did not have enhanced pulmonary vasoconstriction in response to subsequent hypoxic ventilation. Likewise, pulmonary vascular dysfunction, including pulmonary hypertension and altered response to inhaled nitric oxide in CLD, has been reported previously in preterm lambs^{18-20, 41}. Conversely, there is no information about the effects of hyperoxia on the regulation of Kv channels.

It is interesting that the PA and the ductus arteriosus (DA), although adjacent, behave in such opposite ways in response to O_2 and yet share a common pathway for O_2 sensing¹⁰. dPAs exhibit HPV for optimizing gas exchange in the lung. In contrast, the DA is largely open in the hypoxic environment *in utero* and constricts when O_2 levels rise at birth, allowing the lung to take over its postnatal role of gas-exchange. A patent DA is a common complication in premature infants. Decreased O_2 -induced constriction in the preterm rabbit DA is associated with decreased O_2 -sensitive I_K and O_2 -sensitive Kv1.5 expression and overexpression of Kv1.5 in preterm rabbit DA restores O_2 -induced constriction³⁰. In this study we show similar results in dPAs, suggesting the importance for Kv channels in O_2 sensing.

Besides maturational changes in Kv channels, other factors may contribute to the altered response to hypoxia in experimental BPD. The mechanism by which hypoxia is sensed remains unknown. It has been proposed that HPV results from a redox sensor system present in dPAs, but also found in other O_2 -sensing organs¹⁰. A sensor, the proximal portion of the mitochondria transport chain, produces a mediator (reactive oxygen species). This mediator would alter the effector (K⁺ channels) through a process of reduction/oxidation. When the mitochondria detects a hypoxic environment, reactive oxygen species decrease thereby inhibiting

redox-sensitive K⁺ channels. Inhibitors of complex I and III of the electron transport chain in the mitochondria inhibit the formation of reactive oxygen species and mimic HPV in the isolated perfused lung^{11, 42}. In experimental BPD, a loss of O₂ sensing ability caused by chronic exposure to hyperoxia could alter mitochondrial function-reactive oxygen species production, making the pulmonary circulation unable to detect hypoxia and thus failing to constrict.

Abnormal vascular reactivity in older children with a history of severe BPD and pulmonary hypertension has been reported⁴³. Cardiac catheterization of these patients showed that the pulmonary vasculature remained responsive to O₂, but PVR was enhanced in response to hypoxia, suggesting increased HPV in this subpopulation of patients. The discrepancy with our data could be explained by differences in species, but is most likely due to a different timing in the assessment. HPV was assessed at a median of 5 years of age in the clinical study. Our study assessed animals during the neonatal period. As an adaptative and maturational response, the pulmonary vasculature with an initial blunted HPV could become hyperreactive to hypoxia later in life. Indications for such long-term consequences of injury during the perinatal period have been reported in the Fawn-Hooded rat⁴⁴ and more recently in rats exposed during fetal life to hypoxia showing that perinatal hypoxia alters the maturational shift in K⁺ channels and influences pulmonary vascular tone in adulthood⁴⁵. Remarkably, even ambient air may represent relative hyperoxia for infants born too early and impair lung development and function⁴⁶.

In conclusion, HPV is blunted in experimental CLD due, at least in part, to downregulation of O₂-sensitive Kv channels. Hypoxic episodes in premature infants with CLD may result from impaired HPV. We speculate that restoration of O₂-sensitive Kv channels in the pulmonary circulation may decrease episodes of hypoxemia, facilitate management and ultimately improve outcome of premature infants with CLD.

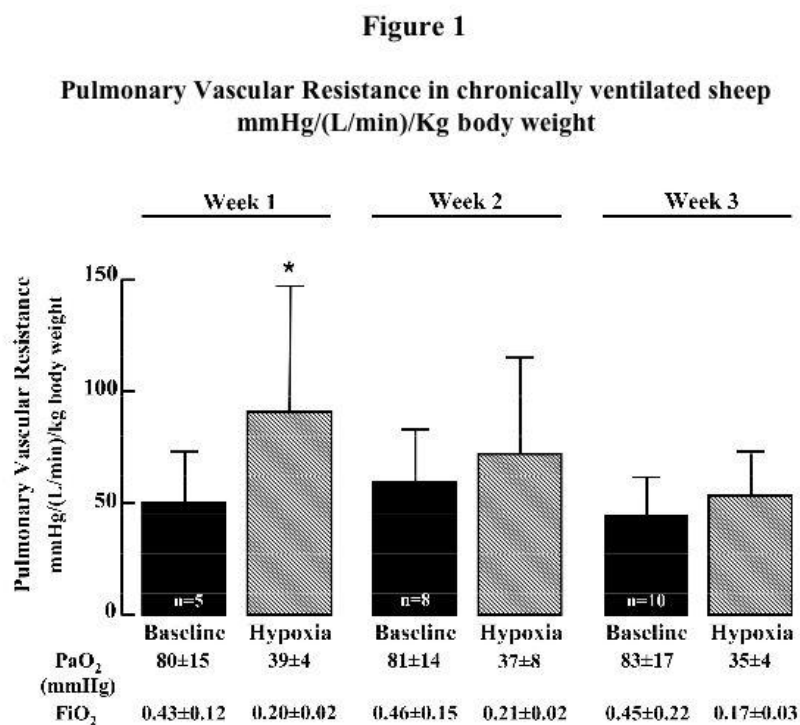


Figure 7.1. Pulmonary vascular response to hypoxia

Pulmonary vascular response to hypoxia induced by a reduction in F_{iO_2} sufficient to lower P_{aO_2} to less than 40 mm Hg at the end of Weeks 1, 2, and 3 of mechanical ventilation in preterm lambs. Pulmonary vascular resistance increased significantly during steady-state hypoxia at the end of Week 1, but this response was lost at the end of Weeks 2 and 3. Values are mean and SD. *Significant difference compared with baseline, $P < 0.05$.

Figure 2
Hypoxic Pulmonary Vasoconstriction

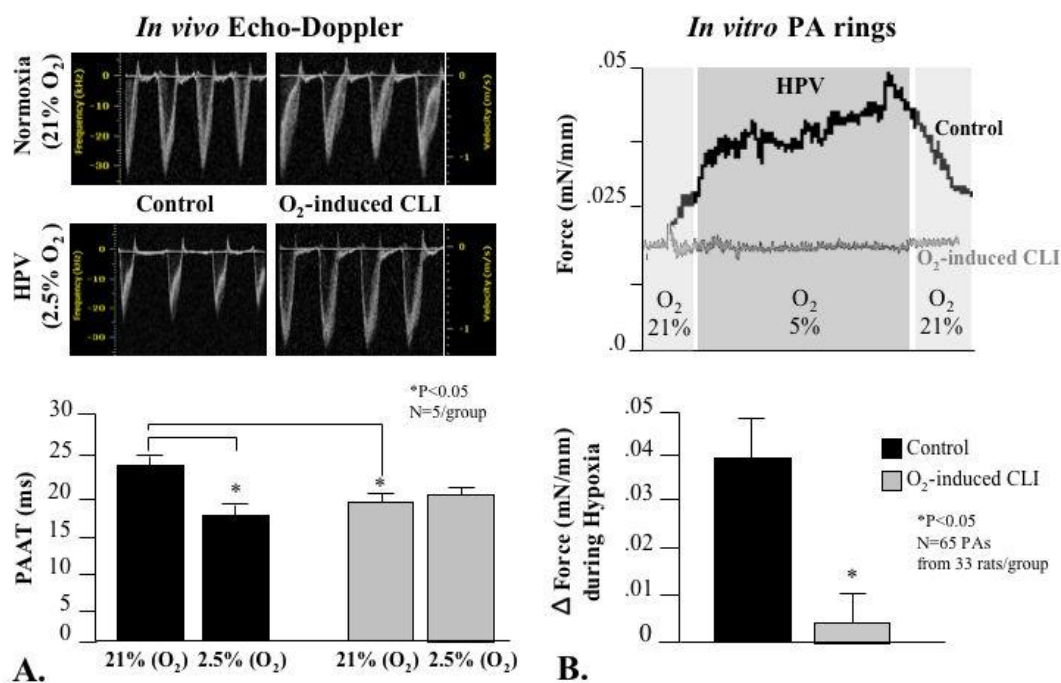


Figure 7. 2. Hypoxic Pulmonary Vasoconstriction

(A) Echo-Doppler showing that the pulmonary arterial acceleration time (PAAT) is significantly decreased in O₂-induced chronic lung injury (CLI) rats as compared with controls. During brief hypoxic exposure, PAAT decreased in controls but not in O₂-induced CLI. (B) Representative trace and mean data showing that distal pulmonary arteries of O₂-induced CLI do not constrict in response to hypoxia as compared with distal pulmonary arteries of room air-housed control rats.

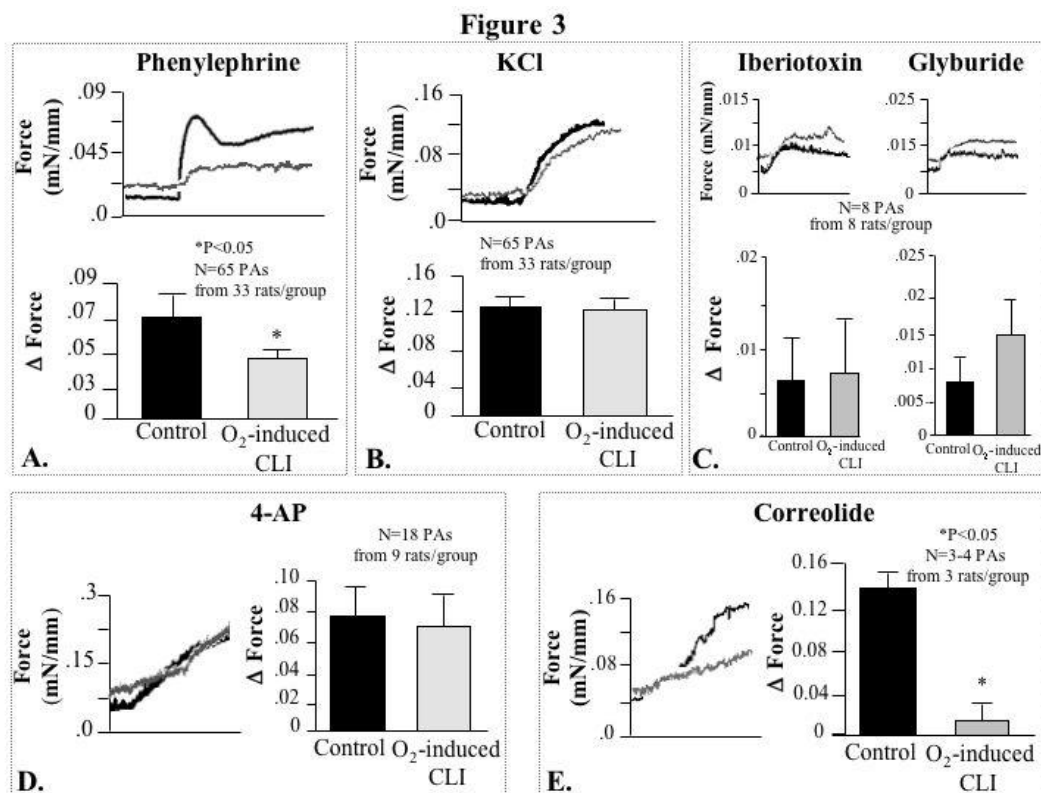


Figure 7.3. Contractile responses from distal pulmonary arteries (dPAs) of newborn rats. Representative trace and mean data \pm SEM in response to (A) phenylephrine, (B) KCl, (C) the calcium-sensitive K⁺ channel inhibitor iberiotoxin and the ATP-sensitive K⁺ channel (KATP) inhibitor glyburide, (D) 4-AP, and (E) to the specific K_v1.x inhibitor correolide. (A) Phenylephrine-induced constriction is significantly decreased in dPAs from O₂-induced chronic lung injury (CLI) rats as compared with with dPAs of room air-housed control rats. (E) The contractile response of O₂-induced CLI arteries to correolide is significantly decreased as compared with normoxic control arteries.

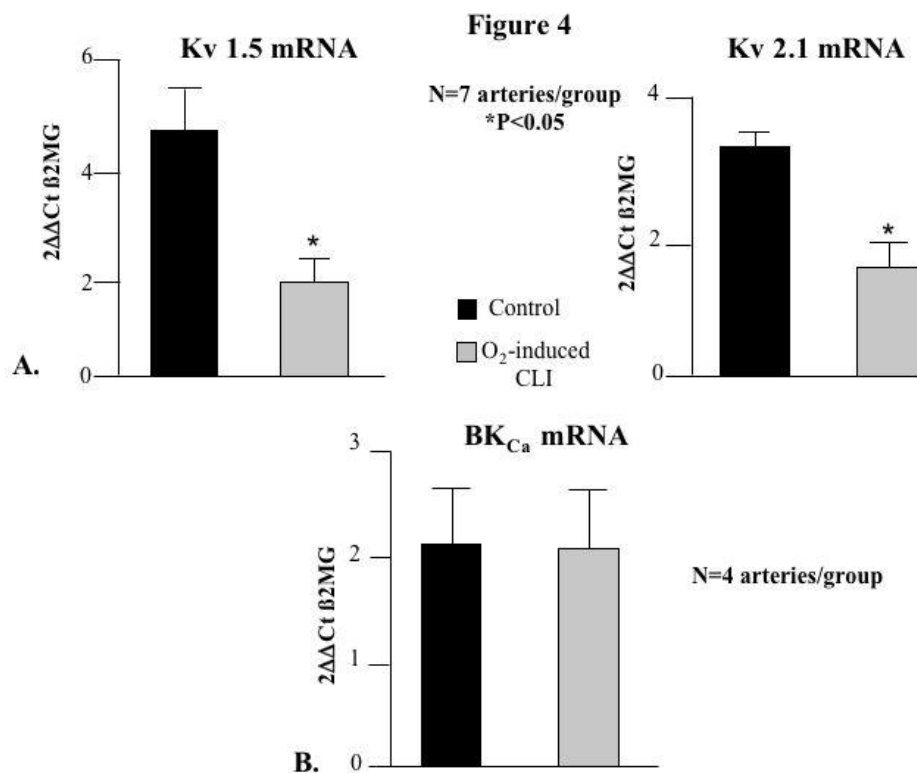


Figure 7.4. Voltage gated K channels mRNA expression in pulmonary arteries of newborn rats. (A) K_v1.5 and K_v2.1 mRNA is decreased in O₂-induced chronic lung injury (CLI) distal pulmonary arteries compared with controls. (B) calcium-sensitive K⁺ channel (BK_{Ca}) mRNA expression in O₂-induced CLI distal pulmonary arteries compared with controls. Mean ± SEM of K_v1.5, 2.1, and calcium-sensitive K⁺ channel (BK_{Ca}) mRNA measured using quantitative real-time polymerase chain reaction.

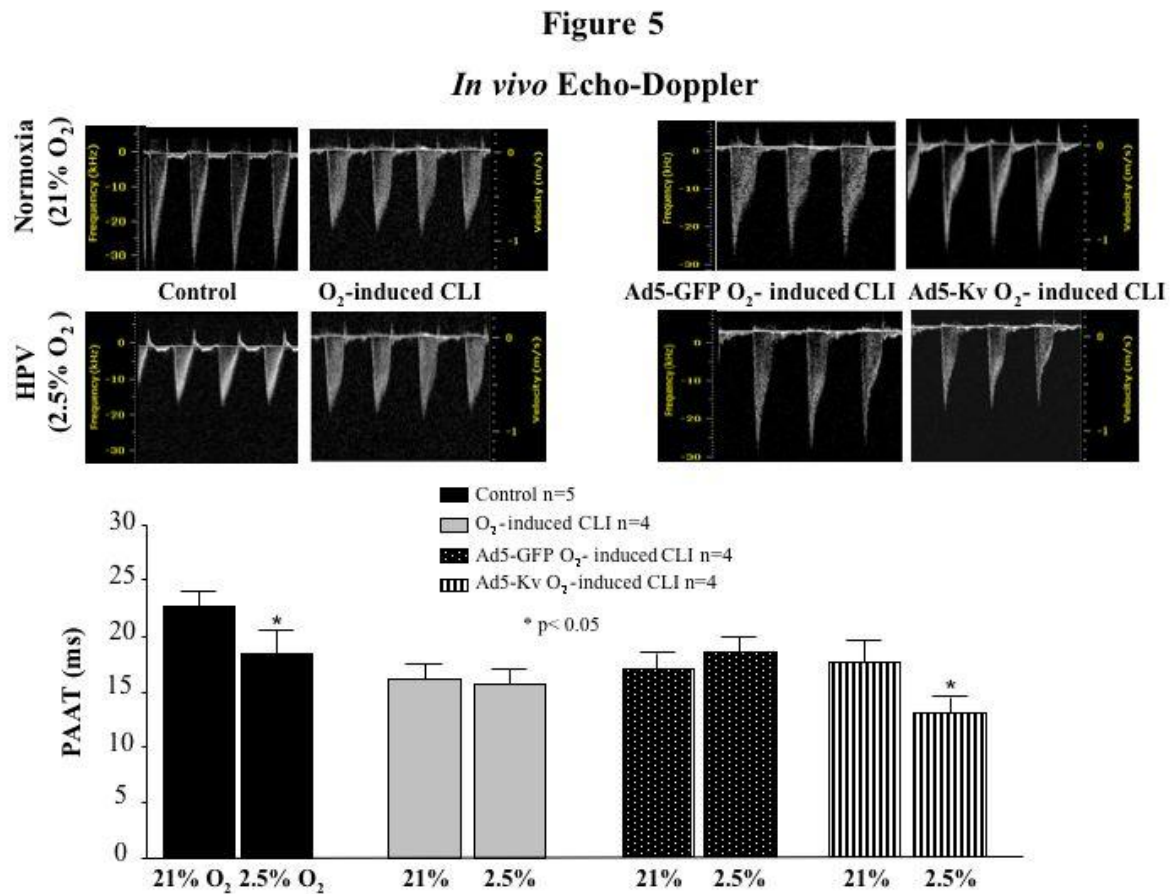


Figure 7. 5. *In vivo* Echo-Doppler. (A) Echo-Doppler shows that the pulmonary arterial acceleration time (PAAT) is significantly decreased in O₂-induced chronic lung injury (CLI) rats, Ad5-K_v O₂-induced CLI, and Ad5-green fluorescent protein (GFP) O₂-induced CLI as compared with controls. During brief hypoxic exposure, PAAT is significantly decreased in controls and Ad5-K_v O₂-induced CLI but not in O₂-induced CLI and Ad5-GFP O₂-induced CLI groups. Representative trace and mean data ± SEM.

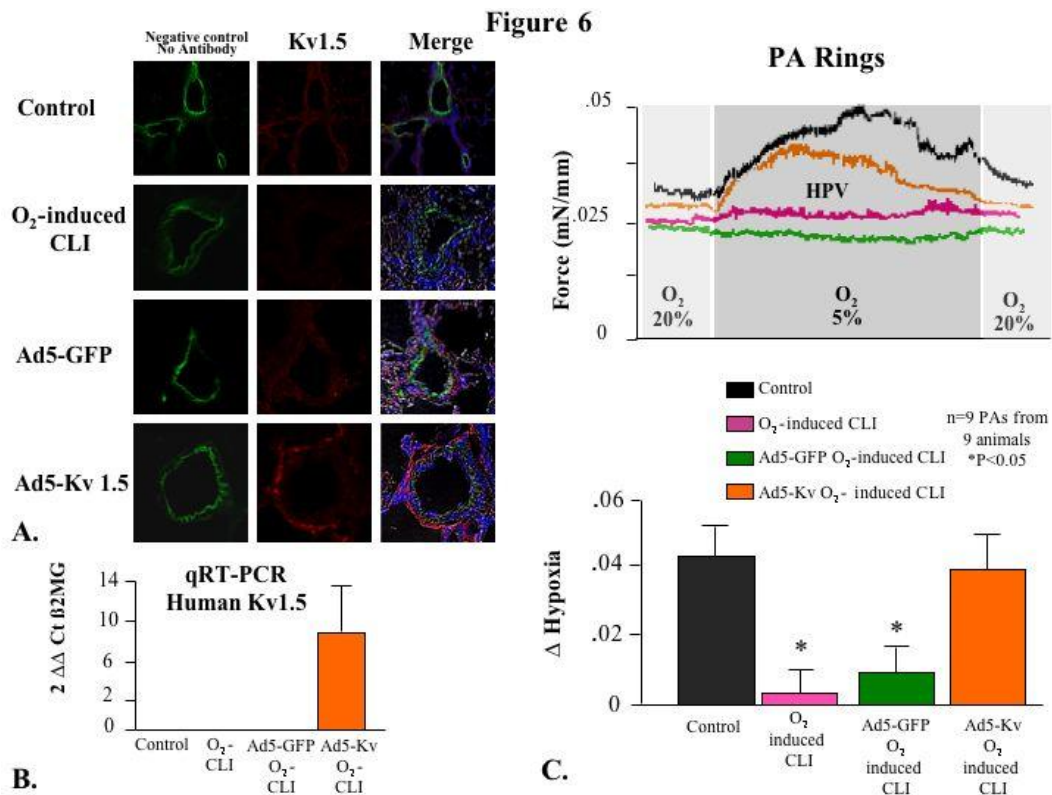


Figure 7.6. Effective K_v1.5 gene transfer in distal pulmonary arteries. (A) Confocal microscopy shows *green* autofluorescence of the elastic lamina in dPAs and *red* fluorescence for K_v1.5 protein; (B) quantitative real-time polymerase chain reaction (qRT-PCR) shows selective expression of Ad5-K_v1.5 mRNA for human K_v1.5 in infected arteries; (C) hypoxic pulmonary vasoconstriction (HPV) is restored in O₂-induced chronic lung injury (CLI) dPAs after intratracheal adenovirus-mediated K_v1.5 gene transfer. Representative trace and mean data \pm SEM shows hypoxic-induced constriction in dPAs of Ad5-K_v1.5 infected rats. Ad5-green fluorescent protein (GFP) and O₂-induced CLI dPAs failed to constrict.

Figure 7

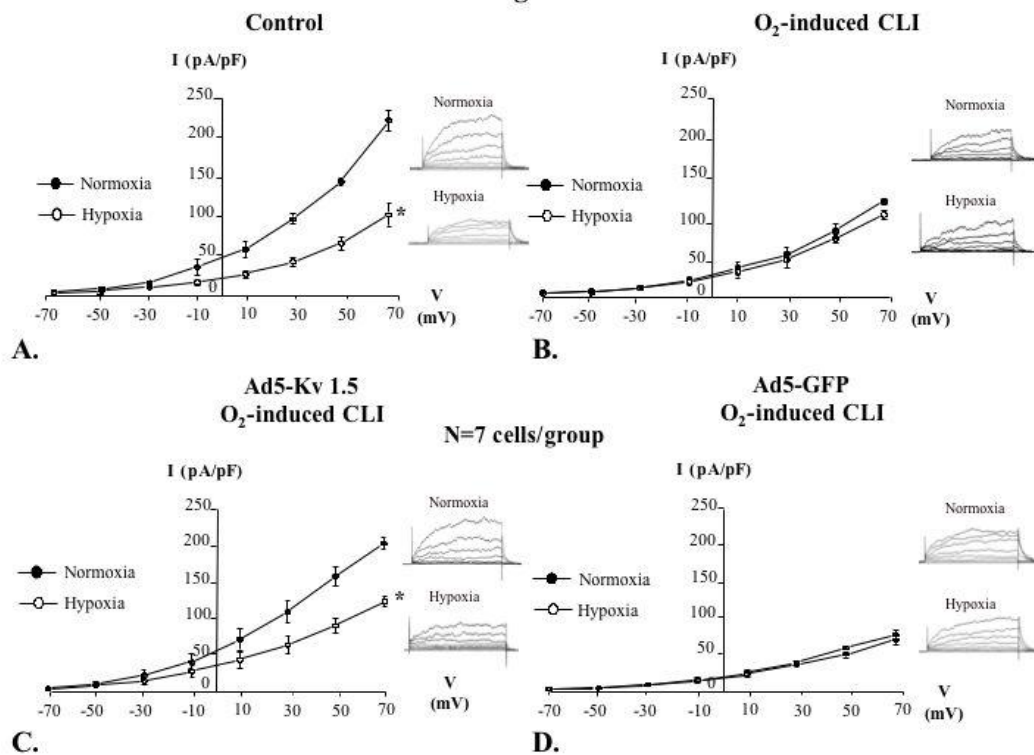


Figure 7.7 Representative patch-clamp recording and mean current density–voltage plots. This figure show hypoxic induced inhibition of whole-cell K^+ current (I_K) in control pulmonary artery smooth muscle cells (A) but not in O_2 -induced chronic lung injury (CLI) PASM (B). Conversely, I_K is restored in PASM isolated from rats that had received intratracheal Ad5- $K_v1.5$ gene therapy (C), but not PASM of Ad5-green fluorescent protein (GFP) infected rats (D).

7.5 ONLINE DATA SUPPLEMENT

Blunted Hypoxic Pulmonary Vasoconstriction in Experimental Neonatal Chronic Lung Disease

Materials and Methods

Induction of chronic lung injury (CLI) in preterm lambs

Preterm lambs (average gestation 124 ± 1 day, weight 2.28 ± 0.16 Kg) were delivered through midline hysterotomy, mechanically ventilated for 3 weeks at a respiratory rate of 20/min yielding a tidal volume of 15 ± 5 ml/Kg, as previously described¹⁸⁻²¹. Peak inspiratory pressure was adjusted to maintain the partial pressure of carbon dioxide in arterial blood (PaCO_2) at ~ 35 - 45 mmHg; FiO_2 was adjusted to keep PaO_2 at ~ 50 - 90 mmHg; and end-expiratory pressure was kept constant at 5-6 cmH₂O. The lambs received intravenous nutrition and enteral feeding of ewe's milk as tolerated. In the first 3 days after birth, each lamb underwent a left thoracotomy while under general anesthesia with iv fentanyl for surgical ligation of the ductus arteriosus and placement of catheters in the pulmonary artery and left atrium and a thermistor wire in the pulmonary artery to measure cardiac output by thermodilution. This allowed for weekly measurements of mean pulmonary arterial (Ppa) and left atrial pressures (Pla) and pulmonary blood flow (Qbl), from which PVR was determined as $(\text{Ppa} - \text{Pla}) / \text{Qbl}$. PVR was measured during a 2-h steady-state baseline period, followed by a 2-h steady-state period of hypoxemia, induced by lowering the FiO_2 so that PaO_2 decreased to < 40 mmHg. Studies were done at the end of weeks 1, 2 and 3 of MV. At the end of each 3-week study, the lambs received iv pentobarbital, 50 mg/kg, followed by a midline sternotomy to open the chest and resect the lungs for subsequent histology and quantitative analysis of alveolar size and number, arterial smooth muscle thickness, and capillary surface density, as previously described¹⁸⁻²¹.

Induction of CLI in newborn rats

Litter size (n=12) was adjusted to provide equal nutrition and growth; dams were switched between normoxic and hyperoxic chambers every 48h to prevent

O₂ toxicity²². After 14d, the pups were euthanized with an intraperitoneal dose of pentobarbital (65mg/kg) for lung resection.

Echo-Doppler in newborn rats

Rats were anesthetized with ketamine (60mg/Kg) and xylazine (7 mg/Kg) IP. Each animal was positioned supine on a mouse imaging stage that was warmed to 37°C. Ultrasound gel used as a coupling fluid between the RMV probe and the skin. Using B-Mode imaging on a Vevo 770B echocardiographic device (Visual Sonics, Inc. ON, Canada), the probe was positioned to obtain a parasternal long axis view of the heart. Doppler imaging was used to measure the pulmonary artery acceleration time (PAAT)²⁶, from the onset of the pulmonary flow to its peak. Control, O₂-CLI, Adv-GFP and Kv 1.5 transfected animals were kept in room air (O₂ saturation 90-95%, Mouse Ox, Starr Life Sciences Corp) and then briefly (~30 sec) exposed to hypoxia (2.5% O₂) until a saturation of ~60% was obtained. PAAT was recorded during baseline (normoxia) and hypoxic challenge.

Organ bath studies in newborn rats

Arterial rings were bathed in Krebs-Henseleit buffer (119 mM NaCl, 3.52 mM KCl, 1.17 mM MgSO₄, 1.18 mM KH₂PO₄, 3.2 mM CaCl₂H₂O, 22.6 mM NaHCO₃, 50 mM Sucrose, 5.5 mM Glucose) bubbled with 21% O₂-5% CO₂-balance N₂ (normoxia, pO₂ ~120 mmHg) or 5% O₂-5% CO₂-balance N₂ (hypoxia, pO₂ ~50 mmHg), and were maintained at 37°C, pH 7.35-7.45. Optimal transmural pressure was determined by stimulation with 80 mM KCl. Subsequent measurements were obtained at the experimentally determined transmural pressure of 17.5 mmHg for control arteries and 24.4 mmHg for O₂-induced CLI arteries. Meclofenamate (10⁻⁵ mol/L) and N^G-nitro-L-arginine methyl ester (10⁻⁴ mol/L) were added to the bath to inhibit synthesis of prostaglandins and nitric oxide, respectively.

Quantitative real-time polymerase chain reaction

Isolated dPAs from newborn rats were analyzed by quantitative real-time polymerase chain reaction (qRT-PCR) as previously described^{29, 30} using purchased primers for human Kv 1.5, rat Kv 1.5, Kv 2.1 and BK_{Ca} (Applied biosystems). Total RNA was extracted using an RNEasy Mini Kit (Qiagen). The TaqMan One-Step RT-PCR Master Mix reagent kit (Applied Biosystems) was used to quantify the copy number of cDNA targets. Levels of mRNA were normalized to a stable control gene (β 2MG, β 2 Microglobulin) and expressed as $2^{-\Delta\Delta Ct}$ (cycle time)^{29, 30}.

Immunofluorescent imaging of lungs from newborn rats

Immunofluorescence was performed on whole lung tissue embedded in optimum cutting temperature compound (OCT) using a Zeiss LSM 510 confocal microscope. 10 μ m frozen sections were cut, incubated 1h at 37°C with Anti-Kv1.5 antibody that was produced in rabbit (Sigma-Aldrich P9357). Slides were exposed to the secondary antibody (tetramethylrhodamine, goat-anti rabbit, Molecular Probes), and nuclear staining was performed using 4',6-diamidino-2-phenyllindole, dihydrochloride (Prolong® Gold, anti-fade reagent with DAPI, Molecular Probes). Slides were imaged at excitation/emission green: 488nm/505 to 530 nm, red: 543 nm/565 to 615 nm, and blue 740 nm/390 to 465 nm). Imaging conditions were kept constant and appropriate controls were applied^{29, 30}.

Adenovirus-mediated gene transfer

A recombinant replication deficient serotype 5 adenovirus vector, carrying genes encoded with green fluorescent protein (GFP) or human Kv1.5 plus GFP, was isolated, precipitated, and concentrated to a final viral titer of 1.5×10^9 pfu/mL, as previously described^{29, 30}. The virus was given intratracheally to CLI rats at P10.

Electrophysiology

Pulmonary artery smooth muscle cells (PASMC) were freshly isolated from dPAs, and their response to hypoxia was studied using a whole cell patch clamping technique. dPAs were dissected and placed in cold enzyme buffer (NaCl 140 nM, KCl 4.2 nM, KH₂PO₄ 1.2 nM, MgCl₂·6H₂O 1.5 nM, HEPES 10 nM). The buffer was then replaced with a solution containing enzyme buffer DTT, BSA and papain (sigma P4762, St. Louis, MO), and the arteries were immersed for 10min at 4°C. The tissue was then incubated for 10min at 37°C in an enzymatic solution containing Ca⁺⁺-free solution and collagenase (sigma C9891, St. Louis, MO). Cells were dispersed by gentle trituration using a Pasteur pipette (room temperature). The cell suspension was centrifuged at 1000 rpm for 5min and the pellet was resuspended in DMEM + PSF 1%. Cells were stored at 4°C, and patch-clamp studies were done the same day. PASMCs were voltage-clamped at -70 mV, and currents were evoked from -70 to +50 mV by steps of 200ms, as previously described²⁹. Current density was calculated by dividing average plateau phase K⁺ current (I_k) by the manually measured capacitance (P_A/P_F). To record E_M, cells were held at their resting E_M in current clamp mode.

Reagents and solutions

All chemicals were purchased from Sigma-Aldrich (St. Louis, MO), unless otherwise specified.

7.6 References

1. Kinsella JP, Greenough A, Abman SH. Bronchopulmonary dysplasia. *Lancet*. 2006;367:1421-1431
2. Abman SH. Bronchopulmonary dysplasia: "A vascular hypothesis". *Am J Respir Crit Care Med*. 2001;164:1755-1756
3. Husain AN, Siddiqui NH, Stocker JT. Pathology of arrested acinar development in postsurfactant bronchopulmonary dysplasia. *Hum Pathol*. 1998;29:710-717
4. Jobe AH, Bancalari E. Bronchopulmonary dysplasia. *Am J Respir Crit Care Med*. 2001;163:1723-1729
5. McCoy KS, Bagwell CE, Wagner M, Sallent J, O'Keefe M, Kosch PC. Spirometric and endoscopic evaluation of airway collapse in infants with bronchopulmonary dysplasia. *Pediatr Pulmonol*. 1992;14:23-27
6. Bhandari A, Panitch HB. Pulmonary outcomes in bronchopulmonary dysplasia. *Semin Perinatol*. 2006;30:219-226
7. von Euler U, and G. Liljestrand. . Observations on the pulmonary arterial blood pressure in the cat. . *Acta Physiol Scand*. 1946. :301-320
8. Robertson TP, Hague D, Aaronson PI, Ward JP. Voltage-independent calcium entry in hypoxic pulmonary vasoconstriction of intrapulmonary arteries of the rat. *J Physiol*. 2000;525 Pt 3:669-680
9. Sato K, Morio Y, Morris KG, Rodman DM, McMurtry IF. Mechanism of hypoxic pulmonary vasoconstriction involves et(a) receptor-mediated inhibition of k(atp) channel. *Am J Physiol Lung Cell Mol Physiol*. 2000;278:L434-442
10. Weir EK, Lopez-Barneo J, Buckler KJ, Archer SL. Acute oxygen-sensing mechanisms. *N Engl J Med*. 2005;353:2042-2055
11. Archer SL, Huang J, Henry T, Peterson D, Weir EK. A redox-based o₂ sensor in rat pulmonary vasculature. *Circ Res*. 1993;73:1100-1112
12. Archer SL, Will JA, Weir EK. Redox status in the control of pulmonary vascular tone. *Herz*. 1986;11:127-141

13. Post JM, Hume JR, Archer SL, Weir EK. Direct role for potassium channel inhibition in hypoxic pulmonary vasoconstriction. *Am J Physiol.* 1992;262:C882-890
14. Weir EK, Archer SL. The mechanism of acute hypoxic pulmonary vasoconstriction: The tale of two channels. *Faseb J.* 1995;9:183-189
15. Archer SL, Souil E, Dinh-Xuan AT, Schremmer B, Mercier JC, El Yaagoubi A, Nguyen-Huu L, Reeve HL, Hampl V. Molecular identification of the role of voltage-gated k⁺ channels, kv1.5 and kv2.1, in hypoxic pulmonary vasoconstriction and control of resting membrane potential in rat pulmonary artery myocytes. *J Clin Invest.* 1998;101:2319-2330
16. Archer SL, Wu XC, Thebaud B, Nsair A, Bonnet S, Tyrrell B, McMurtry MS, Hashimoto K, Harry G, Michelakis ED. Preferential expression and function of voltage-gated, o₂-sensitive k⁺ channels in resistance pulmonary arteries explains regional heterogeneity in hypoxic pulmonary vasoconstriction: Ionic diversity in smooth muscle cells. *Circ Res.* 2004;95:308-318
17. Rey J KB, Van Haaften T, Eaton F, Archer SL, Thébaud B. Hypoxic pulmonary vasoconstriction (h_{pv}) is blunted in experimental bronchopulmonary dysplasia (b_{pd}) in newborn rats. *Presented at the 2007 Pediatric Academic Societies' Annual Meeting. May 7, 2007, Toronto, ON, Canada. Publication 7730.5.*
. 2007
18. Bland RD, Albertine KH, Carlton DP, Kullama L, Davis P, Cho SC, Kim BI, Dahl M, Tabatabaei N. Chronic lung injury in preterm lambs: Abnormalities of the pulmonary circulation and lung fluid balance. *Pediatr Res.* 2000;48:64-74
19. Bland RD, Albertine KH, Carlton DP, MacRitchie AJ. Inhaled nitric oxide effects on lung structure and function in chronically ventilated preterm lambs. *Am J Respir Crit Care Med.* 2005;172:899-906

20. Bland RD, Ling CY, Albertine KH, Carlton DP, MacRitchie AJ, Day RW, Dahl MJ. Pulmonary vascular dysfunction in preterm lambs with chronic lung disease. *Am J Physiol Lung Cell Mol Physiol*. 2003;285:L76-85
21. MacRitchie AN, Albertine KH, Sun J, Lei PS, Jensen SC, Freestone AA, Clair PM, Dahl MJ, Godfrey EA, Carlton DP, Bland RD. Reduced endothelial nitric oxide synthase in lungs of chronically ventilated preterm lambs. *Am J Physiol Lung Cell Mol Physiol*. 2001;281:L1011-1020
22. Frank L, Bucher JR, Roberts RJ. Oxygen toxicity in neonatal and adult animals of various species. *J Appl Physiol*. 1978;45:699-704
23. Roberts RJ, Rendak I, Bucher JR. Lipid peroxidation in the newborn rat: Influence of fasting and hyperoxia on ethane and pentane in expired air. *Dev Pharmacol Ther*. 1983;6:170-178
24. Roberts RJ, Weesner KM, Bucher JR. Oxygen-induced alterations in lung vascular development in the newborn rat. *Pediatr Res*. 1983;17:368-375
25. Wilson WL, Mullen M, Olley PM, Rabinovitch M. Hyperoxia-induced pulmonary vascular and lung abnormalities in young rats and potential for recovery. *Pediatr Res*. 1985;19:1059-1067
26. Ladha F, Bonnet S, Eaton F, Hashimoto K, Korbitt G, Thebaud B. Sildenafil improves alveolar growth and pulmonary hypertension in hyperoxia-induced lung injury. *Am J Respir Crit Care Med*. 2005;172:750-756
27. Belik J, Jankov RP, Pan J, Tanswell AK. Chronic O₂ exposure enhances vascular and airway smooth muscle contraction in the newborn but not adult rat. *J Appl Physiol*. 2003;94:2303-2312
28. Belik J, Pan J, Jankov RP, Tanswell AK. A bronchial epithelium-derived factor reduces pulmonary vascular tone in the newborn rat. *J Appl Physiol*. 2004;96:1399-1405
29. Pozeg ZI, Michelakis ED, McMurtry MS, Thebaud B, Wu XC, Dyck JR, Hashimoto K, Wang S, Moudgil R, Harry G, Sultanian R, Koshal A, Archer SL. In vivo gene transfer of the O₂-sensitive potassium channel kv1.5 reduces pulmonary hypertension and restores hypoxic pulmonary

- vasoconstriction in chronically hypoxic rats. *Circulation*. 2003;107:2037-2044
30. Thebaud B, Michelakis ED, Wu XC, Moudgil R, Kuzyk M, Dyck JR, Harry G, Hashimoto K, Haromy A, Rebeyka I, Archer SL. Oxygen-sensitive kv channel gene transfer confers oxygen responsiveness to preterm rabbit and remodeled human ductus arteriosus: Implications for infants with patent ductus arteriosus. *Circulation*. 2004;110:1372-1379
 31. Mitchell SH, Teague WG. Reduced gas transfer at rest and during exercise in school-age survivors of bronchopulmonary dysplasia. *Am J Respir Crit Care Med*. 1998;157:1406-1412
 32. Hislop AA, Haworth SG. Pulmonary vascular damage and the development of cor pulmonale following hyaline membrane disease. *Pediatr Pulmonol*. 1990;9:152-161
 33. Goodman G, Perkin RM, Anas NG, Sperling DR, Hicks DA, Rowen M. Pulmonary hypertension in infants with bronchopulmonary dysplasia. *J Pediatr*. 1988;112:67-72
 34. Mallory GB, Jr., Chaney H, Mutich RL, Motoyama EK. Longitudinal changes in lung function during the first three years of premature infants with moderate to severe bronchopulmonary dysplasia. *Pediatr Pulmonol*. 1991;11:8-14
 35. Garg M, Kurzner SI, Bautista D, Keens TG. Hypoxic arousal responses in infants with bronchopulmonary dysplasia. *Pediatrics*. 1988;82:59-63
 36. Platoshyn O, Yu Y, Golovina VA, McDaniel SS, Krick S, Li L, Wang JY, Rubin LJ, Yuan JX. Chronic hypoxia decreases k(v) channel expression and function in pulmonary artery myocytes. *Am J Physiol Lung Cell Mol Physiol*. 2001;280:L801-812
 37. Yuan XJ, Wang J, Juhaszova M, Gaine SP, Rubin LJ. Attenuated k⁺ channel gene transcription in primary pulmonary hypertension. *Lancet*. 1998;351:726-727

38. Reeve HL, Weir EK, Archer SL, Cornfield DN. A maturational shift in pulmonary k^+ channels, from ca^{2+} sensitive to voltage dependent. *Am J Physiol*. 1998;275:L1019-1025
39. Lakshminrusimha S, Russell JA, Steinhorn RH, Swartz DD, Ryan RM, Gugino SF, Wynn KA, Kumar VH, Mathew B, Kirmani K, Morin FC, 3rd. Pulmonary hemodynamics in neonatal lambs resuscitated with 21%, 50%, and 100% oxygen. *Pediatr Res*. 2007
40. Lakshminrusimha S, Russell JA, Wedgwood S, Gugino SF, Kazzaz JA, Davis JM, Steinhorn RH. Superoxide dismutase improves oxygenation and reduces oxidation in neonatal pulmonary hypertension. *Am J Respir Crit Care Med*. 2006;174:1370-1377
41. Afshar S, Gibson LL, Yuhanna IS, Sherman TS, Kerecman JD, Grubb PH, Yoder BA, McCurnin DC, Shaul PW. Pulmonary no synthase expression is attenuated in a fetal baboon model of chronic lung disease. *Am J Physiol Lung Cell Mol Physiol*. 2003;284:L749-758
42. Bonnet S, Michelakis ED, Porter CJ, Andrade-Navarro MA, Thebaud B, Haromy A, Harry G, Moudgil R, McMurtry MS, Weir EK, Archer SL. An abnormal mitochondrial-hypoxia inducible factor-1 α -kv channel pathway disrupts oxygen sensing and triggers pulmonary arterial hypertension in fawn hooded rats: Similarities to human pulmonary arterial hypertension. *Circulation*. 2006;113:2630-2641
43. Mourani PM, Ivy DD, Gao D, Abman SH. Pulmonary vascular effects of inhaled nitric oxide and oxygen tension in bronchopulmonary dysplasia. *Am J Respir Crit Care Med*. 2004;170:1006-1013
44. Le Cras TD, Kim DH, Gebb S, Markham NE, Shannon JM, Tuder RM, Abman SH. Abnormal lung growth and the development of pulmonary hypertension in the fawn-hooded rat. *Am J Physiol*. 1999;277:L709-718
45. Marino M, Beny JL, Peyter AC, Bychkov R, Diaceri G, Tolsa JF. Perinatal hypoxia triggers alterations in k^+ channels of adult pulmonary artery smooth muscle cells. *Am J Physiol Lung Cell Mol Physiol*. 2007

46. Hjalmarson O, Sandberg K. Abnormal lung function in healthy preterm infants. *Am J Respir Crit Care Med.* 2002;165:83-87

CHAPTER 8

APPENDIX 2

ANTENATAL SILDENAFIL TREATMENT ATTENUATES PULMONARY HYPERTENSION IN EXPERIMENTAL CONGENITAL DIAPHRAGMATIC HERNIA

Luong, C*, Rey-Parra G.J*, Gilmour G, Sauve Y, Koonen D, Walker D, Todd KG, Gressens P, Kassiri Z, Nadeem K, Vadivel A, Morgan B, Eaton F, Dyck JR, Archer SL, Thébaud B. Antenatal sildenafil treatment attenuates pulmonary hypertension in experimental congenital diaphragmatic hernia. *Circulation*. 2011 May 17;123(19):2120-31. Epub 2011 May 2.

8.1 Introduction

Congenital diaphragmatic hernia (CDH) remains the most life threatening cause of respiratory failure in newborns¹. CDH is a defect of the diaphragm allowing the abdominal content to ascend into the thorax, thereby compromising lung growth *in utero*. CDH occurs in 1/2000 live births². For many years, this malformation was thought to be solely related to a diaphragmatic defect and potentially curable by surgical closure of this defect after birth³. It is now clear that the degree of lung hypoplasia and severity of the pulmonary vascular abnormalities leading to persistent pulmonary hypertension of the newborn (PPHN) are the two main factors limiting outcome in CDH^{4, 5}. Evidence suggests that the malformation includes failure of both alveolar and pulmonary vascular development⁶⁻⁹.

Despite improvements in perinatal care, the mortality (~50%)^{10, 11} and morbidity¹² rate in CDH remains high. Unlike other causes of neonatal respiratory failure, infants with CDH strikingly often present with refractory PPHN resistant to the pulmonary vasodilator, inhaled nitric oxide (NO)^{13, 14}. Even amongst survivors the prognosis is guarded and chronic pulmonary hypertension beyond the neonatal period is increasingly recognized in this patient population^{15, 16}. Consequently, the ultimate therapeutic goal in order to improve survival of infants affected with this devastating malformation, is to promote lung growth before birth and to develop more efficient strategies to treat PPHN¹⁷.

The mechanisms underlying refractory PPHN in CDH remain unknown, but may relate to some combination of (i) altered vasoreactivity (lack of vasodilatation/increased vasoconstriction), (ii) vascular remodeling (smooth muscle cell (SMC) proliferation) and (iii) a hypoplastic pulmonary vascular bed.

Though there are 11 cGMP specific PDE gene families expressed in mammalian SMCs, PDE5 is the most active cGMP-hydrolyzing PDE active under basal, low calcium conditions¹⁸. PDE5 inhibition is used therapeutically in erectile dysfunction and although it is expressed in all visceral and vascular SMCs, it has only a modest effect on systemic blood pressure. In addition, the PDE5 inhibitor

sildenafil dilates the pulmonary vasculature and has antiproliferative effects on human PASMC¹⁹. These properties have been harnessed for the treatment of pulmonary hypertension in adult patients^{20,21}. Consequently, we hypothesized that antenatal PDE5 inhibition with sildenafil would attenuate pulmonary vascular abnormalities in experimental CDH.

8.2 Materials and Methods

All procedures and protocols were approved by the Animal Care and Use Committee at the University of Alberta.

8.2.1 Animal model

Pregnant Sprague–Dawley rats were gavage fed 100 mg of the herbicide nitrofen dissolved in 1 ml olive oil vehicle at embryonic day (E) 9.5 as previously described²². Control animals received olive oil only. Nitrofen is not toxic to adult rodents but induces CDH and lung hypoplasia in the offspring; the incidence of CDH varies depending on the timing of nitrofen administration²². Pregnant Sprague-Dawley rats were randomized to 4 groups: control, nitrofen treatment, nitrofen+sildenafil treatment, and sildenafil treatment alone (sildenafil control). Sildenafil (100 mg/kg/d) was administered from E11.5 to E20.5 by subcutaneous injection. At term (E21.5) fetuses were harvested by cesarean section and assessed for various parameters, outlined below, according to our experimental design. Since not all fetuses develop CDH only those that developed CDH in the nitrofen and nitrofen+sildenafil litters were analyzed. A total of 408 fetal rats were used for analysis.

8.2.2 Plasma sildenafil concentration

Maternal and fetal (E21.5) blood samples were collected at 1h, 2h, 6h, 12h, and 24h post injection. Plasma was isolated from these samples by centrifugation at 10,000 RPM for 10 minutes. Fetal plasma samples were pooled (at 1hr n=10, 2hr n=12, 6hr n=3, 12hr n=5, 24hr n=10) and sildenafil concentrations were

determined by high performance liquid chromatography (HPLC) with mass spectrometric (MS) detection.

Plasma samples were analyzed for sildenafil and its N-desmethyl metabolite by a modification of previously described methodology²³. Briefly, plasma samples (50 μ l) were mixed with internal standard (structurally related analogue of sildenafil) and extracted by solid phase extraction. Extracts were separated by HPLC using a 5 μ m C18 column (50 x 4.6 mm, Hypersil-100, Thermo-Hypersil, Runcorn, UK) and quantified using triple quadrupole mass spectrometric detection in positive ion MRM mode (API 4000, MDS, Sciex, Concord, Ontario, Canada). The quantitation range was 2 to 1000 ng/ml for both analytes.

8.2.3 Lung cGMP levels

Lungs (E21.5) from 5 control, 5 nitrofen-CDH, and 4 nitrofen-CDH+sildenafil rats were harvested and snap frozen in liquid nitrogen. cGMP concentrations were measured with a Cyclic GMP EIA kit (Biomedical Technologies, Inc.) according to the manufacturer's protocol and as previously described²⁴.

8.2.4 Lung morphology

Fetal rat lungs (E21.5) from control, nitrofen-CDH, nitrofen-CDH+sildenafil, and sildenafil control groups were fixed for histology by tracheal instillation of 10% buffered formalin under 20 cm H₂O constant pressure. After ligation of the trachea, the lungs were immersed in fixative overnight. Lungs were processed and embedded in paraffin. Serial sections were taken throughout the medial right lung lobe and stained with Hematoxylin and Eosin (H&E). The stained sections were analyzed with OpenLab Imaging System (Quorum Technologies Inc., Guelph, ON, Canada). Alveolar structure was quantified by the mean linear intercept (Lm) as previously described²⁵.

8.2.5 Western blot analysis

Snap frozen lungs were homogenized on ice in homogenization buffer (50 mM Tris HCl, 150 mM NaCl,) containing protease inhibitor cocktail I and II (Sigma). Samples were sonicated and centrifuged at 10,000 g for 20 min at 4–C. Protein content in the supernatant was determined by the Bradford method using BSA as the standard. Thirty micrograms of protein sample per lane were subjected to SDS-PAGE, and proteins from the gel were transferred to nitrocellulose membranes by electroblotting. Immunodetection was performed with a mouse anti-eNOS polyclonal antibody (610296, BD Sciences, Mississauga, ON, Canada) diluted 1:1,000, a rabbit polyclonal to VEGF antibody (ab46154; Abcam, Cambridge, MA) diluted 1:1000, cGMP-dependent phosphodiesterases Type 5A- antibody (PD5A-112AP, FabGennix Inc., Frisco, TX) diluted 1:500 and a Phospho-specific PDE5A-antibody (PPD5-140AP, FabGennix Inc., Frisco, TX) diluted 1:500 overnight at 4–C. After the blots were washed to remove unbound antibody, secondary antibodies, anti-mouse horseradish peroxidase antibody (1:1,000, Santa Cruz Biotechnology) for eNOS detection, and anti-rabbit horseradish peroxidase (1:3,000, Santa Cruz Biotechnology) for VEGF, PDE5A and Phospho-specific PDE5A detection were applied for 2 h at room temperature. After being washed, bands were visualized by enhanced chemiluminescence using ECL Plus detection (Amersham, Baie d’Urfe, QC, Canada). In addition, each gel was stripped and reprobed with actin as a housekeeping protein to normalize for protein loading.

8.2.6 Barium-gelatin arteriograms and arterial density counts

The main PA of E21.5 rats was cannulated and injected with warmed barium gelatin. The lungs were then fixed by tracheal instillation of formalin at a constant pressure of 20cm H₂O, removed from the body cavity and submerged in formalin for at least 2 days. To assess gross vascular morphology, fixed lungs were imaged using a computed tomography (CT) imaging system (Gamma Medica). For quantitative assessment, lungs were paraffin embedded, sectioned and H&E stained. The number of barium filled vessels was counted in 30 high power fields

(400X) per lung, in 5 animals per group²⁵. Fields containing large airways or major PAs were avoided to maintain consistency of counts between sections.

8.2.7 Medial wall thickness

To assess pulmonary artery remodeling, the percent Medial wall thickness (MWT), a surrogate marker of pulmonary hypertension, was calculated as $(2 \times \text{wall thickness}/\text{external diameter}) \times 100\%$ ²⁶. MWT measurements were performed on small PAs (30–100 μm) on H&E stained lung sections using OpenLab.

8.2.8 Right ventricular hypertrophy

The right ventricle and left ventricle plus septum were weighed separately to determine the ratio (RV/LV+S) as an index of Right ventricular hypertrophy RVH²⁶.

8.2.9 Organ bath studies of newborn rat PAs

Intrapulmonary arteries (diameter <100 μm , length = 2 mm) were mounted in a wire myograph (Myodaq; Danish Myo Technology, Denmark) and bathed in a Krebs-Henseleit buffer bubbled with 21% O₂-5% CO₂-balance N₂²⁷. PAs were precontracted with the thromboxane A₂ analogue U-46619 (10⁻⁷M) and isometric changes in response to NO donor 2-(*N,N*-diethylamino)-diazene-2-oxide (DEANO) (10⁻⁷-10⁻⁵M) were compared between PAs from the 4, age-matched groups. PA relaxation was assessed as a percent of maximal constriction from U-46619. All drugs were purchased from Sigma-Aldrich (Saint Louis, Missouri, USA).

8.2.10 Retina studies

The functional integrity of the retina was assessed using a standard clinical test, the electroretinogram (ERG), which is a non-invasive measure of the electrical changes of the retina in response to light flashes. The ERG was recorded from both eyes of 30 days old rats that had either received antenatal sildenafil

(n=6 rats) or saline injections (n=4 rats). At this age the retina's functional maturity is reached²⁸. In brief, ERG responses (to increasing flash intensities) were recorded in xylazine-ketamine anesthetized rats, firstly, under dark-adaptation (scotopic ERG). Two ERG waves were quantified, the a-wave (reflecting photoreceptor activity) and the b-wave (reflecting activation of the retina circuit downstream to photoreceptors). ERG recordings were then repeated under light adaptation (photopic ERG, under 30 cd/m² luminance background). Finally, photopic ERG responses to flickering flashes (1.37 log cds/m² luminance), presented at increasing frequencies, were recorded. Criterion amplitudes were set at 20 μ V for a- and b-waves and at 5 μ V for flicker amplitudes.

The anatomical integrity of the retina was assessed using Nissl staining on retinal cross sections (to examine the retina's laminar organization; n=4 control and n=4 sildenafil control) as well as with fluorescein angiography on retinal flatmounts (to examine the inner retinal vasculature; n=4 control and n=4 sildenafil). For Nissl staining, retina cryosections were stained in 0.1% cresyl violet solution, dehydrated, cleared in xylene and mounted on glass slides. For fluorescein angiography, rats were transcardiacally perfused with Fluorescein Isothiocyanate Dextran 500,000-conjugate (Sigma). The eyes were removed, post-fixed and then retina flat mounts dissected to be post-fixed. Tissues were mounted on slides and visualized with a Zeiss LSM 510 confocal microscope, and processed with Photoshop 6.0 software (Adobe, San Jose, CA) to adjust contrast levels if required. Two variables were assessed using ImageJ (NIH; <http://rsbweb.nih.gov/ij/index.html>): 1- branching points; 2- density of labeled blood vessels. Four windows were analyzed for the right eye of each animal; these corresponded to the mid-periphery of the retina in the 4 respective quadrants (nasal, temporal, dorsal, ventral).

8.2.11 Brain studies

Brains collected at E21.5 were fixed in formalin and paraffin embedded. Antibodies used for immunostaining were directed against calbindin protein

(CaBP, a marker of a subpopulation of GABAergic interneurons) (1/2000, rabbit polyclonal; SWant, Bellinzona, Switzerland), calretinin (a marker of a subpopulation of GABAergic interneurons) (1/2000, rabbit polyclonal; SWant), glial fibrillary acidic protein (GFAP, a marker of astrocytes) (1/500, rabbit polyclonal; Dako, Glostrup, Denmark), and tomatolectin (a marker of microglia-macrophages) (1/500, biotinylated lectin; Vector, Burlingame, CA). These antibodies were detected using an avidin-biotin-horseradish peroxidase kit (Vector), as instructed by the manufacturer. Diaminobenzidine was used as a chromogen. Immunolabeled cells were quantified at the level of the parietal cortex. Two fields were analyzed in each experimental group for each animal (5/group) and for each marker.

In a separate series of animals (n=4-6) fresh flash-frozen brains from P30.5 rats were mounted in freezing medium and the brains sectioned from the anterior pole to 5 mm posterior to bregma. Adjacent sections 20 μ m thick were slide mounted and used to assess cytoarchitecture, cytogenesis and dying cells. Antibodies recognizing the neuronal cell marker NeuN (1/1000, mouse monoclonal), the astrocyte marker GFAP (1/700, mouse monoclonal) and 5-bromo-2-deoxyuridine a marker of replicating/dividing cells (BrdU, 1/600, mouse monoclonal) were immunoreacted with the sections after which they were incubated with the species relevant secondary IgG antibody, amplified with avidin-biotin complex and visualized with DAB. Semi-quantitative field count score was used to count BrdU positive cells. To identify the presence of degenerating cells, the sections were incubated with Fluorojade-B according to standard protocols. Scores from abutting fields (3-6 fields depending on the size of the brain region) were obtained from the hippocampus, cortex, subventricular zone, basal ganglia (data not shown) and thalamus (data not shown).

8.2.12 Statistical analysis

Statistical analysis was performed using software (SPSS for Windows, version 13; SPSS, Chicago, Ill). Values were expressed as the mean \pm SEM. Comparisons of parameters between 2 groups were made by unpaired Student's t-test. One-way

ANOVA determined significance of litter and rat where relevant. If litter was not significant then comparisons of parameters were made by one-way ANOVA and post-hoc analysis with Student-Newman-Keuls (SNK) test. If a litter effect was significant then statistical analysis was completed with a linear mixed-effects model to account for within litter correlations. Repeated measures ANOVA was used to assess differences in PA relaxation studies. Statistical significance was defined as $P < 0.05$.

8.3 Results

8.3.1 Maternal administered sildenafil crosses the placenta and inhibits PDE5 activity in fetal rat lungs

Maternal and fetal plasma concentrations of sildenafil were measured by HPLC from samples obtained at 1, 2, 6, 12, and 24 hours post injection (Figure 1A). Maternal and fetal plasma concentration profiles followed a similar trend, peaking at about 6h post-maternal administration, indicating that sildenafil effectively crossed the placenta and entered the fetal circulation.

Biological activity of sildenafil in fetal lung was confirmed by measuring cGMP concentrations (Figure 1B), as well as PDE5A expression (Figure 1C) in fetal rat lungs. Nitrofen exposure at E9.5 was associated with a significant decrease in lung cGMP concentration and increased activated PDE5A expression. Sildenafil treatment from E11.5 to E20.5 produced a marked increase in lung cGMP in nitrofen-CDH fetuses and in controls, and a significant attenuation in active PDE5A expression, indicating that sildenafil was biologically active in the fetal lung.

8.3.2 Effects of antenatal sildenafil on body weight, incidence of CDH, and lung hypoplasia

Rats with nitrofen-induced CDH had significantly reduced body weights at E21.5 (Figure 2A). Antenatal sildenafil had no effect in pups with nitrofen-induced CDH.

Sildenafil had no effect on the incidence of CDH (Figure 2B).

The lung weight to body weight ratio (LW/BW), a crude indicator of lung hypoplasia was lower in nitrofen-CDH fetuses as compared to controls (Figure 2C). Antenatal sildenafil decreased LW/BW in normal fetuses. Sildenafil had no effect on LW/BW in the nitrofen-CDH+sildenafil rats.

8.3.3 Antenatal sildenafil improves lung architecture in CDH rats

The Lm was significantly higher in animals with nitrofen-induced CDH as compared with controls (Figure 3A-B). Fetal rats in the nitrofen-CDH+sildenafil group had Lm values that were similar to those of controls (Figure 3B). Sildenafil had no effect on lung architecture in control pups.

8.3.4 Antenatal sildenafil increases pulmonary vessel density in CDH

Nitrofen-CDH animals had significantly fewer pulmonary vessels as compared with controls (Figure 4A-B). Sildenafil significantly increased pulmonary vessel count in nitrofen-CDH animals but decreased pulmonary vessel density in control animals. This was associated with increased lung eNOS and VEGF protein expression (Figure 4C).

8.3.5 Antenatal sildenafil attenuates features of pulmonary hypertension in CDH

Albeit MWT was increased in rats with nitrofen-induced CDH as compared with controls and antenatal sildenafil decreased MWT in animals with nitrofen-induced CDH (Figure 5A), using the appropriate linear mixed model taking both litter and rat effect into account these differences were not statistically significant.

RVH was significantly greater in nitrofen-CDH animals as compared with control (Figure 5B). Antenatal sildenafil treatment attenuated RVH in animals with nitrofen-induced CDH. Sildenafil had no effect on RVH in control rats. RV weight was significantly reduced in control-sildenafil treated animals. LV weight was significantly reduced in both nitrofen CDH and nitrofen-CDH+Sildenafil treated animals.

8.3.6 Antenatal sildenafil enhances PA responsiveness to the NO donor, DEANO

The contractile response of PAs in response to U46619 was similar between groups (Figure 5C). PAs from fetal rats with nitrofen-induced CDH relaxed less to DEANO as compared with controls, paralleling the attenuated response to inhaled NO seen in infants with CDH (Figure 5D). In contrast, PAs from nitrofen-induced CDH animals treated with sildenafil showed an enhanced response to the DEANO. Relaxation of these vessels at the highest DEANO concentration approached precontraction levels.

8.3.7 Retina studies

Antenatal sildenafil had no side effects on retinal function (as assessed by ERG, Figure 6A) or anatomy (Nissl staining, Figure 6B and fluorescein angiography, Figure 6C). All ERG components, including a- and b-waves as well oscillatory potentials (not illustrated) had similar amplitudes and implicit times (not illustrated) between the two groups studied (control versus sildenafil, Figure 6A). Nissl staining shows that all layers were identical between both groups (Figure 6B). Likewise, retinas from both control and sildenafil-exposed rats had similar blood vessel patterns as observed on flatmounts (Figure 6C). There were no difference between control and treated groups in arterial density (0.17 ± 0.02 vs. 0.17 ± 0.03 , $P=0.42$) or number of branching points (122 ± 8 vs 100 ± 21 , $P=0.07$).

8.3.8 Sildenafil does not affect brain maturation

Parietal neocortexes of E21.5 pups were collected. Antenatal sildenafil had no detectable effect on the density of GFAP-positive astrocytes, tomatolectin-positive microglia-macrophages, calretinin-positive and CaBP-positive interneurons (data not shown). Likewise, at P30 no difference were found in brain GFAP (Figure 7A), NeuN (Figure 7B) and BrDU (Figure 7C) immunoreactivity

between groups. Fluorochrome staining for dying/degenerating cells was negative in both groups (Figure 7D).

8.4 Discussion

We show that maternal sildenafil treatment enhances pulmonary vessel density, reverses RVH and improves the pulmonary vasodilatory response to NO in the nitrofen-induced CDH rat model. This is achieved without significant effect on retinal structure and function (P30), and brain development assessed by histology (E21.5 and P30). Our data suggest the opportunity of further exploring the therapeutic potential of sildenafil as a prenatal medical therapy for CDH.

CDH remains one of the greatest challenges in perinatal medicine²⁹. Many infants with CDH respond poorly to inhaled NO^{13, 14}. Survivors with severe PPHN and hypoplastic lungs, suffer significant morbidity, and show a new emerging pattern of severe late and chronic pulmonary hypertension^{15, 16}. In humans, CDH can be accurately diagnosed at about 22 weeks gestation during routine ultrasound exam and is thus amenable to antenatal therapies. Over the past decades a number of surgical strategies have attempted to improve lung growth before birth^{1, 30}. The idea of the herein proposed antenatal use of sildenafil for regression of PPHN parallels the use of antenatal glucocorticoid treatment for women with threatened preterm labor to mature the fetal lung and prevent postnatal complications in premature infants³¹. By analogy, we reasoned that antenatal sildenafil, an approved and safe medication in adults, could have similar beneficial effects on lung vascular development in CDH.

Experimental nitrofen-induced CDH in rats is a well-established and reliable model that recapitulates the pulmonary abnormalities described in human CDH including lung hypoplasia and pulmonary vascular remodeling³². While the mechanism by which nitrofen induces the diaphragmatic defect and lung hypoplasia are not fully understood^{17, 33}, the herbicide also affects overall fetal growth suggesting potential systemic effects³⁴. Studies of nitrofen metabolism in pregnant rats suggest that its teratogenicity is not mediated via generation of mutagenic intermediates through nitro-reduction of the parent compound. Rather, the embryo is exposed to the parent compound

alone and appears to be a deep compartment for accumulation of nitrofen³⁵. This is further corroborated by lung explant studies that show that removing the lung leads to spontaneous recovery unless repeatedly treated with nitrofen³⁶.

Recent evidence suggest that interactions between airways and blood vessels are critical for normal lung development³⁷. In 1959, Liebow observed that the alveolar septa in centrilobular emphysema were remarkably thin and almost avascular³⁸. He postulated that a reduction in the blood supply of the small precapillary blood vessels might induce the disappearance of alveolar septa. Pharmacological Vascular Endothelial Growth Factor (VEGF)-inhibition in neonatal and adult rats leads to arrested alveolar development^{25, 39} and loss of alveoli⁴⁰, respectively. These data suggest that inhibition of vascular growth itself may directly impair postnatal lung development. We and others showed that VEGF-driven angiogenesis reverses postnatal hyperoxia-induced alveolar hypoplasia^{25, 41}. Consequently, enhancing vascular growth before birth may be a therapeutic strategy to promote lung growth in CDH. We previously showed that sildenafil promotes lung angiogenesis *in vitro* and in the developing lung postnatally⁴².

There have been several studies from various laboratories using the nitrofen-induced CDH model, including several that have shown decreased lung eNOS and VEGF expression in CDH vs control lungs⁴³⁻⁴⁵. More interestingly, NO and VEGF promotes airway branching in normal and CDH lung explants^{36, 46, 47} and *in vivo*, inhaled NO prolongs survival in CDH rat pups and this effect could be enhanced with prenatal glucocorticoids^{48, 49}. Here we investigated if administration of antenatal sildenafil could have a beneficial effect on the hypoplastic nitrofen lung *in vivo*. Consistent with previous studies in this model, we show that antenatal sildenafil from E11.5-20.5 improved lung maturation and increased vessel density in rats with nitrofen-induced CDH. Accordingly, decreased lung eNOS and VEGF protein expression in nitrofen-induced CDH was restored by antenatal sildenafil. Hara et al had previously shown that antenatal tracheal occlusion (another therapeutic strategy to promote lung growth in CDH¹) increases VEGF-A protein expression and suggested that VEGF-A mediates

previously described changes in lung vascular and parenchymal development caused by tracheal occlusion⁴³. Similar data were reported by Cloutier et al in mice⁵⁰. The mechanism by which sildenafil increases lung eNOS and VEGF expression remains speculative. It is suggested that sildenafil activates K_{ATP} channels and induces nitrate-like effects, which induces the production of interstitial adenosine. Adenosine is thought to increase VEGF protein and mRNA expression by adenosine receptors⁵¹. Sildenafil also activates phosphorylation and activation of eNOS expression and this might contribute to the up-regulation of VEGF expression⁵². Finally, Sildenafil may increase VEGF expression through induction of thioredoxin-1 and hemeoxygenase-1⁵³ both known to upregulate VEGF expression.

Intriguingly, normal rats that received antenatal sildenafil had decreased lung vessel density at term as compared with controls. The mechanisms underlying this finding are unclear and require further investigation. The few teratogenicity studies have suggested sildenafil to be safe during pregnancy in a variety of species^{23, 54}.

In addition to lung hypoplasia, PH is a limiting factor of survival in CDH. PH in CDH is characterized by PA remodeling with excessive muscularization of preacinar arteries, reduced external diameter of pre- and intra-alveolar arteries and increased medial wall thickness⁵⁵ and poor response to inhaled NO^{14} . In addition to acting as a vasodilator, sildenafil also functions as a potent inhibitor of adult human PASMC proliferation as well as an inducer of apoptosis¹⁹. While antenatal sildenafil attenuated pulmonary smooth media remodeling as assessed by the MWT, the difference was not statistically different in the nitrofen model.

Another interesting finding was that the sildenafil-induced reduction in the RV/LV+S ratio was mostly due to a combined improvement in RV and LV+S. Indeed, nitrofen-induced CDH rats had significant LV hypoplasia, similar to what has been described in the sheep model and in humans with CDH^{56, 57}.

Another important finding of our study was the enhanced pulmonary vasorelaxation in response to DEANO, suggesting that priming of the pulmonary vasculature before birth may enhance the response to postnatal therapies. Given

that sildenafil was administered less than 24 hours prior to delivery, a certain degree of PDE5 inhibition may still be present in the pulmonary vascular tissue so that enhanced vasorelaxation can probably not solely be attributed to attenuation of PA remodeling. This is further supported by the observation that sildenafil significantly reduces pulmonary vascular resistance in normal and ductus arteriosus ligated fetal sheep in response to birth-related stimuli such as oxygen and shear stress^{58,59}.

The sildenafil dose chosen for the pregnant rats was 100mg/kg/day based on previous studies that examined the pharmacokinetics of sildenafil in rodents²³. In chronic *in vivo* studies in rats this dose yielded mean free plasma concentrations comparable to levels obtained in humans at doses of 1 mg/kg/d. This reflects the near 100-fold higher rate of metabolism of sildenafil in rats. At this dose, there were no adverse visual and neurological effects seen in the offspring. We did not investigate changes that may have occurred in pregnant dams that were treated with sildenafil. This is important to note as there have been a small number of cases that have suggested a possible relationship between central serous chorioretinopathy and optic neuropathy with sildenafil use in humans⁶⁰. Furthermore, although there is no proven association between Sildenafil use and central serous chorioretinopathy or optic neuropathy it is prudent to consider cessation of sildenafil therapy in a patient that experiences sudden loss of vision⁶⁰. Further clinical challenges include the choice of the timing (e.g. introducing maternal sildenafil treatment early enough during gestation to positively impact outcome), dosing and length of treatment. Other limitations of this study include the lack of survival data and, inherent to the small animal model, the lack of physiologic data. Experiments in the fetal sheep model are underway to answer these questions. Finally, in this study, data from littermates were treated as independent observations. This is a common assumption in studies using the nitrofen model, as nitrofen does not affect all the offspring in a comparable manner with regards to presence and severity of the diaphragmatic defect, degree of lung hypoplasia, or growth restriction, even within the same litter.

In conclusion, antenatal treatment with sildenafil improves lung structure, increases vessel density, decreases RVH, and enhances dilatation to NO in experimental, nitrofen-induced CDH in rats. We speculate that the sildenafil-induced pulmonary arterial tissue PDE5 inhibition resulted in enhanced DEANO-dependent relaxation in the fetuses. Antenatal strategies may improve responsiveness to postnatal pulmonary vasodilator therapies and ultimately the outcome of infants with CDH. The relative pulmonary vascular specificity of sildenafil, its low cost, and its post-marketing safety makes it an attractive therapeutic option for infants with CDH.

Figure 1

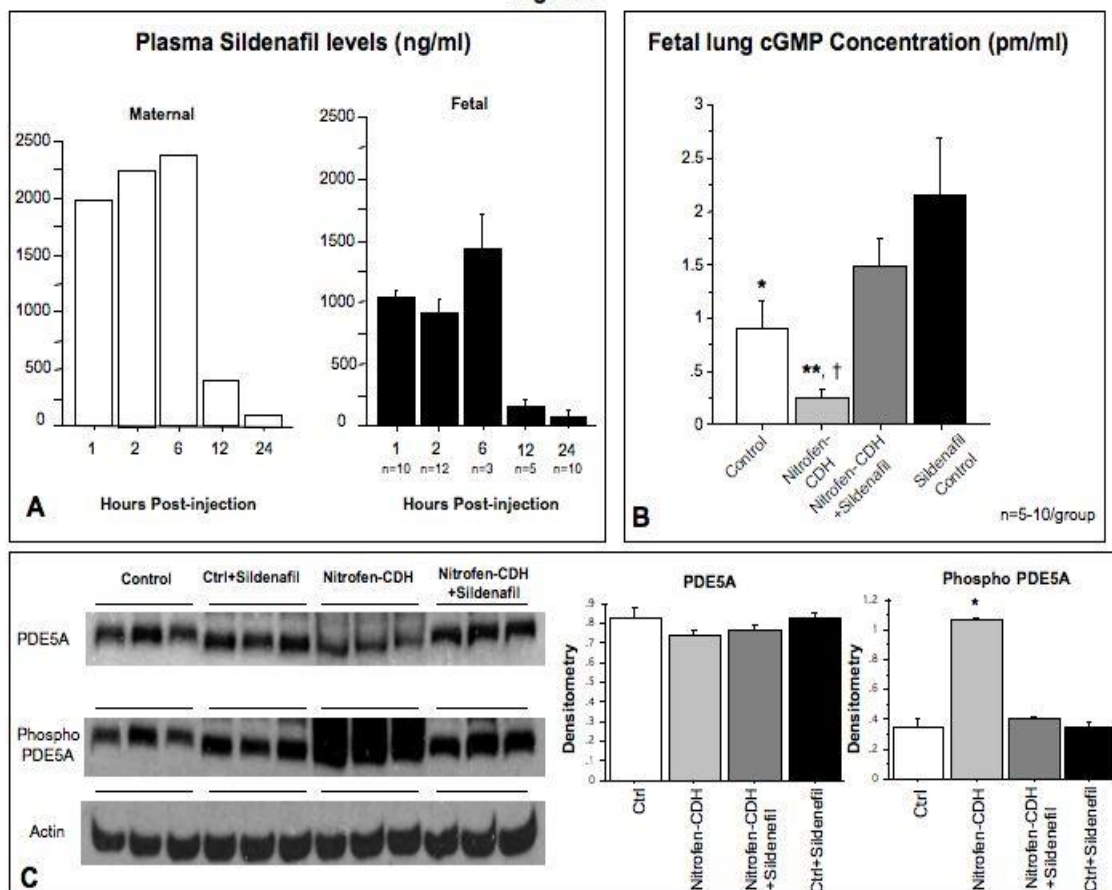


Figure 8.1. Sildenafil crosses the placenta and increases fetal lung cGMP and alters protein expression in fetal rat lungs. **A.** Plasma Sildenafil levels in single maternal rat and pooled fetal rat samples at 1, 2, 6, 12, and 24 hours post administration. **B.** Fetal lung concentrations of cGMP is significantly decreased in nitrofen-CDH as compared to control. cGMP concentration is restored in CDH animals treated with antenatal Sildenafil. (ANOVA $P < 0.02$; P -value: *Control vs CDH 0.045, Control vs CDH+Sildenafil 0.15, *Control vs Sildenafil Control 0.046, **CDH vs CDH+Sildenafil 0.0002, †CDH vs Sildenafil Control 0.0001, CDH+Sildenafil vs Sildenafil Control 0.24). **C.** Western blot assessing E21.5 lung expression of PDE5A and active phosphorylated PDE5A demonstrate an increase in phosphorylated PDE5A as compared with all other groups. (PDE5A ANOVA $P = 0.29$; Phosphorylated PDE5A, ANOVA $P < 0.0001$; SNK P -values: *Control vs CDH < 0.05 , Control vs CDH+Sildenafil > 0.05 , Control vs Sildenafil Control > 0.05 , *CDH vs CDH+Sildenafil < 0.05 , *CDH vs Sildenafil Control < 0.05 , CDH+Sildenafil vs Sildenafil Control > 0.05)

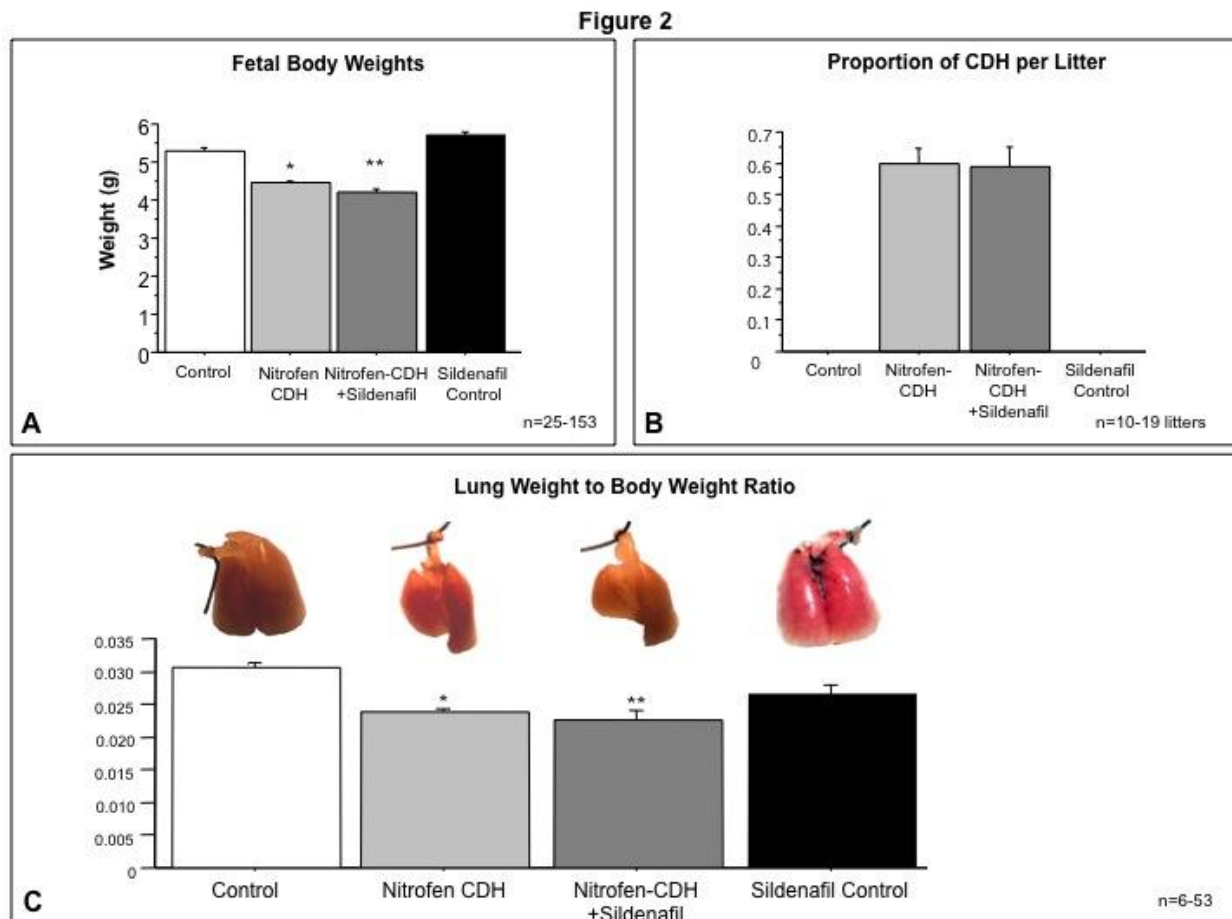


Figure 8.2. Effect of antenatal sildenafil on body weight (BW), incidence of CDH, and LW/BW ratio. **A.** Nitrofen significantly decreased fetal BW and this was not improved by antenatal treatment with sildenafil. (Linear mixed model ANOVA $P < 0.0001$; P-values: *Control vs CDH 0.005, **Control vs CDH+Sildenafil 0.002, Control vs Sildenafil Control 1.0, CDH vs CDH+Sildenafil 1.00, CDH vs Sildenafil Control 0.11, CDH+Sildenafil vs Sildenafil Control 0.04). **B.** The incidence of CDH in the offspring of nitrofen-fed dams was $0.596 \pm 0.052\%$. Sildenafil had no effect on the incidence of CDH ($0.589 \pm 0.061\%$, $P = 0.91$). **C.** LW/BW ratio was significantly decreased in the nitrofen-CDH group. Sildenafil had no effect on LW/BW ratio in nitrofen-CDH. (Linear mixed model ANOVA $P < 0.0001$; P-values: *Control vs CDH 0.002, **Control vs CDH+Sildenafil 0.001, Control vs Sildenafil Control 0.748, CDH vs CDH+Sildenafil 0.90, CDH vs Sildenafil Control 1.0, CDH+Sildenafil vs Sildenafil Control 0.40).

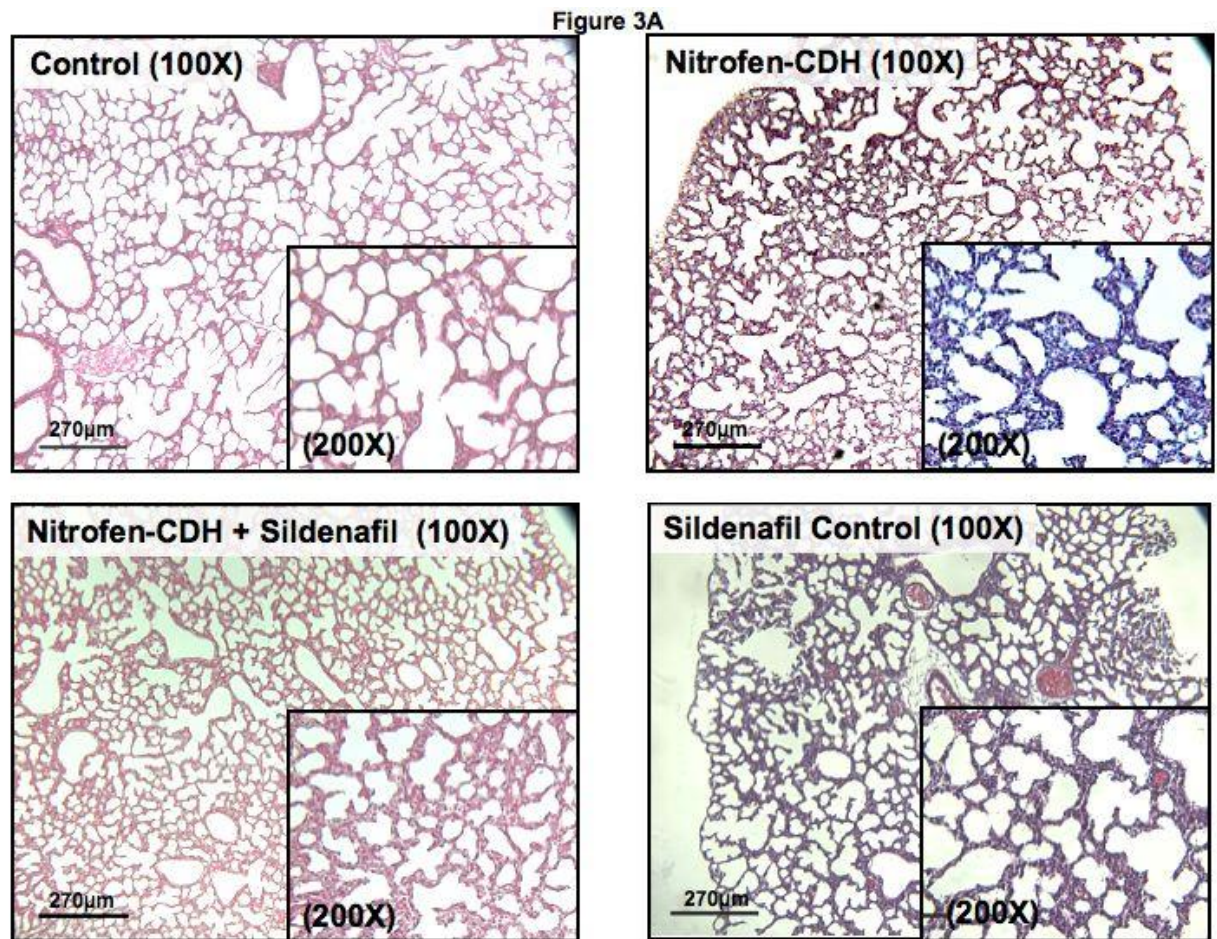


Figure 8.3. Effect of antenatal sildenafil on lung morphometry.

A. Representative H&E stained sections of the treatment groups showing thickened mesenchyme in nitrofen-induced CDH.

Figure 3B

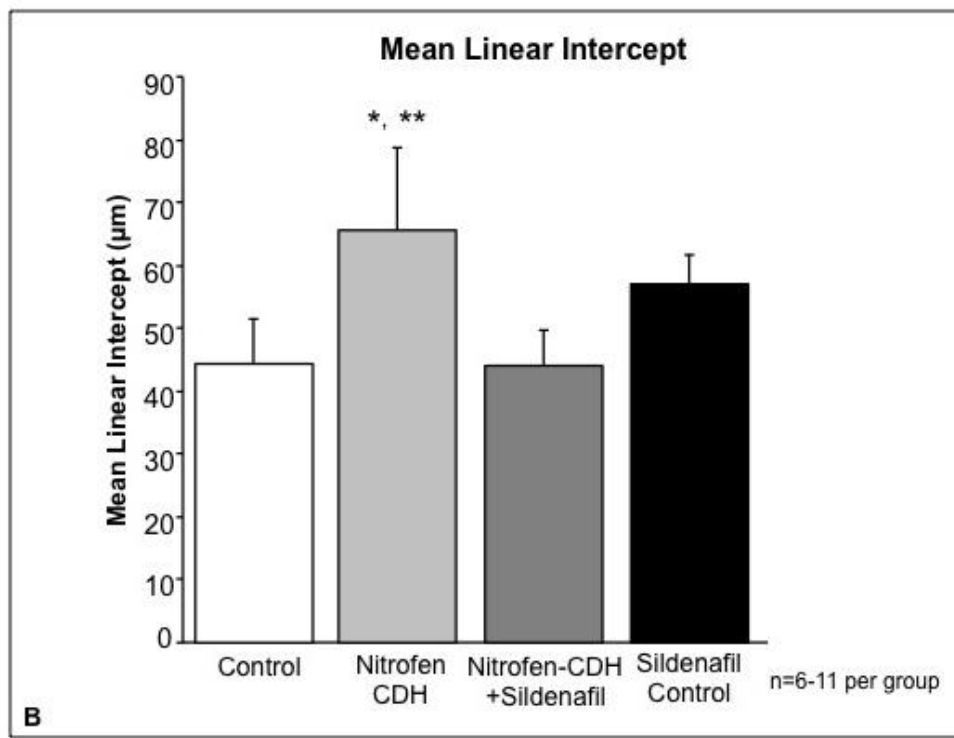


Figure 8.3. Effect of antenatal sildenafil on lung morphometry.

B. Nitrofen-induced CDH lungs had increased mean linear intercept as compared to controls. Sildenafil decreased the mean linear intercept in CDH animals and had no effect in control animals. (Linear mixed model ANOVA $P=0.001$; P-values: *Control vs CDH 0.002, Control vs CDH+Sildenafil 1.00, Control vs Sildenafil Control 0.07, **CDH vs CDH+Sildenafil 0.005, CDH vs Sildenafil Control 0.38, CDH+Sildenafil vs Sildenafil Control 0.14)

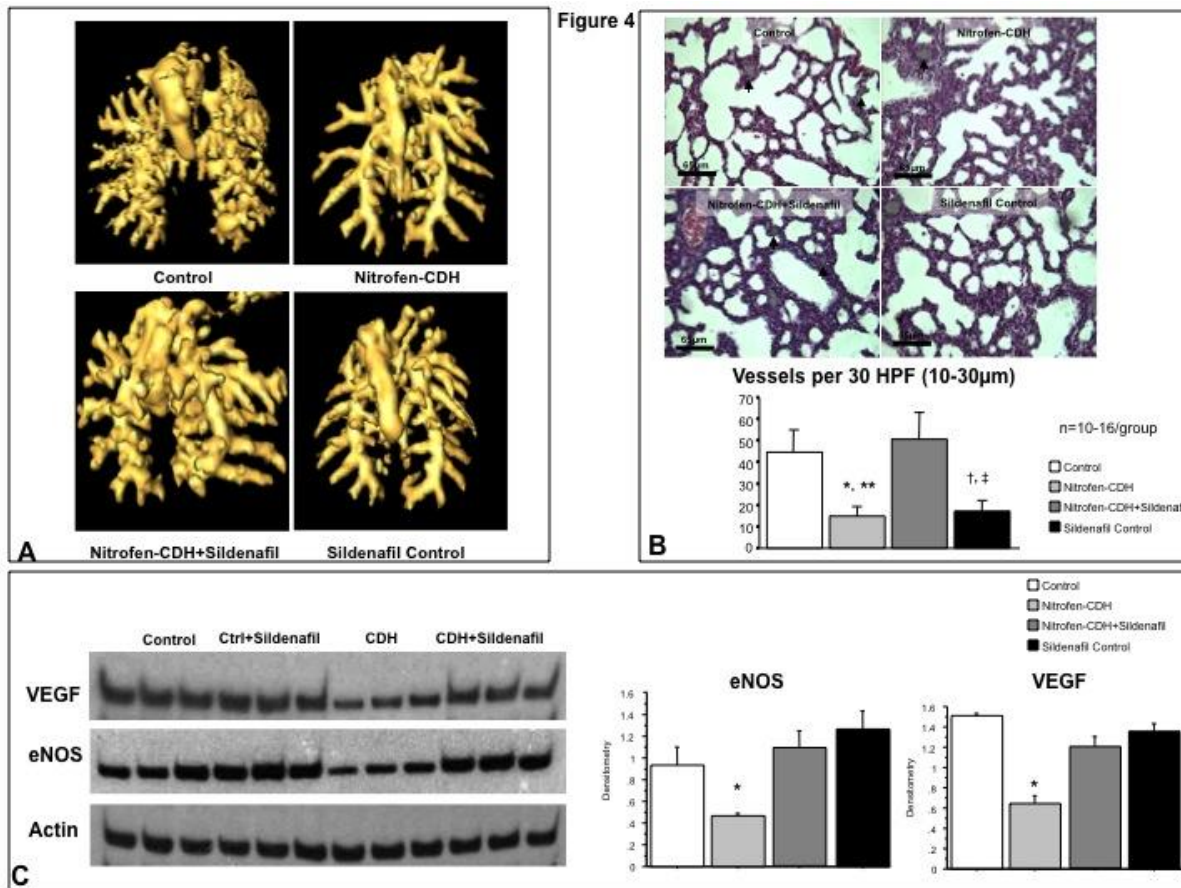


Figure 8.4. Antenatal sildenafil improves lung capillary density and lung expression of eNOS and VEGF. **A.** Representative CT-scan of barium injected pulmonary vessels. **B.** Representative H&E stained sections of barium-injected pulmonary vessels. Quantification demonstrates decreased density of pulmonary vessels in nitrofen-CDH rats. Antenatal sildenafil restores vessel density (Linear mixed model ANOVA $P < 0.0001$; P-value: *Control vs CDH 0.004, Control vs CDH+Sildenafil 1.0, †Control vs Sildenafil Control 0.02, **CDH vs CDH+Sildenafil 0.002, CDH vs Sildenafil Control 1.0, ‡CDH+Sildenafil vs Sildenafil Control 0.007). **C.** Western blots for eNOS and VEGF expression in E21.5 fetal rat lungs. eNOS and VEGF expression is decreased in nitrofen-CDH animals and is increased with antenatal sildenafil treatment. (eNOS ANOVA $P = 0.019$; SNK P-values: *Control vs CDH < 0.05 , Control vs CDH+Sildenafil > 0.05 , Control vs Sildenafil Control > 0.05 , *CDH vs CDH+Sildenafil < 0.05 , *CDH vs Sildenafil Control < 0.05 , CDH+Sildenafil vs Sildenafil Control > 0.05 ; VEGF ANOVA $P < 0.0001$; SNK P-values: *Control vs CDH < 0.05 , †Control vs CDH+Sildenafil < 0.05 , Control vs Sildenafil Control > 0.05 , *CDH vs CDH+Sildenafil < 0.05 , *CDH vs Sildenafil Control < 0.05 , CDH+Sildenafil vs Sildenafil Control > 0.05).

Figure 5

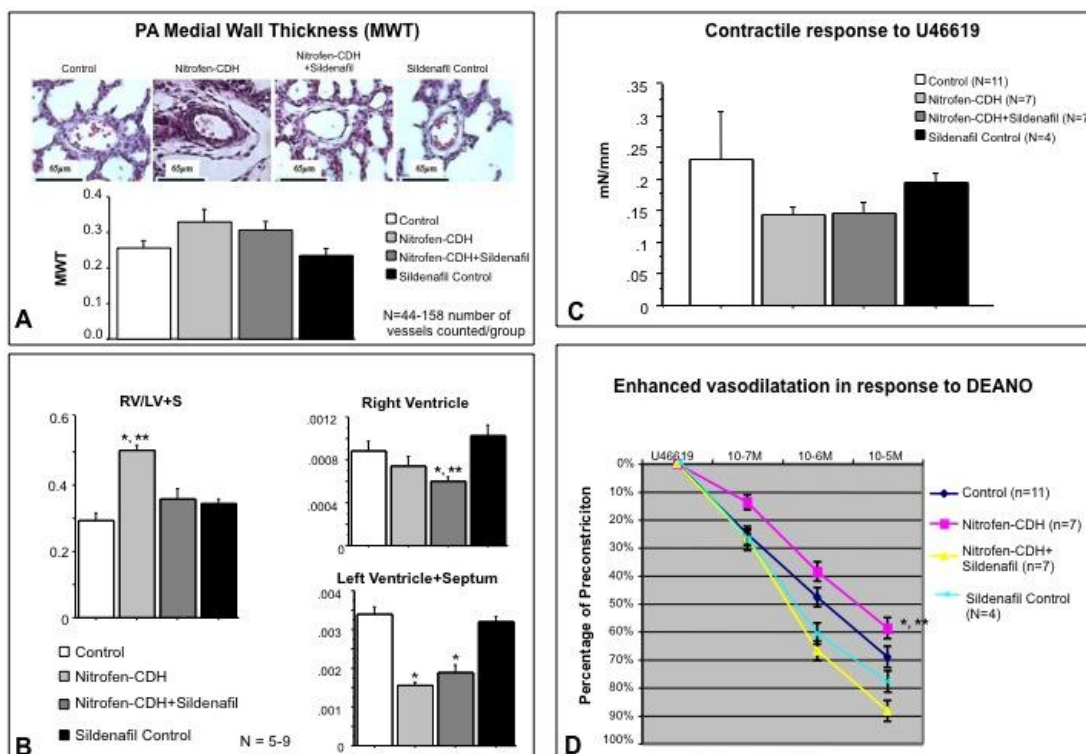


Figure 5. Antenatal sildenafil treatment attenuates features of pulmonary hypertension in the nitrofen-induced rat model of CDH. **A.** Medial wall thickness ratio. Using the appropriate linear mixed model taking both litter and rat effect into account there were no significant differences between CDH vs CDH+Sildenafil treated rats. **B.** Right ventricular hypertrophy in nitrofen-CDH rats was significantly reduced by sildenafil. (RV/LV+S Linear mixed model ANOVA $P=0.005$; P-values: *Control vs CDH 0.006, Control vs CDH+Sildenafil 1.0, Control vs Sildenafil Control 1.0, **CDH vs CDH+Sildenafil 0.03, CDH vs Sildenafil Control 0.055, CDH+Sildenafil vs Sildenafil Control 1.0; RV weights ANOVA $P<0.02$; P-values: Control vs CDH 0.30, *Control vs CDH+Sildenafil 0.04, Control vs Sildenafil Control 0.27, CDH vs CDH+Sildenafil 0.35, *CDH vs Sildenafil Control 0.04, **CDH+Sildenafil vs Sildenafil Control 0.003; LV+S weights ANOVA $P<0.0001$; P-values: *Control vs CDH <0.0001 , *Control vs CDH+Sildenafil <0.0001 , Control vs Sildenafil Control 0.40, CDH vs CDH+Sildenafil 0.23, *CDH vs Sildenafil Control <0.0001 , *CDH+Sildenafil vs Sildenafil Control <0.0001). **C.** The contractile response of PAs to U46619 was similar between groups (P-values: Control vs CDH 0.27, Control vs CDH+Sildenafil 0.39, Control vs Sildenafil Control 0.67, CDH vs CDH+Sildenafil 0.97, CDH vs Sildenafil Control 0.59, CDH+Sildenafil vs Sildenafil Control 0.67). **D.** PAs of nitrofen-CDH rats relaxed significantly less than controls in response to the NO donor DEANO. Antenatal treatment with sildenafil significantly enhanced relaxation of Nitrofen-CDH PAs. P-values *Control vs CDH <0.05 , ** CDH+Sildenafil vs CDH <0.0

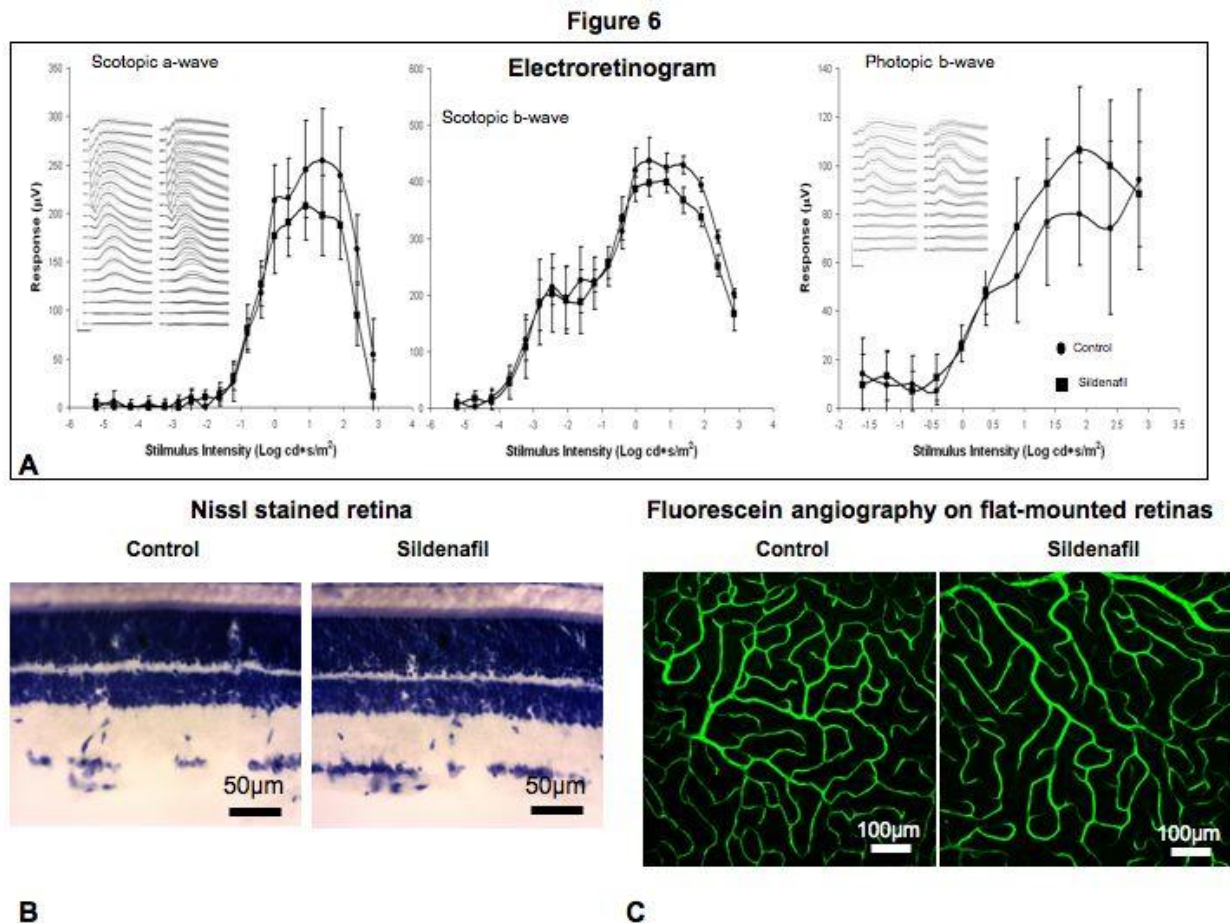


Figure 8.6. Sildenafil has no adverse effects on the Retina. **A.** ERG recordings showed no differences in retinal function between untreated controls (circle) and treated sildenafil (square) groups. Average ERG traces (\pm SEM) from control and treated groups are respectively displayed on the left and right columns of insets shown in the scotopic (a-wave graph) and photopic intensity response series. ERG recordings were done at age P30 bilaterally from 6 rats per group ($n=12$ eyes total per group); one eye per animal was used: the eye yielding the highest mixed scotopic a-wave amplitude was selected for each animal. Scale bar: vertical = 200 μV , horizontal: 50 msec. **B.** Anatomical analysis with Nissl staining (two panels on the left) and **C.** Fluorescein angiography (two panels on the right) showed no differences between the retinas of control and sildenafil groups. Scale bar = 50 μm in all panels.

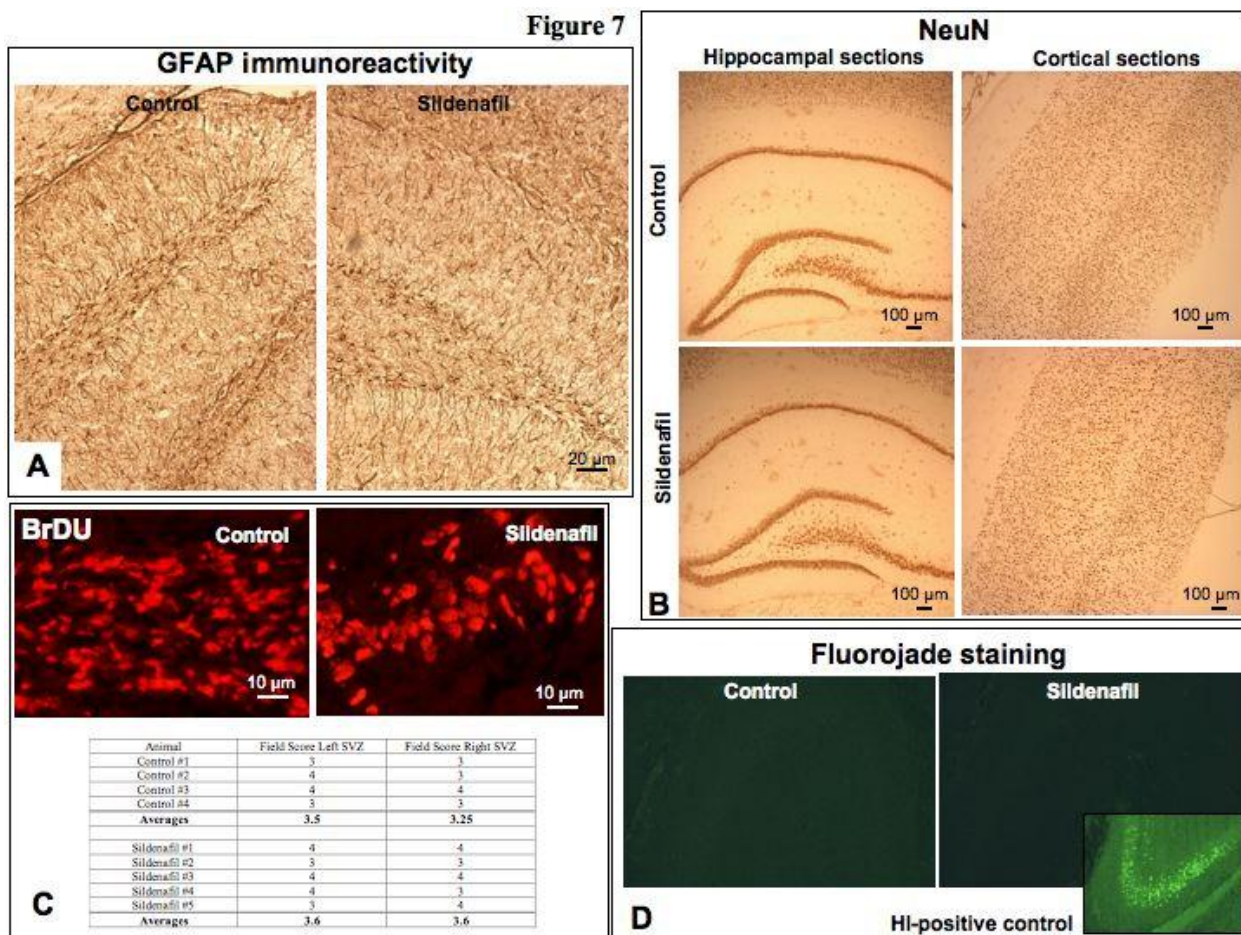


Figure 8.7. Sildenafil has no adverse effects on the neonatal brain at postnatal day 30. Immunoreactivity for GFAP (glial activation) in the Hippocampus (A), NeuN (neuronal cell-specific marker) in the cortex (left) and hippocampus (right) (B) and BrDU in the subventricular zone (SVZ) (C) of control and antenatally exposed sildenafil rats. No differences were noted between groups. D. Fluorojade staining of the hippocampus for dying/degenerating cells. No positive staining was observed in either control or sildenafil-treated rats. Insert: HI-positive control.

8.5 References

1. Harrison MR, Keller RL, Hawgood SB, Kitterman JA, Sandberg PL, Farmer DL, Lee H, Filly RA, Farrell JA, Albanese CT. A randomized trial of fetal endoscopic tracheal occlusion for severe fetal congenital diaphragmatic hernia. *N Engl J Med.* 2003;349:1916-1924
2. Langham MR, Jr., Kays DW, Ledbetter DJ, Frentzen B, Sanford LL, Richards DS. Congenital diaphragmatic hernia. Epidemiology and outcome. *Clin Perinatol.* 1996;23:671-688
3. Puri P, Wester T. Historical aspects of congenital diaphragmatic hernia. *Pediatr Surg Int.* 1997;12:95-100
4. Bohn D. Congenital diaphragmatic hernia. *Am J Respir Crit Care Med.* 2002;166:911-915
5. Thebaud B, Mercier JC, Dinh-Xuan AT. Congenital diaphragmatic hernia. A cause of persistent pulmonary hypertension of the newborn which lacks an effective therapy. *Biol Neonate.* 1998;74:323-336
6. Bohn D, Tamura M, Perrin D, Barker G, Rabinovitch M. Ventilatory predictors of pulmonary hypoplasia in congenital diaphragmatic hernia, confirmed by morphologic assessment. *J Pediatr.* 1987;111:423-431
7. Geggel RL, Murphy JD, Langleben D, Crone RK, Vacanti JP, Reid LM. Congenital diaphragmatic hernia: Arterial structural changes and persistent pulmonary hypertension after surgical repair. *J Pediatr.* 1985;107:457-464
8. Kitagawa M, Hislop A, Boyden EA, Reid L. Lung hypoplasia in congenital diaphragmatic hernia. A quantitative study of airway, artery, and alveolar development. *Br J Surg.* 1971;58:342-346
9. Naeye RL, Shochat SJ, Whitman V, Maisels MJ. Unsuspected pulmonary vascular abnormalities associated with diaphragmatic hernia. *Pediatrics.* 1976;58:902-906
10. Reickert CA, Hirschl RB, Atkinson JB, Dudell G, Georgeson K, Glick P, Greenspan J, Kays D, Klein M, Lally KP, Mahaffey S, Ryckman F, Sawin R, Short BL, Stolar CJ, Thompson A, Wilson JM. Congenital diaphragmatic hernia survival and use of extracorporeal life support at

- selected level iii nurseries with multimodality support. *Surgery*. 1998;123:305-310
11. Wenstrom KD, Weiner CP, Hanson JW. A five-year statewide experience with congenital diaphragmatic hernia. *Am J Obstet Gynecol*. 1991;165:838-842
 12. Muratore CS, Kharasch V, Lund DP, Sheils C, Friedman S, Brown C, Utter S, Jaksic T, Wilson JM. Pulmonary morbidity in 100 survivors of congenital diaphragmatic hernia monitored in a multidisciplinary clinic. *J Pediatr Surg*. 2001;36:133-140
 13. Inhaled nitric oxide in full-term and nearly full-term infants with hypoxic respiratory failure. The neonatal inhaled nitric oxide study group. *N Engl J Med*. 1997;336:597-604
 14. Finer NN, Barrington KJ. Nitric oxide for respiratory failure in infants born at or near term. *Cochrane Database Syst Rev*. 2006:CD000399
 15. Keller RL, Moore P, Teitel D, Hawgood S, McQuitty J, Fineman JR. Abnormal vascular tone in infants and children with lung hypoplasia: Findings from cardiac catheterization and the response to chronic therapy. *Pediatr Crit Care Med*. 2006;7:589-594
 16. Kinsella JP, Ivy DD, Abman SH. Pulmonary vasodilator therapy in congenital diaphragmatic hernia: Acute, late, and chronic pulmonary hypertension. *Semin Perinatol*. 2005;29:123-128
 17. Greer JJ, Babiuk RP, Thebaud B. Etiology of congenital diaphragmatic hernia: The retinoid hypothesis. *Pediatr Res*. 2003;53:726-730
 18. Bender AT, Beavo JA. Cyclic nucleotide phosphodiesterases: Molecular regulation to clinical use. *Pharmacol Rev*. 2006;58:488-520
 19. Wharton J, Strange JW, Moller GM, Growcott EJ, Ren X, Franklyn AP, Phillips SC, Wilkins MR. Antiproliferative effects of phosphodiesterase type 5 inhibition in human pulmonary artery cells. *Am J Respir Crit Care Med*. 2005;172:105-113
 20. Michelakis E, Tymchak W, Lien D, Webster L, Hashimoto K, Archer S. Oral sildenafil is an effective and specific pulmonary vasodilator in

- patients with pulmonary arterial hypertension: Comparison with inhaled nitric oxide. *Circulation*. 2002;105:2398-2403
21. Michelakis ED, Tymchak W, Noga M, Webster L, Wu XC, Lien D, Wang SH, Modry D, Archer SL. Long-term treatment with oral sildenafil is safe and improves functional capacity and hemodynamics in patients with pulmonary arterial hypertension. *Circulation*. 2003;108:2066-2069
 22. Thebaud B, Tibboel D, Rambaud C, Mercier JC, Bourbon JR, Dinh-Xuan AT, Archer SL. Vitamin A decreases the incidence and severity of nitrofen-induced congenital diaphragmatic hernia in rats. *Am J Physiol*. 1999;277:L423-429
 23. Walker DK, Ackland MJ, James GC, Muirhead GJ, Rance DJ, Wastall P, Wright PA. Pharmacokinetics and metabolism of sildenafil in mouse, rat, rabbit, dog and man. *Xenobiotica*. 1999;29:297-310
 24. Thebaud B, Michelakis E, Wu XC, Harry G, Hashimoto K, Archer SL. Sildenafil reverses O₂ constriction of the rabbit ductus arteriosus by inhibiting type 5 phosphodiesterase and activating BK(Ca) channels. *Pediatr Res*. 2002;52:19-24
 25. Thebaud B, Ladha F, Michelakis ED, Sawicka M, Thurston G, Eaton F, Hashimoto K, Harry G, Haromy A, Korbitt G, Archer SL. Vascular endothelial growth factor gene therapy increases survival, promotes lung angiogenesis, and prevents alveolar damage in hyperoxia-induced lung injury: Evidence that angiogenesis participates in alveolarization. *Circulation*. 2005;112:2477-2486
 26. McMurtry MS, Bonnet S, Wu X, Dyck JR, Haromy A, Hashimoto K, Michelakis ED. Dichloroacetate prevents and reverses pulmonary hypertension by inducing pulmonary artery smooth muscle cell apoptosis. *Circ Res*. 2004;95:830-840
 27. Rey-Parra GJ, Archer SL, Bland RD, Albertine KH, Carlton DP, Cho SC, Kirby B, Haromy A, Eaton F, Wu X, Thebaud B. Blunted hypoxic pulmonary vasoconstriction in experimental neonatal chronic lung disease. *Am J Respir Crit Care Med*. 2008;178:399-406

28. Pinilla I, Lund RD, Sauve Y. Contribution of rod and cone pathways to the dark-adapted electroretinogram (erg) b-wave following retinal degeneration in rcs rats. *Vision Res.* 2004;44:2467-2474
29. Stege G, Fenton A, Jaffray B. Nihilism in the 1990s: The true mortality of congenital diaphragmatic hernia. *Pediatrics.* 2003;112:532-535
30. Harrison MR, Adzick NS, Flake AW, Jennings RW, Estes JM, MacGillivray TE, Chueh JT, Goldberg JD, Filly RA, Goldstein RB. Correction of congenital diaphragmatic hernia in utero: Vi. Hard-earned lessons. *J Pediatr Surg.* 1993;28:1411-1417; discussion 1417-1418
31. Liggins GC, Howie RN. A controlled trial of antepartum glucocorticoid treatment for prevention of the respiratory distress syndrome in premature infants. *Pediatrics.* 1972;50:515-525
32. Wilcox DT, Irish MS, Holm BA, Glick PL. Animal models in congenital diaphragmatic hernia. *Clin Perinatol.* 1996;23:813-822
33. Manson JM. Mechanism of nitrofen teratogenesis. *Environ Health Perspect.* 1986;70:137-147
34. Zeman FJ, Heng H, Hoogenboom ER, Kavlock RJ, Mahboob S. Cell number and size in selected organs of fetuses of rats malnourished and exposed to nitrofen. *Teratog Carcinog Mutagen.* 1986;6:339-347
35. Brown TJ, Manson JM. Further characterization of the distribution and metabolism of nitrofen in the pregnant rat. *Teratology.* 1986;34:129-139
36. Muehlethaler V, Kunig AM, Seedorf G, Balasubramaniam V, Abman SH. Impaired vegf and nitric oxide signaling after nitrofen exposure in rat fetal lung explants. *Am J Physiol Lung Cell Mol Physiol.* 2008;294:L110-120
37. Stenmark KR, Abman SH. Lung vascular development: Implications for the pathogenesis of bronchopulmonary dysplasia. *Annu Rev Physiol.* 2005;67:623-661
38. Liebow AA. Pulmonary emphysema with special reference to vascular changes. *Am Rev Respir Dis.* 1959;80:67-93
39. Jakkula M, Le Cras TD, Gebb S, Hirth KP, Tudor RM, Voelkel NF, Abman SH. Inhibition of angiogenesis decreases alveolarization in the

- developing rat lung. *Am J Physiol Lung Cell Mol Physiol*. 2000;279:L600-607
40. Kasahara Y, Tuder RM, Taraseviciene-Stewart L, Le Cras TD, Abman S, Hirth PK, Waltenberger J, Voelkel NF. Inhibition of vegf receptors causes lung cell apoptosis and emphysema. *J Clin Invest*. 2000;106:1311-1319.
 41. Kunig AM, Balasubramaniam V, Markham NE, Morgan D, Montgomery G, Grover TR, Abman SH. Recombinant human vegf treatment enhances alveolarization after hyperoxic lung injury in neonatal rats. *Am J Physiol Lung Cell Mol Physiol*. 2005;289:L529-535
 42. Ladha F, Bonnet S, Eaton F, Hashimoto K, Korbitt G, Thebaud B. Sildenafil improves alveolar growth and pulmonary hypertension in hyperoxia-induced lung injury. *Am J Respir Crit Care Med*. 2005;172:750-756
 43. Hara A, Chapin CJ, Ertsey R, Kitterman JA. Changes in fetal lung distension alter expression of vascular endothelial growth factor and its isoforms in developing rat lung. *Pediatr Res*. 2005;58:30-37
 44. North AJ, Moya FR, Mysore MR, Thomas VL, Wells LB, Wu LC, Shaul PW. Pulmonary endothelial nitric oxide synthase gene expression is decreased in a rat model of congenital diaphragmatic hernia. *Am J Respir Cell Mol Biol*. 1995;13:676-682
 45. Shinkai T, Shima H, Solari V, Puri P. Expression of vasoactive mediators during mechanical ventilation in nitrofen-induced diaphragmatic hernia in rats. *Pediatr Surg Int*. 2005;21:143-147
 46. Shinkai M, Shinkai T, Montedonico S, Puri P. Effect of vegf on the branching morphogenesis of normal and nitrofen-induced hypoplastic fetal rat lung explants. *J Pediatr Surg*. 2006;41:781-786
 47. Shinkai M, Shinkai T, Pirker ME, Montedonico S, Puri P. Effect of nitric oxide on the development of nitrofen-induced fetal hypoplastic lung explants. *J Pediatr Surg*. 2005;40:17-21

48. Kluth D, Buhner, Nestoris S, Tander B, Werner C, Lambrecht W. Inhaled nitric oxide increases survival rates in newborn rats with congenital diaphragmatic hernia. *Eur J Pediatr Surg.* 1997;7:90-92
49. Mann O, Huppertz C, Langwieler TE, Tander B, Bloechle C, Izbicki JR, Lambrecht W, Kluth D. Effect of prenatal glucocorticoids and postnatal nitric oxide inhalation on survival of newborn rats with nitrofen-induced congenital diaphragmatic hernia. *J Pediatr Surg.* 2002;37:730-734
50. Cloutier M, Maltais F, Piedboeuf B. Increased distension stimulates distal capillary growth as well as expression of specific angiogenesis genes in fetal mouse lungs. *Exp Lung Res.* 2008;34:101-113
51. Gu JW, Brady AL, Anand V, Moore MC, Kelly WC, Adair TH. Adenosine upregulates vegf expression in cultured myocardial vascular smooth muscle cells. *Am J Physiol.* 1999;277:H595-602
52. Zhao X, Lu X, Feng Q. Deficiency in endothelial nitric oxide synthase impairs myocardial angiogenesis. *Am J Physiol Heart Circ Physiol.* 2002;283:H2371-2378
53. Vidavalur R, Penumathsa SV, Zhan L, Thirunavukkarasu M, Maulik N. Sildenafil induces angiogenic response in human coronary arteriolar endothelial cells through the expression of thioredoxin, hemeoxygenase and vascular endothelial growth factor. *Vascul Pharmacol.* 2006;45:91-95
54. Abbott D, Comby P, Charuel C, Graepel P, Hanton G, Leblanc B, Lodola A, Longeart L, Paulus G, Peters C, Stadler J. Preclinical safety profile of sildenafil. *International Journal of Impotence Research.* 2004;16:498-504
55. O'Toole SJ, Irish MS, Holm BA, Glick PL. Pulmonary vascular abnormalities in congenital diaphragmatic hernia. *Clin Perinatol.* 1996;23:781-794
56. Karamanoukian HL, Glick PL, Wilcox DT, O'Toole SJ, Rossman JE, Azizkhan RG. Pathophysiology of congenital diaphragmatic hernia. Xi: Anatomic and biochemical characterization of the heart in the fetal lamb cdh model. *J Pediatr Surg.* 1995;30:925-928; discussion 929

57. Vogel M, McElhinney DB, Marcus E, Morash D, Jennings RW, Tworetzky W. Significance and outcome of left heart hypoplasia in fetal congenital diaphragmatic hernia. *Ultrasound Obstet Gynecol.* 35:310-317
58. Jaillard S, Larrue B, Deruelle P, Delelis A, Rakza T, Butrous G, Storme L. Effects of phosphodiesterase 5 inhibitor on pulmonary vascular reactivity in the fetal lamb. *Ann Thorac Surg.* 2006;81:935-942
59. Larrue B, Jaillard S, Lorthioir M, Roubliova X, Butrous G, Rakza T, Warembourg H, Storme L. Pulmonary vascular effects of sildenafil on the development of chronic pulmonary hypertension in the ovine fetus. *Am J Physiol Lung Cell Mol Physiol.* 2005;288:L1193-1200
60. Fraunfelder FW, Fraunfelder FT. Central serous chorioretinopathy associated with sildenafil. *Retina.* 2008;28:606-609